CARM1 AND MUSCLE ATROPHY

THE ROLE OF CARM1

DURING SKELETAL MUSCLE ATROPHY

By DEREK W. STOUTH, B.Sc. Kin (Honours), MSc.

A Thesis Submitted to the School of Graduate Studies in Partial Fulfillment of the Requirements for the Degree Doctor of Philosophy

DOCTOR OF PHILOSOPHY (2021)

Department of Kinesiology, McMaster University, Hamilton, Ontario

TITLE: The role of CARM1 during skeletal muscle atrophy

AUTHOR: Derek W. Stouth, B.Sc. Kin (Honours), MSc.

SUPERVISOR: Dr. Vladimir Ljubicic

NUMBER OF PAGES: 198

Lay Abstract

While muscle wasting and weakness remains a widespread issue, the mechanisms that control muscle atrophy are not entirely understood. Previous evidence suggests that coactivator-associated arginine methyltransferase 1 (CARM1) regulates skeletal muscle remodeling. However, the role of CARM1 during muscle atrophy is unknown. Therefore, the purpose of this work was to investigate the function of CARM1 during muscle wasting. We generated mice with CARM1 deleted in skeletal muscle and studied the impact of CARM1 deficiency on the loss of skeletal muscle mass during muscle disuse, food deprivation, and aging. We found that CARM1 is required to maintain muscle mass under basal conditions. Interestingly, knocking out CARM1 in muscle attenuated the progression of denervation- and fasting-induced atrophy. However, CARM1 deletion in muscle resulted in lower muscle strength and a reduced lifespan. CARM1 deficiency did not prevent aging-induced muscle loss. Overall, these findings advance our understanding of CARM1 in skeletal muscle biology.

Abstract

Coactivator-associated arginine methyltransferase 1 (CARM1) is emerging as an important player in skeletal muscle biology. We sought to elucidate the role of CARM1 in mediating muscle mass and function, as well as in the induction and progression of the muscle atrophy program. To this end, we engineered CARM1 skeletal muscle-specific knockout (mKO) mice and employed distinct, but complementary models of muscle atrophy, including neurogenic muscle disuse, food deprivation, and the sarcopenia of aging. CARM1 mKO resulted in reduced muscle mass and myofiber cross-sectional area concomitant with dysregulated autophagic and atrophic signaling, which indicates the requirement of CARM1 for the maintenance of muscle biology. Interestingly, CARM1 deletion mitigated the progression of both denervation- and fasting-induced skeletal muscle atrophy as compared to wild-type (WT) mice. Key mechanistic findings revealed that CARM1 interacts with the master neuromuscular regulator AMPK and attenuates the expression and activity of its downstream autophagy and atrophy networks. Surprisingly, both male and female mKO mice have a significantly shorter lifespan versus their WT littermates, revealed by a ~50% reduction in survival at 22-months-old, which is equivalent to ~70 years-old in humans. As such, we observed significantly reduced functional outcomes of integrative physiology in old mKO mice compared to old WT animals, such as strength and motor performance. Taken together, these results indicate that skeletal muscle CARM1 is indispensable for maintaining muscle mass, function, and lifespan. Targeting the interplay between CARM1 and AMPK may offer a viable therapeutic strategy for combating life-limiting muscle wasting conditions.

Acknowledgements

To Athan, Tiffany, Nicole, Alex, Sean, Andrew, Erin, Rozhin, and Stephanie – Thank you for all the support and for making the Integrative Neuromuscular Biology Laboratory such an enjoyable experience and fun place to be. You will all be missed!

To Todd – Thank you for all your support, kindness, and technical assistance over the years.

To Dr. MacDonald – Thank you for taking me on as a volunteer and undergraduate research assistant in my third year. Thank you for connecting me with Dr. Tang and co-supervising my undergraduate thesis. These experiences sparked my interest and passion for research.

To Dr. Tang – Thank you for agreeing to co-supervise my undergraduate thesis and for your valuable mentorship.

To Dr. Parise – Thank you for agreeing to serve on my MSc Supervisory Committee and agreeing to serve again on my PhD Supervisory Committee.

To Dr. Phillips – Thank you for agreeing to serve on my PhD Supervisory Committee.

To my friends – Thank you for the fun times and providing insights on life.

To my family – Thank you for all the love, support, and encouragement.

To Vlad – I would like to thank Vlad for taking me on as a MSc student and allowing me to pursue a PhD thereafter. Thank you for all the opportunities that you have given me and for always taking the time to discuss my data and life. You are a true friend. Thank you for all your support and encouragement. Thank you!

Table of Contents

List of figures and tables

Chapter 1:

Chapter 2:

Chapter 3:

Chapter 4:

Chapter 5:

List of Abbreviations

CSA ..... cross-sectional area

TA ..... tibialis anterior

EDL ..... extensor digitorum longus

SOL ..... soleus

GAST ..... gastrocnemius

AMPK ..... AMP-activated protein kinase

PGC-1α ..... peroxisome proliferator-activated receptor-γ coactivator-1α

Tfam ..... mitochondrial transcription factor A

Nrf ..... nuclear respiratory factor

CREB ..... cAMP response element-binding protein

MEF2 ..... myocyte enhancer factor 2

HDAC ..... histone deacetylase

SIRT1 ..... silent mating type information regulator 2 homologue 1

LKB1 ..... liver kinase B1

CAMKK2 ..... calcium/calmodulin-dependent protein kinase kinase 2

ADaM ..... allosteric drug and metabolite

ACC ..... acetyl-coenzyme A carboxylase

TBC1D1 ..... TBC1 domain family member 1

TSC2 ..... tuberous sclerosis complex 2

mTOR ..... mammalian target of rapamycin

MFF ..... mitochondrial fission factor

ULK1 ..... unc-51-like autophagy-activating kinase 1

TFEB ..... transcription factor EB

GLUT4 ..... glucose transporter 4

FOXO ..... Forkhead box O

PI3K ..... phosphatidylinositol 3-kinase PI3K

Atg14 ..... autophagy-related 14

LC3 ..... microtubule-associated protein 1A/1B-light chain 3

Lamp1 ..... lysosomal associated membrane protein 1

TEM ..... Transmission electron microscopy

MuRF1 ..... muscle RING finger 1

MAFbx ..... muscle atrophy F-box

Akt ..... protein kinase B

NMJ ..... neuromuscular junction

PRMTs ..... Protein arginine methyltransferases

SAM ..... S-adenosylmethionine

MMA ..... monomethylarginine

SAH ..... S-adenosylhomocysteine

ADMA ..... asymmetric dimethylarginine

SDMA ..... symmetric dimethylarginine

CARM1 ..... coactivator-associated arginine methyltransferase 1

BAF155 ..... SWI/SNF chromatin remodeling complex BAF155

PABP1 ..... poly(A)-binding protein 1

Thesis format and organization

This thesis contains material from the Ph.D. work of Derek W. Stouth and has been prepared in the "sandwich" format as outlined in the McMaster University School of Graduate Studies' Guide for the Preparation of Theses. The thesis includes a general introduction (Chapter 1), followed by 3 studies that have been prepared as separate manuscripts (Chapters 2-4), and is concluded with a general discussion (Chapter 5). The candidate is first author on all manuscripts.

Declaration of Academic Achievement

Contribution to papers with multiple authorship

Chapter 2 (Study 1):
Stouth, D. W., vanLieshout, T. L., Ng, S. Y., Webb, E. K., Manta, A., Moll, Z., & Ljubicic, V. (2020). CARM1 Regulates AMPK Signaling in Skeletal Muscle. iScience, 23(11), 101755.

Contributions:
D.W.S. and V.L. conceived and designed the study; D.W.S. and T.L.v. generated and maintained CARM1 mKO mice; D.W.S. performed denervation surgeries, quantitative real-time RT-PCRs, western blot and immunoprecipitation experiments; D.W.S. and Z.M. conducted H&E staining analyses; E.K.W. and A.M. assisted with western blot procedures; D.W.S. and A.M. executed SDH staining technique; S.Y.N. performed MK-8722 experiments; all authors participated in data analysis and interpretation of results; D.W.S. and V.L. drafted and edited the manuscript.

Chapter 3 (Study 2):
Stouth, D. W., vanLieshout, T. L., Ng, S. Y., Mikhail, A., Webb, E. K., Gilotra, K.S., Markou, M., Pineda, H.C., Bettencourt-Mora, B.G., Noor, H., Moll, Z., Bittner, M.E., & Ljubicic, V. Skeletal muscle-specific CARM1 deletion hinders autophagy flux and prevents fasting-induced atrophy

Contributions:
D.W.S. and V.L. conceived and designed the study; D.W.S. and T.L.v. generated and maintained CARM1 mKO mice; D.W.S. performed all experiments and most analyses. S.Y.N., A.M., E.K.W., K.S.G., M.M., H.C.P., B.G.B., H.N., Z.M., and M.E.B. assisted with analyses; all authors participated in data analysis and interpretation of results; D.W.S. and V.L. drafted and edited the manuscript.

Chapter 4 (Study 3):
Stouth, D. W., vanLieshout, T. L., Ng, S. Y., Mikhail, A., Webb, E. K., Gilotra, K.S., Markou, M., Pineda, H.C., Bettencourt-Mora, B.G., Ryan T., Kwiecien, J.M., Vasam, G., Menzies, K.J., & Ljubicic, V.
Contributions:
D.W.S. and V.L. conceived and designed the study; D.W.S. and T.L.v. generated and maintained CARM1 mKO mice; D.W.S. performed all experiments and most analyses. S.Y.N., A.M., E.K.W., K.S.G., M.M., H.C.P., B.G.B., T.R., J.M.K., G.V. and K.J.M. assisted with analyses; all authors participated in data analysis and interpretation of results; D.W.S. and V.L. drafted and edited the manuscript.

Chapter 1: Introduction

1.1 Overview

1.1.1 Introduction to skeletal muscle.

Skeletal muscle accounts for approximately 40% of total body mass in humans and is imperative for locomotion, posture, breathing, along with other movements (Janssen et al., 2000). Besides motility, muscle plays a critical role in whole body metabolism, serving as a primary site for glucose uptake and storage, as well as a reservoir for amino acids. Each skeletal muscle consists of vascularized and cylindrical multinucleated cells, termed skeletal muscle fibers, that extend the length of the muscle. The myonuclei are located near the muscle fiber periphery, situated just below the sarcolemma, and its quantity determines the content of DNA for gene transcription (Shenkman et al., 2010). Within the sarcolemma, lies mitochondria, glycogen granules, and myofibrils. Myofibrils are bundles of protein myofilaments composed of actin and myosin that span from one end of the muscle fiber to the other. The actin and myosin myofilaments form highly ordered units called sarcomeres, which are linked end to end.

Along the surface of the sarcolemma are tubelike invaginations, called transverse tubules, that extend to the interior of muscle cells and permit rapid transmission of action potentials. The transverse tubules are associated with the sarcoplasmic reticulum, which surrounds myofibrils and stores calcium ions. Upon neuronal stimulation, calcium ions are released from the sarcoplasmic reticulum, and through a series of steps, enable actin and myosin myofilaments to slide past one another. The shortening of sarcomeres causes skeletal muscle contraction and essentially locomotion, posture, breathing, and other movements.

Skeletal muscle fibers can be classified as either slow twitch (type I) or fast twitch (type II), based on the specific myosin heavy chain isoform they express. Fast twitch fibers can be further distinguished as types IIA and IIX in humans, while subtypes IIA, IIB, and IIX exist in rodents (Egan and Zierath, 2013). Type I fibers typically have smaller cross-sectional area (CSA), along with greater capillaries per fiber, mitochondrial density, satellite cell count, and neuromuscular junction size versus type II fibers (Qaisar et al., 2016). With more myoglobin and mitochondria, type I fibers are red, highly oxidative and hold substantial endurance capacity. In contrast, type II fibers are whiter in appearance and possess greater force generation plus contraction velocity. Subtypes IIB and IIX are also the most glycolytic and fatigue the quickest.

1.1.2 Skeletal muscle plasticity.

The proportion of type I, IIA, IIB, and IIX myofibers, respectively, in murine tibialis anterior (TA), extensor digitorum longus (EDL), soleus (SOL) and gastrocnemius (GAST) muscles are approximately as follows: TA = 0%, 30%, 45%, 25%; EDL = 5%, 20%, 50%, 25%; SOL = 40%, 50%, 5%, 5%; GAST = 0%, 25%, 55%, 20% (Bloemberg and Quadrilatero, 2012; Stark et al., 2015). Notably, these percentages are plastic since skeletal muscle is a highly malleable tissue that perpetually remodels in response to disparate stimuli. For instance, chronic muscle use promotes a slower, more oxidative profile, whereas chronic muscle disuse elicits induction of the fast, glycolytic myogenic program, plus atrophy. These adaptations are driven by various intracellular signaling molecules such as AMP-activated protein kinase (AMPK), peroxisome proliferator-

activated receptor-γ coactivator-1α (PGC-1α), and mitochondrial transcription factor A (Tfam).

AMPK is a major sensor of intracellular energy demand and serves as a master regulator of muscle phenotype plasticity (Mounier et al., 2015; Kjobsted et al., 2018; Steinberg and Carling, 2019). AMPK is sensitive to increased cellular AMP:ATP and ADP:ATP ratios that occur during metabolic stress. For example, food deprivation, endurance-type exercise, and ischemia are physiological activators of AMPK. AMPK promotes an oxidative muscle phenotype through direct or indirect control over key modifier proteins such as PGC-1α, Tfam, nuclear respiratory factor (Nrf)-1/2, tumor suppressor protein p53, cAMP response element-binding protein (CREB), myocyte enhancer factor 2 (MEF2), histone deacetylase (HDAC) 5, and silent mating type information regulator 2 homologue 1 (SIRT1).

PGC-1α is a transcription coactivator that also functions as a powerful regulator of muscle plasticity. PGC-1α is involved in the coordinated regulation of nuclear- and mitochondrial-encoded genes responsible for a shift in muscle toward a slower, more oxidative phenotype (Lira et al., 2010; Ljubicic et al., 2014). For instance, transgenic and physiological overexpression of PGC-1α results in fiber type transformation, mitochondrial biogenesis, angiogenesis, and other adaptive changes such as resistance to muscle atrophy.

Tfam and Nrf-1/2 are among the transcription factors that are important for muscle remodeling. Indeed, these transcription factors regulate genes that are involved in mitochondrial biogenesis, formation of the electron transport chain complexes I–V, and overall mitochondrial respiratory function (Hood et al., 2019). Tfam and Nrf-1/2 foster the

expression of mitochondrial genes that are encoded in both mitochondrial and nuclear DNA. Both transcription factors contribute towards the slow, oxidative myogenic program.

1.1.3 AMPK and metabolic signaling.

AMPK is a heterotrimer comprised of a catalytic subunit (α) and two non-catalytic regulatory subunits (β and γ) existing as multiple isoforms (α1, α2, β1, β2, γ1, γ2, and γ3). The α subunit possesses a kinase domain that is activated when phosphorylated on residue Thr172 by the upstream liver kinase B1 (LKB1) or calcium/calmodulin-dependent protein kinase kinase 2 (CAMKK2). AMP and ADP induce phosphorylation by LKB1, whereas increased intracellular calcium evokes phosphorylation by CAMKK2. Binding of AMP or ADP to the γ subunit also directly activates AMPK via an allosteric mechanism (Mounier et al., 2015; Kjobsted et al., 2018; Steinberg and Carling, 2019). Importantly, AMPK activity can be modulated pharmacologically by compounds that deplete ATP (i.e., metformin) or directly bind at the allosteric drug and metabolite (ADaM) site (i.e., MK-8722).

AMPK restores energy balance by suppressing anabolic processes that consume ATP, while triggering catabolic processes that regenerate ATP (Garcia and Shaw, 2017; Herzig and Shaw, 2018). In response to energy stress, AMPK inhibits fatty acid synthesis, glycogen synthesis, gluconeogenesis, and protein synthesis. AMPK activation also stimulates catabolic pathways such as fatty acid oxidation, glucose uptake, glycolysis, mitochondrial fission, mitophagy, and autophagy. Direct targets of AMPK that regulate metabolic signaling include acetyl-coenzyme A carboxylase (ACC), TBC1 domain family member 1 (TBC1D1), tuberous sclerosis complex 2 (TSC2), mammalian target of

rapamycin (mTOR), mitochondrial fission factor (MFF), unc-51-like autophagy-activating kinase 1 (ULK1), transcription factor EB (TFEB), and Beclin-1 (Figure 1).

Once activated, AMPK phosphorylates key substrates to elicit metabolic changes. Notably, phosphorylation can either positively or negatively modulate the function of target proteins (Garcia and Shaw, 2017; Herzig and Shaw, 2018). AMPK controls lipid metabolism through inhibitory phosphorylation of ACC1 and ACC2. Phosphorylation of ACC1^{Ser79} and ACC2^{Ser212} impedes fatty acid synthesis, while also promoting fatty acid oxidation (Fullerton et al., 2013; O'Neill et al., 2014). AMPK enhances glucose uptake by phosphorylating TBC1D1 at Ser231, Ser660, and Ser700 sites, which facilitates glucose transporter 4 (GLUT4) translocation to the muscle surface membrane (Vichaiwong et al., 2010). The ability of AMPK to suppress protein synthesis is regulated in large part by inhibition of mTOR. mTOR activity is indirectly controlled by AMPK through phosphorylation of TSC2 at Thr1227 or Ser1345, as well as direct phosphorylation of mTOR^{Thr2446} (Inoki et al., 2003; Cheng et al., 2004). Phosphorylation of MFF at Ser155 and Ser172 by AMPK induces mitochondrial fission (Toyama et al., 2016). AMPK also promotes autophagy by phosphorylating ULK1^{Ser555}, TFEB^{Ser466,467,469}, and Beclin-1^{Ser91,94} (Egan et al., 2011; Kim et al., 2013; Paquette et al., 2021).

1.1.4 Autophagy-lysosome signaling pathway.

Macroautophagy, hereafter named autophagy, is a highly conserved homeostatic process in which cellular proteins, organelles, and other macromolecules are engulfed in a double-membraned autophagosome and delivered to lysosomes for degradation and recycling (Klionsky et al., 2021; Triolo and Hood, 2021). This catabolic mechanism is

critical for muscle health as it can elicit selective removal of damaged or dysfunctional cellular contents, such as mitochondria via mitophagy. Importantly, autophagy is necessary to preserve muscle mass (Masiero et al., 2009) and excessive autophagy contributes to muscle wasting. Autophagic breakdown can be altered in response to various stimuli such as muscle disuse, food deprivation, the sarcopenia of aging, cancer cachexia, and neuromuscular disorders.

Autophagy is a highly dynamic, multi-step process of sequential events that includes initiation, nucleation of a phagophore structure, maturation of the autophagosome, transport of cargo, autophagosome fusion with the lysosome, as well as degradation and recycling of nutrients (Triolo and Hood, 2021). Upstream regulators of the autophagy-lysosome system have been identified such as AMPK, mTOR, ULK1, TFEB, and Forkhead box O (FOXO). Autophagy commences with the activation of ULK1 and induction of a pre-autophagosomal structure. ULK1 is negatively regulated by mTOR and positively regulated by AMPK. Autophagy also begins with AMPK increasing transcriptional activity of FOXO3 and TFEB, which upregulates autophagy-related genes.

Activated ULK1 phosphorylates downstream targets to assemble the phosphatidylinositol 3-kinase (PI3K) complex, partly consisting of autophagy-related 14 (Atg14) and Beclin-1, which is responsible for recruitment of proteins that are needed for autophagosome formation. Maturation and elongation of the autophagosome membrane involves conversion of microtubule-associated protein 1A/1B-light chain 3 (LC3)-I to lipidated LC3-II, as well as autophagosomal proteins p62 and Gabarapl. Mature autophagosomes carrying cargo are then transported via microtubules to lysosomes for

fusion and subsequent degradation of sequestered contents. Degradation, in part, is mediated by lysosomal associated membrane protein 1 (Lamp1), Lamp2, and cathepsin D.

LC3-II is incorporated into the autophagosome membrane during elongation and is commonly employed as an experimental marker to detect and quantify autophagosome formation (Klionsky et al., 2021). However, given the dynamic nature of autophagy, static levels of endogenous LC 3-II protein can result in misinterpretations since the accumulation of autophagosomes is not always indicative of autophagy induction. Indeed, elevated levels of LC3-II may represent either increased production of autophagosomes and/or inability to complete the autophagy-lysosome pathway. Measures of autophagosome flux are required, whereby LC3-II protein levels are assessed in the presence and absence of agents that block the degradation of LC3-II. For example, autophagic flux can be determined by immunoblotting for LC3-II with and without lysosomal inhibitor treatment. Another detection method for evaluating autophagic flux includes quantitation of LC3 colour change with fluorescence microscopy. Transmission electron microscopy (TEM) may also be employed to detect the number of autophagosomes (Mizushima et al., 2010).

1.1.5 Ubiquitin-proteasome signaling pathway.

Muscle atrophy occurs when muscle protein breakdown chronically exceeds muscle protein synthesis and can be characterized by reduced muscle mass, muscle fiber CSA, and contractile protein content (Phillips et al., 2009; Sandri, 2013a). Unloading with reduced neural activity, also known as neurogenic muscle disuse, occurs under many clinical settings such as limb immobilization, bed rest, mechanical ventilation, and spinal cord injury. Under these conditions, loss of skeletal muscle mass leads to muscle weakness,

inactivity, and increased mortality (Bodine and Baehr, 2014). Prolonged fasting, sarcopenia, cancer cachexia, and muscular dystrophies have also been shown to elicit muscle wasting. One of the primary pathways responsible for the increased muscle proteolysis under catabolic conditions is the ATP-dependent, ubiquitin-proteasome pathway.

Ubiquitin–proteasome-dependent proteolysis is a multi-step process that involves polyubiquitination of a targeted protein, specific recognition, and subsequent breakdown by a proteasome (Taillandier et al., 2004). Muscle RING finger 1 (MuRF1) and muscle atrophy F-box (MAFbx) are key ubiquitin-protein ligases that selectively bind and mark substrates for degradation. MuRF1 and MAFbx are upregulated during catabolic conditions and are considered master genes of muscle atrophy (Bodine and Baehr, 2014). For instance, knockout of either MuRF1 or MAFbx mitigates denervation-induced muscle wasting (Bodine et al., 2001a). While increased expression of MuRF1 and MAFbx contribute towards the loss of muscle mass, these two ubiquitin ligases are not solely responsible for driving muscle protein breakdown.

FOXO1 and FOXO3 belong to the FOXO family of transcription factors that are among the key regulators of muscle wasting. Indeed, FOXO1 and FOXO3 govern the transcription of several genes important for the autophagy-lysosome and ubiquitin-proteasome degradation pathways (Sanchez et al., 2014). Specifically, FOXO1 and FOXO3 transcriptionally upregulate MuRF1 and MAFbx in response to various atrophy-inducing stressors (Bodine and Baehr, 2014). Muscle-specific deletion of FOXOs prevents the expression of atrogenes and results in protection from denervation- and fasting-induced

atrophy (Milan et al., 2015). Notably, upstream signaling molecules AMPK and protein kinase B (Akt) exert control over FOXOs via phosphorylation. AMPK promotes the transcription of MuRF1 and MAFbx by phosphorylating FOXO3^{Ser588} and FOXO3^{Ser413} (Kjobsted et al., 2018), whereas Akt-dependent phosphorylation of FOXO1^{Ser256} and FOXO3^{Ser253} suppresses transcriptional activity via nuclear exclusion (Sanchez et al., 2014). Thus, the ubiquitin-proteasome signaling pathway can either be positively or negatively modulated.

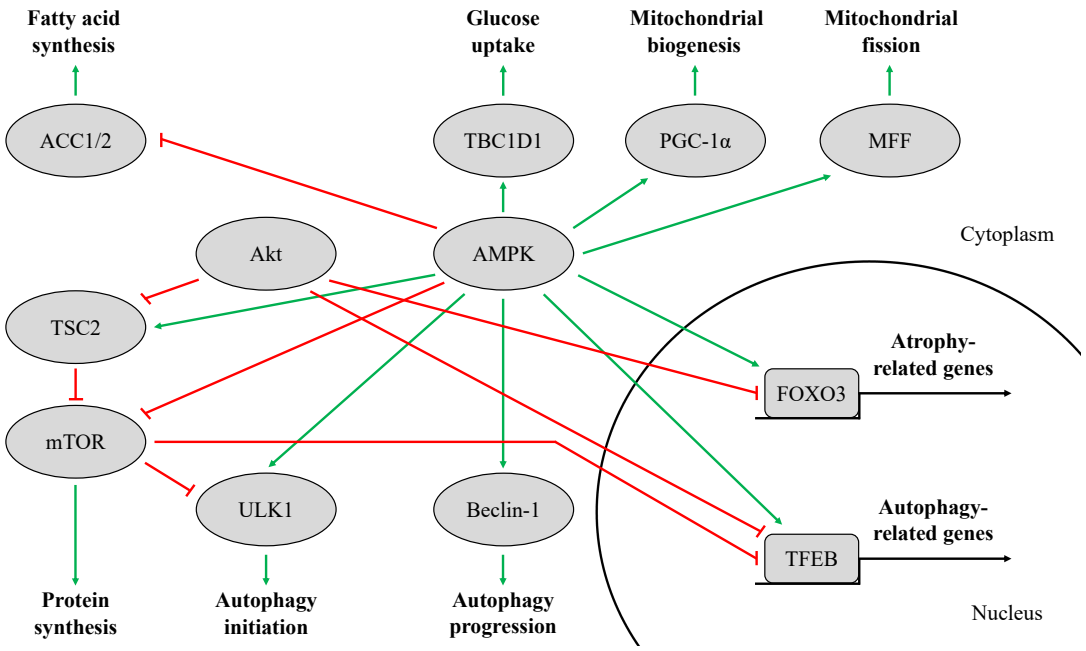

Figure 1. AMPK is a master regulator of metabolism. AMPK controls a wide range of processes, such as lipid metabolism, glucose metabolism, and protein metabolism. AMPK also governs mitochondrial homeostasis, autophagy, and atrophy. AMPK phosphorylates key targets such as ACC1^{Ser79}, ACC2^{Ser212}, TBC1D1$^{Ser231/660/700}$, PGC-1α$^{Thr177/Ser538}$, MFF$^{Ser155/172}$, TSC2$^{Thr1227/Ser1345}$, mTOR^{Thr2446}, ULK1^{Ser555}, Beclin-1$^{Ser91/94}$, TFEB$^{Ser466/467/469}$, and FOXO3$^{Ser413/588}$. Arrows indicate whether the phosphorylation is activating (green) or inhibitory (red) for the function of the target protein.

1.2 Skeletal muscle atrophy

1.2.1 Muscle disuse.

Loss of muscle due to decreased external loading and/or neural activation of a muscle is referred to as disuse atrophy (Atherton et al., 2016). Various models employed to study disuse in humans and rodents include denervation, spinal cord injury, immobilization, hind limb suspension, microgravity, and bed rest. The degree of disuse atrophy depends on the extent to which the load and neural activity are impacted. For example, denervation elicits greater muscle atrophy than other models of disuse such as immobilization and hindlimb suspension (Bodine et al., 2001a). Denervation prevents muscle contraction and results in the absence of trophic factors that travel from nerve to muscle. Notably, immobilization can lead to varying amounts of muscle wasting depending on how completely the joint is restricted from movement and how the fixed joint angle affects muscle length (Spector et al., 1982). The hindlimb suspension model in rodents has less of an effect on neural activity and can be used to study the impact of disuse on muscles of variable physiological function and fiber type composition. Importantly, atrogenes are differentially expressed in different models of disuse (Brocca et al., 2017; Hitachi et al., 2021). Therefore, future studies that aim to investigate potential therapies for treating disuse atrophy should consider the model of disuse.

The rate and severity of disuse atrophy depends on the physiological function and fiber type composition of the muscle, as well as the species-specificity. For instance, spinal cord isolation in rats evokes greater muscle loss in GAST versus TA muscle (Roy et al., 2005). Similarly, the GAST muscle atrophied to a greater extent than the TA following bed

rest in humans (de Boer et al., 2008). The dissimilar response between extensor and flexor muscles is likely due to differences in mechanical loading under normal conditions. Within a particular muscle, type I myofibers appear to atrophy more rapidly than type IIA, IIB, and IIX muscle fibers in response to disuse (Phillips et al., 2009; Bodine, 2013). For example, slow twitch myofibers (type I) were more sensitive to hindlimb unloading than fast twitch myofibers (type II) in rat muscle (Vermaelen et al., 2005). Greater muscle wasting was also observed in type I versus type II muscle fibers after prolonged spaceflight and bed rest in humans (Fitts et al., 2010; Brocca et al., 2012). Despite this work, not all human studies show differential atrophy related to muscle fiber type (Yasuda et al., 2005). A notable difference between human and rodent muscle is that rodents lose relatively more of their muscle mass in a rapid fashion (Phillips et al., 2009; Bodine, 2013). This is likely due to species differences in protein metabolism since total protein turnover in adult rats is approximately 3- to 4-fold higher than adult humans (Phillips et al., 2009). In humans, muscle disuse triggers muscle wasting within 14 days and rates of muscle loss are slightly faster within the first 30 days (Phillips et al., 2009; Bodine, 2013).

Manipulating the expression and/or activity of AMPK, PGC-1α, Akt, mTOR, FOXO1, FOXO3, MuRF1, and MAFbx can protect muscle from disuse atrophy. For instance, transgenic mice with depleted AMPK expression and/or activity are resistant to denervation- and hindlimb unloading-induced muscle wasting (Egawa et al., 2015; Guo et al., 2016). Overexpression of PGC-1α in mice also results in protection from denervation- and hindlimb unloading-evoked muscle atrophy (Sandri et al., 2006; Cannavino et al., 2014; Cannavino et al., 2015; Vainshtein et al., 2015; Wang et al., 2017). Activation of Akt

upregulates mTOR and downregulates FOXOs, leading to opposition of muscle loss elicited by denervation (Brunet et al., 1999; Bodine et al., 2001b). Deletion of FOXOs, MuRF1, and MAFbx can also mitigate denervation- and hindlimb unloading-induced muscle wasting (Bodine et al., 2001a; Milan et al., 2015; Brocca et al., 2017). While disuse atrophy remains a widespread issue, there remains an incomplete understanding of the molecular mechanisms that drive muscle wasting. Thus, continued investigation of putative therapeutic targets that preserve muscle mass during atrophy is warranted.

1.2.2 Prolonged fasting.

Circulating blood glucose levels are governed, in part, by insulin and glucagon hormones. Insulin promotes the storage of glucose via glycogen synthesis in the liver and muscle during the postprandial or well-fed state. In contrast, glucagon stimulates glycogen degradation in the liver and the release of glucose into the blood during the postabsorptive or fasting state. Skeletal muscles are unable to release glucose and muscle glycogen is mainly reserved as a local energy source for exercise. As liver glycogen stores are depleted during prolonged fasting, muscle glycogen can be broken down to lactate and transported to the liver for gluconeogenesis (Jensen et al., 2011). Skeletal muscle is also required to supply the liver with gluconeogenic amino acids for gluconeogenesis in response to prolonged food deprivation (Felig et al., 1970). Increased muscle protein breakdown during fasting can be attributed to the autophagy-lysosome and ubiquitin-proteasome proteolytic systems (Finn and Dice, 2006; Bagherniya et al., 2018). Ultimately, the utilization of amino acids derived from muscle proteins leads to muscle wasting.

Like muscle disuse, prolonged food deprivation is a catabolic condition that results in muscle proteolysis. There is a common set of FOXO-dependent genes that controls both hindlimb unloading- and fasting-induced atrophy. For example, MuRF1 and MAFbx are among the common atrogenes that upregulated in both atrophy models (Brocca et al., 2017). Notably, FOXOs are key transcriptional regulators of the autophagy-lysosome and ubiquitin-proteasome proteolytic pathways (Sanchez et al., 2014). In a similar fashion as neurogenic muscle disuse, absence of FOXOs spares muscle loss during food deprivation by preventing the induction of critical atrogenes (Milan et al., 2015). Elevated levels of PGC-1α during food deprivation also spares muscle mass, in part, by downregulating key atrogenes involved in protein degradation (Sandri et al., 2006). Taken together, a common set of atrogenes are upregulated during different models of atrophy and overlapping countermeasures to prevent muscle loss exist in each condition.

There are important differences between disuse- and fasting-induced muscle atrophy. The overall number of down- and up-regulated mRNAs varies in each muscle atrophy condition (Hitachi et al., 2021). Furthermore, certain genes are differentially expressed between atrophy models. For instance, PGC-1α mRNA expression levels are decreased during denervation and hindlimb unloading (Sacheck et al., 2007; Wang et al., 2017), whereas there is evidence that PGC-1α transcript levels are elevated in response to food deprivation (Canto et al., 2010). Contrary to the various models of muscle disuse, prolonged food deprivation also appears to elicit greater atrophy in faster, more glycolytic muscle compared to their slower, more oxidative counterparts (Wang and Pessin, 2013). For example, higher levels of protein degradation were observed in EDL versus SOL

muscles in rats after fasting (Li and Goldberg, 1976; Dahlmann et al., 1986). The disparate response of muscles to food deprivation is likely due, in part, to diverging autophagic responses. For instance, autophagy levels were higher in EDL versus SOL muscles in mice following food deprivation (Mizushima et al., 2004). Specifically, LC3-II protein levels were greater in rodent fast-twitch muscles compared to slow-twitch muscles after fasting (Ogata et al., 2010). These results suggest that the autophagy-lysosome system is more active in fast-switch muscle following food deprivation. Overall, differences are present between various models of atrophy, and these should be noted when developing therapeutic strategies that aim to attenuate the loss of muscle mass.

The time course of fasting-induced atrophy bears some consideration, as differences exist between species. As discussed earlier, total protein turnover in rodents is higher than humans (Phillips et al., 2009). There is a more rapid and pronounced decline in muscle mass in rodents versus humans after food deprivation. For example, fasting induced-muscle wasting occurs in mice and rats as early as 24 hours (Ogata et al., 2010; Kunkel et al., 2011; Milan et al., 2015), whereas 15 or 40 hours of short-term fasting failed to elicit significant atrophy in healthy human adults (Larsen et al., 2006). Interestingly, genes related to the autophagy-lysosome and ubiquitin-proteasome proteolytic systems were upregulated in healthy human adults following 40 hours of food deprivation (Kunkel et al., 2011). Furthermore, cellular signaling important for protein degradation is altered in human muscle following 72 hours of fasting (Vendelbo et al., 2014). Collectively, despite a similar impact on global skeletal muscle mRNA expression, greater periods of prolonged food deprivation appear to be required to evoke muscle wasting in humans versus rodents.

1.2.3 Sarcopenia of aging.

The progressive loss of muscle mass and strength that occurs with aging, collectively known as sarcopenia, increases the risk for falls, fractures, frailty, physical disability, and mortality (Cruz-Jentoft et al., 2019). As a result, sarcopenia contributes substantially to the loss of independence and reduced quality of life. The sarcopenia of aging appears to begin as early as the fifth decade of life in humans (Janssen et al., 2000; Hughes et al., 2001). Sarcopenia also places a heavy burden on healthcare providers and poses immense financial challenges to the healthcare system. Indeed, estimates of healthcare costs related to sarcopenia previously approached $20 billion per year (Janssen et al., 2004; Norman and Otten, 2019). The average life expectancy in Canada was 79 and 83 years for males and females, respectively, ten years ago (Statistics Canada, 2016). Life expectancy is projected to reach 84 and 87 years for males and females, respectively, in 2036 (Statistics Canada, 2016). Furthermore, the proportion of the Canadian population aged 65 and over was 15% in 2013 and is expected to increase to over 25% by 2061 (Statistics Canada, 2016). Thus, there is a strong rationale for developing suitable lifestyle interventions and therapeutic strategies for combating sarcopenia.

The structural adaptations associated with the sarcopenia of aging in humans and rodents are substantial, including reduced muscle mass, myofiber CSA, and contractile protein content (Lexell et al., 1988). Age-related changes also include the presence of fiber type grouping, centralized myonuclei; and infiltration of non-muscle cells (Tintignac et al., 2015). This multitude of phenotypes suggest that several factors likely contribute to sarcopenia. Sarcopenia is characterized by loss of muscle strength (Larsson et al., 1979),

selective atrophy of type II myofibers (Lexell and Taylor, 1991; Nilwik et al., 2013), and decreased regenerative capacity in response to injury (Joanisse et al., 2016). Despite distinct metabolic rates (Perlman, 2016) and neuromuscular junction (NMJ) morphology (Jones et al., 2017), certain age-related pathways are conserved between humans and rodents (Borsch et al., 2021). Notably, old C57BL6/J mice that are 18-24 months roughly corresponds to 56-69 human years (Jackson et al., 2017; Manzanares et al., 2018; Yanai and Endo 2021). Life expectancy also varies between strains (Jackson et al., 2017). Furthermore, factors that trigger sarcopenia remain to be fully understood. Although there is currently no cure, implementing lifestyle-based interventions such as exercise training and caloric restriction can slow-down sarcopenia. Overall, further investigation is warranted to assess the mechanisms involved in and responsible for driving sarcopenia.

With advancing age, older muscle often presents with compromised NMJ integrity, sarcolemma stability, mitochondrial function, and autophagy (Tintignac et al., 2015). The NMJ is a specialized synapse between a motor neuron and a muscle fiber that plays a fundamental role in generating movement. Although controversial (Jones et al., 2017), there is evidence to support morphological changes in the human NMJ with age (Oda, 1984; Wokke et al., 1990; Soendenbroe et al., 2020). Rodent studies have also demonstrated striking morphological remodeling of the NMJ in response to aging (Burke et al., 2021). For instance, older mice display a higher percentage of NMJ fragmentation and degree of denervation (Valdez et al., 2010; Li et al., 2011; Cheng et al., 2013). Despite these studies, it remains unclear whether NMJ dysfunction as a primary cause of sarcopenia. Furthermore, concomitant with age-related loss of dystrophin, old muscles show more

susceptibility to contraction-induced damage (Hughes et al., 2017). The age-related decline in regenerative capacity of muscle satellite cells is associated with greater tissue fibrosis (Brack et al., 2007; Joanisse et al., 2016). Elevated levels of fibrosis likely contribute towards sarcopenia since excessive accumulation of extracellular matrix components, such as collagen, impairs muscle function and increases muscle susceptibility to re-injury (Mahdy, 2019). Moreover, mitochondria, the organelles responsible for supplying energy through the electron transport chain, are impaired in aging muscle. For example, aged muscle contains reduced organelle content (St-Jean-Pelletier et al., 2017), altered mitochondrial morphology (Leduc-Gaudet et al., 2015), lower respiratory function (Grevendonk et al., 2021; Carter et al., 2018), and higher reactive oxygen species (ROS) emission (Chabi et al., 2008). The accumulation of damaged mitochondria results in motor neuron and muscle fiber death (Alway et al. 2017), possibly culminating in the development of sarcopenia. Autophagy is critical for the preservation of muscle mass (Masiero et al., 2009) through the removal of damaged or dysfunctional cellular components, such as mitochondria via mitophagy. Autophagy inhibition in muscle results in perturbed NMJ morphology and function, as well as muscle strength (Carnio et al., 2014). Importantly, aging alters autophagic flux (Carter et al., 2018), and acute inhibition of autophagy in older mice exacerbates features of sarcopenia (Carnio et al., 2014). Thus, aberrant autophagic processes, along with several other factors, likely contribute to sarcopenia.

The expression and/or activity levels of AMPK, PGC-1α, Akt, mTOR, FOXO1, FOXO3, MuRF1, and MAFbx are influenced by the sarcopenia of aging. Indeed, the responsiveness of AMPK to cellular stress declines with aging (Salminen and Kaarniranta,

2012). This age-related decrease in AMPK activation hinders metabolic signaling and autophagic clearance (Salminen and Kaarniranta, 2012). For instance, AMPK activation is blunted following aerobic exercise in aged muscle, leading to reduced PGC-1α expression, and in turn, mitochondrial biogenesis (Reznick et al., 2007; Lanza et al., 2008). Importantly, loss of AMPK in muscle impairs autophagy and exacerbates the sarcopenia of aging (Bujak et al., 2015). Furthermore, the activity of Akt and its downstream target mTOR are decreased with aging (Cuthbertson et al., 2005; Léger et al., 2008). Anabolic resistance occurs in older muscle after resistance exercise training and this is likely due, in part, to impaired Akt/mTOR hypertrophic signaling (Fry et al., 2011). Interestingly, hyperactivation of mTOR can aggravate the sarcopenia of aging. For example, chronic mTOR activation inhibits autophagy and undermines NMJ function (Castets et al., 2013; Ham et al., 2020). Moreover, evidence from human and rodent studies demonstrate only modest age-related changes in FOXO atrophic signaling (Sanchez et al., 2014). Contrary to muscle disuse and prolonged fasting, MuRF1 and MAFbx expression levels are either unchanged or downregulated in muscle with aging (Edstrom et al., 2006; Sandri et al., 2013b). Altogether, sarcopenia is mechanistically different from other atrophy models.

1.3 CARM1

1.3.1 Introduction to PRMTs.

Protein arginine methyltransferases (PRMTs) are a family of nine enzymes that catalyze the transfer of methyl groups to the guanidine nitrogen atoms of arginine residues on target proteins, thereby affecting their stability, localization, and/or activity (Bedford

and Clarke, 2009; Yang and Bedford, 2013; Blanc and Richard, 2017; Fulton et al., 2019; Guccione and Richard, 2019). Methylation of histones, transcription factors, and other proteins permits PRMTs to regulate cellular processes such as gene transcription, mRNA splicing, DNA repair, signal transduction, protein subcellular localization, and cell cycle progression. PRMTs are generally ubiquitously expressed, and deregulation of these enzymes contributes toward the pathogenesis of various diseases such as cancer. Importantly, arginine methylation is as common an occurrence as the more widely studied and better understood phosphorylation and ubiquitination alterations (Larsen et al., 2016).

PRMTs employ S-adenosylmethionine (SAM) as the universal methyl donor (Guccione and Richard, 2019). SAM is synthesized from methionine and ATP by SAM synthetase. All PRMTs initially catalyze the transfer of a methyl group from SAM to the target protein to produce a monomethylarginine (MMA) mark, along with side product S-adenosylhomocysteine (SAH). The subsequent generation of asymmetric dimethylarginine (ADMA) and symmetric dimethylarginine (SDMA) marks is catalyzed by type I and type II PRMTs, respectively. Type III PRMTs only generate MMA products. Type I PRMTs include PRMT1, PRMT2, PRMT3, PRMT4 (also known as coactivator-associated arginine methyltransferase 1, or CARM1), PRMT6, and PRMT8. Type II PRMTs consist of PRMT5 and PRMT9, whereas type III PRMTs are comprised of PRMT7. Of the nine PRMT family members, PRMT1 and PRMT5 are the enzymes primarily responsible for generating ADMA and SDMA marks, respectively, with PRMT1 performing more than 90% of all methylation in mammalian cells (Yang and Bedford, 2013). Notably, loss of PRMT1 causes

substrate scavenging by other PRMTs (Dhar et al., 2013), highlighting interplay and possible compensatory mechanisms among PRMT family members.

PRMT activity is regulated, in part, by various microRNAs and posttranslational modifications (Guccione and Richard, 2019). Indeed, several microRNAs have been shown to negatively regulate the stability and translation of PRMT mRNAs. Methylation, phosphorylation, and ubiquitination can also influence PRMT stability and function. Furthermore, various clinically relevant PRMT inhibitors have recently emerged (Guccione and Richard, 2019). Particularly, administering small molecule arginine methyltransferase inhibitors may offer therapeutic value in cases where PRMTs are dysregulated.

1.3.2 The importance of CARM1.

CARM1 belongs to the PRMT family of enzymes and is ubiquitously expressed. Importantly, whole-body genetic deletion of CARM1 in mice results in perinatal lethality (Yadav et al., 2003), indicating that this enzyme is indispensable for survival. As a type I PRMT, CARM1 deposits the ADMA mark on target proteins, thereby regulating critical intracellular processes such as autophagy (Bedford and Clarke, 2009). Notably, inhibition of CARM1 impedes autophagy in non-muscle cells (Shin et al., 2016; Yu et al., 2020). Moreover, CARM1 has unique substrate specificity as it methylates proline-rich motifs (Cheng et al., 2018). For instance, SWI/SNF chromatin remodeling complex BAF155 (BAF155me2a^{Arg1064}), and poly(A)-binding protein 1 (PABP1me2a$^{Arg455/Arg460}$) are bona fide CARM1 targets (Lee and Bedford, 2002; Wang et al., 2016). Given that autophagy is among the pathways that mediate protein degradation during atrophy (Sandri, 2013a), an in depth understanding of CARM1 function during autophagy is warranted (Figure 2).

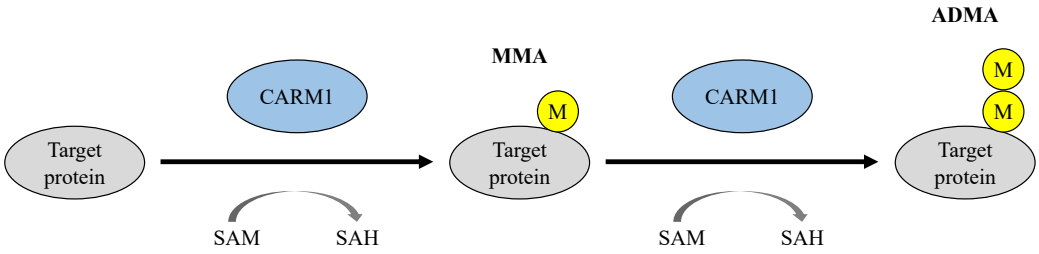

Figure 2. CARM1 methyltransferase activity. CARM1 transfers a methyl group (M) from S-adenosylmethionine (SAM) to arginine residues on target proteins, while also creating the side product S-adenosylhomocysteine (SAH). CARM1 is a type I PRMT that initially generates monomethylarginine (MMA). CARM1 subsequently produces asymmetric dimethylarginine (ADMA), thereby altering the stability, localization, and/or activity of the marked target protein.

Previous work in non-muscle cells revealed that CARM1 is involved in two distinct signaling pathways that positively modulate autophagy. Indeed, these signaling cascades hinge on the methylation of histone and non-histone proteins, respectively. For example, CARM1 methylates histone H3 at arginine 17 (H3R17) and coactivates TFEB to promote the expression of autophagy-related genes (Shin et al., 2016). CARM1 also methylates Pontin chromatin-remodeling factor to facilitate activation of FOXO3-dependent autophagy genes (Yu et al., 2020). In vitro methylation assays confirmed predicted methylation sites of Pontin by CARM1. Upstream of both events, AMPK and SKP2 regulate the stabilization of CARM1. SKP2 is a type of ubiquitin ligase that degrades CARM1 under nutrient-rich conditions (Shin et al., 2016). However, AMPK downregulates SKP2 in response to nutrient stress, and in turn, increases CARM1 stability. Despite these impactful studies, the role of CARM1 during protein degradation remains to be fully

defined. Further investigation is therefore needed to uncover the full molecular mechanism by which CARM1 influences the autophagy-lysosome and ubiquitin-proteasome systems.

Selective inhibitors of CARM1 have recently been identified and will likely serve as useful tools for clarifying the molecular events regulated by CARM1. For instance, TP-064, MS049, and EZM2302 inhibit the methyltransferase activity of CARM1 in vivo with high potency and specificity over other PRMT family proteins (Guccione and Richard, 2019). Interestingly, pharmacological inhibition of CARM1 attenuates tumor growth in murine models of multiple myeloma and acute myeloid leukemia (Drew et al., 2017; Nakayama et al., 2018; Greenblatt et al., 2018). In the future, it will be intriguing to see whether these small molecule inhibitors enter clinical trials and whether their benefits will go beyond treating cancer, perhaps muscle atrophy.

1.3.3 CARM1 in skeletal muscle.

CARM1 is the predominantly expressed PRMT in skeletal muscle (Wang et al., 2012; vanLieshout et al., 2019) and has recently surfaced as an important regulator of skeletal muscle biology. Indeed, previous work suggests that the methyltransferase influences muscle plasticity in rodents and humans (Ljubicic et al., 2012; Stouth et al., 2017; Stouth et al., 2018; vanLieshout et al., 2018; Shen et al., 2018; vanLieshout et al., 2019; vanLieshout and Ljubicic, 2019). Furthermore, various studies showed that CARM1 controls myogenesis during development and regeneration, as well as mediates muscle glycogen metabolism (Chen et al., 2002; Dacwag et al., 2009; Kawabe et al., 2012; Wang et al., 2012; Chang et al., 2018). CARM1 also affects autophagy-lysosome and ubiquitin-proteasome signaling in muscle via a FOXO3-dependent mechanism (Liu et al., 2019). For

example, transient knockdown of CARM1 mitigates denervation-induced muscle atrophy, in part, by downregulating the expression of autophagy and atrophy-related genes. Moreover, elevated CARM1 expression levels following neurogenic muscle disuse are associated with AMPK activation and the initiation of muscle wasting (Stouth et al., 2018). The methyltransferase has been shown to play a direct role in autophagy-lysosome and ubiquitin-proteasome signaling (Kim et al., 2014; Shin et al., 2016; Li et al., 2017; Yu et al., 2020). However, the function of CARM1 in muscle remains to be fully elucidated.

Despite the current limitation in the number of studies investigating the role of CARM1 in muscle, accumulating evidence strongly suggests that this methyltransferase is emerging as a key player in the regulation of muscle homeostasis and plasticity. CARM1 contributes to denervation-induced muscle atrophy by promoting FOXO3 activity (Liu et al., 2019). However, studies have yet to fully explore the molecular mechanism by which CARM1 controls muscle plasticity in response to neurogenic muscle disuse. In addition, there is a knowledge gap pertaining to whether CARM1 function is conserved between muscles and various models of disuse. Although CARM1 is abnormally upregulated in various neuromuscular disorders (Stouth et al., 2017), CARM1 expression and activity has yet to be defined in muscle during food deprivation and sarcopenia. Thus, further studies investing the role of CARM1 during muscle atrophy is warranted to help determine whether altering CARM1 expression and/or activity may offer any therapeutic potential.

1.4 Content of thesis

Skeletal muscle is a highly malleable tissue that perpetually remodels in response to various physiological stimuli. Loss of skeletal mass from disuse occurs frequently in clinical settings such as limb immobilization, bed rest, mechanical ventilation, and spinal cord injury. Prolonged food deprivation, the sarcopenia of aging, cancer cachexia, and neuromuscular disorders can also evoke muscle atrophy. While muscle wasting and weakness remains a widespread issue, there is an incomplete understanding of the mechanisms that drive muscle atrophy, which presents an impediment to developing effective therapeutic strategies to preserve muscle mass under various clinical conditions and chronic diseases.

1.4.1 Purpose and objectives.

Although CARM1 expression and activity are associated with the initiation of the muscle atrophy program (Stouth et al., 2018), and transient knockdown of this methyltransferase attenuates denervation-induced muscle loss (Liu et al., 2019), the regulatory mechanisms by which CARM1 influences muscle mass remains unclear. Thus, the overarching purpose of the current thesis was to examine the role of CARM1 during skeletal muscle atrophy. To develop a more comprehensive understanding of the cellular processes affected by CARM1, we generated CARM1 skeletal muscle-specific knockout (mKO) mice and employed various atrophy-inducing stimuli with distinct molecular signatures. We sought to investigate the impact of CARM1 mKO on the maintenance of skeletal muscle mass under basal conditions, as well as during 1) neurogenic muscle disuse-, 2) fasting-, and 3) the sarcopenia of aging.

1.4.2 Hypotheses.

Previous work has demonstrated that autophagy is indispensable for preserving muscle mass (Masiero et al., 2009) and CARM1 is a crucial component of the autophagy-lysosome signaling pathway (Shin et al., 2016; Yu et al., 2020). Transient knockdown of CARM1 also attenuates skeletal muscle wasting after neurogenic muscle disuse (Liu et al., 2019). The research experiments that comprise this thesis were designed to test the hypotheses that CARM1 is required to maintain muscle mass and that this methyltransferase contributes toward molecular mechanisms responsible for driving 1) denervation-, 2) fasting-, and 3) aging-induced muscle atrophy. Since a common set of protein degradation pathways control the loss of muscle mass for each stimulus (Sandri, 2013a), we initially postulated that skeletal muscle-specific deletion of CARM1 would influence the progression of muscle wasting in response to neurogenic muscle disuse, prolonged food deprivation, and the sarcopenia of aging.

1.5 References

Alway, S. E., Mohamed, J. S., & Myers, M. J. (2017). Mitochondria Initiate and Regulate Sarcopenia. Exercise and sport sciences reviews, 45(2), 58–69.

Andersson, A. M., Olsen, M., Zhernosekov, D., Gaardsvoll, H., Krog, L., Linnemann, D., & Bock, E. (1993). Age-related changes in expression of the neural cell adhesion molecule in skeletal muscle: a comparative study of newborn, adult and aged rats. The Biochemical journal, 290 (Pt 3)(Pt 3), 641–648.

Atherton, P. J., Greenhaff, P. L., Phillips, S. M., Bodine, S. C., Adams, C. M., & Lang, C. H. (2016). Control of skeletal muscle atrophy in response to disuse: clinical/preclinical contentions and fallacies of evidence. American journal of physiology. Endocrinology and metabolism, 311(3), E594–E604.

Bagherniya, M., Butler, A. E., Barreto, G. E., & Sahebkar, A. (2018). The effect of fasting or calorie restriction on autophagy induction: A review of the literature. Ageing research reviews, 47, 183–197.

Bedford, M. T., & Clarke, S. G. (2009). Protein arginine methylation in mammals: who, what, and why. Molecular cell, 33(1), 1–13.

Blanc, R. S., & Richard, S. (2017). Arginine Methylation: The Coming of Age. Molecular cell, 65(1), 8–24.

Bloemberg, D., & Quadrilatero, J. (2012). Rapid determination of myosin heavy chain expression in rat, mouse, and human skeletal muscle using multicolor immunofluorescence analysis. PloS one, 7(4), e35273.

Bodine S. C. (2013). Disuse-induced muscle wasting. The international journal of biochemistry & cell biology, 45(10), 2200–2208.

Bodine, S. C., & Baehr, L. M. (2014). Skeletal muscle atrophy and the E3 ubiquitin ligases MuRF1 and MAFbx/atrogin-1. American journal of physiology. Endocrinology and metabolism, 307(6), E469–E484.

Bodine, S. C., Latres, E., Baumhueter, S., Lai, V. K., Nunez, L., Clarke, B. A., Poueymirou, W. T., Panaro, F. J., Na, E., Dharmarajan, K., Pan, Z. Q., Valenzuela, D. M., DeChiara, T. M., Stitt, T. N., Yancopoulos, G. D., & Glass, D. J. (2001a). Identification of ubiquitin ligases required for skeletal muscle atrophy. Science (New York, N.Y.), 294(5547), 1704–1708.

Bodine, S. C., Stitt, T. N., Gonzalez, M., Kline, W. O., Stover, G. L., Bauerlein, R., Zlotchenko, E., Scrimgeour, A., Lawrence, J. C., Glass, D. J., & Yancopoulos, G. D.

(2001b). Akt/mTOR pathway is a crucial regulator of skeletal muscle hypertrophy and can prevent muscle atrophy in vivo. Nature cell biology, 3(11), 1014–1019.

Börsch, A., Ham, D. J., Mittal, N., Tintignac, L. A., Migliavacca, E., Feige, J. N., Rüegg, M. A., & Zavolan, M. (2021). Molecular and phenotypic analysis of rodent models reveals conserved and species-specific modulators of human sarcopenia. Communications biology, 4(1), 194.

Brack, A. S., Conboy, M. J., Roy, S., Lee, M., Kuo, C. J., Keller, C., & Rando, T. A. (2007). Increased Wnt signaling during aging alters muscle stem cell fate and increases fibrosis. Science (New York, N.Y.), 317(5839), 807–810.

Brocca, L., Cannavino, J., Coletto, L., Biolo, G., Sandri, M., Bottinelli, R., & Pellegrino, M. A. (2012). The time course of the adaptations of human muscle proteome to bed rest and the underlying mechanisms. The Journal of physiology, 590(20), 5211–5230.

Brocca, L., Toniolo, L., Reggiani, C., Bottinelli, R., Sandri, M., & Pellegrino, M. A. (2017). FoxO-dependent atrogenes vary among catabolic conditions and play a key role in muscle atrophy induced by hindlimb suspension. The Journal of physiology, 595(4), 1143–1158.

Brunet, A., Bonni, A., Zigmond, M. J., Lin, M. Z., Juo, P., Hu, L. S., Anderson, M. J., Arden, K. C., Blenis, J., & Greenberg, M. E. (1999). Akt promotes cell survival by phosphorylating and inhibiting a Forkhead transcription factor. Cell, 96(6), 857–868.

Bujak, A. L., Crane, J. D., Lally, J. S., Ford, R. J., Kang, S. J., Rebalka, I. A., Green, A. E., Kemp, B. E., Hawke, T. J., Schertzer, J. D., & Steinberg, G. R. (2015). AMPK activation of muscle autophagy prevents fasting-induced hypoglycemia and myopathy during aging. Cell metabolism, 21(6), 883–890.

Burke, S. K., Fenton, A. I., Konokhova, Y., & Hepple, R. T. (2021). Variation in muscle and neuromuscular junction morphology between atrophy-resistant and atrophy-prone muscles supports failed re-innervation in aging muscle atrophy. Experimental gerontology, 156, 111613. Advance online publication. https://doi.org/10.1016/j.exger.2021.111613

Cannavino, J., Brocca, L., Sandri, M., Bottinelli, R., & Pellegrino, M. A. (2014). PGC1-α over-expression prevents metabolic alterations and soleus muscle atrophy in hindlimb unloaded mice. The Journal of physiology, 592(20), 4575–4589.

Cannavino, J., Brocca, L., Sandri, M., Grassi, B., Bottinelli, R., & Pellegrino, M. A. (2015). The role of alterations in mitochondrial dynamics and PGC-1α over-expression in fast muscle atrophy following hindlimb unloading. The Journal of physiology, 593(8), 1981–1995.

Carnio, S., LoVerso, F., Baraibar, M. A., Longa, E., Khan, M. M., Maffei, M., Reischl, M., Canepari, M., Loefler, S., Kern, H., Blaauw, B., Friguet, B., Bottinelli, R., Rudolf, R., & Sandri, M. (2014). Autophagy impairment in muscle induces neuromuscular junction degeneration and precocious aging. Cell reports, 8(5), 1509–1521.

Carter, H. N., Kim, Y., Erlich, A. T., Zarrin-Khat, D., & Hood, D. A. (2018). Autophagy and mitophagy flux in young and aged skeletal muscle following chronic contractile activity. The Journal of physiology, 596(16), 3567–3584.

Castets, P., Lin, S., Rion, N., Di Fulvio, S., Romanino, K., Guridi, M., Frank, S., Tintignac, L. A., Sinnreich, M., & Rüegg, M. A. (2013). Sustained activation of mTORC1 in skeletal muscle inhibits constitutive and starvation-induced autophagy and causes a severe, late-onset myopathy. Cell metabolism, 17(5), 731–744.

Chabi, B., Ljubicic, V., Menzies, K. J., Huang, J. H., Saleem, A., & Hood, D. A. (2008). Mitochondrial function and apoptotic susceptibility in aging skeletal muscle. Aging cell, 7(1), 2–12.

Chang, N. C., Sincennes, M. C., Chevalier, F. P., Brun, C. E., Lacaria, M., Segalés, J., Muñoz-Cánoves, P., Ming, H., & Rudnicki, M. A. (2018). The Dystrophin Glycoprotein Complex Regulates the Epigenetic Activation of Muscle Stem Cell Commitment. Cell stem cell, 22(5), 755–768.e6.

Chen, S. L., Loffler, K. A., Chen, D., Stallcup, M. R., & Muscat, G. E. (2002). The coactivator-associated arginine methyltransferase is necessary for muscle differentiation: CARM1 coactivates myocyte enhancer factor-2. The Journal of biological chemistry, 277(6), 4324–4333.

Cheng, A., Morsch, M., Murata, Y., Ghazanfari, N., Reddel, S. W., & Phillips, W. D. (2013). Sequence of age-associated changes to the mouse neuromuscular junction and the protective effects of voluntary exercise. PloS one, 8(7), e67970.

Cheng, D., Vemulapalli, V., Lu, Y., Shen, J., Aoyagi, S., Fry, C. J., Yang, Y., Foulds, C. E., Stossi, F., Treviño, L. S., Mancini, M. A., O'Malley, B. W., Walker, C. L., Boyer, T. G., & Bedford, M. T. (2018). CARM1 methylates MED12 to regulate its RNA-binding ability. Life science alliance, 1(5), e201800117.

Cheng, S. W., Fryer, L. G., Carling, D., & Shepherd, P. R. (2004). Thr2446 is a novel mammalian target of rapamycin (mTOR) phosphorylation site regulated by nutrient status. The Journal of biological chemistry, 279(16), 15719–15722.

Cruz-Jentoft, A. J., Bahat, G., Bauer, J., Boirie, Y., Bruyère, O., Cederholm, T., Cooper, C., Landi, F., Rolland, Y., Sayer, A. A., Schneider, S. M., Sieber, C. C., Topinkova, E., Vandewoude, M., Visser, M., Zamboni, M., & Writing Group for the European Working

Group on Sarcopenia in Older People 2 (EWGSOP2), and the Extended Group for EWGSOP2 (2019). Sarcopenia: revised European consensus on definition and diagnosis. Age and ageing, 48(1), 16–31.

Cuthbertson, D., Smith, K., Babraj, J., Leese, G., Waddell, T., Atherton, P., Wackerhage, H., Taylor, P. M., & Rennie, M. J. (2005). Anabolic signaling deficits underlie amino acid resistance of wasting, aging muscle. FASEB journal: official publication of the Federation of American Societies for Experimental Biology, 19(3), 422–424.

Dacwag, C. S., Bedford, M. T., Sif, S., & Imbalzano, A. N. (2009). Distinct protein arginine methyltransferases promote ATP-dependent chromatin remodeling function at different stages of skeletal muscle differentiation. Molecular and cellular biology, 29(7), 1909–1921.

Dahlmann, B., Rutschmann, M., & Reinauer, H. (1986). Effect of starvation or treatment with corticosterone on the amount of easily releasable myofilaments in rat skeletal muscles. The Biochemical journal, 234(3), 659–664.

de Boer, M. D., Seynnes, O. R., di Prampero, P. E., Pisot, R., Mekjavić, I. B., Biolo, G., & Narici, M. V. (2008). Effect of 5 weeks horizontal bed rest on human muscle thickness and architecture of weight bearing and non-weight bearing muscles. European journal of applied physiology, 104(2), 401–407.

Dhar, S., Vemulapalli, V., Patananan, A. N., Huang, G. L., Di Lorenzo, A., Richard, S., Comb, M. J., Guo, A., Clarke, S. G., & Bedford, M. T. (2013). Loss of the major Type I arginine methyltransferase PRMT1 causes substrate scavenging by other PRMTs. Scientific reports, 3, 1311.

Drew, A. E., Moradei, O., Jacques, S. L., Rioux, N., Boriack-Sjodin, A. P., Allain, C., Scott, M. P., Jin, L., Raimondi, A., Handler, J. L., Ott, H. M., Kruger, R. G., McCabe, M. T., Sneeringer, C., Riera, T., Shapiro, G., Waters, N. J., Mitchell, L. H., Duncan, K. W., Moyer, M. P., … Ribich, S. A. (2017). Identification of a CARM1 Inhibitor with Potent In Vitro and In Vivo Activity in Preclinical Models of Multiple Myeloma. Scientific reports, 7(1), 17993.

Edström, E., Altun, M., Hägglund, M., & Ulfhake, B. (2006). Atrogin-1/MAFbx and MuRF1 are downregulated in aging-related loss of skeletal muscle. The journals of gerontology. Series A, Biological sciences and medical sciences, 61(7), 663–674.

Egan, B., & Zierath, J. R. (2013). Exercise metabolism and the molecular regulation of skeletal muscle adaptation. Cell metabolism, 17(2), 162–184.

Egan, D. F., Shackelford, D. B., Mihaylova, M. M., Gelino, S., Kohnz, R. A., Mair, W., Vasquez, D. S., Joshi, A., Gwinn, D. M., Taylor, R., Asara, J. M., Fitzpatrick, J., Dillin, A., Viollet, B., Kundu, M., Hansen, M., & Shaw, R. J. (2011). Phosphorylation of ULK1

(hATG1) by AMP-activated protein kinase connects energy sensing to mitophagy. Science (New York, N.Y.), 331(6016), 456–461.

Egawa, T., Goto, A., Ohno, Y., Yokoyama, S., Ikuta, A., Suzuki, M., Sugiura, T., Ohira, Y., Yoshioka, T., Hayashi, T., & Goto, K. (2015). Involvement of AMPK in regulating slow-twitch muscle atrophy during hindlimb unloading in mice. American journal of physiology. Endocrinology and metabolism, 309(7), E651–E662.

Felig, P., Pozefsky, T., Marliss, E., & Cahill, G. F., Jr (1970). Alanine: key role in gluconeogenesis. Science (New York, N.Y.), 167(3920), 1003–1004.

Finn, P. F., & Dice, J. F. (2006). Proteolytic and lipolytic responses to starvation. Nutrition (Burbank, Los Angeles County, Calif.), 22(7-8), 830–844.

Fitts, R. H., Trappe, S. W., Costill, D. L., Gallagher, P. M., Creer, A. C., Colloton, P. A., Peters, J. R., Romatowski, J. G., Bain, J. L., & Riley, D. A. (2010). Prolonged space flight-induced alterations in the structure and function of human skeletal muscle fibres. The Journal of physiology, 588(Pt 18), 3567–3592.

Fry, C. S., Drummond, M. J., Glynn, E. L., Dickinson, J. M., Gundermann, D. M., Timmerman, K. L., Walker, D. K., Dhanani, S., Volpi, E., & Rasmussen, B. B. (2011). Aging impairs contraction-induced human skeletal muscle mTORC1 signaling and protein synthesis. Skeletal muscle, 1(1), 11.

Fullerton, M. D., Galic, S., Marcinko, K., Sikkema, S., Pulinilkunnil, T., Chen, Z. P., O'Neill, H. M., Ford, R. J., Palanivel, R., O'Brien, M., Hardie, D. G., Macaulay, S. L., Schertzer, J. D., Dyck, J. R., van Denderen, B. J., Kemp, B. E., & Steinberg, G. R. (2013). Single phosphorylation sites in Acc1 and Acc2 regulate lipid homeostasis and the insulin-sensitizing effects of metformin. Nature medicine, 19(12), 1649–1654.

Fulton, M. D., Brown, T., & Zheng, Y. G. (2019). The Biological Axis of Protein Arginine Methylation and Asymmetric Dimethylarginine. International journal of molecular sciences, 20(13), 3322.

Garcia, D., & Shaw, R. J. (2017). AMPK: Mechanisms of Cellular Energy Sensing and Restoration of Metabolic Balance. Molecular cell, 66(6), 789–800.

Greenblatt, S. M., Man, N., Hamard, P. J., Asai, T., Karl, D., Martinez, C., Bilbao, D., Stathias, V., Jermakowicz, A. M., Duffort, S., Tadi, M., Blumenthal, E., Newman, S., Vu, L., Xu, Y., Liu, F., Schurer, S. C., McCabe, M. T., Kruger, R. G., Xu, M., … Nimer, S. D. (2018). CARM1 Is Essential for Myeloid Leukemogenesis but Dispensable for Normal Hematopoiesis. Cancer cell, 33(6), 1111–1127.e5.

Grevendonk, L., Connell, N. J., McCrum, C., Fealy, C. E., Bilet, L., Bruls, Y., Mevenkamp, J., Schrauwen-Hinderling, V. B., Jörgensen, J. A., Moonen-Kornips, E., Schaart, G., Havekes, B., de Vogel-van den Bosch, J., Bragt, M., Meijer, K., Schrauwen, P., & Hoeks, J. (2021). Impact of aging and exercise on skeletal muscle mitochondrial capacity, energy metabolism, and physical function. Nature communications, 12(1), 4773.

Guccione, E., & Richard, S. (2019). The regulation, functions and clinical relevance of arginine methylation. Nature reviews. Molecular cell biology, 20(10), 642–657.

Guo, Y., Meng, J., Tang, Y., Wang, T., Wei, B., Feng, R., Gong, B., Wang, H., Ji, G., & Lu, Z. (2016). AMP-activated kinase α2 deficiency protects mice from denervation-induced skeletal muscle atrophy. Archives of biochemistry and biophysics, 600, 56–60.

Ham, D. J., Börsch, A., Lin, S., Thürkauf, M., Weihrauch, M., Reinhard, J. R., Delezie, J., Battilana, F., Wang, X., Kaiser, M. S., Guridi, M., Sinnreich, M., Rich, M. M., Mittal, N., Tintignac, L. A., Handschin, C., Zavolan, M., & Rüegg, M. A. (2020). The neuromuscular junction is a focal point of mTORC1 signaling in sarcopenia. Nature communications, 11(1), 4510.

Herzig, S., & Shaw, R. J. (2018). AMPK: guardian of metabolism and mitochondrial homeostasis. Nature reviews. Molecular cell biology, 19(2), 121–135.

Hitachi, K., Nakatani, M., Kiyofuji, Y., Inagaki, H., Kurahashi, H., & Tsuchida, K. (2021). An Analysis of Differentially Expressed Coding and Long Non-Coding RNAs in Multiple Models of Skeletal Muscle Atrophy. International journal of molecular sciences, 22(5), 2558.

Hood, D. A., Memme, J. M., Oliveira, A. N., & Triolo, M. (2019). Maintenance of Skeletal Muscle Mitochondria in Health, Exercise, and Aging. Annual review of physiology, 81, 19–41.

Hughes, D. C., Marcotte, G. R., Marshall, A. G., West, D., Baehr, L. M., Wallace, M. A., Saleh, P. M., Bodine, S. C., & Baar, K. (2017). Age-related Differences in Dystrophin: Impact on Force Transfer Proteins, Membrane Integrity, and Neuromuscular Junction Stability. The journals of gerontology. Series A, Biological sciences and medical sciences, 72(5), 640–648.

Hughes, V. A., Frontera, W. R., Wood, M., Evans, W. J., Dallal, G. E., Roubenoff, R., & Fiatarone Singh, M. A. (2001). Longitudinal muscle strength changes in older adults: influence of muscle mass, physical activity, and health. The journals of gerontology. Series A, Biological sciences and medical sciences, 56(5), B209–B217.

Inoki, K., Zhu, T., & Guan, K. L. (2003). TSC2 mediates cellular energy response to control cell growth and survival. Cell, 115(5), 577–590.

Jackson, S. J., Andrews, N., Ball, D., Bellantuono, I., Gray, J., Hachoumi, L., Holmes, A., Latcham, J., Petrie, A., Potter, P., Rice, A., Ritchie, A., Stewart, M., Strepka, C., Yeoman, M., & Chapman, K. (2017). Does age matter? The impact of rodent age on study outcomes. Laboratory animals, 51(2), 160–169.

Janssen, I., Heymsfield, S. B., Wang, Z. M., & Ross, R. (2000). Skeletal muscle mass and distribution in 468 men and women aged 18-88 yr. Journal of applied physiology (Bethesda, Md.: 1985), 89(1), 81–88.

Janssen, I., Shepard, D. S., Katzmarzyk, P. T., & Roubenoff, R. (2004). The healthcare costs of sarcopenia in the United States. Journal of the American Geriatrics Society, 52(1), 80–85.

Jensen, J., Rustad, P. I., Kolnes, A. J., & Lai, Y. C. (2011). The role of skeletal muscle glycogen breakdown for regulation of insulin sensitivity by exercise. Frontiers in physiology, 2, 112.

Joanisse, S., Nederveen, J. P., Baker, J. M., Snijders, T., Iacono, C., & Parise, G. (2016). Exercise conditioning in old mice improves skeletal muscle regeneration. FASEB journal: official publication of the Federation of American Societies for Experimental Biology, 30(9), 3256–3268.

Jones, R. A., Harrison, C., Eaton, S. L., Llavero Hurtado, M., Graham, L. C., Alkhammash, L., Oladiran, O. A., Gale, A., Lamont, D. J., Simpson, H., Simmen, M. W., Soeller, C., Wishart, T. M., & Gillingwater, T. H. (2017). Cellular and Molecular Anatomy of the Human Neuromuscular Junction. Cell reports, 21(9), 2348–2356.

Kawabe, Y., Wang, Y. X., McKinnell, I. W., Bedford, M. T., & Rudnicki, M. A. (2012). Carm1 regulates Pax7 transcriptional activity through MLL1/2 recruitment during asymmetric satellite stem cell divisions. Cell stem cell, 11(3), 333–345.

Kim, D., Lim, S., Park, M., Choi, J., Kim, J., Han, H., Yoon, K., Kim, K., Lim, J., & Park, S. (2014). Ubiquitination-dependent CARM1 degradation facilitates Notch1-mediated podocyte apoptosis in diabetic nephropathy. Cellular signalling, 26(9), 1774–1782.

Kim, J., Kim, Y. C., Fang, C., Russell, R. C., Kim, J. H., Fan, W., Liu, R., Zhong, Q., & Guan, K. L. (2013). Differential regulation of distinct Vps34 complexes by AMPK in nutrient stress and autophagy. Cell, 152(1-2), 290–303.

Kjøbsted, R., Hingst, J. R., Fentz, J., Foretz, M., Sanz, M. N., Pehmøller, C., Shum, M., Marette, A., Mounier, R., Treebak, J. T., Wojtaszewski, J., Viollet, B., & Lantier, L. (2018). AMPK in skeletal muscle function and metabolism. FASEB journal: official publication of the Federation of American Societies for Experimental Biology, 32(4), 1741–1777.

Klionsky, D. J., Abdel-Aziz, A. K., Abdelfatah, S., Abdellatif, M., Abdoli, A., Abel, S., Abeliovich, H., Abildgaard, M. H., Abudu, Y. P., Acevedo-Arozena, A., Adamopoulos, I. E., Adeli, K., Adolph, T. E., Adornetto, A., Aflaki, E., Agam, G., Agarwal, A., Aggarwal, B. B., Agnello, M., Agostinis, P., … Tong, C. K. (2021). Guidelines for the use and interpretation of assays for monitoring autophagy (4th edition)1. Autophagy, 17(1), 1–382.

Kunkel, S. D., Suneja, M., Ebert, S. M., Bongers, K. S., Fox, D. K., Malmberg, S. E., Alipour, F., Shields, R. K., & Adams, C. M. (2011). mRNA expression signatures of human skeletal muscle atrophy identify a natural compound that increases muscle mass. Cell metabolism, 13(6), 627–638.

Lanza, I. R., Short, D. K., Short, K. R., Raghavakaimal, S., Basu, R., Joyner, M. J., McConnell, J. P., & Nair, K. S. (2008). Endurance exercise as a countermeasure for aging. Diabetes, 57(11), 2933–2942.

Larsen, S. C., Sylvestersen, K. B., Mund, A., Lyon, D., Mullari, M., Madsen, M. V., Daniel, J. A., Jensen, L. J., & Nielsen, M. L. (2016). Proteome-wide analysis of arginine monomethylation reveals widespread occurrence in human cells. Science signaling, 9(443), rs9.

Larsen, A. E., Tunstall, R. J., Carey, K. A., Nicholas, G., Kambadur, R., Crowe, T. C., & Cameron-Smith, D. (2006). Actions of short-term fasting on human skeletal muscle myogenic and atrogenic gene expression. Annals of nutrition & metabolism, 50(5), 476–481.

Larsson, L., Grimby, G., & Karlsson, J. (1979). Muscle strength and speed of movement in relation to age and muscle morphology. Journal of applied physiology: respiratory, environmental and exercise physiology, 46(3), 451–456.

Leduc-Gaudet, J. P., Picard, M., St-Jean Pelletier, F., Sgarioto, N., Auger, M. J., Vallée, J., Robitaille, R., St-Pierre, D. H., & Gouspillou, G. (2015). Mitochondrial morphology is altered in atrophied skeletal muscle of aged mice. Oncotarget, 6(20), 17923–17937.

Lee, J., & Bedford, M. T. (2002). PABP1 identified as an arginine methyltransferase substrate using high-density protein arrays. EMBO reports, 3(3), 268–273.

Léger, B., Derave, W., De Bock, K., Hespel, P., & Russell, A. P. (2008). Human sarcopenia reveals an increase in SOCS-3 and myostatin and a reduced efficiency of Akt phosphorylation. Rejuvenation research, 11(1), 163–175B.

Lexell, J., & Taylor, C. C. (1991). Variability in muscle fibre areas in whole human quadriceps muscle: effects of increasing age. Journal of anatomy, 174, 239–249.

Lexell, J., Taylor, C. C., & Sjöström, M. (1988). What is the cause of the ageing atrophy? Total number, size and proportion of different fiber types studied in whole vastus lateralis muscle from 15- to 83-year-old men. Journal of the neurological sciences, 84(2-3), 275–294.

Li, C., Yu, L., Xue, H., Yang, Z., Yin, Y., Zhang, B., Chen, M., & Ma, H. (2017). Nuclear AMPK regulated CARM1 stabilization impacts autophagy in aged heart. Biochemical and biophysical research communications, 486(2), 398–405.

Li, J. B., & Goldberg, A. L. (1976). Effects of food deprivation on protein synthesis and degradation in rat skeletal muscles. The American journal of physiology, 231(2), 441–448.

Li, Y., Lee, Y. i., & Thompson, W. J. (2011). Changes in aging mouse neuromuscular junctions are explained by degeneration and regeneration of muscle fiber segments at the synapse. The Journal of neuroscience: the official journal of the Society for Neuroscience, 31(42), 14910–14919.

Lira, V. A., Benton, C. R., Yan, Z., & Bonen, A. (2010). PGC-1alpha regulation by exercise training and its influences on muscle function and insulin sensitivity. American journal of physiology. Endocrinology and metabolism, 299(2), E145–E161.

Liu, Y., Li, J., Shang, Y., Guo, Y., & Li, Z. (2019). CARM1 contributes to skeletal muscle wasting by mediating FoxO3 activity and promoting myofiber autophagy. Experimental cell research, 374(1), 198–209.

Ljubicic, V., Burt, M., & Jasmin, B. J. (2014). The therapeutic potential of skeletal muscle plasticity in Duchenne muscular dystrophy: phenotypic modifiers as pharmacologic targets. FASEB journal: official publication of the Federation of American Societies for Experimental Biology, 28(2), 548–568.

Ljubicic, V., Khogali, S., Renaud, J. M., & Jasmin, B. J. (2012). Chronic AMPK stimulation attenuates adaptive signaling in dystrophic skeletal muscle. American journal of physiology. Cell physiology, 302(1), C110–C121.

Mahdy M. (2019). Skeletal muscle fibrosis: an overview. Cell and tissue research, 375(3), 575–588.

Manzanares, G., Brito-da-Silva, G., & Gandra, P. G. (2018). Voluntary wheel running: patterns and physiological effects in mice. Brazilian journal of medical and biological research = Revista brasileira de pesquisas medicas e biologicas, 52(1), e7830.

Masiero, E., Agatea, L., Mammucari, C., Blaauw, B., Loro, E., Komatsu, M., Metzger, D., Reggiani, C., Schiaffino, S., & Sandri, M. (2009). Autophagy is required to maintain muscle mass. Cell metabolism, 10(6), 507–515.

Milan, G., Romanello, V., Pescatore, F., Armani, A., Paik, J. H., Frasson, L., Seydel, A., Zhao, J., Abraham, R., Goldberg, A. L., Blaauw, B., DePinho, R. A., & Sandri, M. (2015). Regulation of autophagy and the ubiquitin-proteasome system by the FoxO transcriptional network during muscle atrophy. Nature communications, 6, 6670.

Mizushima, N., Yamamoto, A., Matsui, M., Yoshimori, T., & Ohsumi, Y. (2004). In vivo analysis of autophagy in response to nutrient starvation using transgenic mice expressing a fluorescent autophagosome marker. Molecular biology of the cell, 15(3), 1101–1111.

Mizushima, N., Yoshimori, T., & Levine, B. (2010). Methods in mammalian autophagy research. Cell, 140(3), 313–326.

Mounier, R., Théret, M., Lantier, L., Foretz, M., & Viollet, B. (2015). Expanding roles for AMPK in skeletal muscle plasticity. Trends in endocrinology and metabolism: TEM, 26(6), 275–286.

Nakayama, K., Szewczyk, M. M., Dela Sena, C., Wu, H., Dong, A., Zeng, H., Li, F., de Freitas, R. F., Eram, M. S., Schapira, M., Baba, Y., Kunitomo, M., Cary, D. R., Tawada, M., Ohashi, A., Imaeda, Y., Saikatendu, K. S., Grimshaw, C. E., Vedadi, M., Arrowsmith, C. H., … Brown, P. J. (2018). TP-064, a potent and selective small molecule inhibitor of PRMT4 for multiple myeloma. Oncotarget, 9(26), 18480–18493.

Nilwik, R., Snijders, T., Leenders, M., Groen, B. B., van Kranenburg, J., Verdijk, L. B., & van Loon, L. J. (2013). The decline in skeletal muscle mass with aging is mainly attributed to a reduction in type II muscle fiber size. Experimental gerontology, 48(5), 492–498.

Norman, K., & Otten, L. (2019). Financial impact of sarcopenia or low muscle mass - A short review. Clinical nutrition (Edinburgh, Scotland), 38(4), 1489–1495.

O'Neill, H. M., Lally, J. S., Galic, S., Thomas, M., Azizi, P. D., Fullerton, M. D., Smith, B. K., Pulinilkunnil, T., Chen, Z., Samaan, M. C., Jorgensen, S. B., Dyck, J. R., Holloway, G. P., Hawke, T. J., van Denderen, B. J., Kemp, B. E., & Steinberg, G. R. (2014). AMPK phosphorylation of ACC2 is required for skeletal muscle fatty acid oxidation and insulin sensitivity in mice. Diabetologia, 57(8), 1693–1702.

Oda K. (1984). Age changes of motor innervation and acetylcholine receptor distribution on human skeletal muscle fibres. Journal of the neurological sciences, 66(2-3), 327–338.

Ogata, T., Oishi, Y., Higuchi, M., & Muraoka, I. (2010). Fasting-related autophagic response in slow- and fast-twitch skeletal muscle. Biochemical and biophysical research communications, 394(1), 136–140.

Paquette, M., El-Houjeiri, L., C Zirden, L., Puustinen, P., Blanchette, P., Jeong, H., Dejgaard, K., Siegel, P. M., & Pause, A. (2021). AMPK-dependent phosphorylation is required for transcriptional activation of TFEB and TFE3. Autophagy, 1–19. Advance online publication.

Perlman R. L. (2016). Mouse models of human disease: An evolutionary perspective. Evolution, medicine, and public health, 2016(1), 170–176.

Phillips, S. M., Glover, E. I., & Rennie, M. J. (2009). Alterations of protein turnover underlying disuse atrophy in human skeletal muscle. Journal of applied physiology (Bethesda, Md. : 1985), 107(3), 645–654.

Qaisar, R., Bhaskaran, S., & Van Remmen, H. (2016). Muscle fiber type diversification during exercise and regeneration. Free radical biology & medicine, 98, 56–67.

Reznick, R. M., Zong, H., Li, J., Morino, K., Moore, I. K., Yu, H. J., Liu, Z. X., Dong, J., Mustard, K. J., Hawley, S. A., Befroy, D., Pypaert, M., Hardie, D. G., Young, L. H., & Shulman, G. I. (2007). Aging-associated reductions in AMP-activated protein kinase activity and mitochondrial biogenesis. Cell metabolism, 5(2), 151–156.

Roy, R. R., Zhong, H., Siengthai, B., & Edgerton, V. R. (2005). Activity-dependent influences are greater for fibers in rat medial gastrocnemius than tibialis anterior muscle. Muscle & nerve, 32(4), 473–482.

Sacheck, J. M., Hyatt, J. P., Raffaello, A., Jagoe, R. T., Roy, R. R., Edgerton, V. R., Lecker, S. H., & Goldberg, A. L. (2007). Rapid disuse and denervation atrophy involve transcriptional changes similar to those of muscle wasting during systemic diseases. FASEB journal: official publication of the Federation of American Societies for Experimental Biology, 21(1), 140–155.

Salminen, A., & Kaarniranta, K. (2012). AMP-activated protein kinase (AMPK) controls the aging process via an integrated signaling network. Ageing research reviews, 11(2), 230–241.

Sanchez, A. M., Candau, R. B., & Bernardi, H. (2014). FoxO transcription factors: their roles in the maintenance of skeletal muscle homeostasis. Cellular and molecular life sciences: CMLS, 71(9), 1657–1671.

Sandri M. (2013a). Protein breakdown in muscle wasting: role of autophagy-lysosome and ubiquitin-proteasome. The international journal of biochemistry & cell biology, 45(10), 2121–2129.

Sandri, M., Barberi, L., Bijlsma, A. Y., Blaauw, B., Dyar, K. A., Milan, G., Mammucari, C., Meskers, C. G., Pallafacchina, G., Paoli, A., Pion, D., Roceri, M., Romanello, V.,

Serrano, A. L., Toniolo, L., Larsson, L., Maier, A. B., Muñoz-Cánoves, P., Musarò, A., Pende, M., … Schiaffino, S. (2013b). Signalling pathways regulating muscle mass in ageing skeletal muscle: the role of the IGF1-Akt-mTOR-FoxO pathway. Biogerontology, 14(3), 303–323.

Sandri, M., Lin, J., Handschin, C., Yang, W., Arany, Z. P., Lecker, S. H., Goldberg, A. L., & Spiegelman, B. M. (2006). PGC-1alpha protects skeletal muscle from atrophy by suppressing FoxO3 action and atrophy-specific gene transcription. Proceedings of the National Academy of Sciences of the United States of America, 103(44), 16260–16265.

Shen, N. Y., Ng, S. Y., Toepp, S. L., & Ljubicic, V. (2018). Protein arginine methyltransferase expression and activity during myogenesis. Bioscience reports, 38(1), BSR20171533.

Shenkman, B. S., Turtikova, O. V., Nemirovskaya, T. L., & Grigoriev, A. I. (2010). Skeletal muscle activity and the fate of myonuclei. Acta naturae, 2(2), 59–66.

Shin, H. J., Kim, H., Oh, S., Lee, J. G., Kee, M., Ko, H. J., Kweon, M. N., Won, K. J., & Baek, S. H. (2016). AMPK-SKP2-CARM1 signalling cascade in transcriptional regulation of autophagy. Nature, 534(7608), 553–557.

Soendenbroe, C., Bechshøft, C., Heisterberg, M. F., Jensen, S. M., Bomme, E., Schjerling, P., Karlsen, A., Kjaer, M., Andersen, J. L., & Mackey, A. L. (2020). Key Components of Human Myofibre Denervation and Neuromuscular Junction Stability are Modulated by Age and Exercise. Cells, 9(4), 893.

Spector, S. A., Simard, C. P., Fournier, M., Sternlicht, E., & Edgerton, V. R. (1982). Architectural alterations of rat hind-limb skeletal muscles immobilized at different lengths. Experimental neurology, 76(1), 94–110.

St-Jean-Pelletier, F., Pion, C. H., Leduc-Gaudet, J. P., Sgarioto, N., Zovilé, I., Barbat-Artigas, S., Reynaud, O., Alkaterji, F., Lemieux, F. C., Grenon, A., Gaudreau, P., Hepple, R. T., Chevalier, S., Belanger, M., Morais, J. A., Aubertin-Leheudre, M., & Gouspillou, G. (2017). The impact of ageing, physical activity, and pre-frailty on skeletal muscle phenotype, mitochondrial content, and intramyocellular lipids in men. Journal of cachexia, sarcopenia and muscle, 8(2), 213–228.

Stark, D. A., Coffey, N. J., Pancoast, H. R., Arnold, L. L., Walker, J. P., Vallée, J., Robitaille, R., Garcia, M. L., & Cornelison, D. D. (2015). Ephrin-A3 promotes and maintains slow muscle fiber identity during postnatal development and reinnervation. The Journal of cell biology, 211(5), 1077–1091.

Statistics Canada. (2016). Canadian Demographics at a Glance Second edition. (Catalogue no. 91-003-X). Retrieved from Statistics Canada: https://www150.statcan.gc.ca/n1/pub/91-003-x/91-003-x2014001-eng.htm

Steinberg, G. R., & Carling, D. (2019). AMP-activated protein kinase: the current landscape for drug development. Nature reviews. Drug discovery, 18(7), 527–551.

Stouth, D. W., Manta, A., & Ljubicic, V. (2018). Protein arginine methyltransferase expression, localization, and activity during disuse-induced skeletal muscle plasticity. American journal of physiology. Cell physiology, 314(2), C177–C190.

Stouth, D. W., vanLieshout, T. L., Shen, N. Y., & Ljubicic, V. (2017). Regulation of Skeletal Muscle Plasticity by Protein Arginine Methyltransferases and Their Potential Roles in Neuromuscular Disorders. Frontiers in physiology, 8, 870.

Taillandier, D., Combaret, L., Pouch, M. N., Samuels, S. E., Béchet, D., & Attaix, D. (2004). The role of ubiquitin-proteasome-dependent proteolysis in the remodelling of skeletal muscle. The Proceedings of the Nutrition Society, 63(2), 357–361.

Tintignac, L. A., Brenner, H. R., & Rüegg, M. A. (2015). Mechanisms Regulating Neuromuscular Junction Development and Function and Causes of Muscle Wasting. Physiological reviews, 95(3), 809–852.

Toyama, E. Q., Herzig, S., Courchet, J., Lewis, T. L., Jr, Losón, O. C., Hellberg, K., Young, N. P., Chen, H., Polleux, F., Chan, D. C., & Shaw, R. J. (2016). Metabolism. AMP-activated protein kinase mediates mitochondrial fission in response to energy stress. Science (New York, N.Y.), 351(6270), 275–281.

Triolo, M., & Hood, D. A. (2021). Manifestations of Age on Autophagy, Mitophagy and Lysosomes in Skeletal Muscle. Cells, 10(5), 1054.

Vainshtein, A., Desjardins, E. M., Armani, A., Sandri, M., & Hood, D. A. (2015). PGC-1α modulates denervation-induced mitophagy in skeletal muscle. Skeletal muscle, 5, 9.

Valdez, G., Tapia, J. C., Kang, H., Clemenson, G. D., Jr, Gage, F. H., Lichtman, J. W., & Sanes, J. R. (2010). Attenuation of age-related changes in mouse neuromuscular synapses by caloric restriction and exercise. Proceedings of the National Academy of Sciences of the United States of America, 107(33), 14863–14868.

vanLieshout, T. L., & Ljubicic, V. (2019). The emergence of protein arginine methyltransferases in skeletal muscle and metabolic disease. American journal of physiology. Endocrinology and metabolism, 317(6), E1070–E1080.

vanLieshout, T. L., Bonafiglia, J. T., Gurd, B. J., & Ljubicic, V. (2019). Protein arginine methyltransferase biology in humans during acute and chronic skeletal muscle plasticity. Journal of applied physiology (Bethesda, Md. : 1985), 127(3), 867–880.

Vanlieshout, T. L., Stouth, D. W., Tajik, T., & Ljubicic, V. (2018). Exercise-induced Protein Arginine Methyltransferase Expression in Skeletal Muscle. Medicine and science in sports and exercise, 50(3), 447–457.

Vendelbo, M. H., Møller, A. B., Christensen, B., Nellemann, B., Clasen, B. F., Nair, K. S., Jørgensen, J. O., Jessen, N., & Møller, N. (2014). Fasting increases human skeletal muscle net phenylalanine release and this is associated with decreased mTOR signaling. PloS one, 9(7), e102031.

Vermaelen, M., Marini, J. F., Chopard, A., Benyamin, Y., Mercier, J., & Astier, C. (2005). Ubiquitin targeting of rat muscle proteins during short periods of unloading. Acta physiologica Scandinavica, 185(1), 33–40.

Vichaiwong, K., Purohit, S., An, D., Toyoda, T., Jessen, N., Hirshman, M. F., & Goodyear, L. J. (2010). Contraction regulates site-specific phosphorylation of TBC1D1 in skeletal muscle. The Biochemical journal, 431(2), 311–320.

Wang, S. C., Dowhan, D. H., Eriksson, N. A., & Muscat, G. E. (2012). CARM1/PRMT4 is necessary for the glycogen gene expression programme in skeletal muscle cells. The Biochemical journal, 444(2), 323–331.

Wang, J., Wang, F., Zhang, P., Liu, H., He, J., Zhang, C., Fan, M., & Chen, X. (2017). PGC-1α over-expression suppresses the skeletal muscle atrophy and myofiber-type composition during hindlimb unloading. Bioscience, biotechnology, and biochemistry, 81(3), 500–513.

Wang, L., Zhao, Z., Meyer, M. B., Saha, S., Yu, M., Guo, A., Wisinski, K. B., Huang, W., Cai, W., Pike, J. W., Yuan, M., Ahlquist, P., & Xu, W. (2016). CARM1 Methylates Chromatin Remodeling Factor BAF155 to Enhance Tumor Progression and Metastasis. Cancer cell, 30(1), 179–180.

Wang, Y., & Pessin, J. E. (2013). Mechanisms for fiber-type specificity of skeletal muscle atrophy. Current opinion in clinical nutrition and metabolic care, 16(3), 243–250.

Wokke, J. H., Jennekens, F. G., van den Oord, C. J., Veldman, H., Smit, L. M., & Leppink, G. J. (1990). Morphological changes in the human end plate with age. Journal of the neurological sciences, 95(3), 291–310.

Yadav, N., Lee, J., Kim, J., Shen, J., Hu, M. C., Aldaz, C. M., & Bedford, M. T. (2003). Specific protein methylation defects and gene expression perturbations in coactivator-

associated arginine methyltransferase 1-deficient mice. Proceedings of the National Academy of Sciences of the United States of America, 100(11), 6464–6468.

Yanai, S., & Endo, S. (2021). Functional Aging in Male C57BL/6J Mice Across the Life-Span: A Systematic Behavioral Analysis of Motor, Emotional, and Memory Function to Define an Aging Phenotype. Frontiers in aging neuroscience, 13, 697621.

Yang, Y., & Bedford, M. T. (2013). Protein arginine methyltransferases and cancer. Nature reviews. Cancer, 13(1), 37–50.

Yasuda, N., Glover, E. I., Phillips, S. M., Isfort, R. J., & Tarnopolsky, M. A. (2005). Sex-based differences in skeletal muscle function and morphology with short-term limb immobilization. Journal of applied physiology (Bethesda, Md.: 1985), 99(3), 1085–1092.

Yu, Y. S., Shin, H. R., Kim, D., Baek, S. A., Choi, S. A., Ahn, H., Shamim, A., Kim, J., Kim, I. S., Kim, K. K., Won, K. J., & Baek, S. H. (2020). Pontin arginine methylation by CARM1 is crucial for epigenetic regulation of autophagy. Nature communications, 11(1), 6297.

Chapter 2:

CARM1 regulates AMPK signaling in skeletal muscle

Published in *iScience. 2020 Nov 2;23(11):101755.*

iScience

CellPress
OPEN ACCESS

Article

CARM1 Regulates AMPK Signaling in Skeletal Muscle

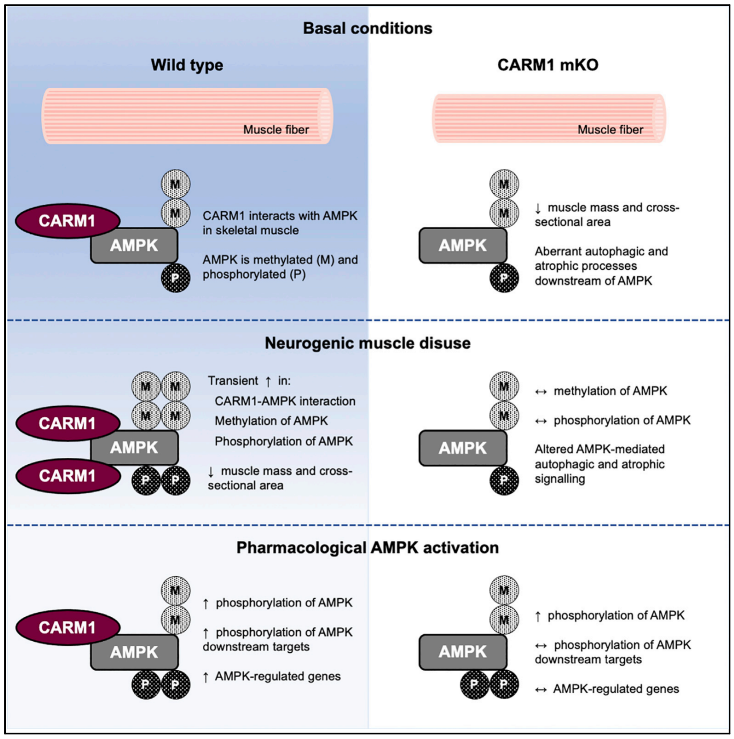

Derek W. Stouth, Tiffany L. vanLieshout, Sean Y. Ng, Erin K. Webb, Alexander Manta, Zachary Moll, Vladimir Ljubicic

ljubicic@mcmaster.ca

HIGHLIGHTS

Role of the arginine methyltransferase CARM1 in muscle biology remains undefined

Skeletal muscle-specific removal of CARM1 alters autophagic and atrophic processes

CARM1 methylates AMPK and mediates AMPK signaling during neurogenic muscle disuse

Targeted pharmacological AMPK stimulation is impacted by CARM1 in skeletal muscle

Stouth et al., iScience 23, 101755
November 20, 2020
https://doi.org/10.1016/j.isci.2020.101755

iScience

CellPress
OPEN ACCESS

Article

CARM1 Regulates AMPK Signaling in Skeletal Muscle

Derek W. Stouth,[1] Tiffany L. vanLieshout,[1] Sean Y. Ng,[1] Erin K. Webb,[1] Alexander Manta,[1] Zachary Moll,[1] and Vladimir Ljubicic[1,2,*]

SUMMARY

Coactivator-associated arginine methyltransferase 1 (CARM1) is an emerging mediator of skeletal muscle plasticity. We employed genetic, physiologic, and pharmacologic approaches to determine whether CARM1 regulates the master neuromuscular phenotypic modifier AMP-activated protein kinase (AMPK). CARM1 skeletal muscle-specific knockout (mKO) mice displayed reduced muscle mass and dysregulated autophagic and atrophic processes downstream of AMPK. We observed altered interactions between CARM1 and AMPK and its network, including forkhead box protein O1, during muscle disuse. CARM1 methylated AMPK during the early stages of muscle inactivity, whereas CARM1 mKO mitigated progression of denervation-induced atrophy and was accompanied by attenuated phosphorylation of AMPK targets such as unc-51 like autophagy-activating kinase 1^{Ser555}. Lower acetyl-coenzyme A corboxylase^{Ser79} phosphorylation, as well as reduced peroxisome proliferator-activated receptor-γ coactivator-1α, was also observed in mKO animals following acute administration of the direct AMPK activator MK-8722. Our study suggests that targeting CARM1-AMPK interplay may have broad impacts on neuromuscular health and disease.

INTRODUCTION

Coactivator-associated arginine methyltransferase 1 (CARM1) belongs to a family of enzymes known as protein arginine methyltransferases (PRMTs) that catalyze the methylation of arginine residues on target proteins, thereby altering intracellular processes (Bedford and Clarke, 2009; Yang and Bedford, 2013; Guccione and Richard, 2019; Fulton et al., 2019). All nine PRMTs synthesize monomethylarginine (MMA), whereas type I (i.e., PRMT1, PRMT2, PRMT3, CARM1, PRMT6, PRMT8) and type II (i.e., PRMT5, PRMT9) PRMTs deposit asymmetric dimethylarginine (ADMA) and symmetric dimethylarginine (SDMA) marks, respectively, on their target molecules. Arginine methylation is an underappreciated post-translational modification that occurs with the same frequency as the more widely studied and better understood phosphorylation and ubiquitination events (Larsen et al., 2016). CARM1 employs S-adenosyl-L-methionine to methylate arginine residues in proline-rich motifs of histones and non-histone proteins to mediate critical functions such as signal transduction, DNA repair, transcriptional control, mRNA splicing, and protein translocation (Bedford and Clarke, 2009; Yang and Bedford, 2013; Guccione and Richard, 2019; Fulton et al., 2019). For instance, CARM1 methylates histone H3 at Arg17 and co-activates transcription factor EB (TFEB) to promote the expression of autophagy-related genes (Shin et al., 2016). CARM1 is ubiquitously expressed, and whole-body genetic deletion of this enzyme in mice results in perinatal lethality (Yadav et al., 2003).

CARM1 has emerged as an important player in skeletal muscle biology. Work from our laboratory indicates that the methyltransferase is a novel regulator of skeletal muscle remodeling in rodents and humans (Ljubicic et al., 2012; Stouth et al., 2017, 2018; Vanlieshout et al., 2018; Shen et al., 2018; vanLieshout and Ljubicic, 2019; vanLieshout et al., 2019). Moreover, a series of elegant studies demonstrate that CARM1 governs myogenesis during development and regeneration, as well as plays a role in muscle glycogen metabolism (Chen et al., 2002; Kawabe et al., 2012; Wang et al., 2012; Chang et al., 2018). Recent data strongly suggest that CARM1 also impacts atrophy and autophagy signaling in muscle. For example, transient knockdown of CARM1 during denervation-induced muscle disuse attenuated the progression of muscle wasting and the expression of the atrophy-related genes via a forkhead box protein O3 (FOXO3)-mediated mechanism (Liu et al., 2019). In an earlier study, we reported that denervation-induced skeletal muscle atrophy was associated with elevated CARM1 expression and arginine methyltransferase activity, as well as

[1]Department of Kinesiology, McMaster University, Hamilton, ON L8S 4L8, Canada

[2]Lead Contact

*Correspondence: ljubicic@mcmaster.ca

https://doi.org/10.1016/j.isci.2020.101755

increased AMP-activated protein kinase (AMPK) activation status (Stouth et al., 2018). AMPK is a master regulator of phenotype determination, maintenance, and plasticity in skeletal muscle (Mounier et al., 2015; Dial et al., 2018; Kjøbsted et al., 2018; Steinberg and Carling, 2019). Notably, AMPK promotes autophagy in skeletal muscle through direct activation of unc-51-like autophagy-activating kinase 1 (ULK1) and FOXO3 (Kjøbsted et al., 2018). AMPK also upregulates atrogenes that drive the ubiquitin-proteasome system such as muscle RING finger 1 (MuRF1) and muscle atrophy F box (MAFbx) during muscle disuse (Kjøbsted et al., 2018). Thus, this collective evidence highlights the roles of CARM1 and AMPK in the orchestration of skeletal muscle remodeling via regulation of autophagy-lysosome and ubiquitin-proteasome signaling pathways.

Recent studies using non-muscle cells directly link CARM1 with AMPK and suggest that these molecules work synergistically to govern autophagic and atrophic networks (Shin et al., 2016; Kim et al., 2014). For instance, under nutrient-deprived conditions, AMPK-dependent phosphorylation of FOXO3 led to increased CARM1 expression and activity levels coincident with the stimulation of pro-autophagic signaling (Shin et al., 2016). In turn, CARM1 induced TFEB, the master transcriptional regulator of the autophagy program. The relationship between CARM1 and AMPK in skeletal muscle is less understood (Ljubicic et al., 2012; Stouth et al., 2018), but may represent a novel, powerful nexus for control of phenotypic plasticity in this tissue. Therefore, in the present study, we employed a combination of genetic, physiologic, and pharmacologic approaches to test the hypothesis that CARM1 interacts with AMPK to affect the kinase's downstream signaling network and muscle phenotype.

RESULTS

Generation of CARM1 Skeletal Muscle-Specific Knockout (mKO) Mice

To examine the function of CARM1 in muscle, we utilized the Cre/*loxP* system to generate mice that lack the enzyme specifically in skeletal muscle (Figure 1A). CARM1 floxed animals (Yadav et al., 2003; Bao et al., 2018) were bred to mice that expressed Cre recombinase under control of the human α-skeletal actin promoter, the activity of which is restricted to skeletal muscle tissue (McCarthy et al., 2012). A significant main effect of genotype was noted on CARM1 transcript levels and a significant interaction between genotype and muscle was also observed (Figure 1B). We found ∼90%–95% lower ($p < 0.05$) CARM1 transcript levels in mKO mice versus their wild-type (WT) littermates in both fast, glycolytic extensor digitorum longus (EDL) muscle and slower, more oxidative soleus (SOL) muscle. Relative to the WT EDL, CARM1 mRNA content was significantly lower by ∼13% in the WT SOL. Immunoblot analyses confirmed that CARM1 protein expression was significantly reduced in various skeletal muscles from mKO mice (Figure 1C). There was a trend ($p = 0.46$) for lower CARM1 protein content in the SOL versus tibialis anterior (TA), EDL, and gastrocnemius (GAST) muscles in WT animals (Figure 1D). CARM1 protein levels were similar between genotypes in other tissues such as the liver and brain (Figure 1E). Furthermore, CARM1 protein expression was similar in WT versus mKO heart muscles (Figures 1F and 1G). Compared with their WT littermates, the average body mass of mKO mice was modestly, but significantly, lower (∼5%; Figure 1H). Heart weights expressed relative to body mass were also similar in WT versus mKO animals (Figure 1I).

CARM1 Deletion in Skeletal Muscle Mitigates Denervation-Induced Atrophy

We previously reported elevated CARM1 expression and methyltransferase activity in response to 3 and 7 days of neurogenic muscle disuse (Stouth et al., 2018). Moreover, transient knockdown of CARM1 in TA muscle blunted the progression of muscle wasting after 4 weeks of denervation (Liu et al., 2019). However, the function of CARM1 during neurogenic muscle disuse remains to be fully understood. As such, we assessed physiological and mechanistic effects of denervation-induced muscle disuse in CARM1 mKO animals. As the average body mass was different between genotypes (Figure 1H), muscle was normalized to total body mass for subsequent analyses. After 3 days of neurogenic disuse elicited by unilateral sciatic nerve transection, a main effect ($p < 0.05$) of denervation on SOL muscle mass was observed in both genotypes (Figure 2A). Indeed, when compared with the contralateral, non-denervated CON limb, SOL muscle mass was significantly reduced by ∼25% and ∼15% in WT and mKO animals, respectively, in the DEN limb after 3 days. We also detected a main effect ($p < 0.05$) of genotype on SOL muscle mass following 3 days of denervation. Relative to the CON limb, TA and GAST muscle mass were significantly lower in WT animals by ∼15% after 3 days in the DEN limb. In contrast, TA and GAST muscle mass were similar between CON and DEN limbs in mKO animals following 3 days of disuse. EDL muscle mass did not differ between CON and DEN limbs in WT and mKO mice after 3 days. In response to 7 days of unilateral hindlimb disuse, we observed a statistical interaction between genotype and treatment (i.e., denervation) for EDL muscle

iScience
Article

CellPress
OPEN ACCESS

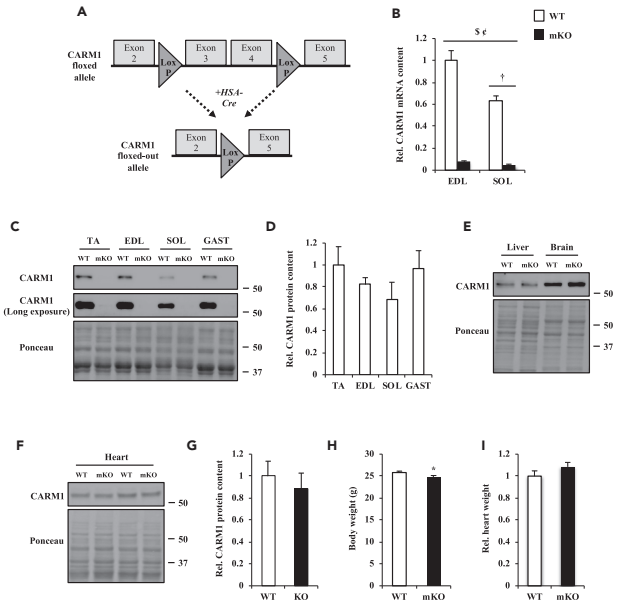

Figure 1. Generation of Skeletal Muscle-Specific Coactivator-Associated Arginine Methyltransferase 1 (CARM1) Knockout (mKO) Mice

(A) Simplified schematic of floxed exon 3 and exon 4 of the CARM1 gene with arrows to indicate deletion by human α-skeletal actin (*HSA*)-driven Cre-recombinase in skeletal muscle.

(B) CARM1 mRNA expression in extensor digitorum longus (EDL) and soleus (SOL) muscles of wild-type (WT) and CARM1 mKO mice. Data are expressed relative to the WT EDL muscle (n = 9–12).

(C) Representative western blots of CARM1 protein content (normal and long exposures) in the tibialis anterior (TA), EDL, SOL, and gastrocnemius (GAST) muscles from WT and mKO mice, as well as a representative Ponceau stain, below. Molecular weights (kDa) are shown at right of blots.

(D) Graphical summary of CARM1 protein expression in TA, EDL, SOL, and GAST muscles of WT animals. Data are expressed as protein content relative to WT TA (n = 9–11).

(E) CARM1 protein content in the liver and brain, along with a typical Ponceau stain. Molecular weights (kDa) are shown on the right (n = 3).

(F) Representative western blot of CARM1 protein content in heart muscles from WT and mKO animals, as well as a representative Ponceau stain, below. Molecular weights (kDa) are shown at the right of blots.

(G) Graphical summary of CARM1 protein expression in heart muscles of WT and mKO animals. Data are expressed as protein content relative to WT heart (n = 14–15).

(H) Body mass of WT and mKO animals (n = 44–51).

(I) Heart weight expressed relative to body mass in WT and mKO mice (n = 12).

Data are expressed relative to the WT value. Data are means ± SEM. Student's t test; *p < 0.05 versus WT. Two-way ANOVA; $p < 0.05 interaction effect of genotype and muscle; ¢p < 0.05 main effect of genotype; †p < 0.05 main effect of muscle.

mass (Figure 2B). Tukey post-hoc analyses revealed that EDL and GAST muscle mass were significantly lower by ~40% and ~30% in the DEN limb, respectively, relative to the CON limb after 7 days in WT mice. However, EDL and GAST muscle weights did not differ between CON and DEN limbs in mKO animals. A main effect ($p < 0.05$) of denervation on TA and SOL muscle mass was observed after 7 days of neurogenic disuse. Relative to the CON limb, TA and SOL muscle weights were significantly lower by ~25%–30% and ~40%–45%, respectively, after 7 days in the DEN limbs of WT and mKO mice. A significant main effect of genotype on TA muscle mass was also detected after 7 days.

CellPress
OPEN ACCESS

iScience
Article

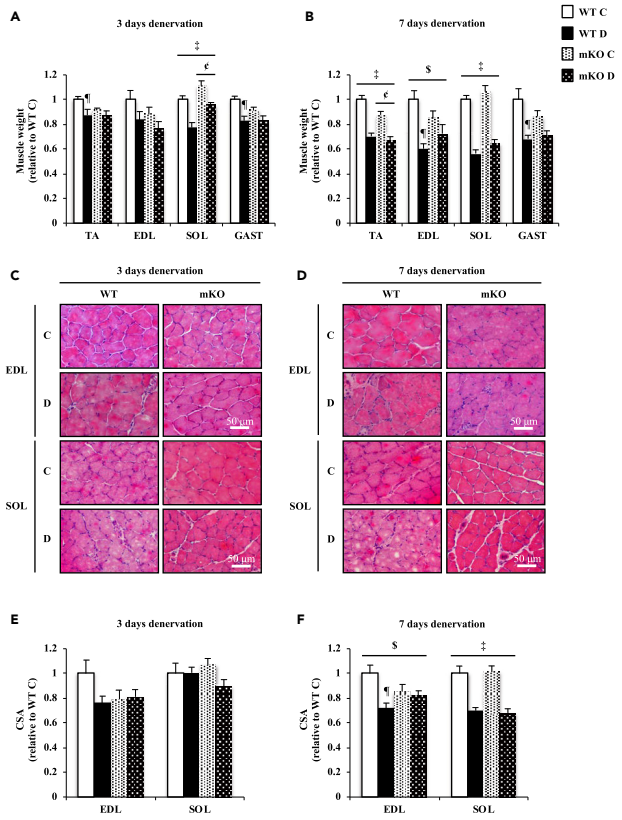

Figure 2. CARM1 Deletion in Skeletal Muscle Mitigates Denervation-Induced Atrophy

TA, EDL, SOL, and GAST muscle mass from the denervated (D) and the contralateral, non-denervated control (C) hindlimbs of WT and mKO mice after 3 (A) and 7 (B) days of denervation. Muscle weights are normalized to body weight, and data are expressed as muscle mass relative to WT C (n = 8–17). Representative images of H&E-stained EDL and SOL muscle cross sections from WT and mKO mice in D and C hindlimbs following 3 (C) and 7 (D) days of denervation. Scale bar, 50 μm. Graphical summaries of the average myofiber cross-sectional area (CSA) of EDL and SOL muscles from WT and mKO mice in D and C hindlimbs after 3 (E) and 7 (F) days of neurogenic muscle disuse. Data are expressed as CSA relative to the WT C (n = 5–9). Data are means ± SEM. Two-way ANOVA; $p < 0.05 interaction effect of genotype and denervation; ¢p < 0.05 main effect of genotype; ‡p < 0.05 main effect of denervation; ¶p < 0.05 versus WT C.

EDL and SOL myofiber cross-sectional area (CSA) was similar between CON and DEN limbs in WT and mKO animals following 3 days of neurogenic muscle disuse (Figures 2C and 2E). However, an interaction ($p < 0.05$) between genotype and denervation for EDL CSA emerged after 7 days (Figures 2D and 2F). Relative to CON, denervation induced a 28% decrease ($p < 0.05$) in EDL CSA in WT animals that was abolished in the absence of CARM1. Moreover, a significant main effect of denervation on SOL CSA was observed in both genotypes following 7 days of unilateral disuse. For instance, when compared with the CON limbs, SOL CSA was significantly reduced by ~30% in the DEN limbs of WT and mKO mice.

iScience
Article

CellPress
OPEN ACCESS

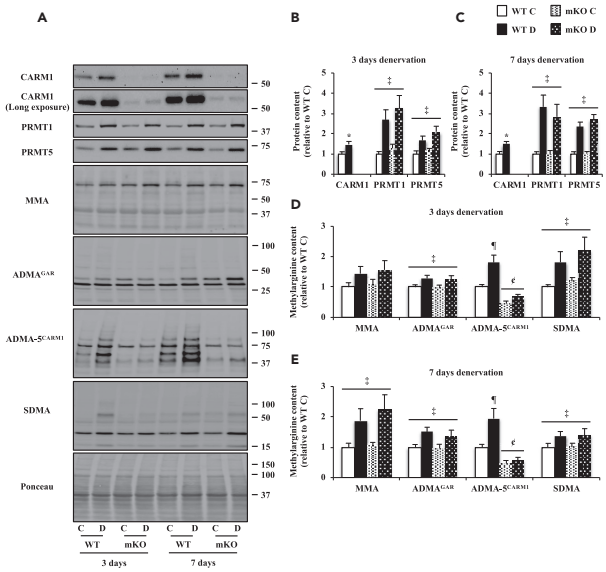

Figure 3. Skeletal Muscle Protein Arginine Methyltransferase (PRMT) Content and Activity Are Elevated in mKO Mice during Neurogenic Disuse

(A) Representative western blots of CARM1 (normal and long exposure), PRMT1, PRMT5, monomethylarginine (MMA), asymmetric dimethylarginine (ADMA) at glycine and arginine-rich motifs (ADMA^{GAR}), ADMA-CARM1 motif (ADMA-5^{CARM1}), and symmetric dimethylarginine (SDMA) levels in C and D TA muscles after 3 and 7 days of unilateral denervation in WT and mKO mice, with a typical Ponceau stain. Molecular weights (kDa) are shown at the right of blots. Graphical summaries of CARM1, PRMT1, and PRMT5 protein expression in TA muscles from the C and D hindlimbs of WT and mKO animals following 3 (B) and 7 (C) days of denervation. Data are expressed as protein content relative to WT C (n = 8–10). Graphical summaries of MMA, ADMA^{GAR}, ADMA-5^{CARM1}, and SDMA methylarginine content in C and D TA muscles of WT and mKO mice after 3 (D) and 7 (E) days. Data are expressed as methylarginine content relative to WT C (n = 6–10). Data are means ± SEM. Student's t test; *p < 0.05 versus WT C. Two-way ANOVA; $p < 0.05 interaction effect of genotype and denervation; ¢p < 0.05 main effect of genotype; ‡p < 0.05 main effect of denervation; ¶p < 0.05 versus WT C.

Skeletal Muscle PRMT Content and Activity Are Elevated in mKO Mice during Neurogenic Disuse

CARM1 protein content was elevated by ~1.5-fold ($p < 0.05$) in DEN versus CON WT limbs following 3 and 7 days of neurogenic muscle disuse (Figures 3A–3C). We wished to determine whether knocking out CARM1 in skeletal muscle elicited adaptations in other PRMTs after denervation. Thus, we examined PRMT1 and PRMT5 protein expression in the TA muscle of mKO animals, as well as markers of type I and type II PRMT activities, such as MMA, ADMA at glycine and arginine-rich motifs (ADMA^{GAR}), and SDMA (Bedford and Clarke, 2009; Yang and Bedford, 2013). We also probed for pan-CARM1-marked substrates (ADMA-5^{CARM1}; Cheng et al. 2018; vanLieshout et al., 2019). A main effect ($p < 0.05$) of denervation on PRMT1 and PRMT5 protein levels was observed in both genotypes after 3 and 7 days (Figures 3A–3C). PRMT1 and PRMT5 expression levels were significantly greater by ~2.5- to 3.3-fold and ~1.7- to 2.6-fold, respectively, in DEN versus CON limbs in WT and mKO mice.

A significant main effect of denervation on ADMA^{GAR} and SDMA content was observed in both genotypes following 3 and 7 days (Figures 3A, 3D, and 3E). Moreover, we detected a main effect ($p < 0.05$) of denervation on MMA content in WT and mKO animals after 7 days. ADMA-5^{CARM1} exhibited a trend toward a

statistically significant interaction between genotype and denervation after 3 and 7 days ($p = 0.08$ and $p = 0.06$, respectively). Specifically, relative to the CON limb, neurogenic muscle disuse induced a significant 1.8- and 1.9-fold increase in ADMA-5^{CARM1} content in the DEN limb after 3 and 7 days, respectively, in WT mice. ADMA-5^{CARM1} did not differ between CON and DEN limbs after 3 and 7 days of denervation in mKO animals. Furthermore, a significant main effect of genotype on ADMA-5^{CARM1} content was detected following 3 and 7 days.

Signaling Molecules That Regulate Skeletal Muscle Remodeling Are Altered in Response to Denervation

We next sought to determine whether CARM1 influences powerful modifiers of skeletal muscle phenotype such as AMPK, peroxisome proliferator-activated receptor-γ coactivator-1α (PGC-1α), tumor-suppressor protein p53, silent mating-type information regulator 2 homolog 1 (SIRT1), mitochondrial transcription factor A (Tfam), and nuclear factor erythroid 2-related factor 2 (Nrf2; Ljubicic et al., 2014; Dial et al., 2018; Hood et al., 2019). To this end, we first examined the activation status (i.e., the phosphorylated form of the protein relative to its total, unphosphorylated content) of AMPK and its target acetyl-coenzyme A carboxylase (ACC), as well as the protein content of downstream phenotypic modifiers PGC-1α and p53 in the TA muscle of WT and mKO animals subjected to denervation. We also assessed SIRT1, PGC-1α, p53, Tfam, and Nrf2 transcript levels in the EDL muscle following neurogenic muscle disuse. A significant interaction between genotype and denervation for phosphorylated AMPK (P-AMPK)^{Thr172} was observed after 3 days of neurogenic muscle disuse in the TA muscle (Figures 4A and 4B). For example, relative to the CON limb, P-AMPK^{Thr172} content in WT animals was significantly greater by 1.8-fold after 3 days in the DEN limb, whereas the phosphorylation of AMPK^{Thr172} did not differ between CON and DEN limbs following 3 days of denervation in mKO animals. In contrast, there were no significant differences for P-AMPK^{Thr172} levels between CON and DEN limbs in WT and mKO mice after 7 days of disuse. Notably, a significant main effect of genotype on P-AMPK^{Thr172} content was detected after 3 days (Figures 4A and 4C). Neither genotype nor denervation had an effect on total AMPK content following 3 and 7 days. An interaction ($p < 0.05$) between genotype and denervation for AMPK activation status was observed after 3 days, along with a significant main effect of genotype. The activation status for AMPK did not differ between CON and DEN limbs in WT and mKO animals following 7 days. A main effect ($p < 0.05$) of genotype on ACC^{Ser79} phosphorylation was observed after 3 days of denervation, along with a trend ($p = 0.06$) toward a main effect of genotype following 7 days (Figures 4A, 4D, and 4E). Total ACC content was similar between CON and DEN limbs in WT and mKO mice after 3 and 7 days of neurogenic muscle disuse. A significant main effect of genotype was detected for ACC activation status following 3 and 7 days. A notable main effect ($p < 0.05$) of denervation was apparent for ACC activation status after 3 days of denervation.

We observed a main effect ($p < 0.05$) of genotype on PGC-1α protein content in TA muscles after 3 and 7 days (Figures 4A, 4F, and 4G). Moreover, a main effect ($p < 0.05$) of denervation on PGC-1α protein expression was detected in both genotypes following 7 days. We observed a significant main effect of denervation on p53 protein content (+3.2-fold) in WT mice after 7 days (Figures 4A and 4G). In contrast, p53 protein levels did not differ between CON and DEN limbs in mKO animals after 7 days of denervation. PGC-1α and p53 stimulate mitochondrial biogenesis in skeletal muscle (Ljubicic et al., 2014; Hood et al., 2019). Thus, we next assessed the expression of protein subunits that are representative of mitochondrial oxidative phosphorylation (OXPHOS) complexes I–V (CI–CV), as well as succinate dehydrogenase (SDH) content in WT and mKO animals. We detected a main effect ($p < 0.05$) of denervation on total OXPHOS expression in both genotypes after 3 and 7 days of denervation (Figures 4A, 4F, and 4G). Qualitative analyses suggest that compared with the control limbs, both WT and mKO EDL muscles displayed reduced SDH staining after 7 days of neurogenic muscle disuse (Figure 4H).

Denervation did not have an effect on SIRT1 mRNA content following 3 or 7 days in the EDL muscle (Figures 4I and 4J). A main effect ($p < 0.05$) of denervation on PGC-1α mRNA expression was observed in both genotypes after 3 and 7 days in the EDL muscles. PGC-1α was significantly lower by ~57%–87% in DEN versus CON limbs in WT and mKO mice (Figures 4I and 4J). An interaction ($p < 0.05$) between genotype and denervation for p53 transcript levels in the EDL muscle emerged after 3 days (Figure 4I). Relative to CON, denervation induced a 3.2-fold increase in p53 mRNA expression in the WT EDL ($p < 0.05$) that was blunted in the absence of CARM1. A significant main effect of denervation on EDL p53 transcript levels was observed in both genotypes after 7 days (Figure 4J). Specifically, when compared with the CON limb, p53 mRNA content was significantly elevated by ~1.8- to 2.2-fold in the DEN EDL following 7 days. We detected a main

iScience
Article

CellPress
OPEN ACCESS

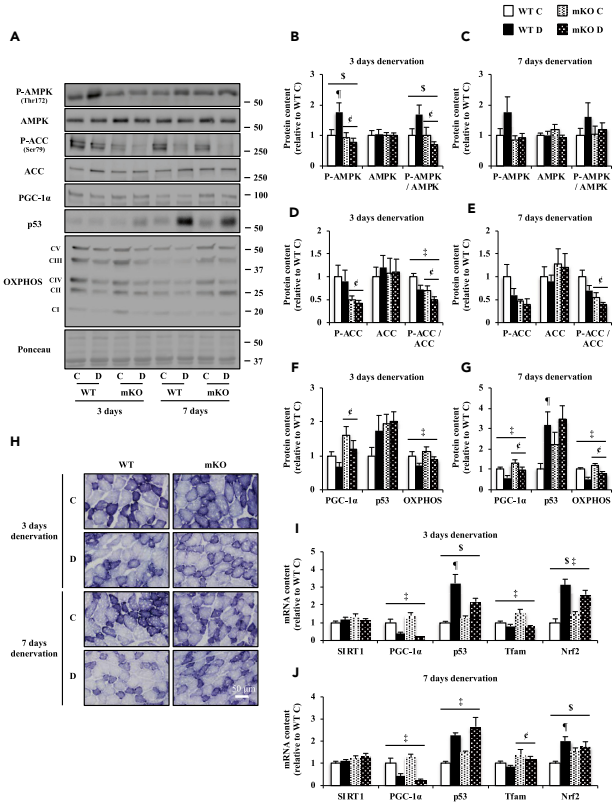

Figure 4. Signaling Molecules That Regulate Skeletal Muscle Remodeling Are Altered in Response to Denervation

(A) Representative western blots of phosphorylated AMP-activated protein kinase (P-AMPK)^{Thr172}, total AMPK, phosphorylated acetyl-coenzyme A carboxylase (P-ACC)^{Ser79}, total ACC, peroxisome proliferator-activated receptor-γ coactivator-1α (PGC-1α), tumor suppressor protein p53 protein content, and proteins indicative of mitochondrial oxidative phosphorylation (OXPHOS) complexes I–V (CI–CV) in C and D TA muscles following 3 and 7 days of unilateral denervation in WT and mKO mice, accompanied by a typical Ponceau stain. Molecular weights (kDa) are shown at the right of blots.

(B–G) Graphical summaries of P-AMPK^{Thr172}, AMPK, AMPK activation status (i.e., the phosphorylated form of the protein relative to the total amount of the protein), P-ACC^{Ser79}, ACC, ACC activation status, PGC-1α, p53, and total OXPHOS protein expression in the C and D TA muscles of WT and mKO mice following 3 and 7 days of neurogenic disuse. Data are expressed as protein content relative to WT C (n = 5–11).

(H) Representative images of succinate dehydrogenase (SDH)-stained EDL muscle cross-sections from WT and mKO mice in D and C hindlimbs following 3 and 7 days of denervation. Scale bar, 50 μm (n = 3–5). Silent mating-type information regulator 2 homolog 1 (SIRT1), PGC-1α, p53, mitochondrial transcription factor A (Tfam), and nuclear factor erythroid 2-related factor 2 (Nrf2) mRNA expression in EDL muscles from the C and D hindlimbs of WT and mKO animals after 3 (I) and 7 (J) days of denervation. Data are expressed as mRNA content relative to WT C (n = 4–8). Data are means ± SEM. Two-way ANOVA; $p < 0.05 interaction effect of genotype and denervation; ¢p < 0.05 main effect of genotype; ‡p < 0.05 main effect of denervation; ¶p < 0.05 versus WT C.

effect ($p < 0.05$) of denervation on Tfam mRNA expression following 3 days of disuse (Figure 4I). Most notable was the significant decline in Tfam mRNA content by ~49% in the DEN versus CON EDL in mKO mice. A main effect ($p < 0.05$) of genotype on Tfam transcript levels was also observed after 7 days (Figure 4J). Statistically significant interactions between genotype and denervation for Nrf2 mRNA levels were observed after 3 and 7 days (Figures 4I and 4J). Following 3 days, Nrf2 mRNA expression in WT and mKO mice was significantly increased by 3.1- and 1.8-fold, respectively, in the DEN versus CON EDL muscles. Relative to CON, denervation induced a 2-fold increase ($p < 0.05$) in Nrf2 mRNA content in WT EDL after 7 days that was abolished in the absence of CARM1.

CARM1 Influences the Muscle Atrophy Program during Neurogenic Muscle Disuse

To examine the impact of CARM1 on the muscle atrophy program, we assessed markers of the autophagy-lysosome pathway and the ubiquitin-proteasome system in WT and mKO animals after disuse. Specifically, we evaluated markers of autophagosome formation such as phosphorylation of ULK1^{Ser555} and lipidation of microtubule-associated protein 1A/1B-light chain 3 (LC3; i.e., the conversion of nonlipidated LC3-I to lipidated LC3-II; Vainshtein et al., 2014). We also analyzed the activation status of FOXO1^{Ser256} and FOXO3^{Ser588} as FOXO1 and FOXO3 regulate the transcription of atrogenes important for proteasome-mediated degradation (Bodine, 2013). The phosphorylation of ULK1^{Ser555} exhibited a trend ($p = 0.14$) toward an interaction between genotype and denervation after 3 days of disuse (Figures 5A and 5B). Relative to the CON limb, P-ULK1^{Ser555} content in WT mice was significantly greater by 1.7-fold following 3 days in the DEN limb, whereas the phosphorylation of ULK1^{Ser555} did not differ between CON and DEN limbs after 3 days of neurogenic muscle disuse in mKO animals. In contrast, similar P-ULK1^{Ser555} levels were detected between CON and DEN limbs in WT and mKO mice after 7 days of disuse (Figures 5A and 5C). Total ULK1 did not differ between CON and DEN limbs following 3 and 7 days of denervation in WT and mKO animals (Figures 5A–5C). The activation status for ULK1 was also similar between CON and DEN limbs in WT and mKO animals following 3 and 7 days. A main effect ($p < 0.05$) of denervation on the phosphorylation of FOXO1^{Ser256} was observed in WT animals after 3 days of disuse in TA muscles (Figures 5A and 5D). We also detected a significant main effect of denervation on the phosphorylation of FOXO1^{Ser256} in both genotypes following 7 days (Figures 5A and 5E). The phosphorylation of FOXO1^{Ser256} was greater by ~1.4- to 2.1-fold in DEN versus CON limbs in WT and mKO mice after denervation. A significant main effect of denervation on total FOXO1 content was observed in both genotypes following 3 days. Relative to the CON limb, neurogenic muscle disuse induced a ~2.1–2.6-fold increase in FOXO1 content in WT and mKO mice. A main effect ($p < 0.05$) of genotype on total FOXO1 protein expression was also detected following 3 days. A significant main effect of denervation on total FOXO1 content was apparent in WT animals following 7 days. A main effect ($p < 0.05$) of denervation on FOXO1 activation status was observed in both genotypes after 3 days. FOXO1 activation status did not differ between CON and DEN limbs following 7 days of denervation in WT and mKO animals. An interaction ($p < 0.05$) between genotype and denervation for the phosphorylation of FOXO3^{Ser588} emerged after 3 days of denervation (Figures 5A and 5F). Moreover, a significant main effect of genotype on FOXO3^{Ser588} phosphorylation was observed in both genotypes following 3 and 7 days of unilateral disuse (Figures 5A, 5F, and 5G). We detected a main effect ($p < 0.05$) of denervation on total FOXO3 content after 3 days. A significant main effect of genotype on FOXO3 activation status was also observed following 3 and 7 days of neurogenic muscle disuse.

We continued to probe the impact of CARM1 on the muscle atrophy program by analyzing atrogenes that are critically important for muscle wasting. Thus, we assessed the protein expression of p62, Beclin1, TFEB, MuRF1, ubiquitinated protein content, as well as LC3-I and LC3-II expression levels in TA muscles from WT and mKO animals following neurogenic muscle disuse (Hood et al., 2019; Vainshtein et al., 2014; Bodine, 2013; Sandri, 2013). A main effect ($p < 0.05$) of denervation on p62, MuRF1, and ubiquitinated protein content was observed in both genotypes following 3 and 7 days of unilateral disuse (Figures 5A, 5H, and 5I). Relative to the CON limb, p62, MuRF1, and ubiquitinated protein content was significantly greater by ~1.7- to 2.9-fold in the DEN limbs of WT and mKO mice. A main effect ($p < 0.05$) of genotype on ubiquitinated protein content was observed after 3 days. Beclin1 and TFEB protein expression levels were not impacted by disuse. A significant main effect of genotype on Beclin1 protein content was observed following 3 and 7 days of denervation. We found a main effect ($p < 0.05$) of denervation on LC3-I (data not shown) and LC3-II content in both genotypes after 7 days (Figures 5A and 5I). For instance, LC3-I and LC3-II expression levels were significantly greater by ~3.3- to 4.4-fold in the DEN limb relative to the CON limb after 7 days in WT and mKO mice. A main effect ($p < 0.05$) of genotype on LC3-II protein content was also detected after 7 days.

iScience
Article

CellPress
OPEN ACCESS

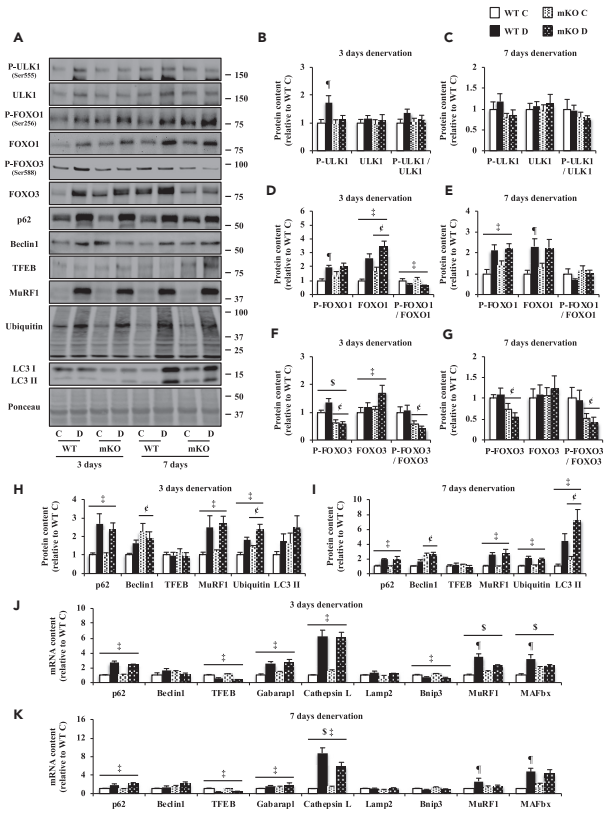

Figure 5. CARM1 Influences the Muscle Atrophy Program during Neurogenic Muscle Disuse

(A) Representative western blots of phosphorylated unc-51 like autophagy-activating kinase 1 (P-ULK1)^{Ser555}, total ULK1, phosphorylated Forkhead box O1 (P-FOXO1)^{Ser256}, total FOXO1, P-FOXO3^{Ser588}, total FOXO3, p62, Beclin1, transcription factor EB (TFEB), muscle RING finger 1 (MuRF1), ubiquitin protein content, microtubule-associated protein 1A/1B-light chain 3 (LC3)-I, and LC3-II in C and D TA muscles following 3 and 7 days of unilateral denervation in WT and mKO mice, accompanied by a typical Ponceau stain. Molecular weights (kDa) are shown on the right of blots.

(B–I) Graphical summaries of P-ULK1^{Ser555}, ULK1, ULK1 activation status, P-FOXO1^{Ser256}, FOXO1, FOXO1 activation status, P-FOXO3^{Ser588}, FOXO3, FOXO3 activation status, as well as p62, Beclin1, TFEB, MuRF1, ubiquitin, and LC3-II protein content in the C and D TA muscles of WT and mKO animals after 3 and 7 days of neurogenic disuse. Data are expressed as protein content relative to WT C (n = 5–11). p62, Beclin1, TFEB, Gabarapl, Cathepsin L, lysosomal-associated membrane protein 2 (Lamp2), BCL2 and adenovirus E1B 19-kDa interacting protein 3 (Bnip3), MuRF1, and muscle atrophy F box (MAFbx) mRNA expression in EDL muscles from the C and D hindlimbs of WT and mKO mice following 3 (J) and 7 (K) days of denervation. Data are expressed as mRNA content relative to WT C (n = 4–8). Data are means ± SEM. Two-way ANOVA; $p < 0.05 interaction effect of genotype and denervation; ¢p < 0.05 main effect of genotype; ‡p < 0.05 main effect of denervation; ¶p < 0.05 versus WT C.

We sought to investigate the effect of CARM1 deletion on the expression of a broad panel of representative atrogenes. To this end, we examined p62, Beclin1, TFEB, Gabarapl, Cathepsin L, lysosomal-associated membrane protein 2 (Lamp2), BCL2, and adenovirus E1B 19-kDa-interacting protein 3 (Bnip3), MuRF1, and

MAFbx transcript levels in EDL muscles from WT and mKO mice. A main effect ($p < 0.05$) of denervation on p62, Gabarapl, and TFEB transcript levels for WT and mKO animals was observed in the EDL muscles after 3 and 7 days of neurogenic muscle disuse (Figures 5J and 5K). In particular, relative to the CON limb, p62 mRNA expression was significantly greater by ~1.9- to 2.7-fold in the DEN EDL muscle in both genotypes. Denervation induced a ~1.9- to 2.6-fold increase ($p < 0.05$) in Gabarapl mRNA content in WT and mKO EDL muscles following 3 days. In contrast, TFEB mRNA content in both genotypes was significantly lower by ~47%–63% in the DEN versus CON EDL after 3 and 7 days. A main effect ($p < 0.05$) of denervation on Bnip3 transcript levels was detected in mKO animals following 3 days. In particular, Bnip3 mRNA expression was lower by ~44% ($p < 0.05$) in mKO animals in the DEN versus CON EDL. Statistically significant interactions between genotype and denervation for Cathepsin L, MuRF1, and MAFbx transcript levels were also observed (Figures 5J and 5K). Specifically, in EDL muscles of DEN versus CON limbs, denervation induced a ~2.7- to 4.7-fold increase ($p < 0.05$) in MuRF1 and MAFbx transcripts in WT animals after 3 and 7 days, whereas no significant changes were observed in the absence of CARM1. An interaction ($p < 0.05$) between genotype and denervation for Cathepsin L transcript levels in the EDL emerged after 7 days (Figure 5K). Relative to the WT CON EDL muscle, denervation induced a ~8.8-fold increase ($p < 0.05$) in Cathepsin L mRNA expression in the WT EDL that was blunted (~3.8-fold) in mKO animals. Beclin1 and Lamp2 mRNA transcripts in the EDL muscles did not differ between CON and DEN limbs following disuse (Figures 5J and 5K).

CARM1 Interacts with AMPK, FOXO1, and TFEB, but Not p53, in Skeletal Muscle during Denervation-Induced Plasticity

Immunoprecipitation (IP) of CARM1 was performed in WT TA muscles to assess potential functional interactions of CARM1 with AMPK, FOXO1, TFEB, and p53. These proteins are well-known mediators of muscle phenotype determination and remodeling (Kjøbsted et al., 2018; Hood et al., 2019), while we and others have previously shown that AMPK and FOXO proteins interact with PRMTs in skeletal muscle (Stouth et al., 2018; Liu et al., 2019; Yamagata et al., 2008). Moreover, TFEB and p53 are validated targets of CARM1 in other cell types (Shin et al., 2016; An et al., 2004). Our data show that CARM1 interacted with AMPK, FOXO1, and TFEB in skeletal muscle *in vivo* (Figure 6A). Interestingly, we did not detect an interaction between CARM1 and p53 (Figure 6A). The interaction between CARM1 and AMPK increased by ~1.5-fold ($p < 0.05$) after 3 days in the DEN versus CON limb (Figures 6A and 6B). Relative to the CON limb, the interaction between CARM1 and FOXO1 was significantly greater by ~1.2-fold in the DEN TA muscle after 3 days, whereas the interaction between CARM1 and TFEB decreased by ~43% ($p < 0.05$) in the DEN limb following 7 days.

CARM1 Methylates AMPK in Muscle *In Vivo*

We were particularly interested in determining whether CARM1 could influence the methylation of AMPK during neurogenic muscle disuse. IP of AMPK was carried out in WT and mKO TA muscles, followed by immunoblotting (IB) for ADMA-5^{CARM1} and $ADMA^{GAR}$. A significant interaction between genotype and denervation for IP of AMPK and IB of ADMA-5^{CARM1} was observed after 3 days of disuse (Figures 6C and 6D). Specifically, in TA muscles with IP of AMPK, denervation induced a ~1.9-fold increase ($p < 0.05$) in ADMA-5^{CARM1} content relative to the CON limb in WT animals, whereas no significant changes were observed in the absence of CARM1. Following IP of AMPK, $ADMA^{GAR}$ content was similar between CON and DEN limbs in the TA muscle of WT and mKO animals after 3 and 7 days (Figures 6C–6E).

CARM1 Regulates AMPK Signaling

Finally, we sought to determine whether CARM1 is required for AMPK activation and downstream signaling in skeletal muscle. As such, we employed the systemic pan-AMPK activator MK-8722 (Myers et al., 2017) to assess pharmacological activation of AMPK and AMPK-mediated, site-specific phosphorylation of ACC in mKO animals. WT and mKO animals were treated with either vehicle (Veh) or MK-8722 by oral gavage. At 3 h post-dose, we observed a main effect ($p < 0.05$) of MK-8722 on P-$AMPK^{Thr172}$ content in both WT and mKO TA muscles (Figures 7A and 7B). For instance, relative to WT Veh and mKO Veh, P-$AMPK^{Thr172}$ content in WT and mKO animals was significantly greater by ~2-fold after MK-8722 administration. Neither genotype nor MK-8722 had an effect on total AMPK content. We also detected a main effect ($p < 0.05$) of MK-8722 on AMPK activation status for both genotypes. The phosphorylation of ACC^{Ser79} exhibited a strong trend ($p = 0.10$) toward an interaction between genotype and MK-8722 in the TA muscle (Figures 7A and 7C). We also observed a main effect ($p < 0.05$) of genotype on P-ACC^{Ser79}. MK-8722 and genotype did not have an effect on total ACC content. An interaction ($p < 0.05$) between genotype and MK-8722 for

iScience
Article

CellPress
OPEN ACCESS

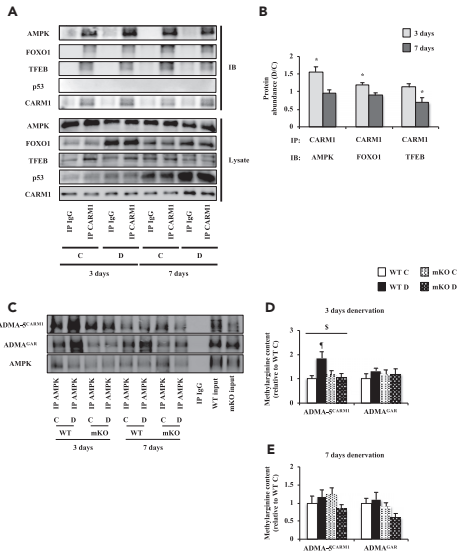

Figure 6. Protein Interactions in Denervated Skeletal Muscle

(A) Representative immunoprecipitation (IP) images of CARM1 or immunoglobulin G (IgG) with subsequent immunoblotting (IB) for AMPK, FOXO1, TFEB, p53, and CARM1 in D and C TA muscles following 3 and 7 days of denervation in WT mice. Western blots of whole muscle lysates (Lysate) for AMPK, FOXO1, TFEB, p53, and CARM1 are also shown.

(B) Graphical summary of CARM1 interactions with AMPK, FOXO1, and TFEB following 3 and 7 days of neurogenic muscle disuse. Data are expressed as protein abundance ratio in D versus C (n = 7–10). Data are means ± SEM. Student's t test; *p < 0.05 D versus C.

(C) Typical images of IP of AMPK with IB for ADMA-5^{CARM1}, ADMA^{GAR}, and AMPK in TA muscles from the C and D hindlimbs of WT and mKO mice following 3 and 7 days of denervation. Representative lanes of IP of IgG, as well as WT and mKO inputs (i.e., whole muscle lysate precleared with IgG) are also shown. Graphical summaries of methylated AMPK levels in WT and mKO animals after 3 (D) and 7 (E) days of denervation. Data are expressed as methylated protein content relative to WT C (n = 5–8). Data are means ± SEM. Two-way ANOVA; $p < 0.05 interaction effect of genotype and denervation; ¶p < 0.05 versus WT C.

ACC activation status emerged 3 h after the dose. Specifically, relative to WT mice treated with Veh, MK-8722 induced a ~1.9-fold increase ($p < 0.05$) in ACC activation status in WT animals, whereas no significant changes were observed in the absence of CARM1. A main effect ($p < 0.05$) of genotype on ACC activation status was also apparent. Furthermore, we detected a significant main effect of genotype on total TBC1 domain family member 1 (TBC1D1), TBC1D1 activation status, phosphorylation of FOXO3^{Ser588}, as well as FOXO3 activation status (Figures 7A, 7D, and 7E).

We further investigated the impact of CARM1 deletion on AMPK signaling by probing a panel of genes downstream of AMPK. In particular, we assessed PGC-1α, p53, Tfam, p62, MuRF1, and MAFbx transcript levels in the EDL because these genes are influenced by AMPK activity (Ljubicic et al., 2014; Ha et al., 2017; Kjøbsted et al., 2018). We detected a main effect ($p < 0.05$) of MK-8722 on PGC-1α and MuRF1 transcript levels in the EDL muscle after treatment (Figure 7F). PGC-1α and MuRF1 exhibited a trend toward an interaction between genotype and MK-8722 after 3 h of the dose ($p = 0.13$ and $p = 0.10$, respectively). A main effect ($p < 0.05$) of genotype on p53 and MAFbx transcript levels was also observed in the EDL muscles. Genotype and MK-8722 did not have an effect on Tfam and p62 mRNA content.

CellPress
OPEN ACCESS

iScience
Article

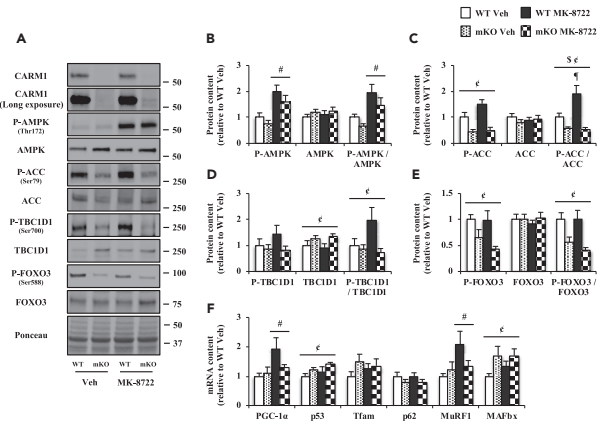

Figure 7. CARM1 Regulates AMPK Signaling

(A) Representative western blots of CARM1 (normal and long exposure), P-AMPK^{Thr172}, total AMPK, P-ACC^{Ser79}, total ACC, phosphorylated TBC1 domain family member 1 (P-TBC1D1)^{Ser700}, total TBC1D1, P-FOXO3^{Ser588}, and FOXO3 protein content in WT and mKO TA muscles after an acute dose (3 h) of vehicle (Veh) or MK-8722, accompanied by a typical Ponceau stain. Molecular weights (kDa) are shown on the right of blots.

(B–E) Graphical summaries of P-AMPK^{Thr172}, AMPK, AMPK activation status, P-ACC^{Ser79}, ACC, ACC activation status, P-TBC1D1^{Ser700}, TBC1D1, TBC1D1 activation status, P-FOXO3^{Ser588}, FOXO3, and FOXO3 activation status in WT and mKO TA muscles following Veh or MK-8722 administration. Data are expressed as protein content relative to WT Veh (n = 6–9).

(F) PGC-1α, p53, Tfam, p62, MuRF1, and MAFbx mRNA expression in EDL muscles from WT and mKO animals following Veh or MK-8722 treatment. Data are expressed as mRNA content relative to WT Veh (n = 6–8). Data are means ± SEM. Two-way ANOVA; $p < 0.05 interaction effect of genotype and MK-8722; ¢p < 0.05 main effect of genotype; #p < 0.05 main effect of MK-8722; ¶p < 0.05 versus WT Veh.

DISCUSSION

Our results show that CARM1 is required to maintain muscle mass and skeletal muscle-specific deletion of CARM1 impacts AMPK signaling. We also demonstrate that CARM1 interacts with and methylates AMPK in skeletal muscle and that this interaction is increased during the early adaptive response to neurogenic muscle disuse. Consistent with this, CARM1 mKO resulted in attenuated phosphorylation of AMPK and proximate autophagic and atrophic signaling following 3 days of denervation. Moreover, we found that in contrast to muscles from WT mice, MK-8722 evoked AMPK site-specific activation of ACC^{Ser79} and TBC1D1^{Ser700}, as well as the gene expression of downstream AMPK targets PGC-1α and MuRF1 did not change in mKO muscles. Collectively, these genetic, physiologic, and pharmacologic data indicate that CARM1 regulates AMPK signaling in skeletal muscle.

We detected muscle-specific differences in the role of CARM1 in the maintenance of skeletal muscle mass. For instance, muscle mass of the fast, glycolytic TA, as well as EDL myofiber CSA, was lower in mKO versus WT mice, whereas SOL muscle mass was greater in mKO animals. These results align with previous work demonstrating that transient knockdown of CARM1 reduces TA muscle weight (Liu et al., 2019). Autophagy is required to maintain muscle mass (Masiero et al., 2009; Carnio et al., 2014), and loss of CARM1 compromises the autophagic process (Shin et al., 2016; Liu et al., 2019). As AMPK promotes autophagy (Kjøbsted et al., 2018; Bujak et al., 2015), in part through stabilization of CARM1 (Shin et al., 2016), it is reasonable to speculate that knocking out CARM1 in skeletal muscle altered AMPK signaling and dysregulated downstream autophagic processes that contributed to the differential muscle phenotype between WT and mKO animals. The experimental evidence revealed here strongly supports this assertion. First, we show that under basal conditions in skeletal muscle CARM1 interacts with AMPK. Second, knocking out CARM1 attenuated basal levels of AMPK-mediated ACC^{Ser79} and FOXO3^{Ser588} phosphorylation. Third, CARM1 mKO resulted in elevated protein content of Beclin1, whose expression levels, as well as dual

regulation of autophagy and apoptosis, are controlled by AMPK-mediated phosphorylation (Kim et al., 2013; Song et al., 2014; Zhang et al., 2016). Fourth, we demonstrate that CARM1 interacts with TFEB and FOXO1, master transcriptional regulators of the autophagy and atrophy programs, respectively. CARM1 exerts transcriptional co-activator function on TFEB (Shin et al., 2016) whereas TFEB regulates AMPK signaling in skeletal muscle (Mansueto et al., 2017). Atrophy-related genes that are governed, in part, by FOXO1 (Bodine, 2013; Milan et al., 2015) were upregulated in response to CARM1 deletion. In particular, MAFbx transcript levels were greater in mKO versus WT muscle. RNA sequencing analysis also revealed disparate atrophy-related gene expression profiles between genotypes, such as increased FOXO1 transcript levels in mKO versus WT animals (data not shown). Finally, we observed augmented PGC-1α content in mKO muscle. AMPK modulates the function of PGC-1α (Dial et al., 2018; Kjøbsted et al., 2018), a transcriptional coactivator that elicits lysosomal and autophagosomal biogenesis in skeletal muscle (Takikita et al., 2010; Halling et al., 2016; Erlich et al., 2018). In all, the data indicate that skeletal muscle phenotypic plasticity in mKO mice is due, at least in part, to altered autophagic signaling mediated by the dissociation of CARM1-AMPK complexes.

It was previously demonstrated that CARM1 knockdown attenuated atrophy and the expression of atrogenes following 28 days of neurogenic muscle disuse (Liu et al., 2019). Consistent with this, the present study shows that knocking out CARM1 in muscle mitigated the progression of denervation-induced skeletal muscle atrophy. This may be due to a specific effect of CARM1 deletion, or possibly to mKO muscles already nearing maximal atrophy, or a combination thereof. We postulate that the induction of PGC-1α in mKO animals resulted in increased protection from relatively short-term (i.e., 3 and 7 days) denervation-induced atrophy, but was unable to preserve muscle mass against a lifetime (i.e., 12 weeks old) of potentially dysregulated atrophy and autophagy signaling and gene expression. Furthermore, our data strongly suggest that CARM1 regulates neurogenic disuse-evoked muscle wasting by way of AMPK. AMPK is activated during various conditions of disuse, whereas AMPK deficiency protects muscle from atrophy (Kjøbsted et al., 2018). AMPK promotes autophagic and proteasomal-mediated protein degradation by phosphorylating ULK1^{Ser555} and FOXO3^{Ser588}, respectively (Kjøbsted et al., 2018). Here, we observed reduced AMPK activation, attenuated downstream stimulatory phosphorylation of ULK^{Ser555} and FOXO3^{Ser588}, as well as mitigated expression levels of FOXO-mediated atrogenes MuRF1 and MAFbx in mKO mice compared with their WT littermates after 3 days of neurogenic muscle disuse. These data suggest that the absence of CARM1 alters AMPK-mediated atrophic signaling during the early adaptive response to denervation. Consistent with this, our IP experiments in WT animals revealed an increased interaction between CARM1 and FOXO1 following 3 days of disuse. As CARM1 modulates the expression of atrophy-related genes by activating FOXO3 via its asymmetric arginine dimethylation (Liu et al., 2019), it is reasonable to posit that CARM1 exerts a similar function on FOXO1 based on the (1) presence of proline-rich CARM1 methylation motifs on FOXO1 at Arg19 and Arg29 (Lee and Bedford, 2002; Gayatri et al., 2016; Cheng et al., 2018) as well as (2) comparable functions between FOXO1 and FOXO3 (Bodine, 2013). Blunted p53 mRNA and protein responses in mKO mice after 3 and 7 days of denervation, respectively, further support the role of a CARM1-AMPK signaling axis in governing muscle phenotype. Indeed, AMPK activation upregulates p53 levels (Imamura et al., 2001) and AMPK-mediated phosphorylation of p53^{Ser15} stabilizes the protein (Jones et al., 2005). Interestingly, we were unable to detect CARM1-p53 interactions in skeletal muscle despite previously observed complexes comprising these molecules (An et al., 2004; O'Brien et al., 2010).

Skeletal muscle-specific PRMT1 deletion results in elevated CARM1 expression (Choi et al., 2019). In contrast, we demonstrate that knocking out CARM1 in skeletal muscle does not influence PRMT1 or PRMT5 content, or their corresponding outputs of global methyltransferase activities ADMA^{GAR} and SDMA, respectively. We also probed methyl-GAR and methyl-CARM1 motifs to assess myocellular ADMA levels, as well as the asymmetric marking of dimethylarginines preferentially performed by CARM1, respectively (Guo et al., 2014; Cheng et al., 2018). We did not observe altered deposition of the ADMA^{GAR} mark in mKO animals, likely because CARM1 does not methylate this motif and because there was no compensatory alteration in PRMT1 activity. Conversely, and as expected, ADMA-5^{CARM1} levels were significantly lower in mKO versus WT mice. We reason that ADMA-5^{CARM1} was not completely ablated in mKO mice due to (1) residual CARM1 activity in cells other than myocytes that typically reside in the muscle and (2) off-target ADMA activity by PRMT1 (Cheng et al., 2018). Denervation elicited increased CARM1 protein and ADMA-5^{CARM1} levels in WT, but not mKO animals, suggesting that CARM1 content and its specific

methyltransferase activity are closely linked during disuse-evoked muscle remodeling. We further demonstrate that denervation-induced methylation of AMPK specifically by CARM1 occurred coincident with increased CARM1-AMPK binding and AMPK activation. Indeed, deposition of ADMA-5^{CARM1} on AMPK was elevated in DEN versus CON muscles following 3 days of disuse in WT animals. In contrast, the ADMA-5^{CARM1} mark on AMPK did not differ between CON and DEN limbs in mKO animals, whereas AMPK ADMA^{GAR} levels remained unchanged in response to denervation in both genotypes. Together these data strongly indicate that CARM1 was solely responsible for the augmented arginine methylation of AMPK during denervation. Our results reveal a CARM1-AMPK mechanism in the skeletal muscle atrophy program during the early adaptive response to neurogenic disuse. A rational hypothesis is that the methyltransferase marks the AMPKα1 subunit at a partially conserved CARM1 ADMA site located at the Arg538 proline-rich motif (Lee and Bedford, 2002; Gayatri et al., 2016; Cheng et al., 2018). Notably, the α-subunit is required for AMPK catalytic activity, and AMPKα1 indirectly promotes muscle atrophy by antagonizing anabolic signaling (Phillips et al., 2009; Kjøbsted et al., 2018).

MK-8722 is a potent pharmacological activator of all 12 AMPK isoforms (Myers et al., 2017; Muise et al., 2019). The compound directly binds to the allosteric drug and metabolite site located at the interface between the α-subunit kinase domain and the carbohydrate-binding module in the β-subunit, which is thought to protect Thr172 from dephosphorylation (Steinberg and Carling, 2019). Our data indicate that whereas CARM1 is dispensable for MK-8722-mediated phosphorylation of AMPK, MK-8722-induced activation status of ACC^{Ser79} and TBC1D1^{Ser700} were abolished in the absence of CARM1. Indeed, AMPK-regulated genes, such as PGC-1α and MuRF1 tended to be blunted in mKO animals after MK-8722 administration, further supporting the assertion that CARM1 affects AMPK signaling. It is interesting to note that, contrary to 3 days of denervation, acute 3-h administration of MK-8722 evoked increased AMPK^{Thr172} phosphorylation in muscles from both WT and mKO animals. These data highlight distinct influences of CARM1 on AMPK during physiological versus pharmacological activation of the kinase. We suspect that a regulatory loop between CARM1 and AMPK exists, as in some conditions CARM1 functions downstream of AMPK (Shin et al., 2016) and the methyltransferase contains a well-defined AMPK phosphorylation motif at Ser501 (Hardie et al., 2016; Steinberg and Carling, 2019).

In summary, this study reveals a CARM1-AMPK mechanism that impacts the maintenance and remodeling of muscle mass via altered downstream autophagic and atrophic signaling. Given the emerging roles for CARM1 in muscle biology (Stouth et al., 2017; vanLieshout et al., 2019), as well as the established functions for AMPK in maintaining and remodeling skeletal muscle phenotype (Mounier et al., 2015; Dial et al., 2018; Kjøbsted et al., 2018; Steinberg and Carling, 2019), targeting this interplay between CARM1-AMPK may therefore provide therapeutic strategies for myopathies such as disuse atrophy, the sarcopenia of aging, or cancer cachexia.

Limitations of the Study

We note several limitations in this study. First, only male mice were examined, at one age and after fixed periods and mode of muscle atrophy. It is possible that female mice or mice of a different age would have different responses to CARM1 mKO, or that different durations of neurogenic disuse, or different models of atrophy (e.g., fasting, unweighting, advanced aging), would differentially impact CARM1-AMPK signaling. Second, we engineered and utilized CARM1 mKO animals to reveal the role of the methyltransferase in skeletal muscle. An inducible CARM1 mKO model, for example, elicited by tamoxifen treatment (McCarthy et al., 2012), would introduce temporal specificity to the removal of CARM1 in muscle and control for any compensatory or confounding adaptations that may have occurred in the animals across a lifetime without the enzyme. Third, the molecular mechanisms of muscle atrophy in humans do not mirror precisely the events that transpire in murine muscle (Atherton et al., 2016). Future work is needed to test and extend the current findings in skeletal muscle from human participants (vanLieshout et al., 2019). Finally, although we demonstrated that CARM1 methylated AMPK in muscle, further research is needed to confirm specific methylation site(s) on the kinase. Other CARM1 targets, as well as the arginine methylome in skeletal muscle, also require identification.

Resource Availability

Lead Contact

Further information and requests for resources and reagents should be directed to and will be fulfilled by the Lead Contact, Dr. Vladimir Ljubicic (ljubicic@mcmaster.ca).

Materials Availability

This study did not generate any unique reagents.

Data and Code Availability

This study did not generate datasets/code.

METHODS

All methods can be found in the accompanying Transparent Methods supplemental file.

SUPPLEMENTAL INFORMATION

Supplemental Information can be found online at https://doi.org/10.1016/j.isci.2020.101755.

ACKNOWLEDGMENTS

We thank Dr. Mark Bedford (MD Anderson Cancer Center, University of Texas) and Dr. Anne Brunet (Department of Genetics, Stanford University School of Medicine) for the gifts of CARM1 floxed mice and the ADMA-5^{CARM1} reagent, as well as the P-FOXO3^{Ser588} antibody, respectively. We also thank Dr. Lawrence Kazak (McGill University, Canada) for assistance with genotyping. We are grateful to members of the Integrative Neuromuscular Biology Laboratory and to colleagues in the Exercise Metabolism Research Group at McMaster University for helpful advice and discussion. This work was funded by the Natural Sciences and Engineering Research Council of Canada (NSERC), the Canada Research Chairs program, and the Ontario Ministry of Economic Development, Job Creation and Trade (MEDJCT). D.W.S., T.L.v., and S.Y.N. are NSERC postgraduate scholars. E.K.W. is an Interdisciplinary Fellow of the Canadian Frailty Network. V.L. is the Canada Research Chair (Tier 2) in Neuromuscular Plasticity in Health and Disease, and is a MEDJCT Early Researcher.

AUTHOR CONTRIBUTIONS

D.W.S. and V.L. conceived and designed the study; D.W.S. and T.L.v. generated and maintained CARM1 mKO mice; D.W.S. performed denervation surgeries, quantitative real-time RT-PCRs, western blot and immunoprecipitation experiments; D.W.S. and Z.M. conducted H&E staining analyses; E.K.W. and A.M. assisted with western blot procedures; D.W.S. and A.M. executed SDH staining technique; S.Y.N. performed MK-8722 experiments; all authors participated in data analysis and interpretation of results; D.W.S. and V.L. drafted and edited the manuscript.

DECLARATION OF INTERESTS

The authors declare no competing interests.

Received: May 15, 2020
Revised: September 28, 2020
Accepted: October 28, 2020
Published: November 20, 2020

REFERENCES

An, W., Kim, J., and Roeder, R.G. (2004). Ordered cooperative functions of PRMT1, p300, and CARM1 in transcriptional activation by p53. Cell *117*, 735–748.

Atherton, P.J., Greenhaff, P.L., Phillips, S.M., Bodine, S.C., Adams, C.M., and Lang, C.H. (2016). Control of skeletal muscle atrophy in response to disuse: clinical/preclinical contentions and fallacies of evidence. Am. J. Physiol. Endocrinol. Metab. *311*, E594–E604.

Bao, J., Rousseaux, S., Shen, J., Lin, K., Lu, Y., and Bedford, M.T. (2018). The arginine methyltransferase CARM1 represses p300●ACT●CREMτ activity and is required for spermiogenesis. Nucleic Acids Res. *46*, 4327–4343.

Bedford, M.T., and Clarke, S.G. (2009). Protein arginine methylation in mammals: who, what, and why. Mol. Cell *33*, 1–13.

Bodine, S.C. (2013). Disuse-induced muscle wasting. Int. J. Biochem. Cell Biol. *45*, 2200–2208.

Bujak, A.L., Crane, J.D., Lally, J.S., Ford, R.J., Kang, S.J., Rebalka, I.A., Green, A.E., Kemp, B.E., Hawke, T.J., Schertzer, J.D., and Steinberg, G.R. (2015). AMPK activation of muscle autophagy prevents fasting-induced hypoglycemia and myopathy during aging. Cell Metab. *21*, 883–890.

Carnio, S., LoVerso, F., Baraibar, M.A., Longa, E., Khan, M.M., Maffei, M., Reischl, M., Canepari, M., Loefler, S., Kern, H., et al. (2014). Autophagy impairment in muscle induces neuromuscular junction degeneration and precocious aging. Cell Rep. *8*, 1509–1521.

Chang, N.C., Sincennes, M.C., Chevalier, F.P., Brun, C.E., Lacaria, M., Segalés, J., Muñoz-Cánoves, P., Ming, H., and Rudnicki, M.A. (2018). The Dystrophin Glycoprotein complex regulates the epigenetic activation of muscle stem cell commitment. Cell Stem Cell *22*, 755–768.e6.

Chen, S.L., Loffler, K.A., Chen, D., Stallcup, M.R., and Muscat, G.E. (2002). The

coactivator-associated arginine methyltransferase is necessary for muscle differentiation: CARM1 coactivates myocyte enhancer factor-2. J. Biol. Chem. *277*, 4324–4333.

Cheng, D., Vemulapalli, V., Lu, Y., Shen, J., Aoyagi, S., Fry, C.J., Yang, Y., Foulds, C.E., Stossi, F., Treviño, L.S., et al. (2018). CARM1 methylates MED12 to regulate its RNA-binding ability. Life Sci. Alliance *1*, e201800117.

Choi, S., Jeong, H.J., Kim, H., Choi, D., Cho, S.C., Seong, J.K., Koo, S.H., and Kang, J.S. (2019). Skeletal muscle-specific Prmt1 deletion causes muscle atrophy via deregulation of the PRMT6-FOXO3 axis. Autophagy *15*, 1069–1081.

Dial, A.G., Ng, S.Y., Manta, A., and Ljubicic, V. (2018). The role of AMPK in neuromuscular biology and disease. Trends Endocrinol. Metab. *29*, 300–312.

Erlich, A.T., Brownlee, D.M., Beyfuss, K., and Hood, D.A. (2018). Exercise induces TFEB expression and activity in skeletal muscle in a PGC-1α-dependent manner. Am. J. Physiol. Cell Physiol. *314*, C62–C72.

Fulton, M.D., Brown, T., and Zheng, Y.G. (2019). The biological Axis of protein arginine methylation and asymmetric dimethylarginine. Int. J. Mol. Sci. *20*, 3322.

Gayatri, S., Cowles, M.W., Vemulapalli, V., Cheng, D., Sun, Z.W., and Bedford, M.T. (2016). Using oriented peptide array libraries to evaluate methylarginine-specific antibodies and arginine methyltransferase substrate motifs. Sci. Rep. *6*, 28718.

Guccione, E., and Richard, S. (2019). The regulation, functions and clinical relevance of arginine methylation. Nat. Rev. Mol. Cell Biol. *20*, 642–657.

Guo, A., Gu, H., Zhou, J., Mulhern, D., Wang, Y., Lee, K.A., Yang, V., Aguiar, M., Kornhauser, J., Jia, X., et al. (2014). Immunoaffinity enrichment and mass spectrometry analysis of protein methylation. Mol. Cell Proteomics *13*, 372–387.

Ha, S., Jeong, S.H., Yi, K., Chung, K.M., Hong, C.J., Kim, S.W., Kim, E.K., and Yu, S.W. (2017). Phosphorylation of p62 by AMP-activated protein kinase mediates autophagic cell death in adult hippocampal neural stem cells. J. Biol. Chem. *292*, 13795–13808.

Halling, J.F., Ringholm, S., Nielsen, M.M., Overby, P., and Pilegaard, H. (2016). PGC-1α promotes exercise-induced autophagy in mouse skeletal muscle. Physiol. Rep. *4*, e12698.

Hardie, D.G., Schaffer, B.E., and Brunet, A. (2016). AMPK: an energy-sensing pathway with multiple inputs and outputs. Trends Cell Biol. *26*, 190–201.

Hood, D.A., Memme, J.M., Oliveira, A.N., and Triolo, M. (2019). Maintenance of skeletal muscle Mitochondria in health, exercise, and aging. Annu. Rev. Physiol. *81*, 19–41.

Imamura, K., Ogura, T., Kishimoto, A., Kaminishi, M., and Esumi, H. (2001). Cell cycle regulation via p53 phosphorylation by a 5′-AMP activated protein kinase activator, 5-aminoimidazole- 4-carboxamide-1-beta-D-ribofuranoside, in a human hepatocellular carcinoma cell line. Biochem. Biophys. Res. Commun. *287*, 562–567.

Jones, R.G., Plas, D.R., Kubek, S., Buzzai, M., Mu, J., Xu, Y., Birnbaum, M.J., and Thompson, C.B. (2005). AMP-activated protein kinase induces a p53-dependent metabolic checkpoint. Mol. Cell *18*, 283–293.

Kawabe, Y., Wang, Y.X., McKinnell, I.W., Bedford, M.T., and Rudnicki, M.A. (2012). Carm1 regulates Pax7 transcriptional activity through MLL1/2 recruitment during asymmetric satellite stem cell divisions. Cell Stem Cell *11*, 333–345.

Kim, D., Lim, S., Park, M., Choi, J., Kim, J., Han, H., Yoon, K., Kim, K., Lim, J., and Park, S. (2014). Ubiquitination-dependent CARM1 degradation facilitates Notch1-mediated podocyte apoptosis in diabetic nephropathy. Cell Signal. *26*, 1774–1782.

Kim, J., Kim, Y.C., Fang, C., Russell, R.C., Kim, J.H., Fan, W., Liu, R., Zhong, Q., and Guan, K.L. (2013). Differential regulation of distinct Vps34 complexes by AMPK in nutrient stress and autophagy. Cell *152*, 290–303.

Kjøbsted, R., Hingst, J.R., Fentz, J., Foretz, M., Sanz, M.N., Pehmøller, C., Shum, M., Marette, A., Mounier, R., Treebak, J.T., et al. (2018). AMPK in skeletal muscle function and metabolism. FASEB J. *32*, 1741–1777.

Larsen, S.C., Sylvestersen, K.B., Mund, A., Lyon, D., Mullari, M., Madsen, M.V., Daniel, J.A., Jensen, L.J., and Nielsen, M.L. (2016). Proteome-wide analysis of arginine monomethylation reveals widespread occurrence in human cells. Sci. Signal. *9*, rs9.

Lee, J., and Bedford, M.T. (2002). PABP1 identified as an arginine methyltransferase substrate using high-density protein arrays. EMBO Rep. *3*, 268–273.

Liu, Y., Li, J., Shang, Y., Guo, Y., and Li, Z. (2019). CARM1 contributes to skeletal muscle wasting by mediating FoxO3 activity and promoting myofiber autophagy. Exp. Cell Res. *374*, 198–209.

Ljubicic, V., Burt, M., and Jasmin, B.J. (2014). The therapeutic potential of skeletal muscle plasticity in Duchenne muscular dystrophy: phenotypic modifiers as pharmacologic targets. FASEB J. *28*, 548–568.

Ljubicic, V., Khogali, S., Renaud, J.M., and Jasmin, B.J. (2012). Chronic AMPK stimulation attenuates adaptive signaling in dystrophic skeletal muscle. Am. J. Physiol. Cell Physiol. *302*, C110–C121.

Mansueto, G., Armani, A., Viscomi, C., D'Orsi, L., De Cegli, R., Polishchuk, E.V., Lamperti, C., Di Meo, I., Romanello, V., Marchet, S., et al. (2017). Transcription factor EB controls metabolic flexibility during exercise. Cell Metab. *25*, 182–196.

Masiero, E., Agatea, L., Mammucari, C., Blaauw, B., Loro, E., Komatsu, M., Metzger, D., Reggiani, C., Schiaffino, S., and Sandri, M. (2009). Autophagy is required to maintain muscle mass. Cell Metab. *10*, 507–515.

McCarthy, J.J., Srikuea, R., Kirby, T.J., Peterson, C.A., and Esser, K.A. (2012). Inducible Cre transgenic mouse strain for skeletal muscle-specific gene targeting. Skelet Muscle *2*, 8.

Milan, G., Romanello, V., Pescatore, F., Armani, A., Paik, J.H., Frasson, L., Seydel, A., Zhao, J., Abraham, R., Goldberg, A.L., et al. (2015). Regulation of autophagy and the ubiquitin-proteasome system by the FoxO transcriptional network during muscle atrophy. Nat. Commun. *6*, 6670.

Mounier, R., Théret, M., Lantier, L., Foretz, M., and Viollet, B. (2015). Expanding roles for AMPK in skeletal muscle plasticity. Trends Endocrinol. Metab. *26*, 275–286.

Muise, E.S., Guan, H.P., Liu, J., Nawrocki, A.R., Yang, X., Wang, C., Rodríguez, C.G., Zhou, D., Gorski, J.N., Kurtz, M.M., et al. (2019). Pharmacological AMPK activation induces transcriptional responses congruent to exercise in skeletal and cardiac muscle, adipose tissues and liver. PLoS One *14*, e0211568.

Myers, R.W., Guan, H.P., Ehrhart, J., Petrov, A., Prahalada, S., Tozzo, E., Yang, X., Kurtz, M.M., Trujillo, M., Gonzalez Trotter, D., et al. (2017). Systemic pan-AMPK activator MK-8722 improves glucose homeostasis but induces cardiac hypertrophy. Science *357*, 507–511.

O'Brien, K.B., Alberich-Jordà, M., Yadav, N., Kocher, O., Diruscio, A., Ebralidze, A., Levantini, E., Sng, N.J., Bhasin, M., Caron, T., et al. (2010). CARM1 is required for proper control of proliferation and differentiation of pulmonary epithelial cells. Development *137*, 2147–2156.

Phillips, S.M., Glover, E.I., and Rennie, M.J. (2009). Alterations of protein turnover underlying disuse atrophy in human skeletal muscle. J. Appl. Physiol. *107*, 645–654.

Sandri, M. (2013). Protein breakdown in muscle wasting: role of autophagy-lysosome and ubiquitin-proteasome. Int. J. Biochem. Cell Biol. *45*, 2121–2129.

Shen, N.Y., Ng, S.Y., Toepp, S.L., and Ljubicic, V. (2018). Protein arginine methyltransferase expression and activity during myogenesis. Biosci. Rep. *38*, 1.

Shin, H.J., Kim, H., Oh, S., Lee, J.G., Kee, M., Ko, H.J., Kweon, M.N., Won, K.J., and Baek, S.H. (2016). AMPK-SKP2-CARM1 signalling cascade in transcriptional regulation of autophagy. Nature *534*, 553–557.

Song, X., Kim, S.Y., Zhang, L., Tang, D., Bartlett, D.L., Kwon, Y.T., and Lee, Y.J. (2014). Role of AMP-activated protein kinase in cross-talk between apoptosis and autophagy in human colon cancer. Cell Death Dis. *5*, e1504.

Steinberg, G.R., and Carling, D. (2019). AMP-activated protein kinase: the current landscape for drug development. Nat. Rev. Drug Discov. *18*, 527–551.

Stouth, D.W., Manta, A., and Ljubicic, V. (2018). Protein arginine methyltransferase expression, localization, and activity during disuse-induced skeletal muscle plasticity. Am. J. Physiol. Cell Physiol. *314*, C177–C190.

Stouth, D.W., vanLieshout, T.L., Shen, N.Y., and Ljubicic, V. (2017). Regulation of skeletal muscle plasticity by protein arginine methyltransferases and their potential roles in neuromuscular disorders. Front Physiol. *8*, 870.

Takikita, S., Schreiner, C., Baum, R., Xie, T., Ralston, E., Plotz, P.H., and Raben, N. (2010). Fiber type conversion by PGC-1α activates lysosomal and autophagosomal biogenesis in both unaffected and Pompe skeletal muscle. PLoS One *5*, e15239.

Vainshtein, A., Grumati, P., Sandri, M., and Bonaldo, P. (2014). Skeletal muscle, autophagy, and physical activity: the ménage à trois of metabolic regulation in health and disease. J. Mol. Med. (Berl) *92*, 127–137.

vanLieshout, T.L., and Ljubicic, V. (2019). The emergence of protein arginine methyltransferases in skeletal muscle and metabolic disease. Am. J. Physiol. Endocrinol. Metab. *317*, E1070–E1080.

vanLieshout, T.L., Bonafiglia, J.T., Gurd, B.J., and Ljubicic, V. (2019). Protein arginine methyltransferase biology in humans during acute and chronic skeletal muscle plasticity. J. Appl. Physiol. *127*, 867–880.

Vanlieshout, T.L., Stouth, D.W., Tajik, T., and Ljubicic, V. (2018). Exercise-induced protein arginine methyltransferase expression in skeletal muscle. Med. Sci. Sports Exerc. *50*, 447–457.

Wang, S.C., Dowhan, D.H., Eriksson, N.A., and Muscat, G.E. (2012). CARM1/PRMT4 is necessary for the glycogen gene expression programme in skeletal muscle cells. Biochem. J. *444*, 323–331.

Yadav, N., Lee, J., Kim, J., Shen, J., Hu, M.C., Aldaz, C.M., and Bedford, M.T. (2003). Specific protein methylation defects and gene expression perturbations in coactivator associated arginine methyltransferase 1-deficient mice. Proc. Natl. Acad. Sci. U S A *100*, 6464–6468.

Yamagata, K., Daitoku, H., Takahashi, Y., Namiki, K., Hisatake, K., Kako, K., Mukai, H., Kasuya, Y., and Fukamizu, A. (2008). Arginine methylation of FOXO transcription factors inhibits their phosphorylation by Akt. Mol. Cell *32*, 221–231.

Yang, Y., and Bedford, M.T. (2013). Protein arginine methyltransferases and cancer. Nat. Rev. Cancer *13*, 37–50.

Zhang, D., Wang, W., Sun, X., Xu, D., Wang, C., Zhang, Q., Wang, H., Luo, W., Chen, Y., Chen, H., and Liu, Z. (2016). AMPK regulates autophagy by phosphorylating BECN1 at threonine 388. Autophagy *12*, 1447–1459.

iScience, Volume *23*

Supplemental Information

CARM1 Regulates AMPK Signaling in Skeletal Muscle

Derek W. Stouth, Tiffany L. vanLieshout, Sean Y. Ng, Erin K. Webb, Alexander Manta, Zachary Moll, and Vladimir Ljubicic

Supplemental Information

Transparent Methods

Animals and genotyping

We utilized the Cre/loxP system to generate skeletal muscle-specific CARM1 knockout (mKO) mice. CARM1 floxed animals (Yadav *et al*., 2003; Bao *et al.,* 2018) were a kind gift from Dr. Mark Bedford (The University of Texas MD Anderson Cancer Centre, Smithville, TX, USA). Floxed CARM1 mice (wild type; WT) were generated as described previously in the mixed C57BL6J/129 background. Human α-skeletal actin (HSA)-Cre mice were obtained from Jackson Laboratories (Bar Harbor, ME, USA). HSA-Cre activity is restricted to skeletal muscle (McCarthy *et al.,* 2012). WT and mKO mice were identified via genotyping, using conventional reverse transcription-polymerase chain reaction (RT-PCR) and gel electrophoresis techniques of DNA extracted from tail tissue. The following primers were used to confirm that WT and mKO mice contained a LoxP site for CARM1 between exon 2 and 3: forward (F)-AGTTGGTGACCCTTGTGTCC, reverse (R)-AGCTGCCAGGACCTCTGATA. The following primers were used to distinguish mKO mice that express Cre recombinase: F-GCGGTCTGGCAGTAAAAACTATC, R-GTGAAACAGCATTGCTGTCACTT. For these studies, 12-week-old WT and mKO mice (~25 g body mass; male) were housed in an environmentally controlled room (23 °C, 12-hour light/12-hour dark cycle) and provided food and water ad libitum. Animals were housed at the Central Animal Facility at McMaster University and all protocols were approved by the University Animal Research Ethics Board operating under the auspices of the Canadian Council for Animal Care.

Animal surgery

To elicit denervation-induced skeletal muscle atrophy, WT and mKO mice underwent unilateral sectioning of the sciatic nerve as described previously (Stouth et al. 2018). This model of acquired neurogenic muscle disuse evokes a rapid, robust, and reproducible remodeling of skeletal muscle, while also allowing for the use of the contralateral, innervated limb to serve as an intra-animal control (Sacheck et al. 2007). Briefly, animals were anesthetized by inhalation of isoflurane (Fresenius Kabi, Bad Homburg, HE, Germany) before surgery and received a 2 mg/kg subcutaneous injection of anafen (Boehringer Ingelheim (Canada) Ltd., Burlington, ON, Canada) for post-operative analgesia. A 1-2 cm skin incision was made in the posterior thigh musculature and blunt dissection was employed to expose the sciatic nerve. Unilateral denervation of the lower limb was induced by excising a ~0.5 cm section of the sciatic nerve in the right hind limb. The overlying musculature was sutured with silk (Ethicon Inc., Somerville, NJ, USA), and the skin was secured using veterinary staples (Mikron Precision Inc., Gardena, CA, USA). WT and mKO mice were subjected to 3 and 7 days of denervation (n = 17-20/ group) followed by euthanasia via cervical dislocation. At each experimental time point, the tibialis anterior (TA), extensor digitorum longus (EDL), soleus (SOL), and gastrocnemius (GAST) muscles from both hind limbs were rapidly excised, weighed, frozen in liquid nitrogen or mounted in optimum cutting temperature compound (Thermo Fisher Scientific Life Sciences, Waltham, MA, USA) then frozen in isopentane cooled with liquid

nitrogen. All muscles were then stored at -80 °C for biochemical analyses. Liver, brain, and heart tissues were also harvested from a small cohort of WT and mKO mice for subsequent analysis of tissue-specific CARM1 expression.

Pharmacological activation of AMPK

A separate cohort of age- and sex-matched WT and mKO animals were treated with vehicle [0.25% (w/v) methylcellulose, 5% (v/v) Polysorbate 80, and 0.02% (w/v) sodium lauryl sulfate in deionized water; Veh] or the next-generation AMPK activator MK-8722 (5 mpk) via oral gavage (n = 6-9/ group), as described previously (Myers et al., 2017). Animals were euthanized via cervical dislocation 3 hours after administration, a time point that corresponds to significantly augmented AMPK site-specific phosphorylation of acetyl–coenzyme A carboxylase (ACC) in skeletal muscle (Myers et al., 2017). The TA and EDL muscles were snap frozen in liquid nitrogen. All tissues were then stored at -80 °C for subsequent biochemical analyses.

Histological analysis

EDL and SOL muscle cross-sections were stained with hematoxylin and eosin (H&E) to assess cross-sectional area (CSA) of individual muscle fibers as described previously (Manta et al. 2019). Briefly, EDL and SOL muscles were first transversely sectioned at 5 μm using a cryostat set at -20°C (Thermo Fisher Scientific Life Sciences, Waltham, MA, USA). Muscle cross-sections were later stained with hematoxylin (Sigma-Aldrich, St. Louis, MO, USA) and eosin (Bioshop Canada Inc., Burlington, ON, Canada), dehydrated with successive 70%, 95%, and 100% ethanol exposures, further dried with xylene (Sigma-Aldrich, St. Louis, MO, USA) and mounted with Permount (Thermo Fisher Scientific Life Sciences, Waltham, MA, USA). H&E-stained muscle sections were imaged using light microscopy at 20x magnification with Nikon Elements Microscopic Imaging Software (Nikon Instruments Inc, Melville, NY, USA). The CSA of 150 myofibers across three individual regions of interest per muscle were measured (NIS-Elements). The investigators performing the image analyses were blinded to all samples (i.e., genotype, treatment, muscle).

EDL muscles were cryosectioned into 8 μm sections and stained for succinate dehydrogenase (SDH) activity as described previously (Thomas et al., 2014). Muscle sections were incubated in a buffer consisting of 0.2 M sodium succinate, 0.2 M phosphate buffer, pH 7.4, and nitro blue tetrazolium (Sigma-Aldrich, St. Louis, MO, USA) at 37°C for one hour. Following the incubation period, muscles were rinsed with distilled water, exposed to 30%, 60%, 90% acetone, and mounted with Permount (Thermo Fisher Scientific Life Sciences, Waltham, MA, USA). Photos of muscle sections were then taken using light microscopy at 20x magnification with Nikon Elements Microscopic Imaging Software (Nikon Instruments Inc, Melville, NY, USA).

RNA isolation and quantitative real-time (q) RT-PCR

Total RNA was isolated from the EDL and SOL muscles as described previously (Stouth et al. 2018). All samples were homogenized in 1 mL of Trizol reagent (Invitrogen, Carlsbad, CA, USA) using stainless steel lysing beads and TissueLyser (Qiagen, Hilden, NRW, Germany) at a frequency of 30 Hz for 5 minutes. Homogenized

samples were then mixed with 200 µL of chloroform (Thermo Fisher Scientific, Waltham, MA, USA), agitated vigorously for 15 seconds and centrifuged at 12,000 x g for 10 minutes. The upper aqueous (RNA) phase was purified using the Total RNA Omega Bio-Tek kit (VWR International, Radnor, PA, USA) as per the instructions provided by the manufacturer. RNA concentration and purity were determined using the NanoDrop 1000 Spectrophotometer (Thermo Fisher Scientific Life Sciences,Waltham, MA, USA). RNA samples were then reverse-transcribed into cDNA using a high-capacity cDNA reverse transcription kit (Thermo Fisher Scientific Life Sciences,Waltham, MA, USA) according to the manufacturer instructions. All individual qRT-PCRs were run in duplicate 6 µL reactions containing GoTaq qPCR Master Mix (Promega, Madison, WI, USA). Data were analyzed using the comparative C_T method (Schmittgen et al. 2008). TATA box-binding protein (TBP) was used as a control housekeeping gene for all experiments, as the C_T values for this gene did not change between non-denervated and denervated muscles within, as well as between, time points (data not shown). This control C_T value was subtracted from the C_T value of the gene of interest [$\Delta C_T = C_{T\ (target\ gene)} - C_{T\ (endogenous\ control)}$]. For our denervation experiment, the mean ΔC_T value from the contralateral, non-denervated control (CON) WT muscle was then subtracted from the ΔC_T values of the denervated (DEN) WT muscle [$\Delta\Delta C_T = \Delta C_{T\ (WT\ DEN)} - C_{T\ (WT\ CON)}$]. This calculation was then repeated for CON and DEN mKO limbs. For the MK-8722 pharmacological intervention, the mean ΔC_T value for the WT Veh group was subtracted from the ΔC_T values of the mKO Veh, WT MK-8722, and mKO MK-8722 treated animals. Results are reported as fold changes using the $\Delta\Delta C_T$ method, calculated as $2^{-\Delta\Delta CT}$.

The following primers were used in our study: CARM1 F-CAACAGCGTCCTCATCCAGT, R-GTCCGCTCACTGAACACAGA; silent mating type information regulator 2 homologue 1 (SIRT1) F-GGAACCTTTGCCTCATCTACA, R-CACCTAGCCTATGACACAACTC; peroxisome proliferator-activated receptor-γ coactivator-1α (PGC-1α) F-AGCCGTGACCAGTGACAACGAG, R-GCTGCATGGTTCTGAGTGCTAAG; tumor-suppressor protein p53 F-CCGACCTATCCTTACCATCATC, R-TTCTTCTGTACGGCGGTCTC; mitochondrial transcription factor A (Tfam) F-TAGGCACCGTATTGCGTGAG, R- GTGCTTTTAGCACGCTCCAC; nuclear factor erythroid 2-related factor 2 (Nrf2) F-TTCTTTCAGCAGCATCCTCTCCAC, R-ACAGCCTTCAATAGTCCCGTCCAG; p62 F-CCCAGTGTCTTGGCATTCTT, R-AGGGAAAGCAGAGGAAGCTC; Beclin1 F-AGGCTGAGGCGGAGAGATT, R- TCCACACTCTTGAGTTCGTCAT; transcription factor EB (TFEB) F-AAGGTTCGGGAGTATCTGTCTG, R-GGGTTGGAGCTGATATGTAGCA; Gabarapl F-CATCGTGGAGAAGGCTCCTA, R-ATACAGCTGGCCCATGGTAG; Cathepsin L F-GTGGACTGTTCTCACGCTCAAG, R-TCCGTCCTTCGCTTCATAGG, lysosomal-associated membrane protein 2 (Lamp2) F-GCTGAACAACAGCCAAATTA, R-CTGAGCCATTAGCCAAATACAT, BCL2 and adenovirus E1B 19-kDa-interacting protein 3 (Bnip3) F-TTCCACTAGCACCTTCTGATGA, R-GAACACCGCATTTACAGAACAA, muscle RING finger 1 (MuRF1) F-CACGTGTGAGGTGCCTACTT, R-

CACCAGCATGGAGATGCAGT, muscle atrophy F-box (MAFbx) F-TGAGCGACCTCAGCAGTTAC, R-ATGGCGCTCCTTCGTACTTC; TBP F-CTGCCACACCAGCTTCTGA, R-TGCAGCAAATCGCTTGGG.

Tissue extracts and Western blotting

Samples were processed as described previously (Stouth et al. 2018). Briefly, frozen TA muscle, heart, liver, and brain were ground to a powder using a porcelain mortar and pestle on liquid nitrogen. Samples were suspended in RIPA buffer (Sigma-Aldrich, St. Louis, MO, USA), supplemented with cOmplete Mini Protease Inhibitor Cocktail (Sigma-Aldrich, St. Louis, MO, USA) and PhosSTOP Phosphatase Inhibitor Cocktail (Sigma-Aldrich, St. Louis, MO, USA). All samples were further homogenized using stainless steel lysing beads and TissueLyser (Qiagen, Hilden, NRW, Germany) at a frequency of 30 Hz for 5 minutes. The lysates were then mixed by end-over end inversion for 60 minutes at 4 °C followed by centrifugation at 14,000 x g for 10 minutes. The supernatants were snap-frozen in liquid nitrogen, and stored at -80 °C for further analysis. The protein concentrations of the supernates were determined using the BCA protein assay (Thermo Fisher Scientific Life Sciences,Waltham, MA, USA). Proteins extracted were resolved on 10-12.5% SDS-PAGE gels or 4-15% precast gradient gels (Bio-Rad Laboratories, Inc., Hercules, CA, USA) and subsequently transferred onto nitrocellulose membranes. After transfer, membranes were stained with Ponceau S solution (Sigma-Aldrich, St. Louis, MO, USA) in order to serve as a loading control (Stouth et al. 2018, Manta et al. 2019, Romero-Calvo et al. 2010). Membranes were washed with 1 x TBST and blocked with 5% milk-TBST or 5% BSA-TBST for one hour before being incubated in a primary antibody overnight at 4 °C with gentle rocking.

We employed antibodies against CARM1 (1:5,000; A300-421A; Bethyl Laboratories, Montgomery, TX, USA), PRMT1 (1:5,000; 07-404; EMD Millipore, Darmstadt, HE, Germany), PRMT5 (1:1,000; 07-405; EMD Millipore, Darmstadt, HE, Germany), MMA (1:1,000; 8015S; Cell Signaling, Danvers, MA, USA), ADMA at glycine and arginine-rich sequences [denoted as $ADMA^{GAR}$ (vanLieshout *et al.* 2019); 1:1,000; 13522; Cell Signaling, Danvers, MA, USA], ADMA-CARM1 motif [denoted as $ADMA\text{-}5^{CARM1}$ (Cheng *et al.* 2018; vanLieshout *et al.* 2019); 1:1,000; another gift from Dr. Mark Bedford, MD Anderson Cancer Center, University of Texas], and SDMA (1:1,000; 13222; Cell Signaling, Danvers, MA, USA) to examine PRMT expression and function. Antibodies against phosphorylated $AMPK^{Thr172}$ (1:1,000; 2535S; Cell Signaling, Danvers, MA, USA), AMPK (1:1,000; 2532S; Cell Signaling, Danvers, MA, USA), phosphorylated ACC^{Ser79} (1:1,000; 3661S; Cell Signaling, Danvers, MA, USA), ACC (1:1,000, 3676S; Cell Signaling, Danvers, MA, USA), PGC-1α (1:200; AB3242; EMD Millipore, Darmstadt, HE, Germany), p53 (1:1,000; 2524S; Cell Signaling, Danvers, MA, USA), and total OXPHOS (1:1,000; ab110413; Abcam, Cambridge, UK) were used to investigate intracellular signalling molecules that regulate the phenotype of skeletal muscle. Antibodies against phosphorylated $ULK1^{Ser555}$ (1:1,000; 5869S; Cell Signaling, Danvers, MA, USA), ULK1 (1:1,000; 8054S; Cell Signaling, Danvers, MA, USA), phosphorylated $FOXO1^{Ser256}$ (1:1,000; 9461S; Cell Signaling, Danvers, MA, USA), FOXO1 (1:1,000; 2880S; Cell Signaling, Danvers, MA, USA), phosphorylated $FOXO3^{Ser588}$ (a kind gift from Dr. Anne Brunet, Department

of Genetics, Stanford University School of Medicine), FOXO3 (1:1,000; 2497S; Cell Signaling, Danvers, MA, USA), p62 (1:1,000; P0067; Sigma-Aldrich, St. Louis, MO, USA), Beclin-1 (1:1,000; 3738S; Cell Signaling, Danvers, MA, USA), TFEB (1:1,000; 4240S; Cell Signaling, Danvers, MA, USA), MuRF1 (1:200; AF5366; R&D Systems, Minneapolis, MN, USA), ubiquitin (1:500; 3933S; Cell Signaling, Danvers, MA, USA), and microtubule-associated protein 1A/1B-light chain 3 (LC3; 1:1,000; 4108S; Cell Signaling, Danvers, MA, USA) were used to identify important markers of the skeletal muscle atrophy program. Antibodies against phosphorylated TBC1D1^{Ser700} (1:1,000; 6929S; Cell Signaling, Danvers, MA, USA) and TBC1D1 (1:1,000; 4629S; Cell Signaling, Danvers, MA, USA) were also employed to assess AMPK activity following acute MK-8722 administration. After overnight incubation in primary antibody, blots were washed with 1 x TBST and incubated in the appropriate secondary antibody (1:2,000; 7074S; Cell Signaling, Danvers, MA, USA) coupled to horseradish peroxidase with gentle rocking at room temperature for one hour. Blots were then washed again with 1 x TBST, followed by visualization with enhanced chemiluminescence (G00069; GE Healthcare Bio-Sciences, Chicago, IL, USA). Blots were developed and analyzed using ImageJ.

Immunoprecipitation (IP)

IP experiments were performed as described previously (Stouth et al. 2018, Philp et al. 2011). Only TA muscles from WT animals were used for IP of CARM1, whereas cohorts of WT and mKO mice were employed for IP of AMPK. For all IP experiments, 200 µg of protein was precleared with 50 µl of protein A agarose suspension (IP02; EMD Millipore, Darmstadt, HE, Germany) and 1 µg of rabbit Immunoglobulin G (IgG; 12-370; EMD Millipore, Darmstadt, HE, Germany). The lysate was mixed by end-over end inversion for 60 minutes at 4 °C followed by centrifugation at 12,000 x g for 10 minutes. Precleared lysate was then rotated by end-over end inversion for 2 hours at 4 °C with either anti-CARM1 (1:100; A300-421A; Bethyl Laboratories, Montgomery, TX, USA) or anti-AMPK (1:100; 2532S; Cell Signaling, Danvers, MA, USA). Next, 50 µl of protein A agarose suspension was added and the samples were mixed by end-over end inversion overnight at 4 °C. The following morning, agarose beads were washed five times with 500 µl of 1 x PBS and centrifugation at 12,000 x g. After suspending each agarose bead complex with equal volumes of 2 x SDS sample buffer (50 µl), samples were boiled for 5 min and centrifuged at 12,000 g for 1 minute. After spinning, only the supernatants were saved for SDS-PAGE (6 µl) separation.

Statistical Analyses

All statistical measures were performed on the raw data sets prior to conversion to the –fold difference values displayed in the graphical summaries. A two-way analysis of variance (ANOVA) was employed to assess the interaction between genotype and muscle for CARM1 mRNA content. A one-way ANOVA was used to evaluate CARM1 protein content in disparate WT muscles. A Student's t test was implemented to assess CARM1 protein content in WT versus mKO heart muscles, as well as to compare body weights and heart weights between genotypes. At each experimental time point in the denervation experiment, a two-way ANOVA was applied to

examine the interaction between genotype and denervation for muscle weight, myofiber CSA, mRNA expression, and protein content. A Student's t test was used to detect differences between DEN and contralateral CON hindlimbs at each time point for CARM1 protein content, as well as the IP experiment of CARM1 in WT mice only. A two-way ANOVA was employed to assess the interaction between genotype and denervation for the IP experiment of AMPK in WT and mKO animals. For the MK-8722 pharmacological study, a two-way ANOVA was also used to examine the interaction between genotype and MK-8722 treatment for mRNA expression and protein content. Tukey post hoc tests were used where appropriate. Data are means ± SEM. Statistical differences were considered significant if $p < 0.05$.

References

Bao, J., Rousseaux, S., Shen, J., Lin, K., Lu, Y. and Bedford, M.T. (2018). The arginine methyltransferase CARM1 represses p300•ACT•CREMτ activity and is required for spermiogenesis. Nucleic Acids Res., 46(9), 4327-4343.

Manta, A., Stouth, D.W., Xhuti, D., Chi, L., Rebalka, I.A., Kalmar, J.M., Hawke, T.J. and Ljubicic, V. (2019). Chronic exercise mitigates disease mechanisms and improves muscle function in myotonic dystrophy type 1 mice. J Physiol., 597(5), 1361-1381.

McCarthy, J.J., Srikuea, R., Kirby, T.J., Peterson, C.A. and Esser, K.A. (2012). Inducible Cre transgenic mouse strain for skeletal muscle-specific gene targeting. Skelet Muscle. 2(1), 8.

Myers, R.W., Guan, H.P., Ehrhart, J., Petrov, A., Prahalada, S., Tozzo, E., Yang, X., Kurtz, M.M., Trujillo, M., Gonzalez, Trotter, D., Feng, D., Xu, S., Eiermann, G., Holahan, M.A., Rubins, D., Conarello, S., Niu, X., Souza, S.C., Miller, C., Liu, J., Lu, K., Feng, W., Li, Y., Painter, R.E., Milligan, J.A., He, H., Liu, F., Ogawa, A., Wisniewski, D., Rohm, R.J., Wang, L., Bunzel, M., Qian, Y., Zhu, W., Wang, H., Bennet, B., LaFranco, Scheuch, L., Fernandez, G.E., Li, C., Klimas, M., Zhou, G., van Heek, M., Biftu, T., Weber, A., Kelley, D.E., Thornberry, N., Erion, M.D., Kemp, D.M. and Sebhat, I.K. (2017). Systemic pan-AMPK activator MK-8722 improves glucose homeostasis but induces cardiac hypertrophy. Science. 357(6350), 507-511.

Philp, A., Chen, A., Lan, D., Meyer, G.A., Murphy, A.N., Knapp, A.E., Olfert, I.M., McCurdy, C.E., Marcotte, G.R., Hogan, M.C., Baar, K. and Schenk, S. (2011). Sirtuin 1 (SIRT1) deacetylase activity is not required for mitochondrial biogenesis or peroxisome proliferator-activated receptor-gamma coactivator-1alpha (PGC-1alpha) deacetylation following endurance exercise. J Biol Chem. 286(35), 30561-70.

Romero-Calvo, I., Ocón, B., Martínez-Moya, P., Suárez, M.D., Zarzuelo, A., Martínez-Augustin, O. and de Medina, F.S. (2010). Reversible Ponceau staining as a loading control alternative to actin in Western blots. Anal Biochem. 401(2), 318-20.

Sacheck, J.M., Hyatt, J.P., Raffaello, A., Jagoe, R.T., Roy, R.R., Edgerton, V.R., Lecker, S.H. and Goldberg, A.L. (2007). Rapid disuse and denervation atrophy involve transcriptional changes similar to those of muscle wasting during systemic diseases. FASEB J., 21(1), 140-55.

214 Schmittgen, T.D. and Livak, K.J. (2008). Analyzing real-time PCR data by the comparative C(T) method. Nat
215 Protoc. 3(6), 1101-8.
216
217 Stouth, D.W., Manta, A. and Ljubicic, V. (2018). Protein arginine methyltransferase expression, localization, and
218 activity during disuse-induced skeletal muscle plasticity. Am J Physiol Cell Physiol., 314(2), C177-C190.
219
220 Thomas, M.M., Trajcevski, K.E., Coleman, S.K., Jiang, M., Di Michele, J., O'Neill, H.M., Lally, J.S., Steinberg,
221 G.R., and Hawke, T.J. (2014). Early oxidative shifts in mouse skeletal muscle morphology with high-fat diet
222 consumption do not lead to functional improvements. Physiological reports, 2(9), e12149.
223
224 Yadav, N., Lee, J., Kim, J., Shen, J., Hu, M.C., Aldaz, C.M. and Bedford, M.T. (2003). Specific protein
225 methylation defects and gene expression perturbations in coactivator associated arginine methyltransferase 1-
226 deficient mice. Proc Natl Acad Sci USA., 100(11), 6464-8.

Chapter 3:

Skeletal muscle-specific CARM1 deletion hinders autophagy flux and prevents fasting-induced atrophy

Skeletal muscle-specific CARM1 deletion hinders autophagy flux and prevents fasting-induced atrophy

Derek W. Stouth,[1] Tiffany L. vanLieshout,[1] Sean Y. Ng,[1] Andrew Mikhail,[1] Erin K. Webb,[1] Kevin S. Gilotra,[1] Matthew Markou,[1] Hannah C. Pineda,[1] Brianna G. Bettencourt-Mora,[1] Haleema Noor,[1] Zachary Moll,[1] Megan E. Bittner,[1] and Vladimir Ljubicic[1,*]

[1]Department of Kinesiology, McMaster University, Hamilton, Ontario, L8S 4L8, Canada

*Correspondence: Tel: 905 525 9140 ext. 24517; Email: ljubicic@mcmaster.ca

Abstract

Coactivator-associated arginine methyltransferase 1 (CARM1) has recently surfaced as a critical regulator of skeletal muscle remodeling. Although CARM1 has been shown to regulate the master neuromuscular phenotypic modifier AMP-activated protein kinase (AMPK) in muscle, the molecular mechanisms by which the methyltransferase modulates muscle plasticity are still nascent. The purpose of this study was to investigate the function of CARM1 within autophagy and atrophy networks during fasting-evoked muscle wasting. We show that CARM1 is required to maintain muscle mass. Furthermore, CARM1 skeletal muscle-specific knockout (mKO) prevents muscle loss during food deprivation. CARM1 deletion resulted in dysregulated autophagic and atrophic signaling downstream of AMPK following fasting. CARM1 mKO altered mitochondrial function, plus markers of mitophagy such as the accumulation of Parkin puncta after food deprivation. We also provide evidence that CARM1 influences autophagy flux, as well as the myonuclear localization of factors important for autophagy and muscle atrophy such as transcription factor EB and Forkhead box O3. Overall, the results demonstrate that CARM1 is required for proper propagation of autophagy during fasting-induced muscle wasting. This study advances our understanding of the role of CARM1 in governing autophagic and atrophic processes crucial for the maintenance and remodeling of muscle mass.

Keywords: Coactivator-associated arginine methyltransferase 1, skeletal muscle, autophagy, atrophy, AMP-activated protein kinase, fasting, mitochondria, mitophagy.

Introduction

Coactivator-associated arginine methyltransferase 1 (CARM1) is a member of the protein arginine methyltransferase (PRMT) family and catalyzes the transfer of methyl groups to arginine residues on target proteins, thereby controlling the stability, localization, and/or activity of marked substrates (Bedford and Clarke, 2009; Yang and Bedford, 2013; Fulton et al., 2019; Guccione and Richard, 2019). Importantly, the occurrence of this post-translational modification is comparable to that of phosphorylation and ubiquitination (Larsen et al., 2016). All nine PRMTs initially deposit the monomethylarginine (MMA) mark on their target molecules. Type I (i.e., PRMT1, PRMT2, PRMT3, CARM1, PRMT6, PRMT8) and type II (i.e., PRMT5, PRMT9) PRMTs subsequently generate asymmetric dimethylarginine (ADMA) and symmetric dimethylarginine (SDMA) marks, respectively. Type III (i.e., PRMT7) only monomethylate. CARM1 is ubiquitously expressed and whole-body genetic deletion of CARM1 results in mice that die perinatally (Yadav et al., 2003). There is also a propensity for CARM1 to methylate proline-rich motifs of histone and non-histone proteins (Cheng et al., 2018). As such, CARM1 regulates diverse cellular processes such as signal transduction, DNA repair, transcriptional control, mRNA splicing, and cell cycle progression, among others.

The involvement of CARM1 in skeletal muscle biology has recently received a great deal of attention. Previous work from our laboratory suggests that this methyltransferase is a critical regulator of skeletal muscle plasticity (Ljubicic et al., 2012; Stouth et al., 2017; Stouth et al., 2018; vanLieshout et al., 2018; Shen et al., 2018; vanLieshout et al., 2019; vanLieshout and Ljubicic, 2019; Stouth et al., 2020). Indeed, as

the most abundant PRMT expressed in skeletal muscle (Wang et al., 2012; vanLieshout et al., 2019), CARM1 maintains muscle mass (Stouth et al., 2020). CARM1 also regulates myogenesis during development and regeneration, along with glycogen metabolism (Chen et al., 2002; Kawabe et al., 2012; Wang et al., 2012; Chang et al., 2018). Notably, CARM1 influences the autophagy-lysosome and ubiquitin-proteasome systems in skeletal muscle (Liu et al., 2019; Stouth et al., 2020). For instance, transient knockdown of CARM1 attenuates the expression of autophagy and atrophy-related genes following neurogenic muscle disuse (Liu et al., 2019). Like the transient knockdown approach, muscle-specific deletion of CARM1 also mitigates the progression of denervation-induced muscle atrophy (Stouth et al., 2020). Together, these studies suggest that CARM1 governs skeletal muscle phenotypic maintenance and remodeling.

There are few studies that have investigated the molecular mechanism by which CARM1 impacts autophagy-lysosome and ubiquitin-proteasome signaling in muscle. This evidence, although limited, supports the assertion that CARM1 promotes AMP-activated protein kinase (AMPK)-mediated protein degradation (Stouth et al., 2020). In this study, we sought to further elucidate the molecular mechanisms whereby CARM1 controls the maintenance and remodeling of muscle phenotype. We selected fasting as an atrophy model since the autophagy-lysosome and ubiquitin-proteasome systems are activated (Sandri, 2013). Prolonged food deprivation also elicits dramatic changes to the mitochondrial network. As such, we employed CARM1 skeletal muscle-specific knockout (mKO) mice to test the hypothesis that CARM1 contributes to autophagic, and atrophic processes involved in fasting-induced muscle wasting.

Results

Skeletal muscle-specific deletion of CARM1 attenuates progression of fasting-induced atrophy. We previously generated CARM1 mKO mice to investigate the function of CARM1 during neurogenic muscle disuse (Stouth et al. 2020). Similar to a transient knockdown approach (Liu et al. 2019), knockout of CARM1 in muscle blunted denervation-induced muscle wasting (Stouth et al. 2020). Since the impact of CARM1 on muscle wasting during food deprivation remains unclear, we sought to employ mKO animals to study the role of CARM1 during fasting-induced muscle atrophy. Immunoblot analysis confirmed deletion of CARM1 in skeletal muscle (Figure 1A). Compared to fed conditions, CARM1 protein and mRNA expression levels were similar in the tibialis anterior (TA) and extensor digitorum longus (EDL) muscles, respectively, following 24 and 48 hours of food deprivation (Figure 1A-C). CARM1 transcript levels were significantly elevated by 2-fold after 24 hours of fasting in the soleus (SOL) muscle (data not shown).

We observed main effects ($p < 0.05$) of genotype and fasting for body mass (Figure 1D). For instance, body mass was 5% lower ($p < 0.05$) in mKO versus wild-type (WT) mice under fed conditions. Food deprivation induced a significant ~10% and ~20% decrease in body mass after 24 and 48 hours, respectively, in both genotypes relative to their respective fed littermates. The relative decline in body mass between fed and 48 hour fasted conditions trended lower in mKO versus WT animals ($p = 0.06$). A main effect ($p < 0.05$) of fasting on muscle mass was observed in the TA, EDL, SOL, and gastrocnemius (GAST; Figure 1E). When compared to WT fed animals, TA muscle mass was significantly

reduced by ~15% in WT mice after 48 hours of fasting. No significant changes in TA muscle mass were detected in mKO animals under fed versus fasting conditions. The relative reduction in EDL muscle mass between fed and 48 hour fasted trended less in mKO versus WT mice ($p = 0.09$), whereas the relative decline in SOL muscle mass was similar between genotypes. Furthermore, a significant main effect of genotype was noted on GAST muscle mass and a significant interaction between genotype and fasting was also found. Relative to the WT fed group, GAST muscle mass decreased by 20% ($p < 0.05$) in WT animals after 48 hours of food deprivation. GAST muscle mass was also significantly lower by 20% in mKO versus WT mice under fed settings. Moreover, GAST muscle mass did not differ between fed and fasted mKO animals. We also detected a significant statistical interaction between genotype and fasting for EDL myofiber cross-sectional area (CSA; Figure 1F, H). Relative to the WT fed group, food deprivation elicited a ~30% decrease ($p < 0.05$) in EDL CSA after 48 hours, which was not observed in the absence of CARM1. SOL myofiber CSA was similar between all groups (Figure 1G, I).

PRMT content and activity are altered in mKO mice after food deprivation. We desired to determine whether knocking out CARM1 in muscle evoked changes in other PRMTs in response to fasting. Here, we assessed mRNA in EDL and SOL muscles, plus protein content in TA muscles for PRMT1, PRMT5, PRMT6, and PRMT7 in WT and mKO animals following food deprivation. We observed a main effect ($p < 0.05$) of fasting on PRMT6 mRNA content in the EDL (Figure 2A). In contrast, PRMT1, PRMT5, and PRMT7 transcript levels were similar in all experimental conditions. Main effects ($p < 0.05$) of fasting and genotype were observed for PRMT5 and PRMT7 transcript levels, respectively,

in the SOL muscle (data not shown). We also detected a significant main effect of genotype on PRMT1 and PRMT6 protein content, whereas PRMT5 and PRMT7 did not change (Figure 2B, C).

We next examined markers of global type I and type II PRMT activities, such as MMA, ADMA, and SDMA (Bedford and Clarke, 2009; Yang and Bedford, 2013). We also assessed asymmetric arginine dimethylation of pan-CARM1-marked substrates (Cheng et al. 2018; Cheng et al., 2020), along with bona fide CARM1 targets SWI/SNF chromatin remodeling complex BAF155 (BAF155me2a^{Arg1064}), and poly(A)-binding protein 1 (PABP1me2a$^{Arg455/Arg460}$). We observed a main effect ($p < 0.05$) of genotype on CARM1 substrate methylargine content (Figure 2B, D). Specifically, relative to the WT fed group, CARM1 deletion resulted in a significant ~45% decrease in CARM1 substrate arginine methylation levels under fed and fasted settings. MMA, ADMA, and SDMA content were similar between genotypes with food deprivation. We detected significant main effects of genotype and fasting for BAF155me2a^{Arg1064} (Figure 2B, E). Food deprivation induced a 40% decrease ($p < 0.05$) in BAF155me2a^{Arg1064} in WT mice after 48 hours relative to their WT fed littermates. Compared to WT fed mice, BAF155me2a^{Arg1064} was significantly lower by ~70% in fed and fasted mKO animals. Total BAF155 protein content was similar between all groups. A significant main effect of genotype on BAF155 activation status (i.e., the methylated form of the protein relative to its total, unmethylated content) was also observed. Main effects ($p < 0.05$) of genotype and fasting were noted on PABP1me2a$^{Arg455/Arg460}$ and a significant interaction between genotype and fasting was detected (Figure 2B, F). Relative to WT fed mice, PABP1me2a$^{Arg455/Arg460}$ significantly

decreased by ~50% in WT animals in response to 24 and 48 hours of food deprivation. PABP1me2a$^{Arg455/Arg460}$ was also lower by ~65% ($p < 0.05$) in fed and fasted mKO muscle versus fed WT mice. Tukey post-hoc analyses revealed similar levels of PABP1me2a$^{Arg455/Arg460}$ in mKO animals between fed and fasted muscle. We observed a significant main effect of fasting on total PABP1 protein content. Furthermore, a main effect ($p < 0.05$) of genotype on PABP1 activation status was detected. Compared to the WT fed group, PABP1 activation status was significantly lower by 60% in mKO mice during fed and fasted conditions.

CARM1 influences metabolic signaling during fasting-induced muscle wasting. Previous work has shown that CARM1 deletion in muscle affects the expression and/or activity of molecules involved in metabolic signaling during neurogenic muscle disuse (Stouth et al. 2020). We wished to determine whether CARM1 was important for metabolic signaling in response to food deprivation. As such, we first assessed peroxisome proliferator-activated receptor-γ coactivator-1α (PGC-1α), mitochondrial transcription factor A (Tfam), and nuclear factor erythroid 2-related factor 2 (Nrf2) transcript levels in EDL and SOL muscles from fed and fasted WT and mKO mice. A significant main effect of genotype on PGC-1α, Tfam, and Nrf2 mRNA content was detected in the EDL muscle (Figure 3A). A main effect ($p < 0.05$) of fasting on Nrf2 transcript levels was also observed in the EDL. Relative to the WT fed group, food deprivation induced a significant 2-fold increase in Nrf2 mRNA content after 24 hours in WT animals. Nrf2 transcript levels were also greater by ~2-fold ($p < 0.05$) following 24 and 48 hours in mKO mice versus their fed

mKO littermates. Furthermore, a significant main effect of fasting on PGC-1α, Tfam, and Nrf2 mRNA content was noted in the SOL muscle (data not shown).

We next examined the activation status of AMPK and its downstream target cAMP response element-binding protein (Creb), as well as protein content of PGC-1α, citrate synthase, and proteins indicative of mitochondrial oxidative phosphorylation (OXPHOS) complexes I–V (CI–CV). A significant main effect ($p < 0.05$) of fasting on phosphorylated AMPK (P-AMPK^{Thr172}) was detected (Figure 3B, C). Compared to the WT fed group, P-AMPK^{Thr172} content was significantly greater by 2.8-fold in WT animals after 48 hours of food deprivation, whereas P-AMPK^{Thr172} was similar between fed and fasted conditions in mKO mice. A main effect ($p < 0.05$) of genotype on total AMPK was observed. Moreover, we noted significant main effects of genotype and fasting on AMPK activation status. Main effects ($p < 0.05$) of genotype and fasting on P-Creb^{Ser133} were also observed (Figure 3B, D). There was a strong trend ($p = 0.05$) towards a main effect of fasting on total Creb protein content. A significant main effect of genotype on Creb activation status was also noted. We observed main effects ($p < 0.05$) of genotype and fasting on PGC-1α protein content (Figure 3B, E). After 48 hours of food deprivation, PGC-1α protein expression was significantly greater by ~2-fold in mKO mice compared to the fed mKO group. A main effect ($p < 0.05$) of fasting on citrate synthase protein content was detected, whereas total OXPHOS expression was similar between conditions.

Given the impact of CARM1 on metabolic signaling, we performed analyses of succinate dehydrogenase (SDH) content, along with mitochondrial respiration and hydrogen peroxide (H_2O_2) emission. Qualitative analyses suggest that compared to the WT

fed group, both WT and mKO EDL muscles displayed greater SDH staining after 24 and 48 hours of food deprivation (Figure 3F). When normalized to muscle fiber bundle weight, we observed a main effect ($p < 0.05$) of genotype on CI-supported state III respiration and CI + II-supported state III respiration, which was not impacted by fasting (Figure 3G-I). A significant main effect of fasting on CI-supported state III H_2O_2 emission was detected in WT and mKO animals after 48 hours of fasting (Figure 3J).

Mitochondrial morphology and mitophagy in mKO animals following food deprivation. To gain further insight into the effects of CARM1 deficiency on mitochondria structure, we next conducted transmission electron microscopy analysis (Figure 4A, B). Mitochondria size was similar in all experimental conditions, regardless of subsarcolemmal (SS) or intermyofibrillar (IMF) location (Figure 4A, C). Mitochondria per unit area exhibited a strong trend towards a main effect of fasting ($p = 0.06$) in the SS region and an interaction ($p = 0.08$) between genotype and fasting in the IMF section (Figure 4A, D). Though mitochondria density in the SS area was similar between genotypes with food deprivation, another solid trend ($p = 0.07$) towards an interaction between genotype and fasting emerged in the IMF space (Figure 4A, E).

We investigated the impact of CARM1 mKO on genes that regulate mitophagy. In particular, we assessed Parkin and BCL2 and adenovirus E1B 19-kDa interacting protein 3 (Bnip3) transcript levels in EDL and SOL muscles from fed and fasted WT and mKO mice. A main effect ($p < 0.05$) of fasting on Parkin and Bnip3 mRNA content was observed in both muscles (data not shown). A significant main effect of fasting on Parkin protein expression was observed and an interaction ($p < 0.05$) between genotype and fasting was

also detected (Figure 4F, G). When compared to the WT fed group, Parkin protein content increased by 2-fold ($p < 0.05$) in WT animals after 24 hours of food deprivation. Parkin protein expression was also significantly greater by 1.7-fold in mKO versus WT muscle under fed conditions. Tukey post-hoc analyses also revealed similar Parkin protein levels between fed and fasted mKO mice. Furthermore, we found significant main effects of genotype and fasting on Bnip3 protein content (Figure 4F, G). Bnip3 protein expression significantly increased by 2.5-fold in WT muscle following 48 hours of food deprivation compared to their fed WT littermates. Bnip3 protein content was greater by 3-fold ($p < 0.05$) in mKO muscle after 48 hours of fasting relative to the fed mKO animals. The relative increase in Bnip3 protein expression between fed and 48 hour fasted groups trended larger in mKO versus WT mice ($p = 0.08$).

EDL myofiber cross-sections were also stained for Parkin and mitochondrial translocase of the outer membrane (Tom20) in WT and mKO animals during food deprivation (Figure 4H, I). We detected a main effect ($p < 0.05$) of fasting on Parkin puncta. Specifically, relative to the WT fed group, fasting induced a significant 1.8-fold increase in Parkin puncta following 24 and 48 hours in WT mice. In contrast, the number of Parkin puncta was similar between fed and fasted mKO animals.

Knockout of CARM1 in muscle results in aberrant autophagy. Previous studies have shown that CARM1 regulates the autophagic process in non-muscle cells in response to nutrient deprivation (Shin et al., 2016). Here, we sought to determine whether CARM1 governs myofiber autophagy. To this end, we administered saline or colchicine to WT and mKO mice under fed and fasted conditions to evaluate autophagosome turnover (Figure

5A). We noted significant main effects of genotype and fasting on the microtubule-associated protein 1A/1B-light chain 3 (LC3)-II/LC3-I ratio (Figure 5A, B). A main effect ($p < 0.05$) of colchicine treatment on the LC3-II/LC3-I ratio was also observed in WT and mKO animals during fed and fasted settings. Furthermore, a significant main effect of genotype on LC3-II protein expression was observed in saline-treated fed and fasted mice (data not shown). We detected a main effect ($p < 0.05$) of colchicine on LC3-II protein expression in WT and mKO animals during fasted conditions. A significant main effect of fasting on LC3-II autophagosome flux emerged (Figure 5C). Despite a 30-fold difference in LC3-II flux between fed and fasted mKO mice versus only a 2.2-fold difference in WT animals, the relative increase in autophagic flux evoked by fasting did not significantly differ between WT and mKO mice. Notably, there was a trend ($p = 0.12$) towards a main effect of genotype on LC3-II autophagosome flux.

Transmission electron microscopy was employed to assess the accumulation of abnormal mitochondria (Figure 5D) and autophagic bodies (Figure 5E) in WT and mKO mice under saline or colchicine-treated conditions in both fed and fasted muscle. A main effect ($p < 0.05$) of colchicine on total number of abnormal mitochondria emerged in both genotypes under fasted settings (Figure 5D, F). Moreover, we observed a main effect ($p < 0.05$) of colchicine on total number of autophagic bodies in WT and mKO mice during food deprivation (Figure 5E, G).

We next investigated autophagy-related and lysosomal genes previously demonstrated to be transcriptionally regulated by CARM1 in non-muscle cells (Shin et al., 2016). mRNA content of microtubule-associated protein 1 light chain 3β (Map1lc3b),

autophagy-related 12 (Atg12), Atg14, vacuolar protein sorting 11 (VPS11), mucolipin 1 (MCOLN1), and cystinosin (CTNS) was examined in EDL and SOL muscles from fed and fasted WT and mKO animals. A main effect ($p < 0.05$) of fasting on Map1lc3b, Atg12, Atg14, VPS11, MCOLN1, and CTNS transcript levels was detected for both muscles (Figure 5H and data not shown). Map1lc3b, Atg12, Atg14, VPS11, MCOLN1, and CTNS mRNA expression levels were similar between genotypes in all experimental conditions. To further understand the role of CARM1 in regulating myofiber autophagy, we also probed for autophagy-related Beclin-1 and Gabarapl, as well as lysosomal cathepsin L mRNA content. We observed main effects of genotype ($p < 0.05$) and fasting ($p = 0.06$) on Beclin-1 mRNA expression in the EDL muscle (Figure 5H). Furthermore, a significant main effect of fasting was detected on Gabarapl transcript levels and a significant interaction between genotype and fasting emerged. For example, Gabarapl mRNA expression was significantly greater by 4.5-fold in WT animals after 48 hours of fasting versus their WT fed littermates. Compared to mKO fed mice, Gabarapl mRNA content was increased 7.5-fold ($p < 0.05$) in mKO animals following 24 hours of food deprivation. We also observed a main effect ($p < 0.05$) of fasting on cathepsin L mRNA content. Relative to the WT fed EDL, cathepsin L mRNA expression was significantly greater by 2.5-fold in WT muscle after 48 hours of fasting. Cathepsin L transcript levels were also elevated by 2.5-fold ($p < 0.05$) in mKO muscle following 24 and 48 hours of food deprivation compared to their fed mKO littermates.

We continued to evaluate the autophagy-lysosome pathway by assessing the activation status of unc-51-like autophagy-activating kinase 1 (ULK1), as well as the

protein expression of S-phase kinase-associated protein 2 (SKP2), transcription factor EB (TFEB), Beclin-1, lysosomal associated membrane protein 1 (Lamp1), Lamp2, and cathepsin D. Main effects of fasting ($p < 0.05$) and genotype ($p = 0.08$) on phosphorylated ULK1 (P-ULK1^{Ser555}) were detected (Figure 5I, J). For example, relative to the WT fed group, food deprivation evoked a significant 1.5-fold increase in P-ULK1^{Ser555} after 48 hours in WT mice. In contrast, similar P-ULK1^{Ser555} levels were detected between fed and fasted mKO animals. Total ULK1 protein content was similar between all groups. Notably, a significant main effect of genotype on ULK1 activation status was observed. A main effect ($p < 0.05$) of genotype on SKP2 protein expression was noted (Figure 5I, K). When compared to the WT fed group, SKP2 protein content was significantly reduced by ~40% in fed and fasted mKO muscle. TFEB protein expression was similar in all experimental conditions. Main effects ($p < 0.05$) of genotype and fasting on Beclin-1 protein content were also observed. We detected a significant main effect of genotype on Lamp1 and Lamp2 protein expression (Figure 5I, L). For instance, Lamp2 protein content was significantly greater by 1.7-fold in mKO versus WT fed muscle. There was also a main effect ($p < 0.05$) of fasting on cathepsin D protein expression in both genotypes. Food deprivation elicited a significant 1.5-fold increase in cathepsin D protein content in WT and mKO mice following 48 hours, relative to their respective fed groups.

CARM1 modulates muscle atrophy signaling during food deprivation. To probe the effect of CARM1 mKO on the muscle atrophy program during fasting, we analyzed atrogenes that are crucial for muscle wasting. As such, we assessed the transcript levels of muscle RING finger 1 (MuRF1), muscle atrophy F box (MAFbx), Forkhead box O1

(FOXO1), and FOXO3 in EDL and SOL muscles (Sartori et al. 2021). We observed a main effect ($p < 0.05$) of fasting on MuRF1, MAFbx, FOXO1, and FOXO3 mRNA content in both muscles for WT and mKO animals (Figure 6A and data not shown). For example, food deprivation induced a significant ~13- and ~10-fold increase in MuRF1 mRNA expression in WT and mKO EDL muscles, respectively, versus their respective fed controls. Compared to the WT fed group, fasting evoked a 4- and 7-fold increase ($p < 0.05$) in MAFbx transcript levels in WT animals after 24 and 48 hours. MAFbx mRNA content was significantly greater by 3-fold in mKO animals following 24 and 48 hours of food deprivation versus the mKO fed group. We noted a significant main effect of genotype of FOXO3 mRNA content. Relative to mKO fed animals, FOXO3 transcript levels were greater by 2.5-fold ($p < 0.05$) in mKO muscle following 24 hours of fasting. A main effect ($p < 0.05$) of fasting on MuRF1, MAFbx, and ubiquitin protein content was detected (Figure 6B, C). For instance, MuRF1 protein expression was significantly greater by ~4-fold in both genotypes after 24 and 48 hours of food deprivation compared to their respective fed control group. We observed a main effect of genotype on MAFbx ($p < 0.05$) and ubiquitin ($p = 0.05$) protein content. Compared to the WT fed group, MAFbx protein expression was significantly greater by 1.8-fold in WT animals following 24 and 48 hours of fasting, whereas MAFbx protein content was similar between fed and fasted conditions in mKO mice.

We next investigated the upstream signaling molecule protein kinase B (Akt). We observed a main effect ($p < 0.05$) of genotype on P-Akt^{Ser473} and total Akt (Figure 6B, D). For example, total Akt protein content was significantly greater by 1.7-fold in fed and

fasted mKO muscle versus the fed WT condition. Akt activation status was similar between all groups. A main effect ($p < 0.05$) of genotype on P-mTOR^{Ser2448} and total mTOR was also detected (Figure 6B, E). Furthermore, mTOR activation status was similar between genotypes with food deprivation. We found a significant main effect of fasting on P-FOXO1^{Ser256}, total FOXO1, and FOXO1 activation status (Figure 6B, F). For instance, FOXO1 activation status was ~60% lower ($p < 0.05$) in WT and mKO animals following 48 hours of fasting versus their respective fed littermates. We also noted a main effect of genotype on P-FOXO1^{Ser256} and total FOXO1. Relative to the WT fed group, P-FOXO1^{Ser256} content was significantly reduced by 50% in WT animals after 48 hours of food deprivation. In contrast, P-FOXO1^{Ser256} did not change between fed and fasted conditions in mKO mice. Moreover, a main effect of fasting on P-FOXO3^{Ser253} ($p < 0.05$) and FOXO3^{Ser253} activation status ($p = 0.05$) was observed (Figure 6B, G). Compared to the WT fed group, food deprivation evoked a significant 40% decrease in P-FOXO3^{Ser253} in WT muscle following 24 and 48 hours. In contrast, levels of P-FOXO3^{Ser253} in mKO animals were similar between fed and fasted muscle. A significant main effect of genotype on total FOXO3 protein content and FOXO3^{Ser253} activation status was also noted.

We analyzed the activation status of AMPK downstream targets FOXO3^{Ser413} and FOXO3^{Ser588} (Kjobsted et al., 2018), as CARM1 and AMPK coregulate autophagic and atrophic signaling (Shin et al., 2016; Li et al., 2017; Stouth et al., 2020). We detected a main effect ($p < 0.05$) of genotype on P-FOXO3^{Ser413} and P-FOXO3^{Ser588}, as well as FOXO3^{Ser588} activation status (Figure 6B, G). For example, relative to the WT fed group,

CARM1 deletion resulted in a significant 1.6-fold increase in P-FOXO3^{Ser413} levels under fed and fasted conditions. FOXO3^{Ser413} activation status was similar between all groups.

CARM1 deletion causes perturbed myonuclear localization of muscle remodeling and autophagic proteins during fasting-induce atrophy. We evaluated myonuclear levels of CARM1, PRMT1, PRMT5, PRMT6, and PRMT7 in WT and mKO GAST muscle to further define their expression during atrophy elicited by food deprivation. We also analyzed the nuclear content of PGC-1α, AMPK, TFEB, FOXO1, and FOXO3, to more comprehensively understand how CARM1 governs myonuclear adaptations to fasting. Compared to fed conditions, nuclear CARM1 protein expression was similar in WT muscle after 24 and 48 hours of food deprivation (Figure 7A, B). Nuclear PRMT1 protein content was similar between genotypes with food deprivation. We detected a main effect ($p < 0.05$) of fasting on PRMT5 and PRMT6 levels in myonuclei. For instance, relative to the WT fed group, fasting induced a significant 30% decrease in nuclear PRMT5 protein expression in WT animals following 24 and 48 hours of food deprivation. We also noted a main effect ($p < 0.05$) of genotype on nuclear PRMT6 protein content. PRMT6 levels in myonuclei were significantly lower by ~50% in fed and fasted mKO muscle versus fed WT mice. Interestingly, we did not detect PRMT6 in cytosolic fractions, whereas conversely, PRMT7 was excluded from myonuclei and found only in the cytosolic compartment (data not shown).

Main effects ($p < 0.05$) of genotype and fasting on nuclear PGC-1α protein expression were observed (Figure 7A, C). Furthermore, a significant main effect of fasting was noted on nuclear P-AMPK^{Thr172} and a significant interaction between genotype and

fasting was also found. When compared to the WT fed group, myonuclear P-AMPK^{Thr172} increased by 5-fold ($p < 0.05$) in WT animals after 48 hours of food deprivation. In contrast, Tukey post-hoc analyses revealed that nuclear P-AMPK^{Thr172} did not significantly change between fed and fasted mKO mice. A significant main effect of genotype on total AMPK in myonuclei was noted. We also found a significant main effect of fasting on nuclear AMPK activation status, as well as a strong trend ($p = 0.08$) towards an interaction between genotype and fasting. Compared to WT fed animals, nuclear AMPK activation status was significantly greater by 5-fold in WT muscle following 48 hours of food deprivation. Fasting induced a 4-fold increase ($p < 0.05$) in myonuclear AMPK activation status in mKO mice after 24 and 48 hours relative to their mKO fed littermates.

A significant interaction between genotype and fasting for nuclear TFEB and FOXO1 protein content emerged (Figure 7A, D, and data not shown). Relative to the WT fed group, total nuclear FOXO1 protein expression was elevated by 2.8-fold ($p < 0.05$) in WT mice following 48 hours food deprivation. Total FOXO1 levels in myonuclei were significantly increased by 2-fold after 24 hours in mKO animals versus their fed mKO littermates. Moreover, a main effect ($p < 0.05$) of genotype on nuclear P-FOXO3^{Ser588}, total FOXO3, and FOXO3 activation status was noted. We also found a significant main effect of fasting on total nuclear FOXO3 protein expression and FOXO3 activation status. Compared to the WT fed group, total FOXO3 levels in myonuclei were significantly greater by 2-fold in WT animals following 48 hours of food deprivation, whereas nuclear FOXO3 content was similar between fed and fasted conditions in mKO mice. Nuclear FOXO3 activation status was lower by ~65% ($p < 0.05$) in fed and fasted mKO mice versus the fed

WT condition. Furthermore, relative to WT fed animals, fasting induced a significant ~50% reduction in FOXO3 activation status in WT myonuclei after 24 and 48 hours. Nuclear FOXO3 activation status was similar between fed and fasted conditions in mKO mice. EDL muscle cross-sections from WT and mKO animals following food deprivation were then stained for wheat germ agglutinin (WGA), 4',6-diamidino-2-phenylindole dihydrochloride (DAPI), and TFEB to quantify TFEB myonuclear localization (Figure 7E, F). We observed a main effect ($p < 0.05$) of fasting on myonuclei positive for TFEB. Compared to the WT fed group, the amount of TFEB positive myonuclei was significantly elevated by 1.8-fold in WT muscle after 24 and 48 hours of food deprivation. Contrary to this, TFEB positive myonuclei in mKO mice was similar between fed and fasted conditions.

Discussion

In this study, we confirm that CARM1 is required to maintain muscle mass and show that muscle-specific deletion of CARM1 attenuates the progression of fasting-induced muscle wasting. CARM1 mKO resulted in altered PRMT biology, as well as perturbed autophagic and atrophic signaling downstream of AMPK after food deprivation. Specifically, we provide evidence that knockout of CARM1 in muscle led to dysregulated AMPK site-specific activation of ULK1^{Ser555} and FOXO3^{Ser588}, along with upregulated PGC-1α, Tfam, and Nrf2 transcript levels. Downstream of these proximal autophagy and atrophy signals, CARM1 also mediated mitochondrial function, markers of mitophagy such as the accumulation of Parkin puncta, autophagy flux, along with TFEB and FOXO3 myonuclear localization, as well as the autophagy gene expression program during food deprivation-evoked muscle atrophy. Taken together, this study supports and extends earlier

work demonstrating that CARM1 is a powerful regulator of autophagy (Shin et al., 2016; Li et al., 2017; Zhou et al., 2019; Yu et al., 2020), particularly in skeletal muscle (Liu et al., 2019; Hu et al., 2020; Stouth et al., 2020), along with mitophagic and atrophic processes critical for the maintenance and remodeling of muscle mass.

Consistent with our recent work (Stouth et al., 2020), we demonstrate that muscle-specific knockout of CARM1 leads to aberrant autophagic processes and elevated muscle atrophy, which aligns with the abundance of evidence that autophagy is required to maintain muscle mass (Triolo and Hood, 2021). We also now present evidence that CARM1 mKO mitigates both fasting- and denervation-induced skeletal muscle wasting (Liu et al., 2019; Stouth et al. 2020) despite the complementary, but in some respects disparate molecular signatures of these atrophy-inducing stimuli (Milan et al., 2015; Brocca et al., 2017). For example, although muscles atrophied to a similar extent during conditions of neurogenic muscle disuse and fasting, we observed in PRMT content and methyltransferase activity, including CARM1, a general upregulation with denervation (Stouth 2020) but largely no effects in response to fasting except for specific reductions in CARM1 function revealed by decreased BAF155me2a^{Arg1064} and PABP1me2a$^{Arg455/Arg460}$ levels. Collectively, these findings indicate that the influence of CARM1, as well as that of other PRMTs, on atrophy-evoked remodeling is at least in part dependent on the mode of skeletal muscle wasting.

It was previously shown that CARM1 and AMPK are part of a signaling axis that controls autophagy (Shin 2016) and that CARM1 modulates AMPK and its downstream signaling network in skeletal muscle (Stouth et al., 2020). Importantly, loss of AMPK in

muscle disrupts the removal of mitochondria tagged for autophagic degradation (Bujak et al., 2015; Laker et al., 2017). The attenuation of fasting-induced muscle wasting in mKO muscles was likely due, at least in part, to lower AMPK activation, along with higher expression of the transcriptional coactivator PGC-1α in mKO mice. PGC-1α overexpression enhances mitochondrial function and preserves mitochondrial mass by minimizing targeting of the organelle for degradation in response to denervation- and fasting-induced atrophy (Vainshtein et al., 2015). Consistent with this, CARM1 mKO led to increased Tfam expression and mitochondrial respiration, and our results strongly suggest that food deprivation decreased mitochondrial content in WT animals but was maintained in mKO mice. Interestingly, we also observed differential levels of mitophagy proteins Parkin and Bnip3 in mKO muscle during fasting. Parkin puncta, which tag mitochondria for degradation, were elevated in WT animals as early as 24 hours after food deprivation, whereas similar accumulations of Parkin were detected between fed and fasted conditions in mKO mice. Our data therefore highlight disparate mitophagic adaptations between genotypes in response to food deprivation. It is tempting to attribute this distinction to overexpression of PGC-1α in mKO muscle determined in this work. When considering this possibility, it should be noted that mitochondrial fragmentation is required for proper mitochondrial turnover to occur, and PGC-1α strongly promotes organelle fusion (Hood et al., 2019). In any case, it will be interesting to examine whether mitophagy flux and/or fission is reduced in mKO animals during muscle wasting.

A main finding of the current study is that CARM1 governs the autophagy-lysosome system in skeletal muscle during food deprivation-evoked muscle atrophy. We

observed lower levels of AMPK-mediated ULK1^{Ser555} phosphorylation, a canonical marker of autophagic activation (Klionsky et al., 2021; Triolo and Hood, 2021), in mKO versus WT muscle after fasting. Moreover, our data strongly suggest that muscle-specific deletion of CARM1 hinders autophagy flux, evidenced by LC3-II content in colchicine experiments during fed and fasted conditions. The upregulation of Beclin-1, Lamp1, and Lamp2 in mKO versus WT muscle during food deprivation further implies that muscle-specific deletion of CARM1 leads to dysregulated autophagosome processing and defective lysosomal clearance. Since hyperactivation of mTOR^{Ser2448} is sufficient to block autophagy and mitigate muscle wasting in response to fasting (Castets et al., 2013; Vendelbo et al., 2014), in part through marking of ULK1^{Ser757} (Klionsky et al., 2021), it is reasonable to speculate that sustained phosphorylation of mTOR^{Ser2448} in mKO muscle plays a key role in attenuating protein breakdown during food deprivation. Furthermore, CARM1 interacts with TFEB in myonuclei (data not shown), and the absence of the methyltransferase influences nuclear TFEB protein levels during fasting-induced muscle atrophy. Since mTOR fosters TFEB nuclear export (Napolitano et al., 2018), we reason that hyperphosphorylation of mTOR^{Ser2448} in mKO mice contributes to impeded TFEB nuclear entry during food deprivation. Despite the relatively lower TFEB myonuclear localization in mKO animals, mRNA levels of TFEB-dependent autophagy and lysosomal genes were similarly induced in WT and mKO mice with fasting (data not shown), which suggests enhanced TFEB transcriptional activity and/or compensatory mechanisms involving TFEB family members, such as TFE3 (Markby and Sakamoto, 2020; Martina et al., 2014; Pastore et al., 2017). Interestingly, myonuclear TFEB content was elevated in WT animals 24 hours

following food deprivation, which likely facilitated AMPK-dependent TFEB transcriptional activity (Paquette et al., 2021). Altogether, these data suggest that CARM1 mKO curtails fasting-induced muscle wasting via alterations in autophagy-lysosomal machinery additional to the transcriptional and post-translational events established here. Further work is necessary to confirm this possibility and to identify the key players.

Akt and AMPK modulate muscle protein breakdown via the downstream FOXO transcriptional network (Sartori et al. 2021). For instance, Akt-induced phosphorylation of FOXO3^{Ser253} suppresses FOXO3-dependent atrogene expression by promoting its nuclear exclusion (Calnan and Brunet, 2008; Sanchez et al., 2014). We found that muscle-specific deletion of CARM1 results in greater Akt^{Ser473} phosphorylation, and that CARM1 interacts with FOXO3 in myonuclei (data not shown). We also show that phosphorylation of FOXO3^{Ser253} decreased in WT mice following food deprivation, whereas no changes were detected in mKO animals between fed and fasted conditions. Concomitantly, nuclear FOXO3 protein content significantly increased in WT muscle after food deprivation, but not in fed and fasted mKO myonuclei. Since deletion of FOXOs spares muscle loss during food deprivation, in part, by preventing the induction of atrogenes (Milan et al., 2015), and CARM1 is required for FOXO3 transcriptional activity during neurogenic muscle disuse (Liu et al., 2019), it is reasonable to posit that CARM1 mKO, in part, protects against fasting-induced atrophy by inhibiting FOXO3-dependent protein degradation. Unlike Akt, AMPK promotes the transcription of atrogenes by phosphorylating FOXO3^{Ser588} and FOXO3^{Ser413} (Kjobsted et al., 2018). Notably, AMPK phosphorylation at both FOXO3 residues upregulates the transcription of MuRF1 and MAFbx, independent of FOXO3

subcellular localization. Consistent with our data and previous work (Stouth et al., 2020), knocking out CARM1 in muscle led to decreased phosphorylation of FOXO3^{Ser588} in the myonuclear compartment. Interestingly, phosphorylation of FOXO3^{Ser413} was greater in mKO versus WT muscle, possibly to compensate for reduced phosphorylation at the FOXO3^{Ser588} site, as interplay between AMPK-specific FOXO3 residues has been previously observed (Greer et al., 2007). This aligns with food deprivation evoking a similar increase in MuRF1 and MAFbx atrogene mRNA content between genotypes. Future studies should focus on investigating the impact of CARM1 on FOXO3-specific atrogenes during atrophy, in order to further our understanding of the role of the methyltransferase in muscle protein breakdown.

In summary, skeletal muscle-specific deletion of CARM1 altered mitochondrial function and mitophagy, as well as autophagic and atrophic signaling downstream of Akt and AMPK, which resulted in protection from fasting-induced muscle wasting. Together with recent observations that demonstrate an attenuation of neurogenic muscle atrophy in CARM1 mKO (Stouth et al., 2020) and knockdown (Liu et al., 2019) conditions along with reports of CARM1-mediated control of autophagy (Shin et al., 2016; Yu et al., 2020), these data strongly suggest that CARM1 is a critical regulator of muscle mass and phenotypic plasticity during atrophy. Further investigation is therefore warranted to determine whether the arginine methyltransferase is a viable therapeutic target for combating muscle wasting in alternative pre-clinical and clinical settings characterized by aberrant mitophagic, autophagic, and atrophic signaling, such as the sarcopenia of aging, cancer cachexia, and neuromuscular disorders.

Materials and methods

Animal model and fasting experiments. Floxed CARM1 (WT) and mKO mice were housed in the McMaster Animal Facilities and all protocols were approved by the Animal Research Ethics Board at McMaster University operating under the regulations of the Canadian Council for Animal Care. CARM1 floxed animals with C57BL6J/129 background (Yadav et al., 2003; Bao et al., 2018) were a kind gift from Dr. Mark Bedford (The University of Texas MD Anderson Cancer Centre, Smithville, TX, USA). We employed the Cre/loxP system to generate mKO mice as described previously (Stouth et al., 2020). Briefly, CARM1 floxed animals were crossed with human α-skeletal actin (HSA)-Cre mice (Jackson Laboratories, Bar Harbor, ME, USA) expressing skeletal muscle-specific Cre recombinase (McCarthy et al., 2012). Progeny were genotyped by obtaining tail clippings for DNA extraction, as well as by performing reverse transcription-polymerase chain reaction (RT-PCR) and gel electrophoresis protocols. The following primers were used to verify that WT and mKO mice contained a LoxP site for CARM1 between exon 2 and 3: forward (F)-AGTTGGTGACCCTTGTGTCC, reverse (R)-AGCTGCCAGGACCTCTGATA. The following primers were used to detect mKO mice that express Cre recombinase: F-GCGGTCTGGCAGTAAAAACTATC, R-GTGAAACAGCATTGCTGTCACTT. WT and mKO animals were studied at 12-weeks of age (~25 g body mass; male) and were housed in an environmentally controlled room (23 °C, 12-hour light/12-hour dark cycle). During fasting experiments, food was removed from mice at the beginning of the active light cycle for a total of 24 or 48 hours prior to

sacrifice and tissue collection. Fed, control mice maintained ad libitum access to food and were sacrificed at the same time as their fasted littermates. Animals (n = 11-21/group) were euthanized via cervical dislocation. TA, EDL, SOL, and GAST muscles were rapidly excised, weighed, frozen in liquid nitrogen or mounted in optimal cutting temperature compound (OCT; Thermo Fisher Scientific Life Sciences, Waltham, MA, USA) then frozen in isopentane cooled with liquid nitrogen. All muscles were then stored at -80 °C for subsequent biochemical analyses.

Autophagy flux calculation. To determine the relative degree of autophagosome turnover, WT and mKO mice received intraperitoneal injections of colchicine (Col; 0.4 mg/kg/day; Sigma-Aldrich, St. Louis, MO, USA) or an equal volume of 0.9% saline (Sal) every 24 hours for two days prior to the day of sacrifice (n = 12-16/group). This dosage of Col is sufficient to disrupt microtubules and inhibit autophagosome-lysosome fusion for autophagic flux calculations (Ju et al., 2010; Carter et al., 2018). Animals were randomly assigned to either fed or 48 hour fasted groups. Western blotting (as described below) of LC3-II was performed in TA whole muscle samples with all conditions represented on one SDS-PAGE gel. LC3-II protein content was quantified using ImageJ and values were corrected for loading via Ponceau S solution (Sigma-Aldrich, St. Louis, MO, USA). Autophagic flux was calculated based on the difference in LC3-II levels between Col- and Sal-treated mice (i.e., fed WT Col – mean fed WT Sal) as described previously (Carter et al., 2018; Klionsky et al., 2021).

Whole muscle protein extraction. Tissues were processed as described previously (Stouth et al., 2018; Stouth et al., 2020). For total protein extraction, frozen TA muscles

were pulverized to a fine powder with a mortar and pestle on liquid nitrogen. Muscle samples were suspended in RIPA buffer (Sigma-Aldrich, St. Louis, MO, USA), supplemented with cOmplete Mini Protease Inhibitor Cocktail (Sigma-Aldrich, St. Louis, MO, USA) and PhosSTOP Phosphatase Inhibitor Cocktail (Sigma-Aldrich, St. Louis, MO, USA). Further homogenization was performed using stainless steel lysing beads and TissueLyser (Qiagen, Hilden, NRW, Germany) at a frequency of 30 Hz for 5 minutes. Lysates were then mixed by end-over end inversion for 60 minutes at 4 °C followed by centrifugation at 14,000 x g for 10 minutes. The supernatants were collected, and protein concentrations were determined using the BCA protein assay (Thermo Fisher Scientific Life Sciences, Waltham, MA, USA). Samples were then stored at -80 °C for further analysis.

Nuclear and cytosolic isolations. Nuclear and cytosolic fractions were isolated from GAST muscles as described previously (Dimauro et al., 2012; Stouth et al., 2018). Briefly, frozen tissue was suspended in STM buffer and minced with sharp scissors on ice. Samples were then homogenized with a micropestle for 2 minutes. After incubating on ice for 30 minutes, samples were vortexed, followed by centrifugation at 800 x g for 15 minutes. The pellet and supernatant were separated for isolating nuclear and cytosolic fractions, respectively. To isolate the nuclear fraction, the pellet was resuspended in STM buffer, vortexed, and then centrifuged at 500 x g for 15 minutes. After repeating the previous centrifugation step at 1,000 x g for 15 minutes, pellet was suspended in NET buffer, which was then vortexed and placed on ice for 30 minutes. Next, samples were sonicated and centrifuged at 9,000 x g for 30 minutes to yield the nuclear fraction. To isolate the cytosolic

fraction, the supernatant set aside earlier also underwent a series of centrifugation steps. Protein concentrations were determined using the BCA protein assay (Thermo Fisher Scientific Life Sciences, Waltham, MA, USA) and fractions were stored at -80 °C for further analysis.

Western blotting. Proteins extracted from whole muscle, as well as nuclear and cytosolic compartments, were separated on 10% SDS-PAGE gels or 4-15% precast gradient gels (Bio-Rad Laboratories, Inc., Hercules, CA, USA) and subsequently transferred onto nitrocellulose membranes. Following transfer, membranes were stained with Ponceau S solution (Sigma-Aldrich, St. Louis, MO, USA) to serve as a loading control (Stouth et al. 2018, Stouth et al., 2020, Romero-Calvo et al. 2010). Membranes were then washed with 1 x TBST and blocked with 5% BSA-TBST for one hour before being incubated in a primary antibody overnight at 4 °C with gentle rocking. The next day, blots were washed with 1 x TBST and incubated in the appropriate secondary antibody (1:2,000; 7074S; Cell Signaling, Danvers, MA, USA) conjugated to horseradish peroxidase with gentle rocking at room temperature for one hour. Blots were then washed again with 1 x TBST, followed by visualization with enhanced chemiluminescence (G00069; GE Healthcare Bio-Sciences, Chicago, IL, USA). Blots were developed with long and short exposures. Protein density was analyzed using ImageJ.

We employed antibodies against CARM1 (1:5,000; A300-421A; Bethyl Laboratories, Montgomery, TX, USA), PRMT1 (1:1,000; 07-404; EMD Millipore, Darmstadt, HE, Germany), PRMT5 (1:1,000; 07-405; EMD Millipore, Darmstadt, HE, Germany), PRMT6 (1:1,000; A300-929A; Bethyl Laboratories, Montgomery, TX, USA),

PRMT7 (1:1,000; sc-376077; Santa Cruz Biotechnology, Dallas, TX, USA), MMA (1:1,000; 8015S; Cell Signaling, Danvers, MA, USA), ADMA (1:1,000; 13522S; Cell Signaling, Danvers, MA, USA), CARM1 substrate (1:1,000; another gift from Dr. Mark Bedford, MD Anderson Cancer Center, University of Texas), SDMA (1:1,000; 13222S; Cell Signaling, Danvers, MA, USA), asymmetrically dimethylated BAF155^{Arg1064} (1:1,000; 94962S; Cell Signaling, Danvers, MA, USA), BAF155 (1:1,000; 11956S; Cell Signaling, Danvers, MA, USA), asymmetrically dimethylated PABP1$^{Arg455/Arg460}$ (1:1,000; 3505S; Cell Signaling, Danvers, MA, USA), and PABP1 (1:1,000; 4992S; Cell Signaling, Danvers, MA, USA) to assess PRMT expression and function.

Antibodies against phosphorylated AMPK^{Thr172} (1:1,000; 2535S; Cell Signaling, Danvers, MA, USA), AMPK (1:1,000; 2532S; Cell Signaling, Danvers, MA, USA), phosphorylated Creb^{Ser133} (1:1,000; 06-519; EMD Millipore, Darmstadt, HE, Germany), Creb (1:1,000; 06-863; EMD Millipore, Darmstadt, HE, Germany), PGC-1α (1:200; AB3242; EMD Millipore, Darmstadt, HE, Germany), citrate synthase (1:1,000; ab96600; Abcam, Cambridge, UK), and total OXPHOS (1:1,000; ab110413; Abcam, Cambridge, UK) were used to examine metabolic signaling. Antibodies against Parkin (1:1,000; 2132S; Cell Signaling, Danvers, MA, USA) and Bnip3 (1:1,000; 3769S; Cell Signaling, Danvers, MA, USA) were used to investigate mitophagy. Antibodies against LC3 (1:1,000; 4108S; Cell Signaling, Danvers, MA, USA), phosphorylated ULK1^{Ser555} (1:1,000; 5869S; Cell Signaling, Danvers, MA, USA), ULK1 (1:1,000; 8054S; Cell Signaling, Danvers, MA, USA), SKP2 (1:1,000; 4313S; Cell Signaling, Danvers, MA, USA), TFEB (1:1,000; 4240S; Cell Signaling, Danvers, MA, USA), Beclin-1 (1:1,000; 3738S; Cell Signaling,

Danvers, MA, USA), Lamp1 (1:1,000; ab24170; Abcam, Cambridge, UK), Lamp2 (1:1,000; ab13524; Abcam, Cambridge, UK), and cathepsin D (1:1,000; 2284S; Cell Signaling, Danvers, MA, USA) were used to evaluate autophagy.

Antibodies against MuRF1 (1:200; AF5366; R&D Systems, Minneapolis, MN, USA), MAFbx (1:1,000; AP2041; ECM Biosciences, Versailles, KY, USA), ubiquitin (1:500; 3933S; Cell Signaling, Danvers, MA, USA), phosphorylated Akt^{Ser473} (1:1,000; 9271S; Cell Signaling, Danvers, MA, USA), Akt (1:1,000; 4691S; Cell Signaling, Danvers, MA, USA), phosphorylated mTOR^{Ser2448} (1:1,000; 2971S; Cell Signaling, Danvers, MA, USA), mTOR (1:1,000; 2972S; Cell Signaling, Danvers, MA, USA), phosphorylated FOXO1^{Ser256} (1:1,000; 9461S; Cell Signaling, Danvers, MA, USA), FOXO1 (1:1,000; 2880S; Cell Signaling, Danvers, MA, USA), phosphorylated FOXO3^{Ser253} (1:1,000; 9466S; Cell Signaling, Danvers, MA, USA), phosphorylated FOXO3^{Ser413} (1:1,000; 8174S; Cell Signaling, Danvers, MA, USA), phosphorylated FOXO3^{Ser588} (1:1,000; a kind gift from Dr. Anne Brunet, Department of Genetics, Stanford University School of Medicine), and FOXO3 (1:1,000; 2497S; Cell Signaling, Danvers, MA, USA) to analyze the muscle atrophy program. We also employed antibodies against Histone H3 (1:1,000; ab18521; Abcam, Cambridge, UK), and glyceraldehyde-3-phosphate dehydrogenase (GAPDH; 1:1,000; ab9483; Abcam, Cambridge, UK) to serve as markers of purity for nuclear and cytosolic fractions, respectively.

Immunoprecipitation (IP). Previously prepared whole muscle lysate and nuclear fractions from TA and GAST, respectively, were used for IP experiments. The IP procedure was carried out as described earlier (Philp et al. 2011; Stouth et al., 2018; Stouth et al.,

2020). For all IP experiments, 200 µg of protein was precleared with 50 µl of protein A agarose suspension (IP02; EMD Millipore, Darmstadt, HE, Germany) and 1 µg of rabbit Immunoglobulin G (IgG; 12-370; EMD Millipore, Darmstadt, HE, Germany). This was followed by end-over-end inversion for 60 minutes at 4 °C followed by centrifugation at 12,000 x g for 10 minutes. Precleared supernatant was then rotated by end-over-end inversion for 2 hours at 4 °C with anti-CARM1 (1:100; A300-421A; Bethyl Laboratories, Montgomery, TX, USA). Next, 50 µl of protein A agarose suspension was added and the samples were mixed by end-over-end inversion overnight at 4 °C. The next day, agarose beads were washed five times with 500 µl of 1 x PBS and centrifuged at 12,000 x g. After suspending each agarose bead complex with equal volumes of 2 x SDS sample buffer (50 µl), samples were boiled for 5 minutes and centrifuged at 12,000 x g for 1 minute. After spinning, only the supernatants were saved for SDS-PAGE (6 µl) separation.

RNA isolation and quantitative real-time (q) RT-PCR. EDL and SOL muscles were used to isolate total RNA and perform qRT-PCR as described previously (Stouth et al. 2018; Stouth et al., 2020). Samples were first homogenized in 1 mL of chilled Trizol reagent (Invitrogen, Carlsbad, CA, USA) using stainless steel lysing beads and TissueLyser (Qiagen, Hilden, NRW, Germany) at a frequency of 30 Hz for 5 minutes. This was followed by adding 200 µL of chloroform (Thermo Fisher Scientific, Waltham, MA, USA), shaking vigorously for 15 seconds, and centrifuging at 12,000 x g for 10 minutes. The upper aqueous (RNA) phase was purified using the Total RNA Omega Bio-Tek kit (VWR International, Radnor, PA, USA). RNA concentration and purity were determined using the NanoDrop 1000 Spectrophotometer (Thermo Fisher Scientific Life Sciences,Waltham,

MA, USA). RNA samples were then reverse-transcribed into cDNA using a high-capacity cDNA reverse transcription kit (Thermo Fisher Scientific Life Sciences,Waltham, MA, USA).

All individual qRT-PCRs were run in duplicate 6 μL reactions containing GoTaq qPCR Master Mix (Promega, Madison, WI, USA). Data were analyzed using the comparative C_T method (Schmittgen and Livak, 2008). Beta-actin (Actb) was used as a control housekeeping gene for all experiments. This control C_T value was subtracted from the C_T value of the gene of interest [$\Delta C_T = C_{T\ (target\ gene)} - C_{T\ (endogenous\ control)}$]. The mean ΔC_T value from the fed WT group (WT Fed) was then subtracted from the ΔC_T values of the fed mKO muscle [$\Delta\Delta C_T = \Delta C_{T\ (mKO\ Fed)} - C_{T\ (WT\ Fed)}$]. This calculation was then repeated for fasted WT and mKO animals. Results are reported as fold changes using the $\Delta\Delta C_T$ method, calculated as $2^{-\Delta\Delta CT}$.

The following primers were used in this study: CARM1 F-CAACAGCGTCCTCATCCAGT, R-GTCCGCTCACTGAACACAGA; PRMT1 F-CACCTTGGCTAATGGGATGAG, R-GTGAAACATGGAGTTGCGGT; PRMT5 F-TCTCCCCACCAGCATTTTCC, R-TGGAGGGCGATTTTGGCTTA; PRMT6 F-TGTCGCTGAGCAAGAAAAGA, R-GACGTCGGAGTAGCACTCGT; PRMT7 F-GCTGCTGTGAAGATTGTGGA, R-CAAACAGCTCCGTGATCAGA; PGC-1α F-AGCCGTGACCAGTGACAACGAG, R-GCTGCATGGTTCTGAGTGCTAAG; Tfam F-TAGGCACCGTATTGCGTGAG, R-GTGCTTTTAGCACGCTCCAC; Nrf2 F-TTCTTTCAGCAGCATCCTCTCCAC, R-ACAGCCTTCAATAGTCCCGTCCAG; Parkin F-GTCTGCAATTTGGTTTGGAGTA, R-GCATCATGGGATTGTCTCTTAAA;

Bnip3 F-TTCCACTAGCACCTTCTGATGA, R-GAACACCGCATTTACAGAACAA; Map1lc3b F-CACTGCTCTGTCTTGTGTAGGTTG, R-TCGTTGTGCCTTTATTAGTGCATC; Atg12 F-TCCGTGCCATCACATACACA, R-TAAGACTGCTGTGGGGCTGA; Atg14 F-AGCGGTGATTTCGTCTATTTCG, R-GCTGTTCAATCCTCATCTTGCAT; VPS11 F-AAAAGAGAGACGGTGGCAATC, R-AGCCCAGTAACGGGATAGTTG; MCOLN1 F-CTGACCCCCAATCCTGGGTAT, R-GGCCCGGAACTTGTCACAT; CTNS F-ATGAGGAGGAATTGGCTGCTT, R-ACGTTGGTTGAACTGCCATTTT; Beclin-1 F-AGGCTGAGGCGGAGAGATT, R-TCCACACTCTTGAGTTCGTCAT; Gabarapl F-CATCGTGGAGAAGGCTCCTA, R-ATACAGCTGGCCCATGGTAG; cathepsin L F-GTGGACTGTTCTCACGCTCAAG, R-TCCGTCCTTCGCTTCATAGG; MuRF1 F-CACGTGTGAGGTGCCTACTT, R-CACCAGCATGGAGATGCAGT; MAFbx F-TGAGCGACCTCAGCAGTTAC, R-ATGGCGCTCCTTCGTACTTC; FOXO1 F-GCTGGGTGTCAGGCTAAGAG, R-GAGGGGTGAAGGGCATCT; FOXO3 F-CGCTGTGTGCCCTACTTCA, R-CCCGTGCCTTCATTCTGA; Actb F-TAGCCATCCAGGCTGTGCTG, R-CAGGATCTTCATGAGGTAGTC.

Histological analyses. Hematoxylin and eosin (H&E) staining was performed on EDL and SOL muscle cross-sections to determine the cross-sectional area (CSA) of individual muscle fibers, as described previously (Stouth et al., 2020). Muscles were first sectioned at 5 μm using a cryostat set at -20 °C (Thermo Fisher Scientific Life Sciences, Waltham, MA, USA). Muscle cross-sections were then stained with hematoxylin (Sigma-Aldrich, St. Louis, MO, USA) and eosin (Bioshop Canada Inc., Burlington, ON, Canada),

dehydrated with successive 70%, 95%, and 100% ethanol exposures, further dried with xylene (Sigma-Aldrich, St. Louis, MO, USA) and mounted with Permount (Thermo Fisher Scientific Life Sciences, Waltham, MA, USA). H&E-stained muscle sections were imaged using light microscopy at 20x magnification with Nikon Elements Microscopic Imaging Software (Nikon Instruments Inc, Melville, NY, USA). The CSA of 150 myofibers across three separate regions of interest per muscle were measured (NIS-Elements). The investigators performing the image analyses were blinded to all samples.

SDH staining of EDL muscle cross-sections was carried out as described previously (Stouth et al., 2020). Briefly, muscles were cryosectioned into 8 μm slices and slides were later incubated in a buffer consisting of 0.2 M sodium succinate, 0.2 M phosphate buffer, pH 7.4, and nitro blue tetrazolium (Sigma-Aldrich, St. Louis, MO, USA) at 37 °C for one hour. Following the incubation step, muscle sections were rinsed with distilled water, exposed to 30%, 60%, and 90% acetone, and mounted with Permount (Thermo Fisher Scientific Life Sciences, Waltham, MA, USA). SDH-stained muscle sections were later imaged using light microscopy at 20x magnification with Nikon Elements Microscopic Imaging Software (Nikon Instruments Inc, Melville, NY, USA).

Preparation of permeabilized muscle fiber bundles. Permeabilization of muscle fibers was conducted as described earlier (Kuznetsov et al., 2008; Hughes et al., 2019). During tissue collection, the proximal half of the TA muscle was sectioned and immediately placed in ice-cold biopsy preservation solution (BIOPS; 10 mM Ca-EGTA solution, 5.77 mM ATP, 6.56 mM MgCl2, 20 mM taurine, 15 mM phosphocreatine, 20 mM imidazole, 0.5 mM dithiothreitol, and 50 mM MES hydrate, pH 7.1). Once fat and

connective tissue were removed, fine tip forceps were used to divide muscle fibers into small muscle bundles (~5 mg) underneath a dissection microscope while on a frozen block. The muscle bundles were then added to BIOPS solution with saponin (50 µg/µl) and mixed by end-over end inversion for 30 minutes at 4 °C. Bundles were also treated with 2,4-dinitrochlorobenzene (CDNB; 35 µM) during permeabilization to deplete glutathione and allow for detectable rates of hydrogen peroxide (H_2O_2) emission. Following permeabilization, samples were incubated in buffer Z (105 mM K-MES, 30 mM KCl, 10 mM KH_2PO_4, 5 mM $MgCl_2$, 1 mM EGTA, 5 mg/mL BSA, pH 7.4) on a rotor at 4 °C for at least 15 minutes until the respiration and H_2O_2 emission trials commenced.

Mitochondrial respiration and H_2O_2 emission. High-resolution measurements of mitochondrial oxygen consumption were assessed with the Oxygraph-2k (Oroboros Instruments, Innsbruck, Austria) as described previously (Shen et al., 2018; Hughes et al., 2019). The chambers were calibrated prior to adding 2 mL of buffer Z, blebbistatin (BLEB; 5µM), and Amplex Red. Following permeabilization and washing, muscle bundles were blotted dry, weighed, and then placed into instrument chambers. All experiments were performed at 37 °C with constant stirring at 750 rpm, and at oxygen concentrations greater than 250 nmol/mL. For ADP-stimulated respiratory kinetics, pyruvate (5 mM) and malate (2 mM) were added to stimulate complex I, followed by maximal ADP (5 mM). In the presence of complex I-specific glutamate (5 mM), succinate (20 mM) was then added to saturate electron entry into complex II. Cytochrome c (10 µM) was added last to verify mitochondrial membrane integrity, with all trials inducing <10% increase in respiration. For analysis, oxygen flux was calculated from the derivative of the oxygen concentration

in the respiratory chamber. Respiration values were then normalized to fiber bundle wet weight (pmol /sec /mg), or citrate synthase protein content determined by Western blot in TA muscle sampled from the same mouse (pmol /sec /citrate synthase arbitrary units), as validated previously (Kuznetsov et al., 2008). Mitochondrial H_2O_2 emission was measured fluorometrically using the O2k-Fluo LED2-Module (Oroboros Instruments, Innsbruck, Austria) as described previously (Buch et al., 2020). Briefly, horseradish peroxidase (1 U/ mL), superoxide dismutase (5 U/ mL), and Amplex Red (10 μM) were added to convert superoxide to H_2O_2. This was accompanied by H_2O_2-mediated conversion of Amplex Red to resorufin. Fluorometric sensor calibrations were performed by adding H_2O_2 titrations (0.1-0.4 μM) before each trial. Mitochondrial H_2O_2 emission values were also normalized to fiber bundle wet weight (pmol /sec /mg), or citrate synthase protein content (pmol /sec /citrate synthase arbitrary units).

Transmission electron microscopy (TEM). Fresh TA muscle was immediately fixed in 2% (v/v) glutaraldehyde in 0.1 mol/L sodium cacodylate buffer pH 7.4 and processed as described earlier (Nilsson et al., 2015). Mitochondria were then quantified as described previously (Monaco et al., 2018; Hughes et al., 2019). Representative micrographs from ten unique fibres were acquired at 15,000x magnification. Each micrograph contained a portion of the subsarcolemmal region adjacent to the nucleus, with most of the image containing the intermyofibrillar area. Blinded quantification of mitochondrial size (mean area, μm^2), distribution (number per μm^2) and density (μm^2 x number per μm^2 x 100) was performed by manually outlining and counting mitochondria in ImageJ. Total number of

abnormal mitochondria and autophagic bodies were also assessed at 15,000x magnification (Klionsky et al., 2021).

Immunofluorescence (IF) microscopy. The immunostaining procedure for Parkin and Tom20 was carried out as described earlier (Bujak et al., 2015). Briefly, EDL muscles embedded in OCT were sectioned into 8 μm slices. Muscle samples were later incubated in 0.2% Triton-x-100 for 30 minutes, 5% Normal Goat Serum for 40 minutes, and then Parkin antibody (1:250; 2132S; Cell Signaling, Danvers, MA, USA) overnight at 4 °C. The next day, muscle sections were incubated in Tom20 antibody (1:50; sc-17764; Santa Cruz Biotechnology, Dallas, TX, USA) for 2 hours at room temperature. Slides were then incubated in goat-anti-rabbit Alexa Fluor 594 (1:500; A-11037; Thermo Fisher Scientific Life Sciences, Waltham, MA, USA) and goat-anti-mouse Alexa Fluor 488 (1:500; A-11029; Thermo Fisher Scientific Life Sciences, Waltham, MA, USA), to visualize Parkin and Tom20, respectively. Samples were subsequently imaged using 60x magnification oil immersion lens with Nikon Elements Microscopic Imaging Software (Nikon Instruments Inc, Melville, NY, USA). For analysis, 6 regions of interest (ROI) were created per animal throughout the muscle cross-section. Images of interest were quantitatively assessed for the number of Parkin puncta by a blinded researcher as previously described (Bujak et al., 2015).

Myonuclear TFEB localization was examined with IF microscopy as described previously (Spaulding et al., 2018; Ng et al., 2019). EDL muscle snap frozen in OCT were cryosectioned into 8 μm slices. To avoid non-specific binding, slides were first blocked with 5% BSA for one hour. Slides were then incubated overnight at 4 °C in a primary

antibody solution targeting TFEB (1:100; A303-673A; Bethyl Laboratories, Montgomery, TX, USA). The following morning, sections were washed three times with 1 x PBS for 10 minutes, exposed to goat-anti-rabbit Alexa Fluor 594 (1:500; A-11037; Thermo Fisher Scientific Life Sciences, Waltham, MA, USA) for 2 hours at room temperature, followed by another three washes with 1 x PBS. Samples were then incubated in a flouorophore-conjugated wheat germ agglutinin (WGA) antibody (1:300; W11261; Thermo Fisher Scientific Life Sciences, Waltham, MA, USA) for 10 minutes and 4',6-diamidino-2-phenylindole dihydrochloride (DAPI; 1:20,000; D9542; Sigma-Aldrich, St. Louis, MO, USA) in 1% BSA in 1 x PBS for 5 minutes to label myonuclei. After the slides were dried, fluorescent mounting medium (S3023; Agilent Technologies, Mississauga, ON, Canada) was applied to mount the slide with a cover slip. Slides were then imaged by confocal microscopy at 20x magnification with Nikon Elements Microscopic Imaging Software (Nikon Instruments Inc, Melville, NY, USA). For each sample, 3-4 ROI were generated to represent approximately 40% of the total muscle CSA. Myonuclear TFEB localization was then determined as the percentage of TFEB positive myonuclei relative to total myonuclei. An average of ~900 myonuclei were counted per sample per time point. The investigators were blinded to all samples prior to commencing IF microscopy analyses.

Statistical Analyses. Statistical tests were performed on the raw data prior to conversion to the -fold differences that appear in graphical summaries. One-way analysis of variance (ANOVA), two-way ANOVA, and Tukey post hoc tests were employed to compare means between experimental groups, as appropriate. A one-way ANOVA was used to probe CARM1 expression in WT muscles under fed and fasted conditions. A two-

way ANOVA was implemented to assess the interaction between genotype and fasting for body weight, muscle weight, myofiber CSA, mRNA and protein content, oxygen and H_2O_2 flux, as well as TEM and IF microscopy analyses. Separate two-way ANOVAs were applied to WT and mKO mice treated with saline or colchicine under fed and fasted conditions. Unpaired *t*-tests between genotypes were carried out to compare relative -fold changes that occurred with fasting. Statistical analyses were assessed using Prism software (GraphPad Software, San Diego, CA, USA). All results are expressed as means ± SEM and statistical differences were considered significant if $p < 0.05$.

Acknowledgements

We thank Dr. Mark Bedford (MD Anderson Cancer Center, University of Texas) and Dr. Anne Brunet (Department of Genetics, Stanford University School of Medicine) for the gifts of CARM1 floxed mice and the CARM1 substrate reagent, as well as the P-FOXO3^{Ser588} antibody, respectively. We also thank Dr. Lawrence Kazak (McGill University, Canada) for assistance with genotyping. We are grateful to members of the Integrative Neuromuscular Biology Laboratory and to colleagues in the Exercise Metabolism Research Group at McMaster University for helpful advice and discussion. This work was funded by the Natural Science and Engineering Research Council of Canada (NSERC), the Canada Research Chairs program, and the Ontario Ministry of Economic Development, Job Creation and Trade (MEDJCT). D.W.S., T.L.V., S.Y.N., and E.K.W. are NSERC postgraduate scholars. E.K.W. is an Interdisciplinary Fellow of the Canadian Frailty Network. V.L. is the Canada Research Chair (Tier 2) in Neuromuscular Plasticity in Health and Disease and is a MEDJCT Early Researcher.

Author Contributions

D.W.S. and V.L. conceived and designed the study; D.W.S. and T.L.v. generated and maintained CARM1 mKO mice; D.W.S. performed all experiments and most analyses. S.Y.N., A.M., E.K.W., K.S.G., M.M., H.C.P., B.G.B., H.N., Z.M., and M.E.B. assisted with analyses; all authors participated in data analysis and interpretation of results; D.W.S. and V.L. drafted and edited the manuscript.

Disclosure statement:

No conflicts of interest, financial or otherwise, are declared by the authors.

References

Bao, J., Rousseaux, S., Shen, J., Lin, K., Lu, Y., & Bedford, M. T. (2018). The arginine methyltransferase CARM1 represses p300•ACT•CREMτ activity and is required for spermiogenesis. Nucleic acids research, 46(9), 4327–4343.

Bedford, M. T., & Clarke, S. G. (2009). Protein arginine methylation in mammals: who, what, and why. Molecular cell, 33(1), 1–13.

Brocca, L., Toniolo, L., Reggiani, C., Bottinelli, R., Sandri, M., & Pellegrino, M. A. (2017). FoxO-dependent atrogenes vary among catabolic conditions and play a key role in muscle atrophy induced by hindlimb suspension. The Journal of physiology, 595(4), 1143–1158.

Buch, B. T., Halling, J. F., Ringholm, S., Gudiksen, A., Kjøbsted, R., Olsen, M. A., Wojtaszewski, J., & Pilegaard, H. (2020). Colchicine treatment impairs skeletal muscle mitochondrial function and insulin sensitivity in an age-specific manner. FASEB journal : official publication of the Federation of American Societies for Experimental Biology, 34(6), 8653–8670.

Bujak, A. L., Crane, J. D., Lally, J. S., Ford, R. J., Kang, S. J., Rebalka, I. A., Green, A. E., Kemp, B. E., Hawke, T. J., Schertzer, J. D., & Steinberg, G. R. (2015). AMPK activation of muscle autophagy prevents fasting-induced hypoglycemia and myopathy during aging. Cell metabolism, 21(6), 883–890.

Calnan, D. R., & Brunet, A. (2008). The FoxO code. Oncogene, 27(16), 2276–2288.

Carter, H. N., Kim, Y., Erlich, A. T., Zarrin-Khat, D., & Hood, D. A. (2018). Autophagy and mitophagy flux in young and aged skeletal muscle following chronic contractile activity. The Journal of physiology, 596(16), 3567–3584.

Castets, P., Lin, S., Rion, N., Di Fulvio, S., Romanino, K., Guridi, M., Frank, S., Tintignac, L. A., Sinnreich, M., & Rüegg, M. A. (2013). Sustained activation of mTORC1 in skeletal muscle inhibits constitutive and starvation-induced autophagy and causes a severe, late-onset myopathy. Cell metabolism, 17(5), 731–744.

Chang, N. C., Sincennes, M. C., Chevalier, F. P., Brun, C. E., Lacaria, M., Segalés, J., Muñoz-Cánoves, P., Ming, H., & Rudnicki, M. A. (2018). The Dystrophin Glycoprotein Complex Regulates the Epigenetic Activation of Muscle Stem Cell Commitment. Cell stem cell, 22(5), 755–768.e6.

Chen, S. L., Loffler, K. A., Chen, D., Stallcup, M. R., & Muscat, G. E. (2002). The coactivator-associated arginine methyltransferase is necessary for muscle differentiation: CARM1 coactivates myocyte enhancer factor-2. The Journal of biological chemistry, 277(6), 4324–4333.

Cheng, D., Gao, G., Di Lorenzo, A., Jayne, S., Hottiger, M. O., Richard, S., & Bedford, M. T. (2020). Genetic evidence for partial redundancy between the arginine methyltransferases CARM1 and PRMT6. The Journal of biological chemistry, 295(50), 17060–17070.

Cheng, D., Vemulapalli, V., Lu, Y., Shen, J., Aoyagi, S., Fry, C. J., Yang, Y., Foulds, C. E., Stossi, F., Treviño, L. S., Mancini, M. A., O'Malley, B. W., Walker, C. L., Boyer, T. G., & Bedford, M. T. (2018). CARM1 methylates MED12 to regulate its RNA-binding ability. Life science alliance, 1(5), e201800117.

Dimauro, I., Pearson, T., Caporossi, D., & Jackson, M. J. (2012). A simple protocol for the subcellular fractionation of skeletal muscle cells and tissue. BMC research notes, 5, 513.

Fulton, M. D., Brown, T., & Zheng, Y. G. (2019). The Biological Axis of Protein Arginine Methylation and Asymmetric Dimethylarginine. International journal of molecular sciences, 20(13), 3322.

Greer, E. L., Oskoui, P. R., Banko, M. R., Maniar, J. M., Gygi, M. P., Gygi, S. P., & Brunet, A. (2007). The energy sensor AMP-activated protein kinase directly regulates the mammalian FOXO3 transcription factor. The Journal of biological chemistry, 282(41), 30107–30119.

Guccione, E., & Richard, S. (2019). The regulation, functions and clinical relevance of arginine methylation. Nature reviews. Molecular cell biology, 20(10), 642–657.

Hood, D. A., Memme, J. M., Oliveira, A. N., & Triolo, M. (2019). Maintenance of Skeletal Muscle Mitochondria in Health, Exercise, and Aging. Annual review of physiology, 81, 19–41.

Hu, R., Wang, M. Q., Liu, L. Y., You, H. Y., Wu, X. H., Liu, Y. Y., Wang, Y. J., Lu, L., Xiao, W., & Wei, L. B. (2020). Calycosin inhibited autophagy and oxidative stress in chronic kidney disease skeletal muscle atrophy by regulating AMPK/SKP2/CARM1 signalling pathway. Journal of cellular and molecular medicine, 24(19), 11084–11099.

Hughes, M. C., Ramos, S. V., Turnbull, P. C., Rebalka, I. A., Cao, A., Monaco, C., Varah, N. E., Edgett, B. A., Huber, J. S., Tadi, P., Delfinis, L. J., Schlattner, U., Simpson, J. A., Hawke, T. J., & Perry, C. (2019). Early myopathy in Duchenne muscular dystrophy is associated with elevated mitochondrial H2 O2 emission during impaired oxidative phosphorylation. Journal of cachexia, sarcopenia and muscle, 10(3), 643–661.

Ju, J. S., Varadhachary, A. S., Miller, S. E., & Weihl, C. C. (2010). Quantitation of "autophagic flux" in mature skeletal muscle. Autophagy, 6(7), 929–935.

Kawabe, Y., Wang, Y. X., McKinnell, I. W., Bedford, M. T., & Rudnicki, M. A. (2012). Carm1 regulates Pax7 transcriptional activity through MLL1/2 recruitment during asymmetric satellite stem cell divisions. Cell stem cell, 11(3), 333–345.

Kjøbsted, R., Hingst, J. R., Fentz, J., Foretz, M., Sanz, M. N., Pehmøller, C., Shum, M., Marette, A., Mounier, R., Treebak, J. T., Wojtaszewski, J., Viollet, B., & Lantier, L. (2018). AMPK in skeletal muscle function and metabolism. FASEB journal : official publication of the Federation of American Societies for Experimental Biology, 32(4), 1741–1777.

Klionsky, D. J., Abdel-Aziz, A. K., Abdelfatah, S., Abdellatif, M., Abdoli, A., Abel, S., Abeliovich, H., Abildgaard, M. H., Abudu, Y. P., Acevedo-Arozena, A., Adamopoulos, I. E., Adeli, K., Adolph, T. E., Adornetto, A., Aflaki, E., Agam, G., Agarwal, A., Aggarwal, B. B., Agnello, M., Agostinis, P., … Tong, C. K. (2021). Guidelines for the use and interpretation of assays for monitoring autophagy (4th edition)1. Autophagy, 17(1), 1–382.

Kuznetsov, A. V., Veksler, V., Gellerich, F. N., Saks, V., Margreiter, R., & Kunz, W. S. (2008). Analysis of mitochondrial function in situ in permeabilized muscle fibers, tissues and cells. Nature protocols, 3(6), 965–976.

Laker, R. C., Drake, J. C., Wilson, R. J., Lira, V. A., Lewellen, B. M., Ryall, K. A., Fisher, C. C., Zhang, M., Saucerman, J. J., Goodyear, L. J., Kundu, M., & Yan, Z. (2017). Ampk phosphorylation of Ulk1 is required for targeting of mitochondria to lysosomes in exercise-induced mitophagy. Nature communications, 8(1), 548.

Larsen, S. C., Sylvestersen, K. B., Mund, A., Lyon, D., Mullari, M., Madsen, M. V., Daniel, J. A., ..., & Nielsen, M. L. (2016). Proteome-wide analysis of arginine monomethylation reveals widespread occurrence in human cells. Science signaling, 9(443), rs9.

Li, C., Yu, L., Xue, H., Yang, Z., Yin, Y., Zhang, B., Chen, M., & Ma, H. (2017). Nuclear AMPK regulated CARM1 stabilization impacts autophagy in aged heart. Biochemical and biophysical research communications, 486(2), 398–405.

Liu, Y., Li, J., Shang, Y., Guo, Y., & Li, Z. (2019). CARM1 contributes to skeletal muscle wasting by mediating FoxO3 activity and promoting myofiber autophagy. Experimental cell research, 374(1), 198–209.

Ljubicic, V., Khogali, S., Renaud, J. M., & Jasmin, B. J. (2012). Chronic AMPK stimulation attenuates adaptive signaling in dystrophic skeletal muscle. American journal of physiology. Cell physiology, 302(1), C110–C121.

Markby, G. R., & Sakamoto, K. (2020). Transcription factor EB and TFE3: new metabolic coordinators mediating adaptive responses to exercise in skeletal muscle?. American journal of physiology. Endocrinology and metabolism, 319(4), E763–E768.

Martina, J. A., Diab, H. I., Lishu, L., Jeong-A, L., Patange, S., Raben, N., & Puertollano, R. (2014). The nutrient-responsive transcription factor TFE3 promotes autophagy, lysosomal biogenesis, and clearance of cellular debris. Science signaling, 7(309), ra9.

McCarthy, J. J., Srikuea, R., Kirby, T. J., ..., & Esser, K. A. (2012). Inducible Cre transgenic mouse strain for skeletal muscle-specific gene targeting. Skeletal muscle, 2(1), 8.

Milan, G., Romanello, V., Pescatore, F., Armani, A., Paik, J. H., Frasson, L., Seydel, A., Zhao, J., Abraham, R., Goldberg, A. L., Blaauw, B., DePinho, R. A., & Sandri, M. (2015). Regulation of autophagy and the ubiquitin-proteasome system by the FoxO transcriptional network during muscle atrophy. Nature communications, 6, 6670.

Monaco, C., Hughes, M. C., Ramos, S. V., Varah, N. E., Lamberz, C., Rahman, F. A., McGlory, C., Tarnopolsky, M. A., Krause, M. P., Laham, R., Hawke, T. J., & Perry, C. (2018). Altered mitochondrial bioenergetics and ultrastructure in the skeletal muscle of young adults with type 1 diabetes. Diabetologia, 61(6), 1411–1423.

Napolitano, G., Esposito, A., Choi, H., Matarese, M., Benedetti, V., Di Malta, C., Monfregola, J., Medina, D. L., ..., & Ballabio, A. (2018). mTOR-dependent phosphorylation controls TFEB nuclear export. Nature communications, 9(1), 3312.

Ng, S. Y., Mikhail, A., & Ljubicic, V. (2019). Mechanisms of exercise-induced survival motor neuron expression in the skeletal muscle of spinal muscular atrophy-like mice. The Journal of physiology, 597(18), 4757–4778.

Nilsson, M. I., MacNeil, L. G., Kitaoka, Y., Suri, R., Young, S. P., Kaczor, J. J., Nates, N. J., Ansari, M. U., Wong, T., Ahktar, M., Brandt, L., Hettinga, B. P., & Tarnopolsky, M. A. (2015). Combined aerobic exercise and enzyme replacement therapy rejuvenates the mitochondrial-lysosomal axis and alleviates autophagic blockage in Pompe disease. Free radical biology & medicine, 87, 98–112.

Paquette, M., El-Houjeiri, L., C Zirden, L., Puustinen, P., Blanchette, P., Jeong, H., Dejgaard, K., Siegel, P. M., & Pause, A. (2021). AMPK-dependent phosphorylation is required for transcriptional activation of TFEB and TFE3. Autophagy, 1–19.

Pastore, N., Vainshtein, A., Klisch, T. J., Armani, A., Huynh, T., Herz, N. J., Polishchuk, E. V., Sandri, M., & Ballabio, A. (2017). TFE3 regulates whole-body energy metabolism in cooperation with TFEB. EMBO molecular medicine, 9(5), 605–621.

Philp, A., Chen, A., Lan, D., Meyer, G. A., Murphy, A. N., Knapp, A. E., Olfert, I. M., McCurdy, C. E., Marcotte, G. R., Hogan, M. C., Baar, K., & Schenk, S. (2011). Sirtuin 1 (SIRT1) deacetylase activity is not required for mitochondrial biogenesis or peroxisome proliferator-activated receptor-gamma coactivator-1alpha (PGC-1alpha) deacetylation following endurance exercise. The Journal of biological chemistry, 286(35), 30561–30570.

Romero-Calvo, I., Ocón, B., Martínez-Moya, P., Suárez, M. D., Zarzuelo, A., Martínez-Augustin, O., & de Medina, F. S. (2010). Reversible Ponceau staining as a loading control alternative to actin in Western blots. Analytical biochemistry, 401(2), 318–320.

Sanchez, A. M., Candau, R. B., & Bernardi, H. (2014). FoxO transcription factors: their roles in the maintenance of skeletal muscle homeostasis. Cellular and molecular life sciences : CMLS, 71(9), 1657–1671.

Sandri M. (2013). Protein breakdown in muscle wasting: role of autophagy-lysosome and ubiquitin-proteasome. The international journal of biochemistry & cell biology, 45(10), 2121–2129.

Sartori, R., Romanello, V., & Sandri, M. (2021). Mechanisms of muscle atrophy and hypertrophy: implications in health and disease. Nature communications, 12(1), 330.

Schmittgen, T. D., & Livak, K. J. (2008). Analyzing real-time PCR data by the comparative C(T) method. Nature protocols, 3(6), 1101–1108.

Shen, N. Y., Ng, S. Y., Toepp, S. L., & Ljubicic, V. (2018). Protein arginine methyltransferase expression and activity during myogenesis. Bioscience reports, 38(1), BSR20171533.

Shin, H. J., Kim, H., Oh, S., Lee, J. G., Kee, M., Ko, H. J., Kweon, M. N., Won, K. J., & Baek, S. H. (2016). AMPK-SKP2-CARM1 signalling cascade in transcriptional regulation of autophagy. Nature, 534(7608), 553–557.

Spaulding, H. R., Kelly, E. M., Quindry, J. C., Sheffield, J. B., Hudson, M. B., & Selsby, J. T. (2018). Autophagic dysfunction and autophagosome escape in the mdx mus musculus model of Duchenne muscular dystrophy. Acta physiologica (Oxford, England), 222(2), 10.1111/apha.12944.

Stouth, D. W., Manta, A., & Ljubicic, V. (2018). Protein arginine methyltransferase expression, localization, and activity during disuse-induced skeletal muscle plasticity. American journal of physiology. Cell physiology, 314(2), C177–C190.

Stouth, D. W., vanLieshout, T. L., Ng, S. Y., Webb, E. K., Manta, A., Moll, Z., & Ljubicic, V. (2020). CARM1 Regulates AMPK Signaling in Skeletal Muscle. iScience, 23(11), 101755.

Stouth, D. W., vanLieshout, T. L., Shen, N. Y., & Ljubicic, V. (2017). Regulation of Skeletal Muscle Plasticity by Protein Arginine Methyltransferases and Their Potential Roles in Neuromuscular Disorders. Frontiers in physiology, 8, 870.

Triolo, M., & Hood, D. A. (2021). Manifestations of Age on Autophagy, Mitophagy and Lysosomes in Skeletal Muscle. Cells, 10(5), 1054.

Vainshtein, A., Desjardins, E. M., Armani, A., Sandri, M., & Hood, D. A. (2015). PGC-1α modulates denervation-induced mitophagy in skeletal muscle. Skeletal muscle, 5, 9.

vanLieshout, T. L., & Ljubicic, V. (2019). The emergence of protein arginine methyltransferases in skeletal muscle and metabolic disease. American journal of physiology. Endocrinology and metabolism, 317(6), E1070–E1080.

vanLieshout, T. L., Bonafiglia, J. T., Gurd, B. J., & Ljubicic, V. (2019). Protein arginine methyltransferase biology in humans during acute and chronic skeletal muscle plasticity. Journal of applied physiology (Bethesda, Md. : 1985), 127(3), 867–880.

Vanlieshout, T. L., Stouth, D. W., Tajik, T., & Ljubicic, V. (2018). Exercise-induced Protein Arginine Methyltransferase Expression in Skeletal Muscle. Medicine and science in sports and exercise, 50(3), 447–457.

Vendelbo, M. H., Møller, A. B., Christensen, B., Nellemann, B., Clasen, B. F., Nair, K. S., Jørgensen, J. O., Jessen, N., & Møller, N. (2014). Fasting increases human skeletal muscle net phenylalanine release and this is associated with decreased mTOR signaling. PloS one, 9(7), e102031.

Wang, S. C., Dowhan, D. H., Eriksson, N. A., & Muscat, G. E. (2012). CARM1/PRMT4 is necessary for the glycogen gene expression programme in skeletal muscle cells. The Biochemical journal, 444(2), 323–331.

Yadav, N., Lee, J., Kim, J., Shen, J., Hu, M. C., Aldaz, C. M., & Bedford, M. T. (2003). Specific protein methylation defects and gene expression perturbations in coactivator-associated arginine methyltransferase 1-deficient mice. Proceedings of the National Academy of Sciences of the United States of America, 100(11), 6464–6468.

Yang, Y., & Bedford, M. T. (2013). Protein arginine methyltransferases and cancer. Nature reviews. Cancer, 13(1), 37–50.

Yu, Y. S., Shin, H. R., Kim, D., Baek, S. A., Choi, S. A., Ahn, H., Shamim, A., Kim, J., Kim, I. S., Kim, K. K., ..., & Baek, S. H. (2020). Pontin arginine methylation by CARM1 is crucial for epigenetic regulation of autophagy. Nature communications, 11(1), 6297.

Zhou, K., Chen, H., Lin, J., Xu, H., Wu, H., Bao, G., Li, J., Deng, X., Shui, X., Gao, W., Ding, J., Xiao, J., & Xu, H. (2019). FGF21 augments autophagy in random-pattern skin flaps via AMPK signaling pathways and improves tissue survival. Cell death & disease, 10(12), 872.

Figure Legends

Figure 1. Fasting-induced atrophy in skeletal muscle specific CARM1 knockout (mKO) mice. A: Representative Western blots of CARM1 protein content (normal and long exposures) in the tibialis anterior (TA) muscle from wild-type (WT) and mKO mice under fed (Fed) and fasted [Fast, 24 and 48 hours (hr)] conditions, as well as a representative Ponceau stain, below. Molecular weights (kDa) are shown at right of blots. **B:** Graphical summary of CARM1 protein expression in TA muscle of WT animals. Data are expressed as protein content relative to Fed (n = 14). **C:** CARM1 mRNA expression in the extensor digitorum longus (EDL) muscle of WT mice during Fed and Fast conditions. Data are expressed relative to the Fed condition (n = 11–12). **D:** Body mass of WT and mKO animals in response to fasting (n = 11-21). **E:** TA, EDL, soleus (SOL), and gastrocnemius (GAST) muscle mass from WT and mKO mice in Fed and Fast conditions. Muscle weight data are expressed relative to WT Fed (n = 8-21). **F-G:** Representative images of H&E-stained EDL and SOL muscle cross sections from WT and mKO mice in Fed and Fast cohorts. Scale bar, 50 μm. **H-I:** Graphical summaries of the average myofiber cross-sectional area (CSA) of EDL and SOL muscles from WT and mKO mice in response to fasting. Data are expressed as CSA relative to the WT Fed (n = 7-10). Data are means ± SEM. Two-way ANOVA; $ $p < 0.05$ interaction effect of genotype and fasting; ¢ $p < 0.05$ main effect of genotype; ‡ $p < 0.05$ main effect of fasting; ¶ $p < 0.05$ versus WT Fed; # $p < 0.05$ versus mKO Fed.

Figure 2. Protein arginine methyltransferase (PRMT) content and activity in mKO animals following fasting-evoked muscle wasting. A: PRMT1, PRMT5, PRMT6, and PRMT7 mRNA expression in EDL muscles from WT and mKO mice during Fed and Fast conditions. Data are expressed as mRNA content relative to WT Fed muscle (n = 9-13). **B:** Representative Western blots of PRMT1, PRMT5, PRMT6, PRMT7, monomethylarginine (MMA), asymmetric dimethylarginine (ADMA), asymmetric arginine dimethylated CARM1 substrates, symmetric dimethylarginine (SDMA), asymmetrically dimethylated SWI/SNF chromatin remodeling complex BAF155 (BAF155me2a^{Arg1064}), total BAF155, asymmetrically dimethylated poly(A)-binding protein 1 (PABP1me2a$^{Arg455/Arg460}$), and total PABP1 in TA muscles from WT and mKO animals in Fed and Fast cohorts, accompanied by a typical Ponceau stain. Molecular weights (kDa) are shown at the right of blots. **C-F:** Graphical summaries of PRMT1, PRMT5, PRMT6, PRMT7, MMA, ADMA, CARM1 substrate, SDMA, BAF155me2a ^{Arg1064}, BAF155, BAF155 activation status (i.e., the methylated form of the protein relative to the total amount of the protein), PABP1me2a $^{Arg455/Arg460}$, PABP1, and PABP1 activation status in WT and mKO mice after fasting. Data are expressed as protein content relative to WT Fed (n = 8-14). Data are means ± SEM. Two-way ANOVA; $ $p < 0.05$ interaction effect of genotype and fasting; ¢ $p < 0.05$ main effect of genotype; ‡ $p < 0.05$ main effect of fasting; ¶ $p < 0.05$ versus WT Fed.

Figure 3. CARM1 regulates metabolic signaling during fasting-induced muscle atrophy. A: Peroxisome proliferator-activated receptor-γ coactivator-1α (PGC-1α), mitochondrial transcription factor A (Tfam), and nuclear factor erythroid 2-related factor 2 (Nrf2) mRNA expression in EDL muscles from WT and mKO mice under Fed and Fast

conditions. Data are expressed as mRNA content relative to WT Fed (n = 9-13). **B:** Representative Western blots of phosphorylated AMP-activated protein kinase (P-AMPK^{Thr172}), total AMPK, phosphorylated cAMP response element-binding protein (P-Creb^{Ser133}), total Creb, PGC-1α, citrate synthase, and proteins indicative of mitochondrial oxidative phosphorylation (OXPHOS) complexes I–V (CI–CV) in WT and mKO TA muscles following fasting, accompanied by a typical Ponceau stain. Molecular weights (kDa) are shown at the right of blots. **C-E:** Graphical summaries of P-AMPK^{Thr172}, AMPK, AMPK activation status, P-Creb^{Ser133}, Creb, Creb activation status, PGC-1α, citrate synthase, and total OXPHOS protein expression in WT and mKO TA muscles in response to fasting. Data are expressed as protein content relative to WT Fed (n = 9–21). **F:** Representative images of succinate dehydrogenase (SDH)-stained EDL muscle cross-sections from WT and mKO mice after food deprivation. Scale bar, 50 μm (n = 5–6). **G:** Representative oxygraph trace from high-resolution respirometry showing mass-specific oxygen flux (red line) that is calculated by the change in slope of oxygen concentration (blue line) in the respiratory chamber. Pyruvate (P) and malate (M) were added as complex I-specific substrates, followed by maximal (5 mM) ADP (D)-stimulated state III respiration. In the presence of complex I-specific glutamate (G), succinate (S) was added to induce complex II-supported respiration. **H-I:** Complex I-supported state III respiration and Complex I + II-supported state III respiration in WT and mKO TA muscle under Fed and 48 hr Fast conditions (n = 11-14). **J**: Complex I-supported state III H_2O_2 emission in WT and mKO animals after 48 hr Fast (n = 8-11). Data are means ± SEM. Two-way

ANOVA; ¢ $p < 0.05$ main effect of genotype; ‡ $p < 0.05$ main effect of fasting; ¶ $p < 0.05$ versus WT Fed; # $p < 0.05$ versus mKO Fed.

Figure 4. Mitochondrial morphology and mitophagy in mKO mice during fasting-evoked muscle atrophy. A: Representative transmission electron micrographs of mitochondria and myonuclei (*) within the subsarcolemmal (SS) and intermyofibrillar (IMF) regions of TA muscle in WT and mKO mice under Fed and 48 hr Fast conditions. Scale bar, 1 μm (n = 4). **B:** Representative image from WT muscle of normal mitochondrial ultrastructure with intact membranes and clearly defined cristae (white arrow). Scale bar, 200 nm. **C-E:** Transmission electron micrographs were analysed for mitochondrial size (mean area, μm^2), distribution (# per μm^2), and density (μm^2 x # per μm^2 x 100) within the SS and IMF areas of the muscle. **F:** Representative Western blots of Parkin, BCL2 and adenovirus E1B 19-kDa interacting protein 3 (Bnip3) in WT and mKO TA muscles during Fed and Fast conditions, accompanied by a typical Ponceau stain. Molecular weights (kDa) are shown at the right of blots. **G:** Graphical summary of Parkin and Bnip3 protein expression levels in WT and mKO animals after fasting. Data are expressed as protein content relative to WT Fed (n = 11-18). **H:** Representative images of EDL muscle cross sections stained for Parkin (red; scale bar, 2 μm) and translocase of the outer membrane of mitochondria (Tom20; green; scale bar, 1 μm) with a merged image. **I:** Graphical summary of Parkin puncta in WT and mKO mice following food deprivation. Data are expressed as number of Parkin puncta per 1000 μm^2 (n = 3). Data are means ± SEM. Two-way ANOVA; $ $p < 0.05$ interaction effect of genotype and fasting; ¢ $p < 0.05$ main effect of genotype; ‡ $p < 0.05$ main effect of fasting; ¶ $p < 0.05$ versus WT Fed; # $p < 0.05$ versus mKO Fed.

Figure 5. Skeletal muscle autophagy is dysregulated in mKO animals during atrophy. **A:** Representative Western blot of microtubule-associated protein 1A/1B-light chain 3 (LC3)-I and LC3-II in TA muscles of WT and mKO mice treated with saline (Sal) or colchicine (Col) under Fed and 48 hr Fast conditions, accompanied by a typical Ponceau stain. Molecular weights (kDa) are shown at the right of blots. **B-C:** Graphical summaries of LC3-II/LC3-I ratio, as well as LC3-II flux in WT and mKO animals administered Sal or Col under Fed and 48 hr Fast conditions. Data are expressed as protein content relative to Sal WT Fed (n = 12-16). **D-E:** Representative images from mKO muscles of abnormal mitochondrial ultrastructure (black arrow) with disrupted membranes, loss of cristae, and vacuolization, as well as a double-membrane autophagic vacuole (yellow arrow). Scale bar, 200 nm. **F-G:** Graphical summaries of total number of abnormal mitochondria and autophagic bodies in WT and mKO mice treated with Sal or Col under Fed and 48 hr Fast conditions. **H:** Autophagy-related 14 (Atg14), Beclin-1, Gabarapl, and Cathepsin L mRNA expression in EDL muscles from WT and mKO animals under Fed and Fast conditions. Data are expressed as mRNA content relative to WT Fed (n = 9-13). **I:** Representative Western blots of phosphorylated unc-51-like autophagy-activating kinase 1 (P-ULK1^{Ser555}), total ULK1, S-phase kinase-associated protein 2 (SKP2), transcription factor EB (TFEB), Beclin-1, lysosomal associated membrane protein 1 (Lamp1), Lamp2, and cathepsin D in WT and mKO TA muscles after food deprivation, accompanied by a typical Ponceau stain. Molecular weights (kDa) are shown at the right of blots. **J-L:** Graphical summaries of P-ULK1^{Ser555}, ULK1, ULK1 activation status, SKP2, TFEB, Beclin-1, Lamp1, Lamp2, and cathepsin D protein expression in WT and mKO animals following

fasting. Data are expressed as protein content relative to WT Fed (n = 9-18). Data are means ± SEM. Two-way ANOVA; $ $p < 0.05$ interaction effect of genotype and fasting; ¢ $p < 0.05$ main effect of genotype; ‡ $p < 0.05$ main effect of fasting; § $p < 0.05$ main effect of Col; ¶ $p < 0.05$ versus WT Fed; # $p < 0.05$ versus mKO Fed.

Figure 6. CARM1 regulates the muscle atrophy program during fasting-induced muscle wasting. A: Muscle RING finger 1 (MuRF1), muscle atrophy F box (MAFbx), and Forkhead box O3 (FOXO3) mRNA expression in EDL muscles from WT and mKO mice during Fed and Fast conditions. Data are expressed as mRNA content relative to WT Fed (n = 9-13). **B:** Representative Western blots of MuRF1, MAFbx, ubiquitin protein content, phosphorylated protein kinase B (P-Akt^{Ser473}), total Akt, phosphorylated mammalian target of rapamycin (P-mTOR^{Ser2448}), total mTOR, P-FOXO1^{Ser256}, total FOXO1, P-FOXO3^{Ser253}, P-FOXO3^{Ser413}, P-FOXO3^{Ser588}, and total FOXO3 in WT and mKO TA muscles after food deprivation, accompanied by a typical Ponceau stain. Molecular weights (kDa) are shown at the right of blots. **C-G:** Graphical summaries of MuRF1, MAFbx, ubiquitin protein content, P-Akt^{Ser473}, Akt, Akt activation status, P-mTOR^{Ser2448}, mTOR, mTOR activation status, P-FOXO1^{Ser256}, FOXO1, FOXO1 activation status, P-FOXO3^{Ser253}, P-FOXO3^{Ser413}, P-FOXO3^{Ser588}, FOXO3, and FOXO3 activation statuses in WT and mKO animals in response to fasting. Data are expressed as protein content relative to WT Fed (n = 9-20). Data are means ± SEM. Two-way ANOVA; $ $p < 0.05$ interaction effect of genotype and fasting; ¢ $p < 0.05$ main effect of genotype; ‡ $p < 0.05$ main effect of fasting; ¶ $p < 0.05$ versus WT Fed; # $p < 0.05$ versus mKO Fed.

Figure 7. Altered myonuclear localization of muscle remodeling and autophagic proteins in mKO animals after fasting. A: Representative Western blots of CARM1 (normal and long exposures), PRMT1, PRMT5, PRMT6, PRMT7, PGC-1α, P-AMPK^{Thr172}, total AMPK, TFEB, P-FOXO3^{Ser588}, total FOXO3, Histone H3 (normal and long exposures), and glyceraldehyde-3-phosphate dehydrogenase (GAPDH; normal and long exposures) in myonuclei isolated from WT and mKO GAST muscles following food deprivation, accompanied by a typical Ponceau stain. Molecular weights (kDa) are shown at the right of blots. **B-D:** Graphical summaries of nuclear CARM1, PRMT1, PRMT5, PRMT6, PGC-1α, P-AMPK^{Thr172}, AMPK, AMPK activation status, TFEB, P-FOXO3^{Ser588}, FOXO3, and FOXO3 activation status in WT and mKO mice after fasting. Data are expressed as nuclear protein content relative to WT Fed (n = 11-13). **E:** Representative images of EDL muscle cross sections stained for wheat germ agglutinin (WGA; green), 4',6-diamidino-2-phenylindole dihydrochloride (DAPI; blue), and TFEB (red). Scale bar of merged image, 50 μm. Higher magnifications are inset with TFEB positive myonuclei (white arrows). Scale bar of inset, 10 μm. **F:** Graphical summary of nuclear TFEB content in WT and mKO animals following food deprivation. Data are expressed as TFEB positive myonuclei relative to WT Fed (n = 6). Data are means ± SEM. Two-way ANOVA; $ $p < 0.05$ interaction effect of genotype and fasting; ¢ $p < 0.05$ main effect of genotype; ‡ $p < 0.05$ main effect of fasting; ¶ $p < 0.05$ versus WT Fed; # $p < 0.05$ versus mKO Fed.

Figure 1

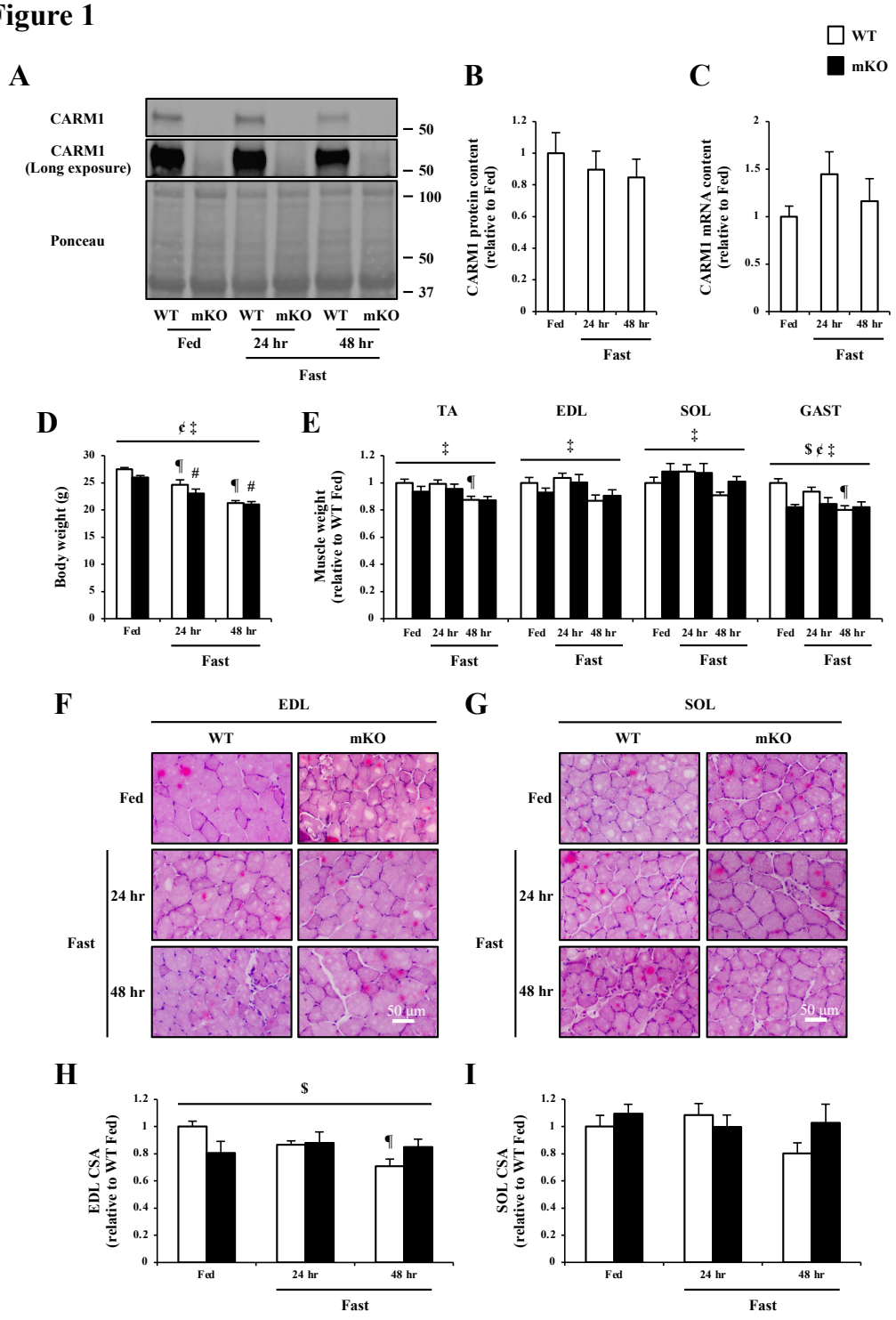
A
CARM1
CARM1 (Long exposure)
Ponceau
50
50
100
50
37
WT mKO WT mKO WT mKO
Fed
24 hr
48 hr
Fast
B
CARM1 protein content (relative to Fed)
C
CARM1 mRNA content (relative to Fed)
WT
mKO
D
Body weight (g)
E
TA
EDL
SOL
GAST
Muscle weight (relative to WT Fed)
F
EDL
WT
mKO
Fed
24 hr
48 hr
Fast
50 μm
G
SOL
H
EDL CSA (relative to WT Fed)
I
SOL CSA (relative to WT Fed)

Figure 2

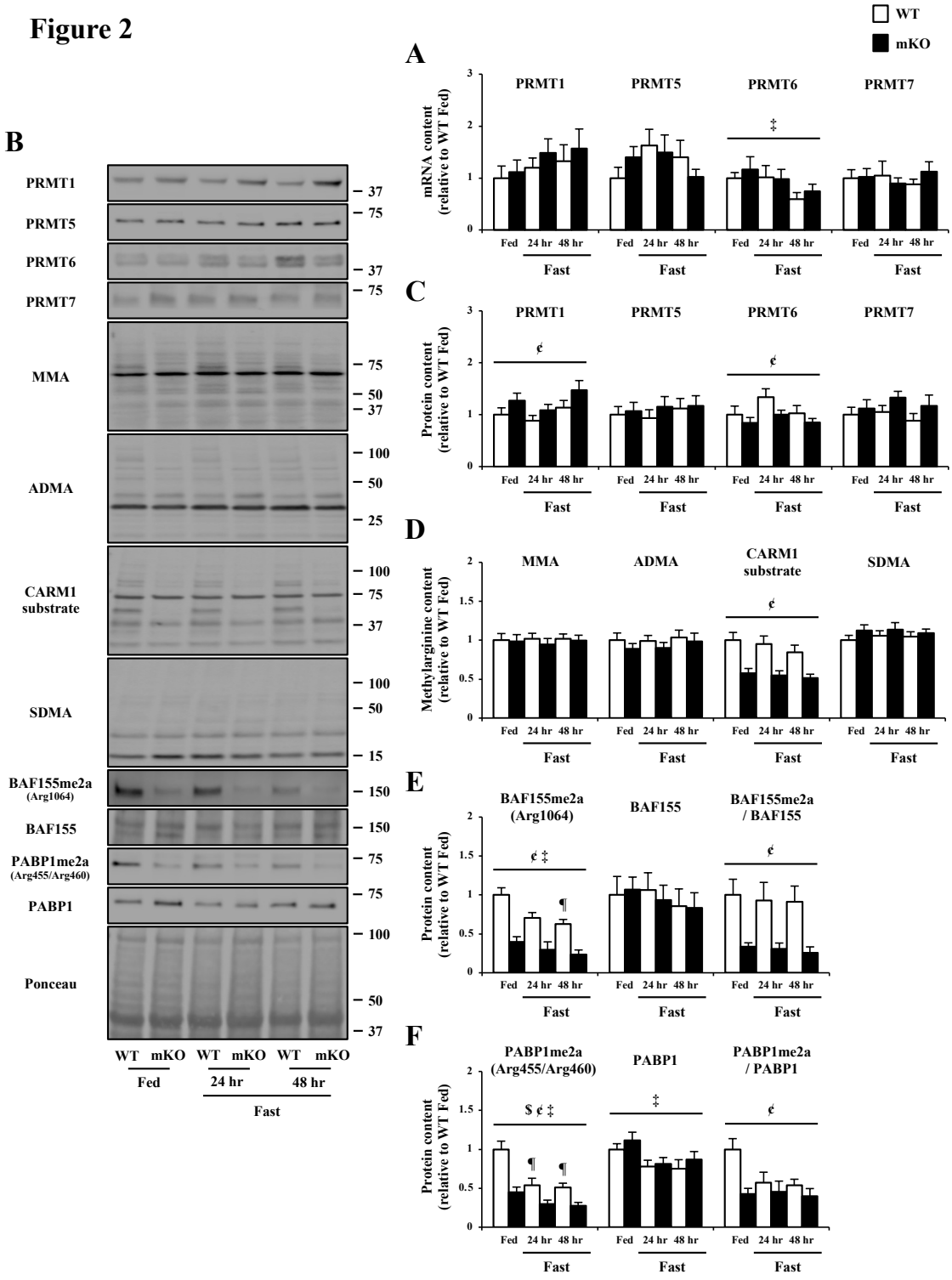
B
PRMT1
PRMT5
PRMT6
PRMT7
MMA
ADMA
CARM1 substrate
SDMA
BAF155me2a (Arg1064)
BAF155
PABP1me2a (Arg455/Arg460)
PABP1
Ponceau
WT mKO WT mKO WT mKO
Fed
24 hr
48 hr
Fast
A
C
D
E
F
WT
mKO
mRNA content (relative to WT Fed)
Protein content (relative to WT Fed)
Methylarginine content (relative to WT Fed)
PRMT1
PRMT5
PRMT6
PRMT7
MMA
ADMA
CARM1 substrate
SDMA
BAF155me2a (Arg1064)
BAF155
BAF155me2a / BAF155
PABP1me2a (Arg455/Arg460)
PABP1
PABP1me2a / PABP1
Fed 24 hr 48 hr
Fast

Figure 3

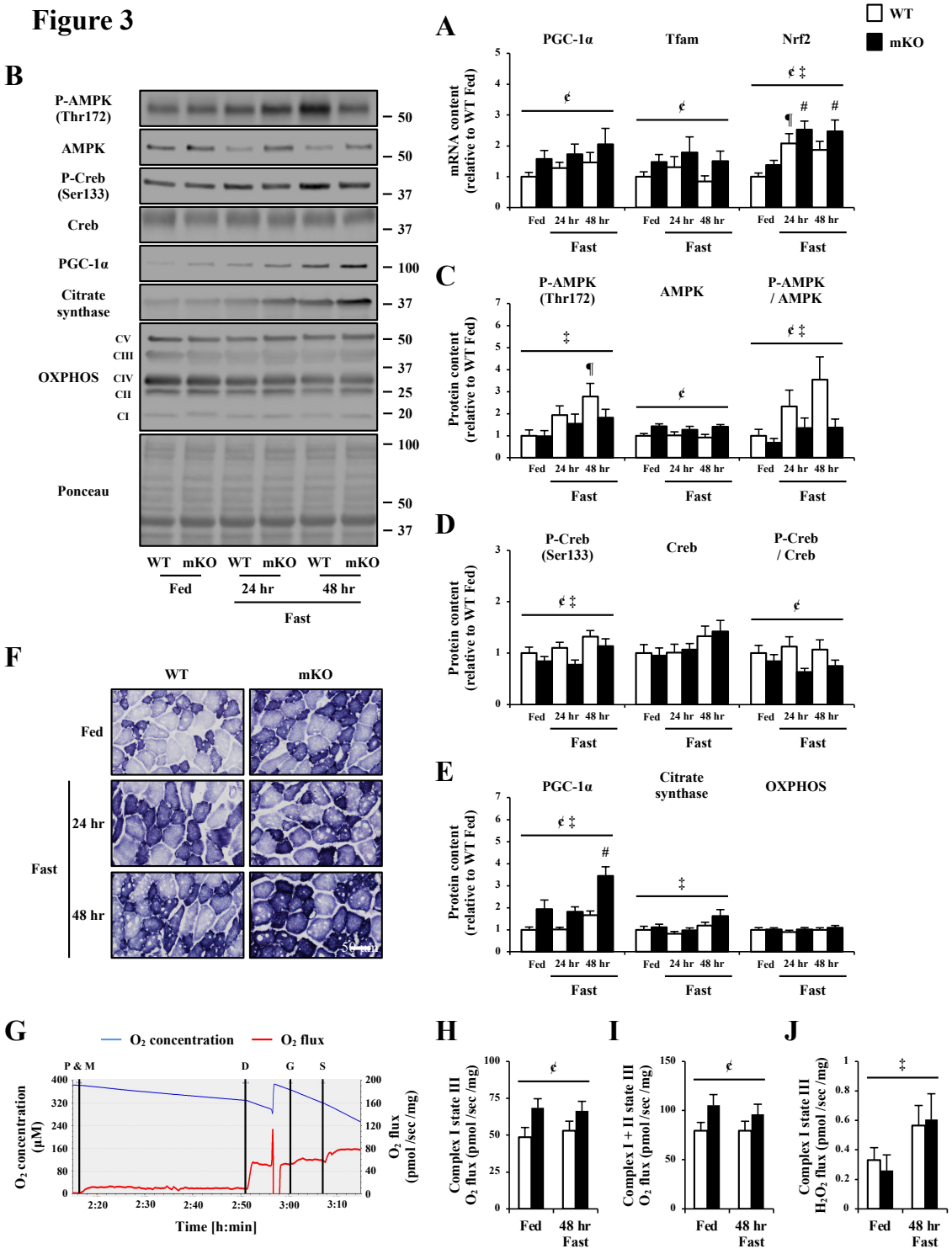
A
WT
mKO
PGC-1α
Tfam
Nrf2
mRNA content (relative to WT Fed)
Fed
24 hr
48 hr
Fast
B
P-AMPK (Thr172)
AMPK
P-Creb (Ser133)
Creb
PGC-1α
Citrate synthase
OXPHOS
CV
CIII
CIV
CII
CI
Ponceau
WT
mKO
C
P-AMPK (Thr172)
AMPK
P-AMPK / AMPK
Protein content (relative to WT Fed)
D
P-Creb (Ser133)
Creb
P-Creb / Creb
E
PGC-1α
Citrate synthase
OXPHOS
F
WT
mKO
Fed
24 hr
48 hr
Fast
G
O2 concentration
O2 flux
P & M
D
G
S
O2 concentration (μM)
O2 flux (pmol/sec/mg)
Time [h:min]
H
Complex I state III O2 flux (pmol/sec/mg)
I
Complex I + II state III O2 flux (pmol/sec/mg)
J
Complex I state III H2O2 flux (pmol/sec/mg)

Figure 4

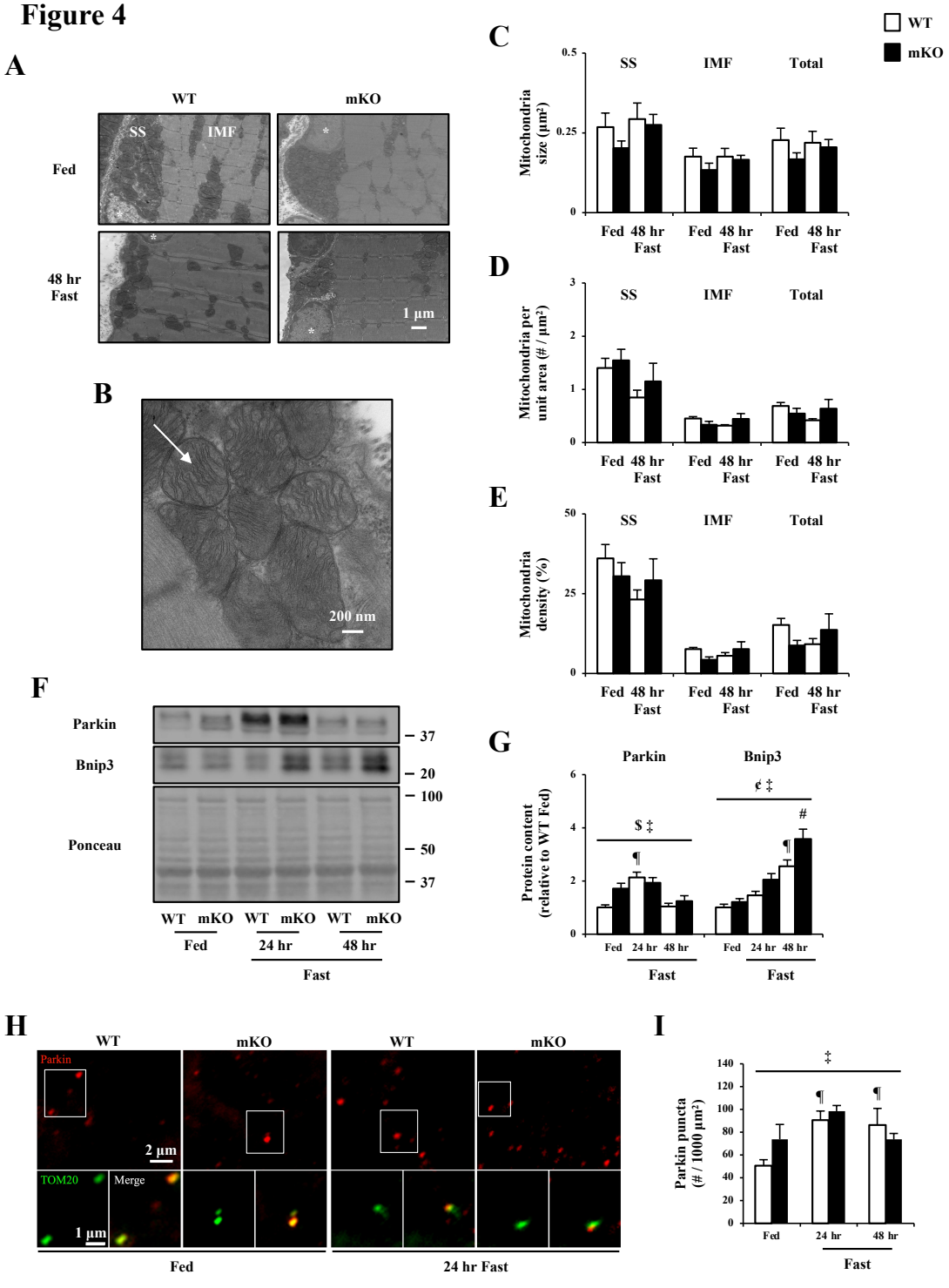
A
WT
mKO
SS
IMF
Fed
48 hr Fast
1 µm
B
200 nm
C
WT
mKO
SS
IMF
Total
Mitochondria size (µm²)
0.5
0.25
0
Fed 48 hr Fast
D
Mitochondria per unit area (# / µm²)
3
2
1
0
E
Mitochondria density (%)
50
25
0
F
Parkin
Bnip3
Ponceau
37
20
100
50
37
WT mKO WT mKO WT mKO
Fed
24 hr
48 hr
Fast
G
Parkin
Bnip3
Protein content (relative to WT Fed)
$ ‡
¶
¢ ‡
#
¶
Fed 24 hr 48 hr
Fast
H
WT
mKO
WT
mKO
Parkin
2 µm
TOM20
Merge
1 µm
Fed
24 hr Fast
I
Parkin puncta (# / 1000 µm²)
‡
¶
¶
140
120
100
80
60
40
20
0
Fed
24 hr
48 hr
Fast

Figure 5

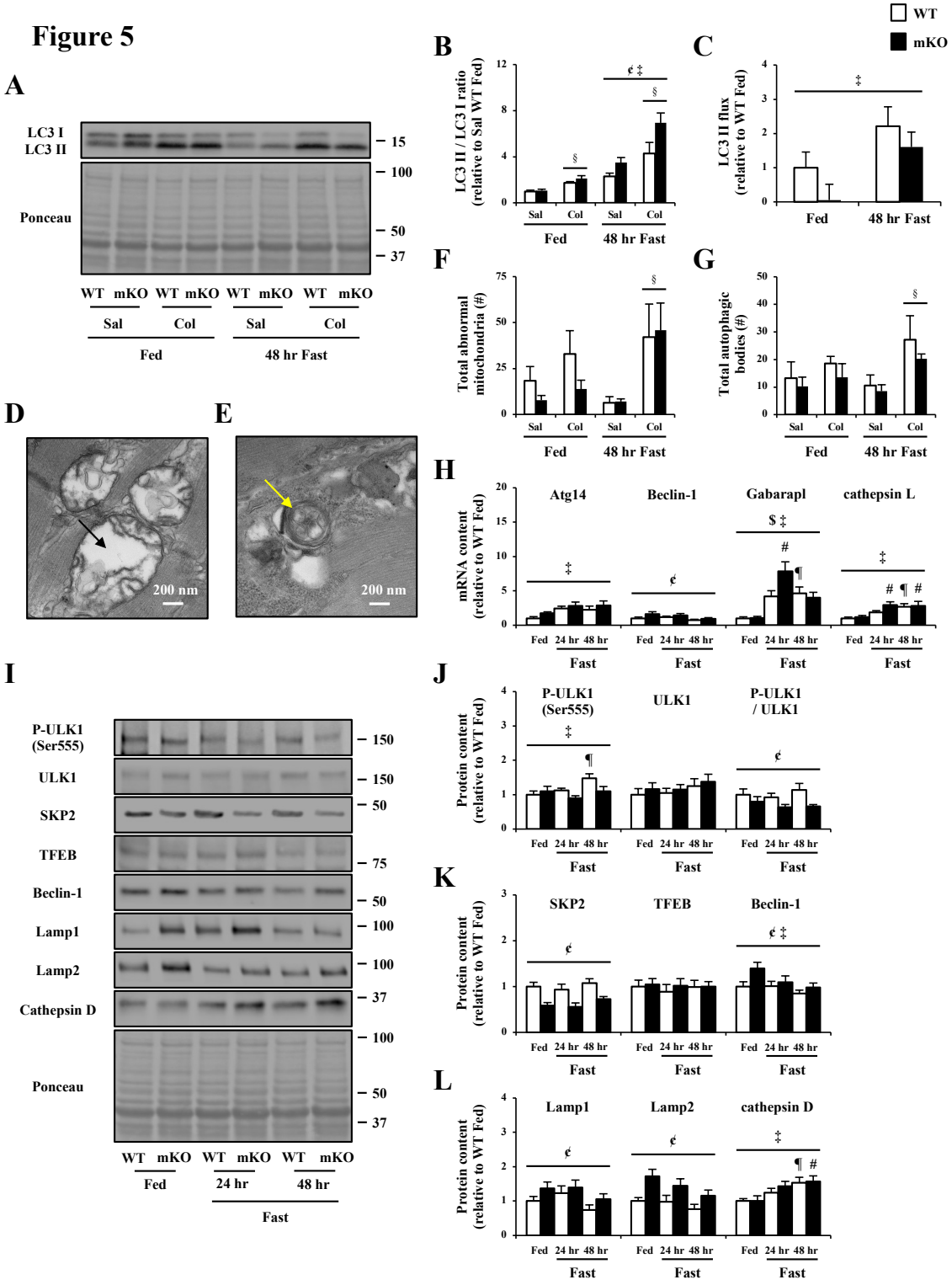
A
LC3 I
LC3 II
Ponceau
15
100
50
37
WT mKO WT mKO WT mKO WT mKO
Sal Col Sal Col
Fed 48 hr Fast
B
LC3 II / LC3 I ratio (relative to Sal WT Fed)
C
LC3 II flux (relative to WT Fed)
WT
mKO
F
Total abnormal mitochondria (#)
G
Total autophagic bodies (#)
D
200 nm
E
200 nm
H
mRNA content (relative to WT Fed)
Atg14
Beclin-1
Gabarapl
cathepsin L
Fed 24 hr 48 hr
Fast
I
P-ULK1 (Ser555)
ULK1
SKP2
TFEB
Beclin-1
Lamp1
Lamp2
Cathepsin D
Ponceau
150
150
50
75
50
100
100
37
100
50
37
WT mKO WT mKO WT mKO
Fed 24 hr 48 hr
Fast
J
Protein content (relative to WT Fed)
P-ULK1 (Ser555)
ULK1
P-ULK1 / ULK1
K
SKP2
TFEB
Beclin-1
L
Lamp1
Lamp2
cathepsin D

Figure 6

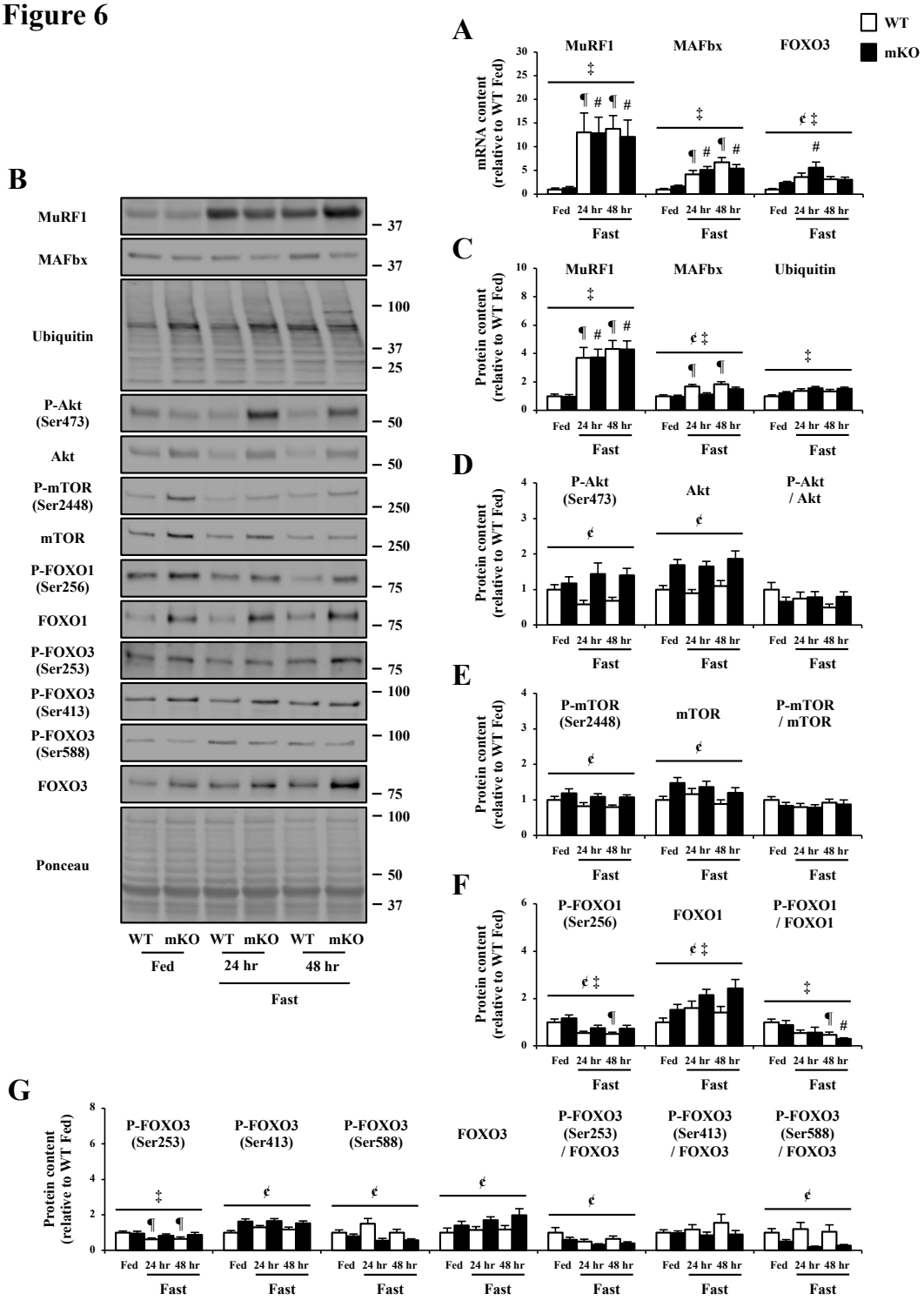
A
WT
mKO
MuRF1
MAFbx
FOXO3
mRNA content (relative to WT Fed)
Fed 24 hr 48 hr
Fast
B
MuRF1
MAFbx
Ubiquitin
P-Akt (Ser473)
Akt
P-mTOR (Ser2448)
mTOR
P-FOXO1 (Ser256)
FOXO1
P-FOXO3 (Ser253)
P-FOXO3 (Ser413)
P-FOXO3 (Ser588)
FOXO3
Ponceau
37
37
100
37
25
50
50
250
250
75
75
75
100
100
75
100
50
37
WT mKO WT mKO WT mKO
Fed
24 hr
48 hr
Fast
C
MuRF1
MAFbx
Ubiquitin
Protein content (relative to WT Fed)
D
P-Akt (Ser473)
Akt
P-Akt / Akt
E
P-mTOR (Ser2448)
mTOR
P-mTOR / mTOR
F
P-FOXO1 (Ser256)
FOXO1
P-FOXO1 / FOXO1
G
P-FOXO3 (Ser253)
P-FOXO3 (Ser413)
P-FOXO3 (Ser588)
FOXO3
P-FOXO3 (Ser253) / FOXO3
P-FOXO3 (Ser413) / FOXO3
P-FOXO3 (Ser588) / FOXO3

Figure 7

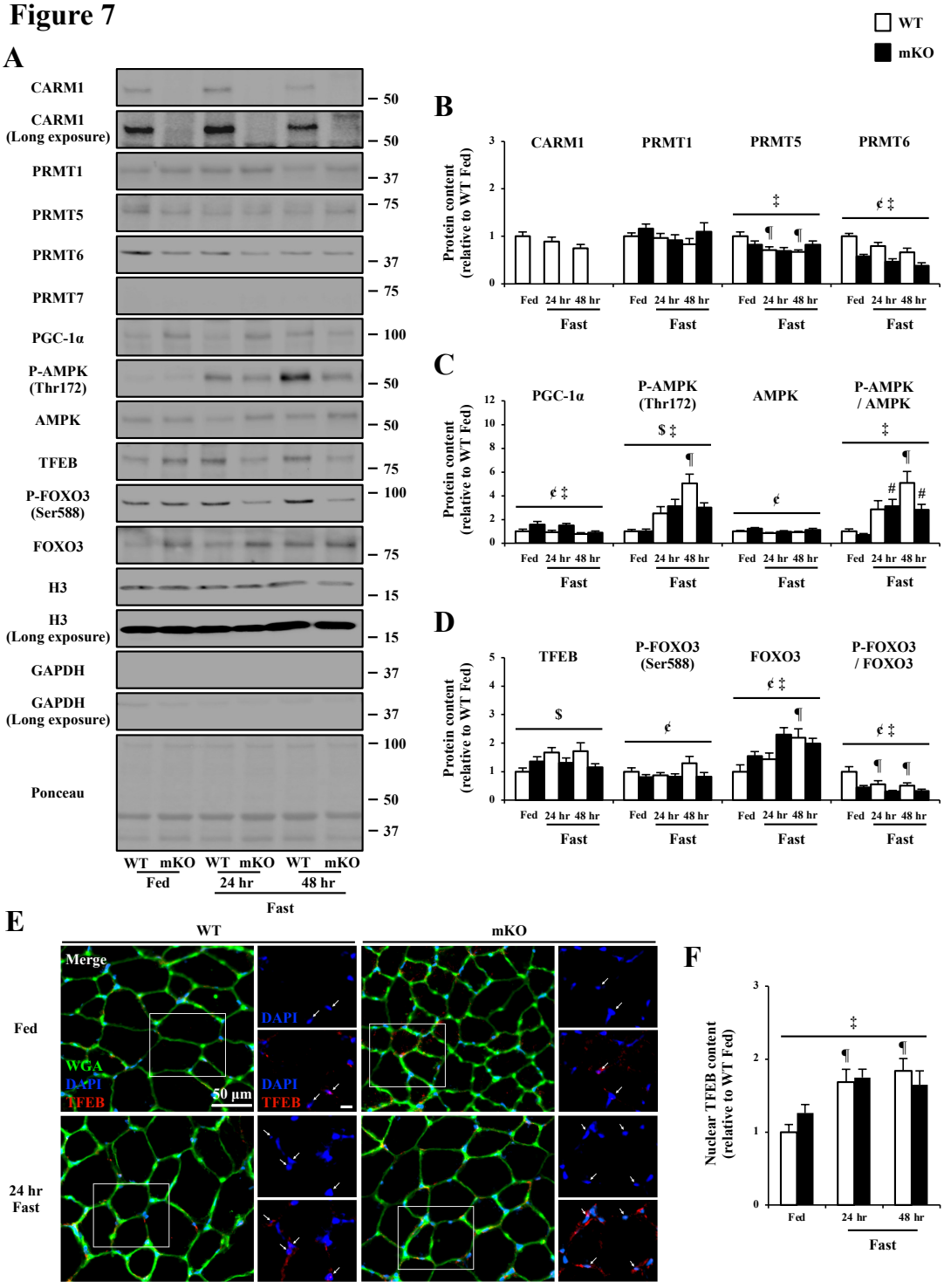
A
CARM1
CARM1 (Long exposure)
PRMT1
PRMT5
PRMT6
PRMT7
PGC-1α
P-AMPK (Thr172)
AMPK
TFEB
P-FOXO3 (Ser588)
FOXO3
H3
H3 (Long exposure)
GAPDH
GAPDH (Long exposure)
Ponceau
50
50
37
75
37
75
100
50
50
75
100
75
15
15
37
37
100
50
37
WT mKO WT mKO WT mKO
Fed
24 hr
48 hr
Fast
WT
mKO
B
CARM1
PRMT1
PRMT5
PRMT6
Protein content (relative to WT Fed)
Fed 24 hr 48 hr
Fast
C
PGC-1α
P-AMPK (Thr172)
AMPK
P-AMPK / AMPK
D
TFEB
P-FOXO3 (Ser588)
FOXO3
P-FOXO3 / FOXO3
E
WT
mKO
Fed
24 hr Fast
Merge
WGA
DAPI
TFEB
50 μm
DAPI
F
Nuclear TFEB content (relative to WT Fed)
Fed
24 hr
48 hr
Fast

Chapter 4:

Skeletal muscle CARM1 is vital for a healthy, long life

Skeletal muscle CARM1 is vital for a healthy, long life

Derek W. Stouth,[1] Tiffany L. vanLieshout,[1] Sean Y. Ng,[1] Andrew Mikhail,[1] Erin K. Webb,[1] Kevin S. Gilotra,[1] Matthew Markou,[1] Hannah C. Pineda,[1] Brianna G. Bettencourt-Mora,[1] Timothy Ryan,[2] Jacek M. Kwiecien,[3] Goutham Vasam[4], Keir J. Menzies[4], and Vladimir Ljubicic[1,*]

[1]Department of Kinesiology, McMaster University, Hamilton, Ontario, L8S 4L8, Canada

[2]McMaster University and David Braley Research Institute, Hamilton, Ontario, L8S 4K1, Canada

[3]Department of Pathology and Molecular Medicine, McMaster University, Hamilton, Ontario, L8S 4L8, Canada

[4]Interdisciplinary School of Health Sciences, University of Ottawa, Ottawa, Ontario, K1H 8M5, Canada

[*]**Correspondence:** Tel: 905 525 9140 ext. 24517; Email: ljubicic@mcmaster.ca

Abstract

Coactivator-associated arginine methyltransferase 1 (CARM1) has recently come into view as an important modifier of skeletal muscle phenotypic plasticity. Although CARM1 appears to be indispensable for preserving muscle mass, the impact of CARM1 deletion during the sarcopenia of aging remains to be elucidated. The purpose of this study was to investigate the function of CARM1 during the progressive loss of muscle mass and strength with age. Survival analysis revealed that male and female CARM1 skeletal muscle-specific knockout (mKO) mice have a significantly shorter lifespan compared to their wild type (WT) littermates. For instance, survival was ~50% lower in mKO versus WT animals after 22 months, which is comparable to ~70 years-old in humans. We also show that CARM1 mKO impairs muscle function across the lifespan and does not protect muscle from aging-induced atrophy. Moreover, aging evoked changes in skeletal muscle PRMT biology, as well as metabolic, autophagic, and atrophic signaling. CARM1 mKO affected autophagic and atrophic processes downstream of the master neuromuscular phenotypic modifier AMP-activated protein kinase (AMPK). CARM1 deletion also influenced metrics of mitochondrial biogenesis, function, and mitophagy. Collectively, these results highlight the importance of CARM1 for combating the progressive and generalized loss of skeletal muscle mass and strength that occurs with age. Manipulating the expression and/or activity of CARM1 in skeletal muscle may offer a viable therapeutic strategy for mitigating sarcopenia.

Keywords: CARM1, AMPK, autophagy, atrophy, aging, sarcopenia.

Introduction

Coactivator-associated arginine methyltransferase 1 (CARM1) is a type of protein arginine methyltransferase (PRMT) that catalyzes the methylation of arginine residues on target proteins (Bedford and Clarke, 2009; Yang and Bedford, 2013; Fulton et al., 2019; Guccione and Richard, 2019). All nine PRMTs first transfer the monomethylarginine (MMA) mark on their target molecules. The subsequent production of asymmetric dimethylarginine (ADMA) is catalyzed by type I PRMTs (i.e., PRMT1, PRMT2, PRMT3, CARM1, PRMT6, PRMT8), whereas sequential generation of symmetric dimethylarginine (SDMA) is catalyzed by type II PRMTs (i.e., PRMT5, PRMT9). Type III PRMTs (i.e., PRMT7) only deposit MMA. Arginine methylation impacts the stability, localization, and/or activity of marked substrates. The frequency of this post-translational modification is also on par with phosphorylation and ubiquitination (Larsen et al., 2016). Particularly, CARM1 methylates proline-rich motifs on marked histone and non-histone proteins (Cheng et al., 2018), thereby controlling intracellular processes such as signal transduction, DNA repair, transcriptional control, mRNA splicing, and cell cycle progression. CARM1 is ubiquitously expressed and full-body CARM1 knockout mice die shortly after birth (Yadav et al., 2003). Dysregulation of CARM1 is also well documented in human diseases such as cancer (Bedford and Clarke, 2009; Yang and Bedford, 2013; Fulton et al., 2019; Guccione and Richard, 2019). Overall, asymmetric arginine dimethylation of pan-CARM1-marked substrates regulates a wide range of cellular events.

Recent work has revealed that CARM1 is an important regulator of skeletal muscle biology. CARM1 is the most abundantly expressed PRMT in rodent and human skeletal

muscle (Wang et al., 2012; vanLieshout et al., 2019). We previously provided evidence that CARM1 is involved in skeletal muscle remodeling and required to maintain muscle mass (Ljubicic et al., 2012; Stouth et al., 2017; Stouth et al., 2018; vanLieshout et al., 2018; Shen et al., 2018; vanLieshout et al., 2019; vanLieshout and Ljubicic, 2019; Stouth et al., 2020). Other laboratories have demonstrated that CARM1 modulates myogenesis during development, regeneration, as well as glycogen metabolism (Chen et al., 2002; Kawabe et al., 2012; Wang et al., 2012; Chang et al., 2018). Interestingly, transient knockdown and knockout of CARM1 in muscle attenuates the progression of denervation-induced atrophy (Liu et al., 2019; Stouth et al., 2020). Indeed, CARM1 contributes to skeletal muscle wasting by mediating the autophagy-lysosome and ubiquitin-proteasome systems. Given that muscle atrophy and weakness with aging remains a pressing and widespread issue, a comprehensive understanding of the regulatory mechanism by which CARM1 influences the sarcopenia of aging is needed.

CARM1 destabilization leads to the dysfunction of autophagy in aged hearts (Li et al., 2017) and the loss of CARM1 is associated with cellular senescence (Pang et al., 2013). The master neuromuscular phenotypic modifier AMP-activated protein kinase (AMPK) stabilizes CARM1 (Shin et al., 2016; Li et al., 2017). Skeletal muscle-specific deletion of CARM1 also results in aberrant autophagic and atrophic processes downstream of AMPK (Stouth et al., 2020). Muscle AMPK is required for the induction of autophagy and loss of AMPK in muscle accelerates the aging process (Bujak et al., 2015). Since autophagy impairment in muscle induces precocious aging (Carnio et al., 2014), we sought to test the hypothesis that knocking out CARM1 in muscle would exacerbate the sarcopenia of aging.

Results

CARM1 skeletal muscle-specific knockout (mKO) mice have a decreased lifespan and reduced functional capacity. To examine the role of CARM1 during the sarcopenia of aging, male and female wild type (WT) and mKO animals (Stouth et al., 2020) were aged for 3, 12, 18, and 22 months. Immunoblot analysis confirmed knockout of CARM1 in skeletal muscle (Figure 1A). Similar to observations in cardiac muscle (Li et al., 2017), CARM1 protein content in the tibialis anterior (TA) was similar across the lifespan (Figure 1B). We noted main effects ($p < 0.05$) of genotype and aging for body mass in male and female mice (Figure 1C). A statistically significant difference was also identified in lifespan according to genotype ($p < 0.05$) in males and females. For instance, the median survival time was 20 months for WT mice, whereas the median survival time was 19 months for mKO animals (Figure 1D). Furthermore, at the endpoint of 22 months, the probability of survival of WT mice was ~2-fold higher as compared to their mKO counterparts (WT 45% vs. mKO 25%).

An open field activity monitoring system was employed to assess locomotor and behavioral activities in male WT and mKO animals after 3, 12, 18, and 22 months of aging (Figure 1E). There was a trend ($p = 0.35$) towards a main effect of aging on total distance traveled (Figure 1F). A battery of tests were also applied to examine muscle strength and balance in male WT and mKO mice in response to aging. Main effects ($p < 0.05$) of genotype and aging were detected for forelimb grip strength and all limb grip strength, as well as latency to fall during a balance endurance test (Figure 1G-I). For example, forelimb grip strength was 20% lower ($p < 0.05$) in mKO versus WT animals following 3 months.

Aging induced a significant 25-40% decrease in forelimb grip strength after 12, 18, and 22 months in both genotypes relative to their respective 3-month-old littermates. Furthermore, time endured during the balance assessment was 65-85% lower ($p < 0.05$) in WT and mKO mice following 12, 18, and 22 months of aging compared to their respective 3-month groups. We noted a significant main effect of aging on cage hang time and rotarod performance in both genotypes (Figure 1J, K). Relative to 3-month-old WT and mKO animals, aging elicited a significant 70-85% decline in cage hang time, as well as a 40-55% ($p < 0.05$) decrease in rotarod time, in both genotypes after 12, 18, and 22 months.

The impact of muscle specific CARM1 deletion on the sarcopenia of aging. We previously reported lower muscle mass and myofiber cross-sectional area (CSA) in young mKO mice compared to their age-matched WT counterparts (Stouth et al., 2020). We next sought to determine whether CARM1 is critical for the maintenance of muscle mass during sarcopenia in male animals. A main effect ($p < 0.05$) of aging on muscle mass was observed in the TA, extensor digitorum longus (EDL), soleus (SOL), and gastrocnemius (GAST; Figure 2A). We detected a significant main effect of genotype on TA, EDL, and GAST muscle mass, along with an interaction ($p < 0.05$) between genotype and aging for SOL and GAST muscle mass. Aging evoked a significant 25-35% decline in TA muscle mass following 12, 18, and 22 months in both genotypes relative to their respective 3-month-old littermates. Compared to 3-month-old WT mice, EDL muscle mass decreased by 30% ($p < 0.05$) in WT animals after 22 months of aging. EDL muscle mass was also significantly lower by 35% in mKO mice following 12 months versus 3-month-old mKO littermates. Relative to the 3-month-old mKO group, SOL muscle mass was decreased by 30-40% (p

< 0.05) in mKO animals following 12, 18, 22 months of aging, whereas SOL muscle mass did not significantly change in WT mice with aging. Moreover, GAST muscle mass was 20% ($p < 0.05$) lower in mKO versus WT animals after 3 months. Aging induced a significant 35% and 30% decrease in GAST muscle mass in WT and mKO mice, respectively, following 18 and 22 months relative to their respective 3-month-old group. The relative decline in GAST muscle mass between 3 and 22 months was lower in mKO versus WT animals ($p < 0.05$). We also observed significant main effects of aging and genotype for centrally located nuclei and CSA, respectively, in the EDL muscle (Figure 2B, D-F). In the SOL muscle, centrally located nuclei and CSA were similar between genotypes with aging (Figure 2C, G and data not shown).

Skeletal muscle PRMT content and activity in mKO mice during aging. We next characterized the impact of muscle-specific CARM1 deletion on PRMT content in male animals across the lifespan. We noted a main effect ($p < 0.05$) of aging on PRMT1 and PRMT7 protein content in the TA (Figure 3A, B). For instance, aging induced a significant 5.5- and 4.5-fold increase in PRMT7 protein expression in WT mice after 18 and 22 months, respectively, versus 3-month-old WT muscle. Compared to the 3-month-old mKO group, aging evoked a 4- and 3-fold increase ($p < 0.05$) in PRMT7 protein content in mKO animals following 18 and 22 months, respectively. In contrast, PRMT5 and PRMT6 protein expression levels were similar between all groups across the lifespan.

We investigated markers of global type I and type II PRMT activities, such as MMA, ADMA, and SDMA (Bedford and Clarke, 2009; Yang and Bedford, 2013), along with asymmetric arginine dimethylation of pan-CARM1-marked substrates (Cheng et al.

2018; vanLieshout et al., 2019) in mKO mice with aging. We also assessed bona fide CARM1 targets SWI/SNF chromatin remodeling complex BAF155 (BAF155me2a^{Arg1064}), and poly(A)-binding protein 1 (PABP1me2a$^{Arg455/Arg460}$). Main effects ($p < 0.05$) of genotype and aging were observed for CARM1 substrate and SDMA methylargine content, respectively (Figure 3A, C). For example, CARM1 substrate arginine dimethylation levels were ~50% lower in mKO versus WT mice across the lifespan. There was a trend ($p = 0.09$) for lower CARM1 substrate methylargine content in WT muscle with aging. MMA and ADMA content were similar in all experimental conditions. We detected significant main effects of genotype and aging, plus an interaction ($p < 0.05$) between genotype and aging for BAF155me2a^{Arg1064} (Figure 3A, D). Aging elicited a significant 35% decline in BAF155me2a^{Arg1064} in WT animals after 12, 18, and 22 months relative to their 3-month-old WT littermates. BAF155me2a^{Arg1064} was 80-90% lower ($p < 0.05$) in mKO animals compared to their WT counterparts across the lifespan. Total BAF155 protein content was similar between genotypes with aging. There were also significant main effects of genotype and aging on BAF155 activation status (i.e., the methylated form of the protein relative to its total, unmethylated content). For instance, BAF155 activation status decreased by 60% ($p < 0.05$) in WT mice following 12 months versus the 3-month-old WT group. BAF155 activation status was also significantly lower in mKO muscle across the lifespan versus WT animals. Furthermore, main effects ($p < 0.05$) of genotype and aging were noted on PABP1me2a$^{Arg455/Arg460}$ (Figure 3A, E). Aging induced a significant 45% decrease ($p < 0.05$) in PABP1me2a$^{Arg455/Arg460}$ in WT mice following 22 months relative to the 3-month-old WT group. Main effects ($p < 0.05$) of aging and genotype were also observed for total

PABP1 protein content and PABP1 activation status, respectively. Aging induced a significant 40% decrease in total PABP1 protein expression in mKO muscles after 22 months relative to 3-month-old mKO animals. PABP1 activation status was significantly lower by 45-55% in mKO animals compared to WT across the lifespan.

***Metabolic signaling in mKO muscle across the lifespan*.** Since CARM1 influences metabolic processes during neurogenic muscle disuse (Stouth et al., 2020), we next sought to determine the impact of CARM1 mKO on metabolic signaling in male mice following 3, 12, 18, and 22 months of aging. We assessed the activation status of AMPK and its downstream target acetyl-coenzyme A carboxylase (ACC), as well as p38 mitogen-activated protein kinase (p38) in TA muscles. We also examined protein content of peroxisome proliferator-activated receptor-γ coactivator-1α (PGC-1α), p53, citrate synthase, and proteins indicative of mitochondrial oxidative phosphorylation (OXPHOS) complexes I–V (CI–CV). A main effect ($p < 0.05$) of aging on phosphorylated AMPK (P-AMPK^{Thr172}), total AMPK protein content, and AMPK activation status was observed (Figure 4A, B). A significant main effect of genotype on AMPK activation status was also noted. We detected a main effect ($p < 0.05$) of aging on P-ACC^{Ser79} and total ACC (Figure 4A, C). Compared to 3-month-old WT animals, aging induced a significant 45% decrease in P-ACC^{Ser79} and total ACC levels in WT muscle after 22 months. There was a strong trend ($p = 0.09$) towards a main effect of genotype on ACC activation status. We observed a main effect ($p < 0.05$) of aging on P-p38$^{Thr180/Tyr182}$, total p38, and p38 activation status (Figure 4A, D). We also noted a significant main effect of genotype on P-p38$^{Thr180/Tyr182}$. For instance, P-p38$^{Thr180/Tyr182}$ increased by ~3-fold ($p < 0.05$) in WT mice following 12

and 18 months, relative to the 3-month-old WT group. When compared to 3-month-old mKO muscle, P-p38$^{Thr180/Tyr182}$ was significantly greater by 3.5-fold in mKO animals after 12 months. Aging elicited a significant 3-fold increase in p38 activation status in WT and mKO mice following 22 months, compared to their respective 3-month-old group.

We noted a main effect ($p < 0.05$) of genotype on PGC-1α and total OXPHOS protein content (Figure 4A, E), whereby their expression was higher in mKO animals compared to WT. There was also a significant main effect of aging on p53 and citrate synthase protein expression. Aging induced a 3.5-7-fold increase ($p < 0.05$) in p53 protein content in both genotypes after 18 and 22 months, relative to their respective 3-month-old littermates. Aging also evoke a 50% decrease ($p < 0.05$) in citrate synthase protein content in WT mice after 18 and 22 months, relative to 3-month-old WT muscle.

We next evaluated succinate dehydrogenase (SDH) content, as well as mitochondrial respiration and hydrogen peroxide (H_2O_2) emission in male WT and mKO animals with aging. Qualitative histochemical staining for SDH in the EDL muscle revealed more intense SDH staining in 22-month old male mKO mice versus their age-matched WT counterparts. We observed a trend towards a main effect of genotype on CI-supported state III respiration ($p = 0.24$) and CI + II-supported state III respiration ($p = 0.22$), when normalized to muscle fiber bundle weight. A significant main effect of genotype on CI-supported state III H_2O_2 emission was also detected (Figure 4G-I).

Mitochondrial morphology and mitophagy in mKO animals during the sarcopenia of aging. To further understand the impact of CARM1 mKO on mitochondrial biology, we performed transmission electron microscopy (TEM) analysis in male TA

muscle following 3 and 22 months of aging (Figure 5A, B). In both the subsarcolemmal (SS) and intermyofibrillar (IMF) regions, mitochondrial size was similar in all groups (Figure 5A, C). We detected a main effect ($p < 0.05$) of genotype on mitochondria per unit area in the SS location (Figure 5A, D). Total mitochondria per unit area also displayed a strong trend ($p = 0.08$) towards a main effect of genotype. Mitochondrial density was similar in all experimental conditions in the SS and IMF sections (Figure 5A, E). We also evaluated the total number of abnormal mitochondria (Figure 5F) and autophagic bodies (Figure 5G) in WT and mKO animals with aging. A trend towards a main effect of aging on total number of abnormal mitochondria ($p = 0.09$) and autophagic bodies ($p = 0.11$) emerged (Figure 5H, I). To complement the TEM analyses, we examined markers of mitophagy in the TA muscle, such as Parkin and BCL2 and adenovirus E1B 19-kDa interacting protein 3 (Bnip3) protein content. A main effect ($p < 0.05$) of aging on Parkin protein expression was detected (Figure 5J, K). We also observed a main effect of genotype on Parkin ($p = 0.08$) and Bnip3 ($p < 0.05$) protein content levels.

The effect of CARM1 mKO on autophagy signaling with aging. Previous work has demonstrated that CARM1 modulates autophagy in muscle (Liu et al., 2019, Hu et al., 2020; Stouth et al., 2020). In this study, we analyzed the autophagy-lysosome pathway by measuring the microtubule-associated protein 1A/1B-light chain 3 (LC3)-II/LC3-I ratio and unc-51-like autophagy-activating kinase 1 (ULK1) activation status, along with p62, S-phase kinase-associated protein 2 (SKP2), transcription factor EB (TFEB), Beclin-1, lysosomal associated membrane protein 1 (Lamp1), Lamp2, and cathepsin D protein content in TA muscles from male WT and mKO mice with aging. We noted a main effect

($p < 0.05$) of genotype on LC3-I, LC3-II, and p62 protein expression (Figure 6A, B). There was also a significant main effect of aging on LC3-I protein content and a trend ($p = 0.11$) towards a main effect of genotype on LC3-II/LC3-I ratio. We detected main effects ($p < 0.05$) of genotype and aging on P-ULK1^{Ser555} (Figure 6A, C). Significant main effects of aging and genotype were also observed for total ULK1 protein content and ULK1 activation status, respectively. For instance, aging induced a 1.5-fold increase ($p < 0.05$) in total ULK1 in WT muscle after 12 months relative to their 3-month-old WT littermates. Main effects ($p < 0.05$) of genotype and aging were noted on SKP2, TFEB, Beclin-1, Lamp1, and Lamp2 protein expression levels (Figure 6A, D, E). For example, aging elicited a significant ~60% decrease in Lamp1 protein content in WT and mKO muscle following 22 months, compared to their respective 3-month-old groups. We also detected a main effect ($p < 0.05$) of aging on cathepsin D protein expression.

CARM1 and the muscle atrophy program during sarcopenia. We next examined muscle atrophy processes in the TA muscle of male WT and mKO mice after 3, 12, 18, and 22 months of aging. We evaluated the ubiquitin-proteasome degradation pathway by assessing Muscle RING finger 1 (MuRF1), muscle atrophy F box (MAFbx), and ubiquitin protein content, along with activation of FOXO1 and FOXO3 transcription factors. We also measured the activation status of mammalian target of rapamycin (mTOR), as well as upstream signaling molecules protein kinase B (Akt) and tuberous sclerosis complex 2 (TSC2). We observed a main effect ($p < 0.05$) of aging on MuRF1 and MAFbx protein content (Figure 7A, B). For instance, aging induced a significant 55% decrease in MuRF1 protein expression in WT muscles following 22 months relative to the 3-month-old WT

group. There was also a main effect ($p < 0.05$) of genotype on ubiquitin protein content, with a greater level of ubiquitin marked proteins in the mKO groups relative to the WT.

Significant main effects of aging and genotype were detected for P-Akt^{Ser473} and total Akt, respectively (Figure 7A, C). Main effects ($p < 0.05$) of aging and genotype were also noted for Akt activation status. Compared to the 3-month-old WT group, Akt activation status was significantly greater by 2.3-fold in WT animals after 12 months of aging, whereas Akt activation status was similar between all timepoints in mKO mice. We observed a main effect ($p < 0.05$) of genotype on P-TSC2^{Ser1387} and total TSC2 protein content (Figure 7A, D). There was also a significant main effect of aging on total TSC2 and TSC2 activation status. For example, TSC2 activation status was significantly greater by 1.6-fold in WT muscle following 18 months relative to the 3-month-old WT condition. We found a main effect ($p < 0.05$) of genotype on P-mTOR^{Ser2448} and total mTOR, along with a main effect ($p < 0.05$) of aging on P-mTOR^{Ser2448} levels (Figure 7A, E). mTOR activation status was similar between all groups.

A significant main effect of aging on P-FOXO1^{Ser256} was detected (Figure 7A, F). We also noted main effects ($p < 0.05$) of genotype and aging on total FOXO1 and FOXO1 activation status. Compared to 3-month-old mKO mice, total FOXO1 protein content was significantly higher by 1.7-fold in 12-month-old mKO animals. FOXO1 activation status was greater by 2-fold ($p < 0.05$) in WT muscle following 22 months of aging versus the 3-month-old WT group. In contrast, FOXO1 activation status did not significantly differ in mKO muscle with aging. We observed a main effect ($p < 0.05$) of genotype on P-FOXO3^{Ser253}, P-FOXO3^{Ser413}, P-FOXO3^{Ser588}, and total FOXO3 protein levels (Figure 7A,

G). Significant main effects of genotype and aging on FOXO3^{Ser588} activation status were also found. FOXO3^{Ser253} and FOXO3^{Ser413} activation status were similar between genotypes in all age groups.

Discussion

The progressive decline in muscle mass and function with advancing age, termed sarcopenia, is a global issue in dire need of attention. Here, we provide evidence that CARM1 mKO decreases life expectancy, as well as hinders muscle strength and balance across the lifespan. We also reaffirm that CARM1 is required to maintain muscle mass. Interestingly, CARM1 mKO did not prevent further loss of muscle mass with aging. An adaptive response to aging was noted for skeletal muscle PRMT biology, along with metabolic, autophagic, and atrophic changes. CARM1 mKO altered AMPK activation in response to aging, along with downstream autophagic and atrophic events, such as AMPK-site specific phosphorylation of ULK1^{Ser555} and FOXO3^{Ser588}. Markers of mitochondrial biogenesis, function, and mitophagy were also affected by CARM1 deletion. Overall, these data suggest that skeletal muscle CARM1 is critical for maintaining a healthy, long life.

We found muscle- and atrophy-specific differences in the role of CARM1 in the preservation of skeletal muscle mass. For instance, muscle mass of the faster, more glycolytic EDL was lower in mKO versus WT mice after 3 months, whereas SOL muscle mass was greater in mKO animals. As CARM1 deletion in EDL and SOL muscles differentially affect denervation-induced muscle atrophy (Stouth et al., 2020), we postulate that CARM1 function during atrophy is muscle dependent. Moreover, autophagy is required to maintain muscle mass (Masiero et al., 2009), and aberrant autophagic

breakdown in CARM1 mKO mice likely contributed to reductions in muscle mass. Autophagy is critical for the maintenance of cell health through the removal of damaged or dysfunctional cellular components (Triolo and Hood, 2021), and dysregulated autophagy can exacerbate the sarcopenia of aging (Carnio et al., 2014). In this study, we demonstrate that CARM1 mKO decreases survival and worsens muscle function with aging. Unlike neurogenic muscle disuse (Liu et al., 2019; Stouth et al. 2020), muscle-specific deletion of CARM1 did not mitigate the progression of aging-induced muscle loss. CARM1 expression and activity levels were increased following denervation (Stouth et al., 2020), whereas CARM1 was generally downregulated with aging. As such, these data strongly suggest that the role of CARM1 during atrophy-inducing conditions depends, in part, on the stimuli evoking muscle loss. It is notable that any atrophy-induced changes in CARM1 methyltransferase activity, such as the marking of CARM1 substrates, were significantly reduced in mKO animals. This suggests that the requirement for PRMTs, and for CARM1 specifically, may be integral to the maintenance and plasticity of muscle mass during other atrophic conditions, such as cancer cachexia or neuromuscular disorders.

It was previously demonstrated that CARM1 and AMPK are members of a signaling cascade that governs autophagy (Shin et al., 2016; Li et al., 2017; Yu et al., 2020), and that CARM1 regulates AMPK-mediated autophagic processes in skeletal muscle (Stouth et al., 2020). Like CARM1, muscle AMPK is required for proper autophagic breakdown (Bujak et al., 2015). Growing evidence indicates that the sensitivity of AMPK to cellular stress declines with aging. As such, the curtailed responsiveness of AMPK diminishes autophagic clearance in older muscle (Salminen and Kaarniranta, 2012). Since

AMPK deletion accelerates aging-induced myopathy (Bujak et al., 2015), it is reasonable to speculate that CARM1 mKO provokes precocious features of sarcopenia by modulating AMPK and its downstream signaling network. Here, we noted an inverted U-shaped pattern for AMPK activation following 3, 12, 18, and 22 months of aging in mice, which is equivalent to approximately 20, 43, 56, and 70 years-old in humans (Jackson et al., 2017; Manzanares et al., 2018; Yanai and Endo 2021). We observed reduced AMPK activation, as well as attenuated downstream stimulatory phosphorylation of ULK^{Ser555} and FOXO3^{Ser588} in mKO animals compared to their WT littermates with aging. The activity of ULK1^{Ser555} and FOXO3^{Ser588} is crucial for the activation of muscle autophagy and transcription of atrogenes, respectively (Kjobsted et al., 2018; Triolo and Hood, 2021). Interestingly, elevated phosphorylation of AMPK targets TSC2^{Ser1387} and FOXO3^{Ser413} were noted in mKO versus WT mice, perhaps to counteract the downregulation of ULK^{Ser555} and FOXO3^{Ser588}. CARM1 mKO also resulted in greater accumulation of TFEB and Beclin-1 protein content with aging, whose autophagic activity is controlled by AMPK, suggestive of perturbed autophagosomal breakdown (Herzig and Shaw, 2018; Triolo and Hood, 2021). Together, these findings suggest that knocking out CARM1 alters AMPK-mediated autophagic signaling across the lifespan, which likely contributes to myopathy in mKO animals with aging.

Skeletal muscle-specific deletion of CARM1 influenced the activation of Akt and its downstream effectors mTOR and FOXO3 (Mammucari et al., 2008) across the lifespan. A main finding of the current study is that CARM1 mKO led to greater phosphorylation of mTOR^{Ser2448} with aging. Although mTOR promotes skeletal muscle hypertrophy

(Drummond et al., 2009), sustained mTOR activation inhibits autophagy via direct phosphorylation of ULK1^{Ser757} and TFEB^{Ser211} (Klionsky et al., 2021). Hyperactivation of mTOR is sufficient to induce molecular signatures of sarcopenia, such as neuromuscular junction (NMJ) instability. Conversely, chronic mTOR inhibition attenuates sarcopenia (Ham et al., 2020). Since mTOR impedes autophagy (Klionsky et al., 2021), and autophagy disruption elicits NMJ degeneration and precocious aging (Carnio et al., 2014), it is reasonable to speculate that hyperphosphorylation of mTOR^{Ser2448} in CARM1 mKO mice contributed to impaired muscle function across the lifespan. Moreover, phosphorylation of FOXO3^{Ser253} was greater in mKO animals compared to WT littermates with aging. Since Akt-induced phosphorylation of FOXO3^{Ser253} suppresses FOXO3 transcriptional activity by promoting its nuclear exclusion, and FOXO3, in part, controls autophagy-related genes (Calnan and Brunet, 2008; Sanchez et al., 2014), it is reasonable to posit that aberrant FOXO3-dependent autophagic processes played a role in aggravating sarcopenia in CARM1 mKO mice. Collectively, these data suggest that CARM1 mKO advances age-related decrements in whole-body muscle function by manipulating mTOR and FOXO3 activity. The dearth of in vivo studies currently limits our understanding about the physiological impact of CARM1 in aging muscle. Future studies should address whether CARM1 mKO influences myonuclear translocation of TFEB and FOXO3, as well as NMJ integrity across the lifespan. Further elucidation of the molecular mechanisms by which CARM1 deletion affects the maintenance and remodeling of muscle phenotype will facilitate the discovery of therapeutic strategies for attenuating sarcopenia.

Consistent with our previous study (Stouth et al., 2020), CARM1 mKO modulated indicators of mitochondrial biogenesis, function, and mitophagy. Mitochondrial biogenesis and function decline with aging (Carter et al., 2015), and are largely governed by AMPK and its downstream target PGC-1α (Herzig and Shaw, 2018). In this study, we observed higher levels of PGC-1α and total OXPHOS protein content. This aligned with greater mitochondria per unit area in mKO versus WT animals, plus a trend toward increased mitochondrial respiration and decreased H_2O_2 emission in mKO muscle. SDH staining also appeared raised in mKO mice compared to their WT littermates, especially after 22 months of aging. Although transgenic overexpression of PGC-1α in muscle improves NMJ function (Arnold et al., 2014), PGC-1α overexpression does not prevent aging-induced muscle atrophy (Yeo et al., 2019). Given that mitochondrial biogenesis can serve as a compensatory mechanism for mitochondrial degradation (Garrido-Maraver et al., 2015), and PGC-1α overexpression (Vainshtein et al., 2015), we reason that CARM1 mKO evoked elevated PGC-1α expression to counteract mitochondria loss by mitophagy. With aging, mitochondria become fragmented and reactive oxygen species emission increases (Hood et al., 2019). Here, we show aberrant mitophagy in mKO animals during the sarcopenia of aging. There was an inverted U-shaped curve, plus greater Parkin and Bnip3 protein content across the lifespan in mKO versus WT mice. Since aging increases mitophagy flux (Carter et al., 2018), and abnormal mitophagy is implicated in muscle wasting with aging (Carter et al., 2015; Hood et al., 2019), we speculate that dysregulated mitophagy in CARM1 mKO animals, in part, exacerbates the sarcopenia of aging. Further work is needed to confirm whether skeletal muscle-specific deletion of CARM1 impairs mitophagy flux. In all, the

data suggest that CARM1 is important for regulating mitochondrial biogenesis, function, and mitophagy during the aging process.

In summary, the progressive loss of muscle mass and function that occurs with aging, collectively known as sarcopenia, increases the risk of frailty, morbidity, and mortality. This study extends previous work (Stouth et al., 2020) and advances our mechanistic understanding of the role of CARM1 during the sarcopenia of aging. We show that mKO mice have a significantly shorter lifespan compared to their WT littermates. Furthermore, we provide evidence that CARM1 mKO results in aberrant autophagy and exacerbates the sarcopenia of aging. Ultimately, targeting the expression and/or activity of CARM1 in skeletal muscle may offer a novel therapeutic approach for combating sarcopenia.

Materials and methods

Animals. We employed the Cre/loxP system to generate mKO mice as described previously (Stouth et al., 2020). CARM1 floxed animals (Yadav et al., 2003; Bao et al., 2018) were a kind gift from Dr. Mark Bedford (The University of Texas MD Anderson Cancer Centre, Smithville, TX, USA) and produced in the mixed C57BL6J/129 background. Human α-skeletal actin (HSA)-Cre mice with HSA-Cre activity restricted to skeletal muscle (McCarthy et al., 2012) were obtained from Jackson Laboratories (Bar Harbor, ME, USA). Floxed CARM1 (wild type; WT) and mKO animals were identified by performing conventional reverse transcription-polymerase chain reaction (RT-PCR) and gel electrophoresis techniques on DNA extracted from tail clippings. We used the following primers to confirm that WT and mKO mice contained a LoxP site for CARM1 between

exon 2 and 3: forward (F)-AGTTGGTGACCCTTGTGTCC, reverse (R)-AGCTGCCAGGACCTCTGATA. The following primers were used to detect mKO animals that express Cre recombinase: F-GCGGTCTGGCAGTAAAAACTATC, R-GTGAAACAGCATTGCTGTCACTT.

Male and female WT and mKO mice were aged for 3, 12, 18, and 22 months. Animals were housed in an environmentally controlled room (23 °C, 12-hour light/12-hour dark cycle) across the lifespan and had access to food and water ad libitum. All protocols for maintaining aging mouse colonies were approved by the Animal Research Ethics Board at McMaster University operating under the regulations of the Canadian Council for Animal Care. At each experimental time point, the tibialis anterior (TA), extensor digitorum longus (EDL), soleus (SOL), and gastrocnemius (GAST) muscles were rapidly removed, weighed, frozen in liquid nitrogen or mounted in optimal cutting temperature compound (OCT; Thermo Fisher Scientific Life Sciences, Waltham, MA, USA) then frozen in isopentane cooled with liquid nitrogen. All muscles were then stored at -80 °C for biochemical analyses.

Survival experiment. Male and female WT and mKO mice (n = 29-48 /group) were followed until the predetermined humane end-point criteria were fulfilled, or until 22 months of aging, whichever occurred first. Mice were considered at end of life if they displayed the following: non-responsiveness to being touched, gasping respiratory pattern or a respiration rate of less than 90 breaths /minute, failure to eat or drink, severe skin lesions, palpable tumors, and/or rectal prolapse. Animals were euthanized when the veterinary staff, blinded to genotype, confirmed the fulfilment of the end-point criteria. We

selected the 22-month timepoint because it captures an advanced aging phenotype in these mice, roughly corresponding to 70 years old in humans (Jackson et al., 2017; Manzanares et al., 2018; Yanai and Endo 2021). Furthermore, we chose 22 months since only approximately 25% of mKO animals were still alive at this timepoint. Clinical frailty and pathologic assessments were performed by a clinical research veterinarian (T.R., McMaster University) and veterinary pathologist (J.M.K., McMaster University), respectively, who were blinded to genotype.

Performance testing. Locomotor and behavioral activities of male and female WT and mKO mice were examined after 3, 12, 18, and 22 months of aging using an open field activity monitoring system (Auto-Track v5.04; Columbus Instruments, Columbus, OH, USA) as described previously (Tatem et al. 2014). Following the acclimation period, total distance traveled, and anxiety-like behavior were calculated for animals placed in test chambers for 60 minutes. All tests were performed at least two days prior to tissue collection.

Grip strength, hanging, and rotarod running tests were also performed in male and female WT and mKO animals across the lifespan as described previously (Aartsma-Rus and van Putten, 2014). To assess forelimb and all limb grip strength, a metal grid was attached to a force transducer (Chatillon Force Measurement Products; AMETEK Test & Calibration instruments, AMETEK, Inc., Berwyn, PA, USA) set to peak tension mode. Upon grasping the grid, mice were pulled by the tail until their grasp was broken. Maximum peak tension from the best of three trials was used for the grip strength analyses. To examine balance, coordination, and muscle coordination, we performed hanging tests using

either a pen or cage lid and rotarod running. Suspended animals were positioned on a pen, such that all limbs were used to balance on the pen. Mice placed on top of a cage lid were positioned so that all four limbs grasped the lid while hanging. A fixed limit of 5 minutes was set for all balance and hanging tests. For rotarod running (Rotamex; Columbus Instruments, Columbus, OH, USA), the steady speed was set at xx rotations per minute (rpm). We employed preprogrammed rotarod settings of 0.25 RPM (increment speed), 1.875 (increment seconds), 0 RPM (start speed), and 40 RPM (end speed). The maximum peak tension, balance, hanging time, and rotarod running time from the best of three trials were recorded.

Whole muscle protein extraction and Western blotting. TA muscles were processed as described previously (Stouth et al., 2020). To homogenize whole muscle, frozen tissues were ground to a powder with a mortar and pestle on liquid nitrogen. These samples were suspended in RIPA buffer (Sigma-Aldrich, St. Louis, MO, USA), supplemented with cOmplete Mini Protease Inhibitor Cocktail (Sigma-Aldrich, St. Louis, MO, USA) and PhosSTOP Phosphatase Inhibitor Cocktail (Sigma-Aldrich, St. Louis, MO, USA). All samples were then further homogenized with stainless steel lysing beads and TissueLyser (Qiagen, Hilden, NRW, Germany) at a frequency of 30 Hz for 5 minutes. The lysates were mixed by end-over end inversion for 60 minutes at 4 °C prior to centrifugation at 14,000 x g for 10 minutes. The supernatants were snap-frozen in liquid nitrogen and stored at -80 °C for further analysis. Protein concentrations were later determined using the BCA protein assay (Thermo Fisher Scientific Life Sciences, Waltham, MA, USA).

Proteins extracted from whole muscle were separated on 10% SDS-PAGE gels or 4-15% precast gradient gels (Bio-Rad Laboratories, Inc., Hercules, CA, USA) and subsequently transferred onto nitrocellulose membranes. After transfer, membranes were stained with Ponceau S solution (Sigma-Aldrich, St. Louis, MO, USA) in order to serve as a loading control (Romero-Calvo et al. 2010; Stouth et al. 2018; Stouth et al., 2020). Membranes were washed with 1 x TBST and blocked with 5% BSA-TBST for one hour before being incubated in a primary antibody overnight at 4 °C with gentle rocking. The following morning, blots were washed with 1 x TBST and incubated in the appropriate secondary antibody (1:2,000; 7074S; Cell Signaling, Danvers, MA, USA) coupled to horseradish peroxidase with gentle rocking at room temperature for one hour. Blots were then washed again with 1 x TBST, followed by visualization with enhanced chemiluminescence (G00069; GE Healthcare Bio-Sciences, Chicago, IL, USA) under short and long exposures. Protein content was assessed using ImageJ.

Antibodies against CARM1 (1:5,000; A300-421A; Bethyl Laboratories, Montgomery, TX, USA), PRMT1 (1:1,000; 07-404; EMD Millipore, Darmstadt, HE, Germany), PRMT5 (1:1,000; 07-405; EMD Millipore, Darmstadt, HE, Germany), PRMT6 (1:1,000; A300-929A; Bethyl Laboratories, Montgomery, TX, USA), PRMT7 (1:1,000; sc-376077; Santa Cruz Biotechnology, Dallas, TX, USA), MMA (1:1,000; 8015S; Cell Signaling, Danvers, MA, USA), ADMA (1:1,000; 13522S; Cell Signaling, Danvers, MA, USA), CARM1 substrate (1:1,000; another gift from Dr. Mark Bedford, MD Anderson Cancer Center, University of Texas), SDMA (1:1,000; 13222S; Cell Signaling, Danvers, MA, USA), asymmetrically dimethylated BAF155^{Arg1064} (1:1,000; 94962S; Cell Signaling,

Danvers, MA, USA), BAF155 (1:1,000; 11956S; Cell Signaling, Danvers, MA, USA), asymmetrically dimethylated PABP1$^{Arg455/Arg460}$ (1:1,000; 3505S; Cell Signaling, Danvers, MA, USA), and PABP1 (1:1,000; 4992S; Cell Signaling, Danvers, MA, USA) were used to examine PRMT expression and function.

We employed antibodies against phosphorylated AMPK^{Thr172} (1:1,000; 2535S; Cell Signaling, Danvers, MA, USA), AMPK (1:1,000; 2532S; Cell Signaling, Danvers, MA, USA), phosphorylated ACC^{Ser79} (1:1,000; 3661S; Cell Signaling, Danvers, MA, USA), ACC (1:1,000; 3676S; Cell Signaling, Danvers, MA, USA), phosphorylated p38$^{Thr180/Tyr182}$ (1:1,000; 9215S; Cell Signaling, Danvers, MA, USA), p38 (1:1,000; 9212S; Cell Signaling, Danvers, MA, USA), PGC-1α (1:200; AB3242; EMD Millipore, Darmstadt, HE, Germany), p53 (1:1,000; 2524S; Cell Signaling, Danvers, MA, USA), citrate synthase (1:1,000; ab96600; Abcam, Cambridge, UK), and total OXPHOS (1:1,000; ab110413; Abcam, Cambridge, UK) to assess metabolic signaling. Antibodies against Parkin (1:1,000; 2132S; Cell Signaling, Danvers, MA, USA) and Bnip3 (1:1,000; 3769S; Cell Signaling, Danvers, MA, USA) were used as markers of mitophagy. Antibodies against LC3 (1:1,000; 4108S; Cell Signaling, Danvers, MA, USA), p62 (1:1,000; P0067; Sigma-Aldrich, St. Louis, MO, USA), phosphorylated ULK1^{Ser555} (1:1,000; 5869S; Cell Signaling, Danvers, MA, USA), ULK1 (1:1,000; 8054S; Cell Signaling, Danvers, MA, USA), SKP2 (1:1,000; 4313S; Cell Signaling, Danvers, MA, USA), TFEB (1:1,000; 4240S; Cell Signaling, Danvers, MA, USA), Beclin-1 (1:1,000; 3738S; Cell Signaling, Danvers, MA, USA), Lamp1 (1:1,000; ab24170; Abcam, Cambridge, UK), Lamp2 (1:1,000; ab13524; Abcam,

Cambridge, UK), and cathepsin D (1:1,000; 2284S; Cell Signaling, Danvers, MA, USA) were employed to investigate the autophagy-lysosome pathway.

Antibodies against MuRF1 (1:200; AF5366; R&D Systems, Minneapolis, MN, USA), MAFbx (1:1,000; AP2041; ECM Biosciences, Versailles, KY, USA), ubiquitin (1:500; 3933S; Cell Signaling, Danvers, MA, USA), phosphorylated Akt^{Ser473} (1:1,000; 9271S; Cell Signaling, Danvers, MA, USA), Akt (1:1,000; 4691S; Cell Signaling, Danvers, MA, USA), phosphorylated TSC2^{Ser1387} (1:1,000; 23402S; Cell Signaling, Danvers, MA, USA), TSC2 (1:1,000; 4308S; Cell Signaling, Danvers, MA, USA), phosphorylated mTOR^{Ser2448} (1:1,000; 2971S; Cell Signaling, Danvers, MA, USA), mTOR (1:1,000; 2972S; Cell Signaling, Danvers, MA, USA), phosphorylated FOXO1^{Ser256} (1:1,000; 9461S; Cell Signaling, Danvers, MA, USA), FOXO1 (1:1,000; 2880S; Cell Signaling, Danvers, MA, USA), phosphorylated FOXO3^{Ser253} (1:1,000; 9466S; Cell Signaling, Danvers, MA, USA), phosphorylated FOXO3^{Ser413} (1:1,000; 8174S; Cell Signaling, Danvers, MA, USA), phosphorylated FOXO3^{Ser588} (1:1,000; a kind gift from Dr. Anne Brunet, Department of Genetics, Stanford University School of Medicine), and FOXO3 (1:1,000; 2497S; Cell Signaling, Danvers, MA, USA) were used to evaluate the muscle atrophy program.

Histological analyses. EDL and SOL muscle cross-sections were stained with hematoxylin and eosin (H&E) to measure cross-sectional area (CSA) and centrally located nuclei of individual muscle fibers as performed previously (Manta et al., 2019; Stouth et al., 2020). Briefly, muscle samples were first transversely sectioned at 5 μm using a cryostat set at -20°C (Thermo Fisher Scientific Life Sciences, Waltham, MA, USA). Muscle cross-sections were then stained with hematoxylin (Sigma-Aldrich, St. Louis, MO, USA) and

eosin (Bioshop Canada Inc., Burlington, ON, Canada), dehydrated with successive 70%, 95%, and 100% ethanol exposures, further dried with xylene (Sigma-Aldrich, St. Louis, MO, USA) and mounted with Permount (Thermo Fisher Scientific Life Sciences, Waltham, MA, USA). H&E-stained muscle sections were imaged using light microscopy at 20x magnification with Nikon Elements Microscopic Imaging Software (Nikon Instruments Inc, Melville, NY, USA). CSA and total number of centrally located myonuclei were quantified for 150 myofibers across three individual regions per muscle (NIS-Elements). All investigators performing the image analyses were blinded.

EDL muscles were cut into 8 µm cryosections and stained for succinate dehydrogenase (SDH) activity as described previously (Stouth et al., 2020). Muscle samples were incubated in a buffer consisting of 0.2 M sodium succinate, 0.2 M phosphate buffer, pH 7.4, and nitro blue tetrazolium (Sigma-Aldrich, St. Louis, MO, USA) at 37°C for one hour. After the incubation step, muscle sections were rinsed with distilled water, exposed to 30%, 60%, 90% acetone, and mounted with Permount (Thermo Fisher Scientific Life Sciences, Waltham, MA, USA). Photos of muscle sections were later captured using light microscopy at 20x magnification with Nikon Elements Microscopic Imaging Software (Nikon Instruments Inc, Melville, NY, USA).

Permeabilization of muscle fibers. Preparation of permeabilized muscle fiber bundles was carried out as described earlier (Kuznetsov et al., 2008; Hughes et al., 2019). Immediately after excision, the proximal half of the TA muscle was placed in ice-cold biopsy preservation solution (BIOPS; 10 mM Ca-EGTA solution, 5.77 mM ATP, 6.56 mM MgCl2, 20 mM taurine, 15 mM phosphocreatine, 20 mM imidazole, 0.5 mM dithiothreitol,

and 50 mM MES hydrate, pH 7.1). Each muscle was trimmed of fat and connective tissue below a dissection microscope while on a frozen block. Fine tip forceps were then used to separate muscle fibers into small muscle bundles (~5 mg). The muscle bundles were placed in BIOPS solution with saponin (50 μg/μl) and mixed by end-over end inversion for 30 minutes at 4 °C. Bundles were also incubated in 2,4-dinitrochlorobenzene (CDNB; 35 μM) during permeabilization to deplete glutathione and allow for detectable rates of hydrogen peroxide (H_2O_2) emission. After permeabilization, samples were treated with buffer Z (105 mM K-MES, 30 mM KCl, 10 mM KH_2PO_4, 5 mM $MgCl_2$, 1 mM EGTA, 5 mg/mL BSA, pH 7.4) on a rotor at 4 °C for at least 15 minutes until the respiration and H_2O_2 emission trials commenced.

Mitochondrial respiration and H_2O_2 emission. High-resolution measurements of mitochondrial oxygen consumption were calculated with the Oxygraph-2k (Oroboros Instruments, Innsbruck, Austria) as performed earlier (Shen et al., 2018; Hughes et al., 2019). The instrument chambers were calibrated prior to adding 2 mL of buffer Z, blebbistatin (BLEB; 5 μM), and Amplex Red. After muscle fiber permeabilization and washing steps, muscle bundles were blotted dry, weighed, and placed into the appropriate chamber. All trials were conducted at 37 °C with constant stirring at 750 rpm, and at oxygen concentrations greater than 250 nmol/mL. For ADP-stimulated respiratory kinetics, pyruvate (5 mM) and malate (2 mM) were initially included to prompt complex I, followed by maximal ADP (5 mM). Succinate (20 mM) was then added, in the presence of complex I-specific glutamate (5 mM), to saturate electron entry into complex II. Cytochrome c (10 μM) was added last to test mitochondrial membrane integrity, with all experiments

demonstrating <10% increase in respiration. For the analysis of the respiration data, oxygen flux was determined from the derivative of the oxygen concentration in the respiratory chamber. Oxygen flux values were normalized to fiber bundle wet weight (pmol/sec/mg), or citrate synthase protein content quantified by Western blot in TA muscle collected from the same mouse (pmol/sec/citrate synthase arbitrary units), as validated previously (Kuznetsov et al., 2008). Mitochondrial H_2O_2 emission was assessed fluorometrically using the O2k-Fluo LED2-Module (Oroboros Instruments, Innsbruck, Austria) as described previously (Buch et al., 2020). Initially, horseradish peroxidase (1 U/mL), superoxide dismutase (5 U/mL), and Amplex Red (10 μM) were added to convert superoxide to H_2O_2 with accompanying H_2O_2-mediated conversion of Amplex Red to resorufin. Fluorometric sensor calibrations were conducted by adding H_2O_2 titrations (0.1-0.4 μM) prior to each experiment. Mitochondrial H_2O_2 emission values were expressed relative to fiber bundle wet weight (pmol/sec/mg), or citrate synthase protein content (pmol/sec/citrate synthase arbitrary units).

Transmission electron microscopy (TEM). TA muscle was immediately fixed in 2% (v/v) glutaraldehyde in 0.1 mol/L sodium cacodylate buffer pH 7.4 and processed as performed previously (Nilsson et al., 2015). Mitochondria were then quantified as described earlier (Monaco et al., 2018; Hughes et al., 2019). Representative micrographs from ten unique fibers (each containing a section of the subsarcolemmal region adjacent to the nucleus, with most of the image containing the intermyofibrillar area) were acquired at 15,000x magnification. Mitochondrial size (mean area, μm^2), distribution (number per μm^2) and density (μm^2 x number per μm^2 x 100) were calculated by manually outlining and

counting mitochondria in ImageJ. Total number of abnormal mitochondria and autophagic bodies were also determined at 15,000x magnification (Klionsky et al., 2021). The investigators conducting the analyses were blinded to all images.

Statistical Analyses. All statistical measures were carried out on the raw data sets prior to conversion to the -fold difference values presented in the graphical summaries. One-way analysis of variance (ANOVA), two-way ANOVA, and Tukey post hoc tests were used to compare means between experimental groups, where suitable. A one-way ANOVA was used to assess CARM1 protein expression in WT muscles following 3, 12, 18, and 22 months of aging. A two-way ANOVA was implemented to evaluate the interaction between genotype and aging for body weight, muscle function, muscle weight, centrally located nuclei, myofiber CSA, protein content, oxygen and H_2O_2 flux, as well as TEM analyses. A log-rank Mantel-Cox test was applied for comparison of survival between genotypes. Unpaired *t*-tests between genotypes were performed to compare relative -fold changes that occurred with aging. Statistical analyses were conducted using Prism software (GraphPad Software, San Diego, CA, USA). Data are means ± SEM and statistical differences were considered significant if $p < 0.05$.

Acknowledgements

We thank Dr. Mark Bedford (MD Anderson Cancer Center, University of Texas) and Dr. Anne Brunet (Department of Genetics, Stanford University School of Medicine) for the gifts of CARM1 floxed mice and the CARM1 substrate reagent, as well as the P-FOXO3^{Ser588} antibody, respectively. We also thank Dr. Lawrence Kazak (McGill University, Canada) for assistance with genotyping. We are grateful to members of the

Integrative Neuromuscular Biology Laboratory and to colleagues in the Exercise Metabolism Research Group at McMaster University for helpful advice and discussion. This work was funded by the Natural Science and Engineering Research Council of Canada (NSERC), the Canada Research Chairs program, and the Ontario Ministry of Economic Development, Job Creation and Trade (MEDJCT). D.W.S., T.L.V., S.Y.N., and E.K.W. are NSERC postgraduate scholars. E.K.W. is an Interdisciplinary Fellow of the Canadian Frailty Network. V.L. is the Canada Research Chair (Tier 2) in Neuromuscular Plasticity in Health and Disease and is a MEDJCT Early Researcher.

Author Contributions

D.W.S. and V.L. conceived and designed the study; D.W.S. and T.L.v. generated and maintained CARM1 mKO mice; D.W.S. performed all experiments and most analyses. S.Y.N., A.M., E.K.W., K.S.G., M.M., H.C.P., B.G.B., T.R., J.M.K., G.V. and K.J.M. assisted with analyses; all authors participated in data analysis and interpretation of results; D.W.S. and V.L. drafted and edited the manuscript.

Disclosure statement

The authors declare no conflicts of interest.

References

Aartsma-Rus, A., & van Putten, M. (2014). Assessing functional performance in the mdx mouse model. Journal of visualized experiments : JoVE, (85), 51303.

Arnold, A. S., Gill, J., Christe, M., Ruiz, R., McGuirk, S., St-Pierre, J., Tabares, L., & Handschin, C. (2014). Morphological and functional remodelling of the neuromuscular junction by skeletal muscle PGC-1α. Nature communications, 5, 3569.

Bao, J., Rousseaux, S., Shen, J., Lin, K., Lu, Y., & Bedford, M. T. (2018). The arginine methyltransferase CARM1 represses p300•ACT•CREMτ activity and is required for spermiogenesis. Nucleic acids research, 46(9), 4327–4343.

Bedford, M. T., & Clarke, S. G. (2009). Protein arginine methylation in mammals: who, what, and why. Molecular cell, 33(1), 1–13.

Buch, B. T., Halling, J. F., Ringholm, S., Gudiksen, A., Kjøbsted, R., Olsen, M. A., Wojtaszewski, J., & Pilegaard, H. (2020). Colchicine treatment impairs skeletal muscle mitochondrial function and insulin sensitivity in an age-specific manner. FASEB journal : official publication of the Federation of American Societies for Experimental Biology, 34(6), 8653–8670.

Bujak, A. L., Crane, J. D., Lally, J. S., Ford, R. J., Kang, S. J., Rebalka, I. A., Green, A. E., Kemp, B. E., Hawke, T. J., Schertzer, J. D., & Steinberg, G. R. (2015). AMPK activation of muscle autophagy prevents fasting-induced hypoglycemia and myopathy during aging. Cell metabolism, 21(6), 883–890.

Calnan, D. R., & Brunet, A. (2008). The FoxO code. Oncogene, 27(16), 2276–2288.

Carnio, S., LoVerso, F., Baraibar, M. A., Longa, E., Khan, M. M., Maffei, M., Reischl, M., Canepari, M., Loefler, S., Kern, H., Blaauw, B., Friguet, B., Bottinelli, R., Rudolf, R., & Sandri, M. (2014). Autophagy impairment in muscle induces neuromuscular junction degeneration and precocious aging. Cell reports, 8(5), 1509–1521.

Carter, H. N., Chen, C. C., & Hood, D. A. (2015). Mitochondria, muscle health, and exercise with advancing age. Physiology (Bethesda, Md.), 30(3), 208–223.

Carter, H. N., Kim, Y., Erlich, A. T., Zarrin-Khat, D., & Hood, D. A. (2018). Autophagy and mitophagy flux in young and aged skeletal muscle following chronic contractile activity. The Journal of physiology, 596(16), 3567–3584.

Chang, N. C., Sincennes, M. C., Chevalier, F. P., Brun, C. E., Lacaria, M., Segalés, J., Muñoz-Cánoves, P., Ming, H., & Rudnicki, M. A. (2018). The Dystrophin Glycoprotein

Complex Regulates the Epigenetic Activation of Muscle Stem Cell Commitment. Cell stem cell, 22(5), 755–768.e6.

Chen, S. L., Loffler, K. A., Chen, D., Stallcup, M. R., & Muscat, G. E. (2002). The coactivator-associated arginine methyltransferase is necessary for muscle differentiation: CARM1 coactivates myocyte enhancer factor-2. The Journal of biological chemistry, 277(6), 4324–4333.

Cheng, D., Vemulapalli, V., Lu, Y., Shen, J., Aoyagi, S., Fry, C. J., Yang, Y., Foulds, C. E., Stossi, F., Treviño, L. S., Mancini, M. A., O'Malley, B. W., Walker, C. L., Boyer, T. G., & Bedford, M. T. (2018). CARM1 methylates MED12 to regulate its RNA-binding ability. Life science alliance, 1(5), e201800117.

Drummond, M. J., Dreyer, H. C., Fry, C. S., Glynn, E. L., & Rasmussen, B. B. (2009). Nutritional and contractile regulation of human skeletal muscle protein synthesis and mTORC1 signaling. Journal of applied physiology (Bethesda, Md. : 1985), 106(4), 1374–1384.

Fulton, M. D., Brown, T., & Zheng, Y. G. (2019). The Biological Axis of Protein Arginine Methylation and Asymmetric Dimethylarginine. International journal of molecular sciences, 20(13), 3322.

Garrido-Maraver, J., Paz, M. V., Cordero, M. D., Bautista-Lorite, J., Oropesa-Ávila, M., de la Mata, M., Pavón, A. D., de Lavera, I., Alcocer-Gómez, E., Galán, F., Ybot González, P., Cotán, D., Jackson, S., & Sánchez-Alcázar, J. A. (2015). Critical role of AMP-activated protein kinase in the balance between mitophagy and mitochondrial biogenesis in MELAS disease. Biochimica et biophysica acta, 1852(11), 2535–2553. https://doi.org/10.1016/j.bbadis.2015.08.027

Guccione, E., & Richard, S. (2019). The regulation, functions and clinical relevance of arginine methylation. Nature reviews. Molecular cell biology, 20(10), 642–657.

Ham, D. J., Börsch, A., Lin, S., Thürkauf, M., Weihrauch, M., Reinhard, J. R., Delezie, J., Battilana, F., Wang, X., Kaiser, M. S., Guridi, M., Sinnreich, M., Rich, M. M., Mittal, N., Tintignac, L. A., Handschin, C., Zavolan, M., & Rüegg, M. A. (2020). The neuromuscular junction is a focal point of mTORC1 signaling in sarcopenia. Nature communications, 11(1), 4510.

Herzig, S., & Shaw, R. J. (2018). AMPK: guardian of metabolism and mitochondrial homeostasis. Nature reviews. Molecular cell biology, 19(2), 121–135.

Hood, D. A., Memme, J. M., Oliveira, A. N., & Triolo, M. (2019). Maintenance of Skeletal Muscle Mitochondria in Health, Exercise, and Aging. Annual review of physiology, 81, 19–41.

Hu, R., Wang, M. Q., Liu, L. Y., You, H. Y., Wu, X. H., Liu, Y. Y., Wang, Y. J., Lu, L., Xiao, W., & Wei, L. B. (2020). Calycosin inhibited autophagy and oxidative stress in chronic kidney disease skeletal muscle atrophy by regulating AMPK/SKP2/CARM1 signalling pathway. Journal of cellular and molecular medicine, 24(19), 11084–11099.

Hughes, M. C., Ramos, S. V., Turnbull, P. C., Rebalka, I. A., Cao, A., Monaco, C., Varah, N. E., Edgett, B. A., Huber, J. S., Tadi, P., Delfinis, L. J., Schlattner, U., Simpson, J. A., Hawke, T. J., & Perry, C. (2019). Early myopathy in Duchenne muscular dystrophy is associated with elevated mitochondrial H2 O2 emission during impaired oxidative phosphorylation. Journal of cachexia, sarcopenia and muscle, 10(3), 643–661.

Jackson, S. J., Andrews, N., Ball, D., Bellantuono, I., Gray, J., Hachoumi, L., Holmes, A., Latcham, J., Petrie, A., Potter, P., Rice, A., Ritchie, A., Stewart, M., Strepka, C., Yeoman, M., & Chapman, K. (2017). Does age matter? The impact of rodent age on study outcomes. Laboratory animals, 51(2), 160–169.

Kawabe, Y., Wang, Y. X., McKinnell, I. W., Bedford, M. T., & Rudnicki, M. A. (2012). Carm1 regulates Pax7 transcriptional activity through MLL1/2 recruitment during asymmetric satellite stem cell divisions. Cell stem cell, 11(3), 333–345.

Kjøbsted, R., Hingst, J. R., Fentz, J., Foretz, M., Sanz, M. N., Pehmøller, C., Shum, M., Marette, A., Mounier, R., Treebak, J. T., Wojtaszewski, J., Viollet, B., & Lantier, L. (2018). AMPK in skeletal muscle function and metabolism. FASEB journal : official publication of the Federation of American Societies for Experimental Biology, 32(4), 1741–1777.

Klionsky, D. J., Abdel-Aziz, A. K., Abdelfatah, S., Abdellatif, M., Abdoli, A., Abel, S., Abeliovich, H., Abildgaard, M. H., Abudu, Y. P., Acevedo-Arozena, A., Adamopoulos, I. E., Adeli, K., Adolph, T. E., Adornetto, A., Aflaki, E., Agam, G., Agarwal, A., Aggarwal, B. B., Agnello, M., Agostinis, P., … Tong, C. K. (2021). Guidelines for the use and interpretation of assays for monitoring autophagy (4th edition)1. Autophagy, 17(1), 1–382.

Kuznetsov, A. V., Veksler, V., Gellerich, F. N., Saks, V., Margreiter, R., & Kunz, W. S. (2008). Analysis of mitochondrial function in situ in permeabilized muscle fibers, tissues and cells. Nature protocols, 3(6), 965–976.

Larsen, S. C., Sylvestersen, K. B., Mund, A., Lyon, D., Mullari, M., Madsen, M. V., Daniel, J. A., Jensen, L. J., & Nielsen, M. L. (2016). Proteome-wide analysis of arginine monomethylation reveals widespread occurrence in human cells. Science signaling, 9(443), rs9.

Li, C., Yu, L., Xue, H., Yang, Z., Yin, Y., Zhang, B., Chen, M., & Ma, H. (2017). Nuclear AMPK regulated CARM1 stabilization impacts autophagy in aged heart. Biochemical and biophysical research communications, 486(2), 398–405.

Liu, Y., Li, J., Shang, Y., Guo, Y., & Li, Z. (2019). CARM1 contributes to skeletal muscle wasting by mediating FoxO3 activity and promoting myofiber autophagy. Experimental cell research, 374(1), 198–209.

Ljubicic, V., Khogali, S., Renaud, J. M., & Jasmin, B. J. (2012). Chronic AMPK stimulation attenuates adaptive signaling in dystrophic skeletal muscle. American journal of physiology. Cell physiology, 302(1), C110–C121.

Mammucari, C., Schiaffino, S., & Sandri, M. (2008). Downstream of Akt: FoxO3 and mTOR in the regulation of autophagy in skeletal muscle. Autophagy, 4(4), 524–526.

Manta, A., Stouth, D. W., Xhuti, D., Chi, L., Rebalka, I. A., Kalmar, J. M., Hawke, T. J., & Ljubicic, V. (2019). Chronic exercise mitigates disease mechanisms and improves muscle function in myotonic dystrophy type 1 mice. The Journal of physiology, 597(5), 1361–1381.

Manzanares, G., Brito-da-Silva, G., & Gandra, P. G. (2018). Voluntary wheel running: patterns and physiological effects in mice. Brazilian journal of medical and biological research = Revista brasileira de pesquisas medicas e biologicas, 52(1), e7830.

Masiero, E., Agatea, L., Mammucari, C., Blaauw, B., Loro, E., Komatsu, M., Metzger, D., Reggiani, C., Schiaffino, S., & Sandri, M. (2009). Autophagy is required to maintain muscle mass. Cell metabolism, 10(6), 507–515.

McCarthy, J. J., Srikuea, R., Kirby, T. J., Peterson, C. A., & Esser, K. A. (2012). Inducible Cre transgenic mouse strain for skeletal muscle-specific gene targeting. Skeletal muscle, 2(1), 8.

Monaco, C., Hughes, M. C., Ramos, S. V., Varah, N. E., Lamberz, C., Rahman, F. A., McGlory, C., Tarnopolsky, M. A., Krause, M. P., Laham, R., Hawke, T. J., & Perry, C. (2018). Altered mitochondrial bioenergetics and ultrastructure in the skeletal muscle of young adults with type 1 diabetes. Diabetologia, 61(6), 1411–1423.

Nilsson, M. I., MacNeil, L. G., Kitaoka, Y., Suri, R., Young, S. P., Kaczor, J. J., Nates, N. J., Ansari, M. U., Wong, T., Ahktar, M., Brandt, L., Hettinga, B. P., & Tarnopolsky, M. A. (2015). Combined aerobic exercise and enzyme replacement therapy rejuvenates the mitochondrial-lysosomal axis and alleviates autophagic blockage in Pompe disease. Free radical biology & medicine, 87, 98–112.

Pang, L., Tian, H., Chang, N., Yi, J., Xue, L., Jiang, B., Gorospe, M., Zhang, X., & Wang, W. (2013). Loss of CARM1 is linked to reduced HuR function in replicative senescence. BMC molecular biology, 14, 15.

Romero-Calvo, I., Ocón, B., Martínez-Moya, P., Suárez, M. D., Zarzuelo, A., Martínez-Augustin, O., & de Medina, F. S. (2010). Reversible Ponceau staining as a loading control alternative to actin in Western blots. Analytical biochemistry, 401(2), 318–320.

Salminen, A., & Kaarniranta, K. (2012). AMP-activated protein kinase (AMPK) controls the aging process via an integrated signaling network. Ageing research reviews, 11(2), 230–241.

Sanchez, A. M., Candau, R. B., & Bernardi, H. (2014). FoxO transcription factors: their roles in the maintenance of skeletal muscle homeostasis. Cellular and molecular life sciences : CMLS, 71(9), 1657–1671.

Shen, N. Y., Ng, S. Y., Toepp, S. L., & Ljubicic, V. (2018). Protein arginine methyltransferase expression and activity during myogenesis. Bioscience reports, 38(1), BSR20171533.

Shin, H. J., Kim, H., Oh, S., Lee, J. G., Kee, M., Ko, H. J., Kweon, M. N., Won, K. J., & Baek, S. H. (2016). AMPK-SKP2-CARM1 signalling cascade in transcriptional regulation of autophagy. Nature, 534(7608), 553–557.

Stouth, D. W., Manta, A., & Ljubicic, V. (2018). Protein arginine methyltransferase expression, localization, and activity during disuse-induced skeletal muscle plasticity. American journal of physiology. Cell physiology, 314(2), C177–C190.

Stouth, D. W., vanLieshout, T. L., Ng, S. Y., Webb, E. K., Manta, A., Moll, Z., & Ljubicic, V. (2020). CARM1 Regulates AMPK Signaling in Skeletal Muscle. iScience, 23(11), 101755.

Stouth, D. W., vanLieshout, T. L., Shen, N. Y., & Ljubicic, V. (2017). Regulation of Skeletal Muscle Plasticity by Protein Arginine Methyltransferases and Their Potential Roles in Neuromuscular Disorders. Frontiers in physiology, 8, 870.

Tatem, K. S., Quinn, J. L., Phadke, A., Yu, Q., Gordish-Dressman, H., & Nagaraju, K. (2014). Behavioral and locomotor measurements using an open field activity monitoring system for skeletal muscle diseases. Journal of visualized experiments : JoVE, (91), 51785.

Triolo, M., & Hood, D. A. (2021). Manifestations of Age on Autophagy, Mitophagy and Lysosomes in Skeletal Muscle. Cells, 10(5), 1054.

Vainshtein, A., Desjardins, E. M., Armani, A., Sandri, M., & Hood, D. A. (2015). PGC-1α modulates denervation-induced mitophagy in skeletal muscle. Skeletal muscle, 5, 9.

vanLieshout, T. L., & Ljubicic, V. (2019). The emergence of protein arginine methyltransferases in skeletal muscle and metabolic disease. American journal of physiology. Endocrinology and metabolism, 317(6), E1070–E1080.

vanLieshout, T. L., Bonafiglia, J. T., Gurd, B. J., & Ljubicic, V. (2019). Protein arginine methyltransferase biology in humans during acute and chronic skeletal muscle plasticity. Journal of applied physiology (Bethesda, Md. : 1985), 127(3), 867–880.

Vanlieshout, T. L., Stouth, D. W., Tajik, T., & Ljubicic, V. (2018). Exercise-induced Protein Arginine Methyltransferase Expression in Skeletal Muscle. Medicine and science in sports and exercise, 50(3), 447–457.

Wang, S. C., Dowhan, D. H., Eriksson, N. A., & Muscat, G. E. (2012). CARM1/PRMT4 is necessary for the glycogen gene expression programme in skeletal muscle cells. The Biochemical journal, 444(2), 323–331.

Yadav, N., Lee, J., Kim, J., Shen, J., Hu, M. C., Aldaz, C. M., & Bedford, M. T. (2003). Specific protein methylation defects and gene expression perturbations in coactivator-associated arginine methyltransferase 1-deficient mice. Proceedings of the National Academy of Sciences of the United States of America, 100(11), 6464–6468.

Yanai, S., & Endo, S. (2021). Functional Aging in Male C57BL/6J Mice Across the Life-Span: A Systematic Behavioral Analysis of Motor, Emotional, and Memory Function to Define an Aging Phenotype. Frontiers in aging neuroscience, 13, 697621.

Yang, Y., & Bedford, M. T. (2013). Protein arginine methyltransferases and cancer. Nature reviews. Cancer, 13(1), 37–50.

Yeo, D., Kang, C., Gomez-Cabrera, M. C., Vina, J., & Ji, L. L. (2019). Intensified mitophagy in skeletal muscle with aging is downregulated by PGC-1alpha overexpression in vivo. Free radical biology & medicine, 130, 361–368.

Yu, Y. S., Shin, H. R., Kim, D., Baek, S. A., Choi, S. A., Ahn, H., Shamim, A., Kim, J., Kim, I. S., Kim, K. K., Won, K. J., & Baek, S. H. (2020). Pontin arginine methylation by CARM1 is crucial for epigenetic regulation of autophagy. Nature communications, 11(1), 6297.

Zhou, K., Chen, H., Lin, J., Xu, H., Wu, H., Bao, G., Li, J., Deng, X., Shui, X., Gao, W., Ding, J., Xiao, J., & Xu, H. (2019). FGF21 augments autophagy in random-pattern skin flaps via AMPK signaling pathways and improves tissue survival. Cell death & disease, 10(12), 872.

Figure Legends

Figure 1. Survival and integrative physiology of skeletal muscle specific CARM1 knockout (mKO) mice throughout the lifespan. A: Representative Western blots of CARM1 protein content (normal and long exposures) in the tibialis anterior (TA) muscle from wild-type (WT) and mKO mice following 3, 12, 18, and 22 months (m) of aging, as well as a representative Ponceau stain, below. Molecular weights (kDa) are shown at right of blots. **B:** Graphical summary of CARM1 protein expression in TA muscle of male WT animals. Data are expressed as protein content relative to 3 m (n = 11-16). **C:** Body mass of WT and mKO mice across the lifespan. Data are collected from male and female animals (n = 73-84). **D:** Survival curve of WT and mKO mice. Data are collected from male and female animals (n = 73-84). Log-rank Mantel-Cox test; * $p < 0.05$ WT versus mKO. **E:** Representative locomotion traces of 3, 12, 18, and 22 m WT and mKO male mice taken after one hour in the open field chamber. **F-G:** Graphical summaries of ambulation (total distance traveled; n = 5-21) and anxiety-like behavior (activity spent in central region of test chamber; n = 5-21) in male WT and mKO animals following one hour. **H-K:** Indices of muscle function in male WT and mKO mice were assessed by forelimb grip strength, as well as latency to fall during pen, cage hang, and rotarod tests (n = 9-21). Data are means ± SEM. Two-way ANOVA; ∉ $p < 0.05$ main effect of genotype; ‡ $p < 0.05$ main effect of aging; ¶ $p < 0.05$ versus WT 3 m; # $p < 0.05$ versus mKO 3 m.

Figure 2. Sarcopenia of aging in WT and mKO animals. A: TA, extensor digitorum longus (EDL), soleus (SOL), and gastrocnemius (GAST) muscle mass from male WT and

mKO mice after 3, 12, 18, and 22 m of aging. Muscle mass is normalized to body weight and data are expressed relative to WT 3 m (n = 9-21). **B-D:** Representative images of hematoxylin and eosin (H&E)-stained EDL and SOL muscle cross sections from WT and mKO animals with aging. Inset, representative image of centrally located myonuclei (white arrow). Scale bar, 50 μm. **E:** Number of EDL myofibers with centrally located nuclei per total number of fibers analyzed. Myofibers containing centrally located nuclei are expressed relative to WT 3 m (n = 10-17). **F-G:** Graphical summaries of the average myofiber cross-sectional area (CSA) of EDL and SOL muscles from WT and mKO mice with aging. Data are expressed as CSA relative to WT 3 m (n = 10-18). Data are means ± SEM. Two-way ANOVA; $ $p < 0.05$ interaction effect of genotype and aging; ¢ $p < 0.05$ main effect of genotype; ‡ $p < 0.05$ main effect of aging; ¶ $p < 0.05$ versus WT 3 m; # $p < 0.05$ versus mKO 3 m.

Figure 3. Protein arginine methyltransferase (PRMT) content and activity in mKO mice with aging. A: Representative Western blots of PRMT1, PRMT5, PRMT6, PRMT7, monomethylarginine (MMA), asymmetric dimethylarginine (ADMA), ADMA-marked CARM1 substrates, symmetric dimethylarginine (SDMA), ADMA-marked SWI/SNF chromatin remodeling complex BAF155 (BAF155me2a^{Arg1064}), total BAF155, ADMA-marked poly(A)-binding protein 1 (PABP1me2a$^{Arg455/Arg460}$), and total PABP1 in TA muscles from male WT and mKO animals with aging, accompanied by a typical Ponceau stain. Molecular weights (kDa) are shown at the right of blots. **B-E:** Graphical summaries of PRMT1, PRMT5, PRMT6, PRMT7, MMA, ADMA, CARM1 substrate, SDMA,

BAF155me2a ^{Arg1064}, BAF155, BAF155 activation status (i.e., the methylated form of the protein relative to the total amount of the protein), PABP1me2a $^{Arg455/Arg460}$, PABP1, and PABP1 activation status in WT and mKO mice following 3, 12, 18, and 22 m of aging. Data are expressed as protein content relative to WT 3 m (n = 8-16). Data are means ± SEM. Two-way ANOVA; $ $p < 0.05$ interaction effect of genotype and aging; ¢ $p < 0.05$ main effect of genotype; ‡ $p < 0.05$ main effect of aging; ¶ $p < 0.05$ versus WT 3 m; # $p < 0.05$ versus mKO 3 m.

Figure 4. Metabolic signaling in mKO animals during sarcopenia. A: Representative Western blots of phosphorylated AMP-activated protein kinase (P-AMPK^{Thr172}), total AMPK, phosphorylated acetyl–coenzyme A carboxylase (P-ACC^{Ser79}), total ACC, phosphorylated p38 mitogen-activated protein kinase (P-p38$^{Thr180/Tyr182}$), total p38, peroxisome proliferator-activated receptor-γ coactivator-1α (PGC-1α), proteins indicative of mitochondrial oxidative phosphorylation (OXPHOS) complexes I–V (CI–CV), p53, and citrate synthase in male WT and mKO TA muscles with aging, accompanied by a typical Ponceau stain. Molecular weights (kDa) are shown at the right of blots. **B-E:** Graphical summaries of P-AMPK^{Thr172}, AMPK, AMPK activation status, P-ACC^{Ser79}, ACC, ACC activation status, P-p38$^{Thr180/Tyr182}$, p38, p38 activation status, PGC-1α, total OXPHOS, p53, and citrate synthase protein expression in WT and mKO TA muscles after 3, 12, 18, and 22 m of aging. Data are expressed as protein content relative to WT 3 m (n = 8-16). **F:** Representative images of succinate dehydrogenase (SDH)-stained EDL muscle cross-sections from WT and mKO mice during sarcopenia. Scale bar, 50 μm (n = 8-10). **G-H:**

Complex I-supported state III respiration and Complex I + II-supported state III respiration in WT and mKO TA muscle following 3 and 22 m of aging (n = 8-10). **I**: Complex I-supported state III H_2O_2 emission in WT and mKO animals after 3 and 22 m (n = 7-9). Data are means ± SEM. Two-way ANOVA; ¢ $p < 0.05$ main effect of genotype; ‡ $p < 0.05$ main effect of aging; ¶ $p < 0.05$ versus WT 3 m; # $p < 0.05$ versus mKO 3 m.

Figure 5. Mitochondrial biology in young and old mKO mice. A: Representative transmission electron micrographs of myonuclei (white asterisk), as well as mitochondria within the subsarcolemmal (SS) and intermyofibrillar (IMF) regions of WT and mKO TA muscles from male mice after 3 and 22 m of aging. Scale bar, 1 μm (n = 4-6). **B:** Representative image from a mKO 3 m animal of normal mitochondrial ultrastructure with intact inner and outer membranes and clearly defined cristae (white arrow). Scale bar, 200 nm. **C-E:** Transmission electron micrographs were assessed for mitochondrial size (mean area, μm^2), distribution (# per μm^2), and density (μm^2 x # per μm^2 x 100) within the SS and IMF areas of the muscle. **F-G:** Representative images from a mKO 22 m mouse of abnormal mitochondrial ultrastructure (black arrow) with disrupted membrane systems, loss of cristae, and vacuolization, as well as a double-membrane autophagic vacuole (yellow arrow). Scale bar, 200 nm. **H-I:** Graphical summaries of total number of abnormal mitochondria and autophagic bodies in WT and mKO animals following 3 and 22 m of aging. **J:** Representative Western blots of Parkin, BCL2 and adenovirus E1B 19-kDa interacting protein 3 (Bnip3) in WT and mKO TA muscles with aging, accompanied by a typical Ponceau stain. Molecular weights (kDa) are shown at the right of blots. **K:**

Graphical summary of Parkin and Bnip3 protein expression levels in WT and mKO mice after 3, 12, 18, and 22 m of aging. Data are expressed as protein content relative to WT 3 m (n = 9-16). Data are means ± SEM. Two-way ANOVA; ¢ $p < 0.05$ main effect of genotype; ‡ $p < 0.05$ main effect of aging.

Figure 6. Impact of muscle-specific deletion of CARM1 on autophagy with aging. A: Representative Western blots of microtubule-associated protein 1A/1B-light chain 3 (LC3)-I, LC3-II, p62, phosphorylated unc-51-like autophagy-activating kinase 1 (P-ULK1^{Ser555}), total ULK1, S-phase kinase-associated protein 2 (SKP2), transcription factor EB (TFEB), Beclin-1, lysosomal associated membrane protein 1 (Lamp1), Lamp2, and cathepsin D in male WT and mKO TA muscles with aging, accompanied by a typical Ponceau stain. Molecular weights (kDa) are shown at the right of blots. **B-E:** Graphical summaries of LC3-I, LC3-II, LC3-II/LC3-I ratio, p62, P-ULK1^{Ser555}, ULK1, ULK1 activation status, SKP2, TFEB, Beclin-1, Lamp1, Lamp2, and cathepsin D protein expression in WT and mKO mice following 3, 12, 18, and 22 m of aging. Data are expressed as protein content relative to WT 3 m (n = 9-16). Data are means ± SEM. Two-way ANOVA; ¢ $p < 0.05$ main effect of genotype; ‡ $p < 0.05$ main effect of aging; ¶ $p < 0.05$ versus WT 3 m; # $p < 0.05$ versus mKO 3 m.

Figure 7. The muscle atrophy program in mKO animals during sarcopenia. A: Representative Western blots of Muscle RING finger 1 (MuRF1), muscle atrophy F box (MAFbx), ubiquitin protein content, phosphorylated protein kinase B (P-Akt^{Ser473}), total

Akt, phosphorylated tuberous sclerosis complex 2 (P-TSC2^{Ser1387}), total TSC2, phosphorylated mammalian target of rapamycin (P-mTOR^{Ser2448}), total mTOR, phosphorylated Forkhead box O1 (P-FOXO1^{Ser256}) total FOXO1, P-FOXO3^{Ser253}, P-FOXO3^{Ser413}, P-FOXO3^{Ser588}, and total FOXO3 in male WT and mKO TA muscles with aging, accompanied by a typical Ponceau stain. Molecular weights (kDa) are shown at the right of blots. **B-G:** Graphical summaries of MuRF1, MAFbx, ubiquitin protein content, P-Akt^{Ser473}, Akt, Akt activation status, P-TSC2^{Ser1387}, TSC2, TSC2 activation status, P-mTOR^{Ser2448}, mTOR, mTOR activation status, P-FOXO1^{Ser256}, FOXO1, FOXO1 activation status, P-FOXO3^{Ser253}, P-FOXO3^{Ser413}, P-FOXO3^{Ser588}, FOXO3, and FOXO3 activation status in WT and mKO animals after 3, 12, 18, and 22 m of aging. Data are expressed as protein content relative to WT 3 m (n = 8-16). Data are means ± SEM. Two-way ANOVA; ¢ $p < 0.05$ main effect of genotype; ‡ $p < 0.05$ main effect of aging; ¶ $p < 0.05$ versus WT 3 m; # $p < 0.05$ versus mKO 3 m.

Figure 1

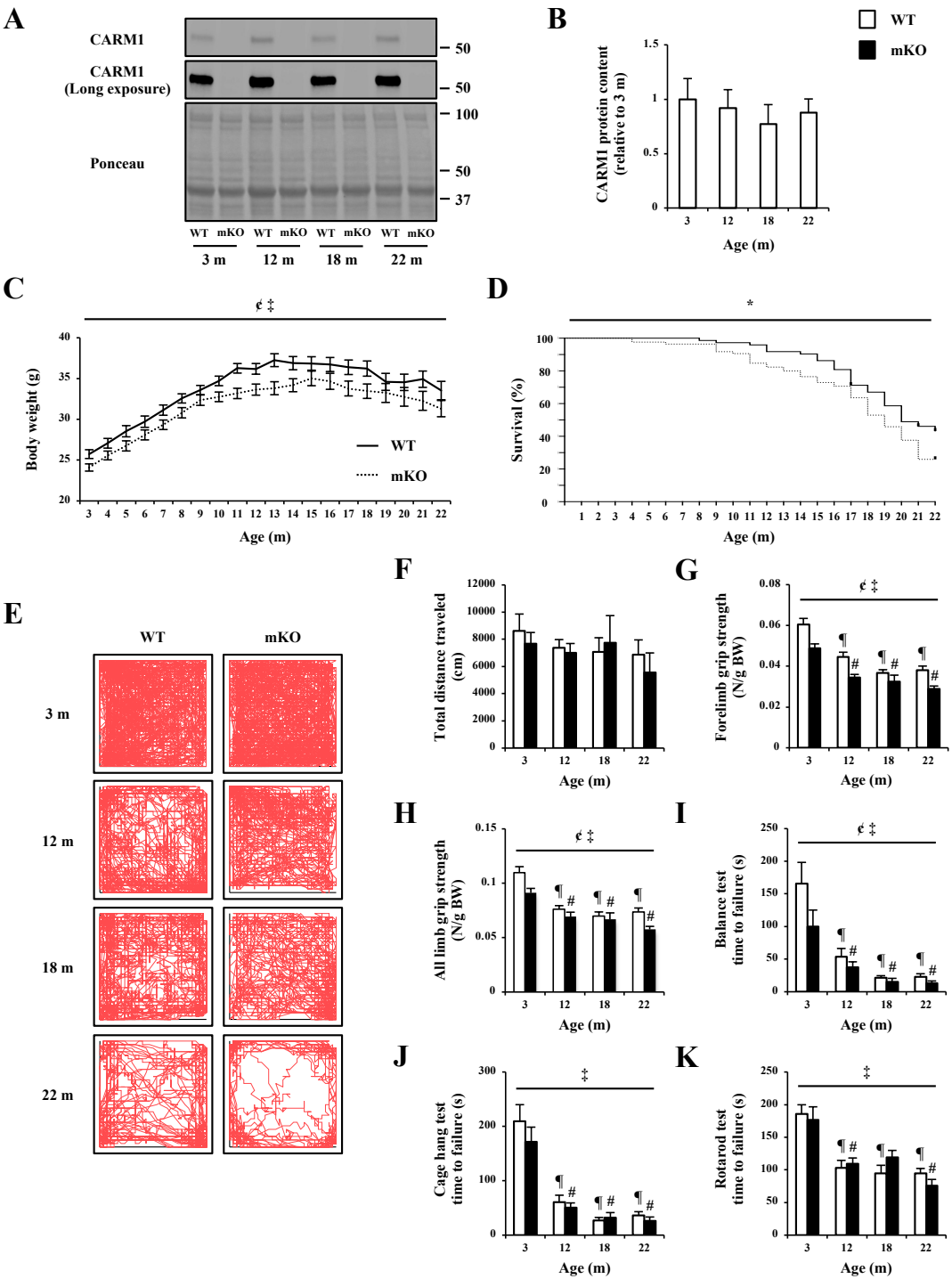
A
CARM1
CARM1 (Long exposure)
Ponceau
50
50
100
50
37
WT mKO WT mKO WT mKO WT mKO
3 m
12 m
18 m
22 m
B
WT
mKO
CARM1 protein content (relative to 3 m)
Age (m)
C
Body weight (g)
WT
mKO
Age (m)
D
Survival (%)
Age (m)
E
WT
mKO
3 m
12 m
18 m
22 m
F
Total distance traveled (cm)
Age (m)
G
Forelimb grip strength (N/g BW)
Age (m)
H
All limb grip strength (N/g BW)
Age (m)
I
Balance test time to failure (s)
Age (m)
J
Cage hang test time to failure (s)
Age (m)
K
Rotarod test time to failure (s)
Age (m)

Figure 2

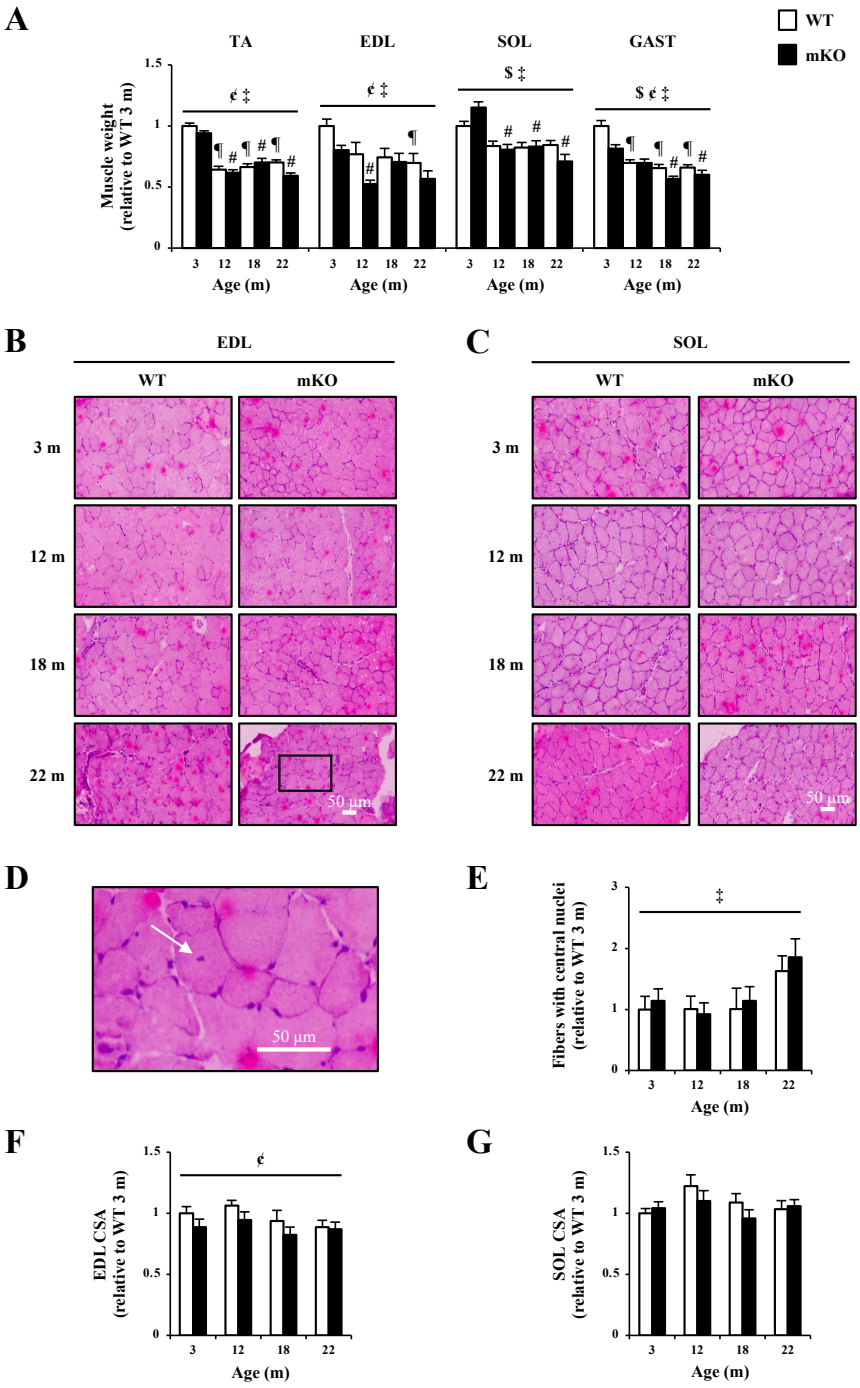
A
WT
mKO
TA
EDL
SOL
GAST
Muscle weight (relative to WT 3 m)
Age (m)
B
EDL
WT
mKO
3 m
12 m
18 m
22 m
50 µm
C
SOL
D
E
Fibers with central nuclei (relative to WT 3 m)
F
EDL CSA (relative to WT 3 m)
G
SOL CSA (relative to WT 3 m)

Figure 3

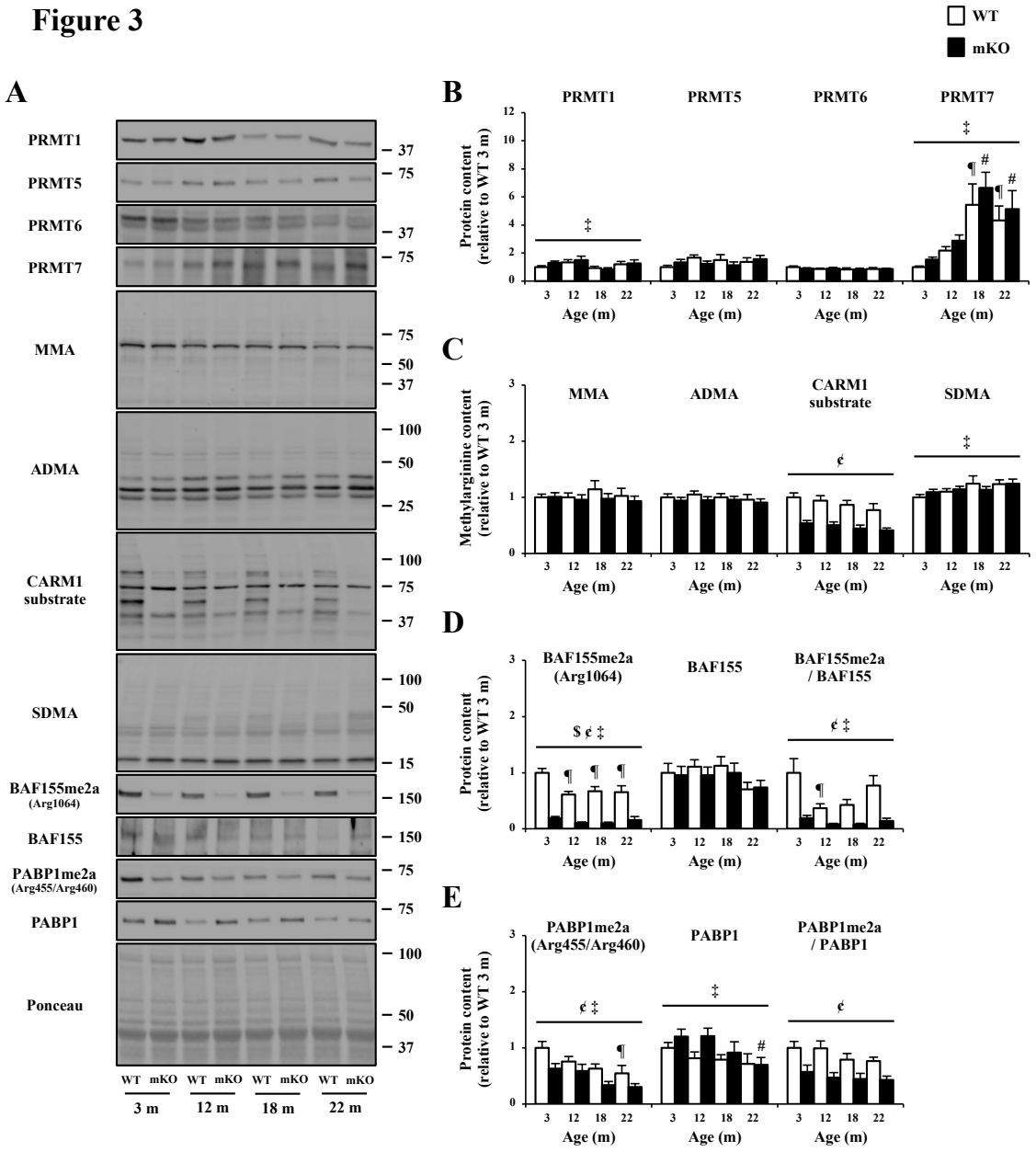
A
PRMT1
PRMT5
PRMT6
PRMT7
MMA
ADMA
CARM1 substrate
SDMA
BAF155me2a (Arg1064)
BAF155
PABP1me2a (Arg455/Arg460)
PABP1
Ponceau
WT mKO WT mKO WT mKO WT mKO
3 m 12 m 18 m 22 m
B
PRMT1 PRMT5 PRMT6 PRMT7
Protein content (relative to WT 3 m)
Age (m)
C
MMA ADMA CARM1 substrate SDMA
Methylarginine content (relative to WT 3 m)
D
BAF155me2a (Arg1064) BAF155 BAF155me2a / BAF155
E
PABP1me2a (Arg455/Arg460) PABP1 PABP1me2a / PABP1
WT
mKO

Figure 4

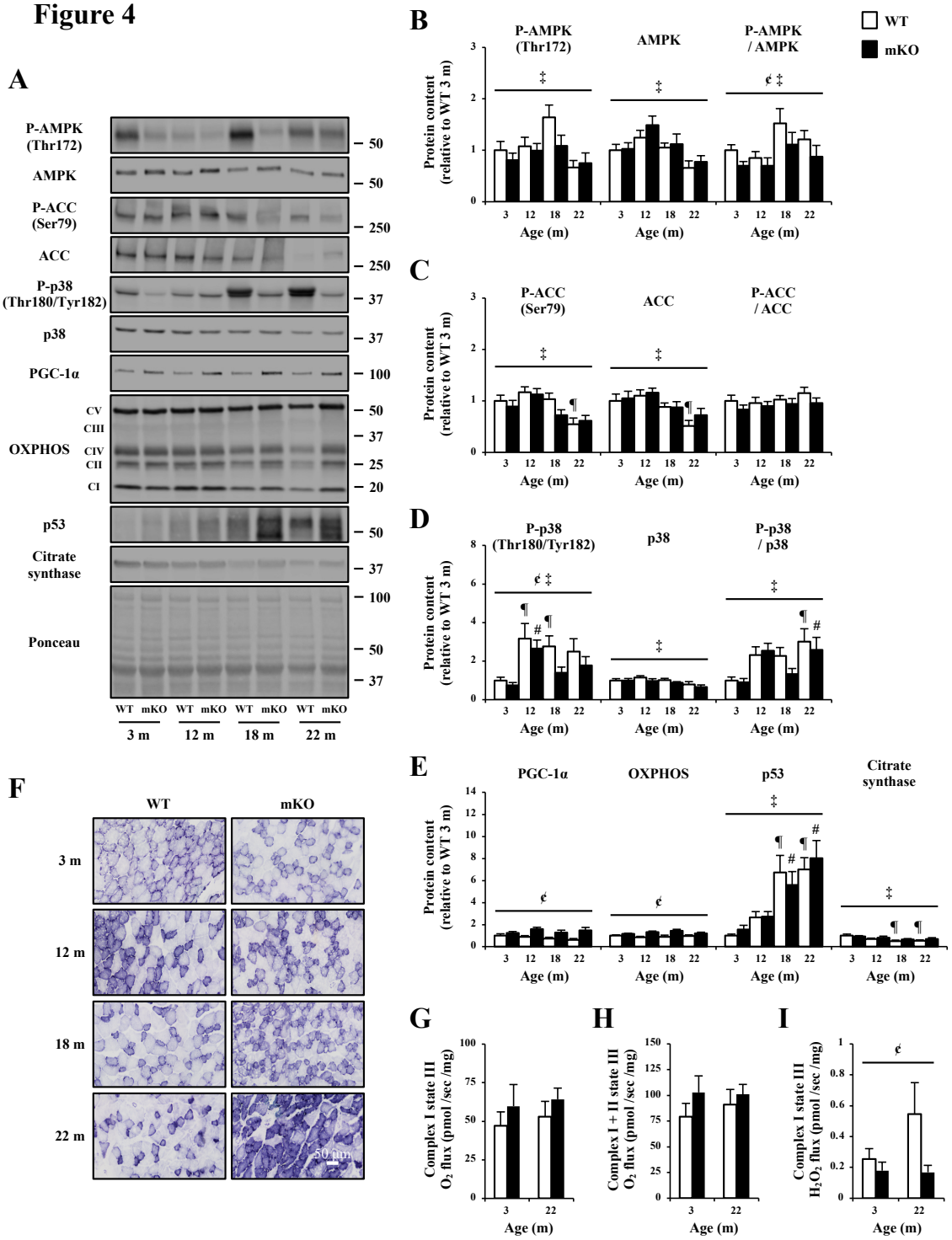
A
P-AMPK (Thr172)
AMPK
P-ACC (Ser79)
ACC
P-p38 (Thr180/Tyr182)
p38
PGC-1α
OXPHOS
CV
CIII
CIV
CII
CI
p53
Citrate synthase
Ponceau
50
50
250
250
37
37
100
50
37
25
20
50
37
100
50
37
WT mKO WT mKO WT mKO WT mKO
3 m
12 m
18 m
22 m
B
P-AMPK (Thr172)
AMPK
P-AMPK / AMPK
WT
mKO
Protein content (relative to WT 3 m)
Age (m)
C
P-ACC (Ser79)
ACC
P-ACC / ACC
D
P-p38 (Thr180/Tyr182)
p38
P-p38 / p38
E
PGC-1α
OXPHOS
p53
Citrate synthase
F
WT
mKO
3 m
12 m
18 m
22 m
50 μm
G
Complex I state III O2 flux (pmol /sec /mg)
H
Complex I + II state III O2 flux (pmol /sec /mg)
I
Complex I state III H2O2 flux (pmol /sec /mg)

Figure 5

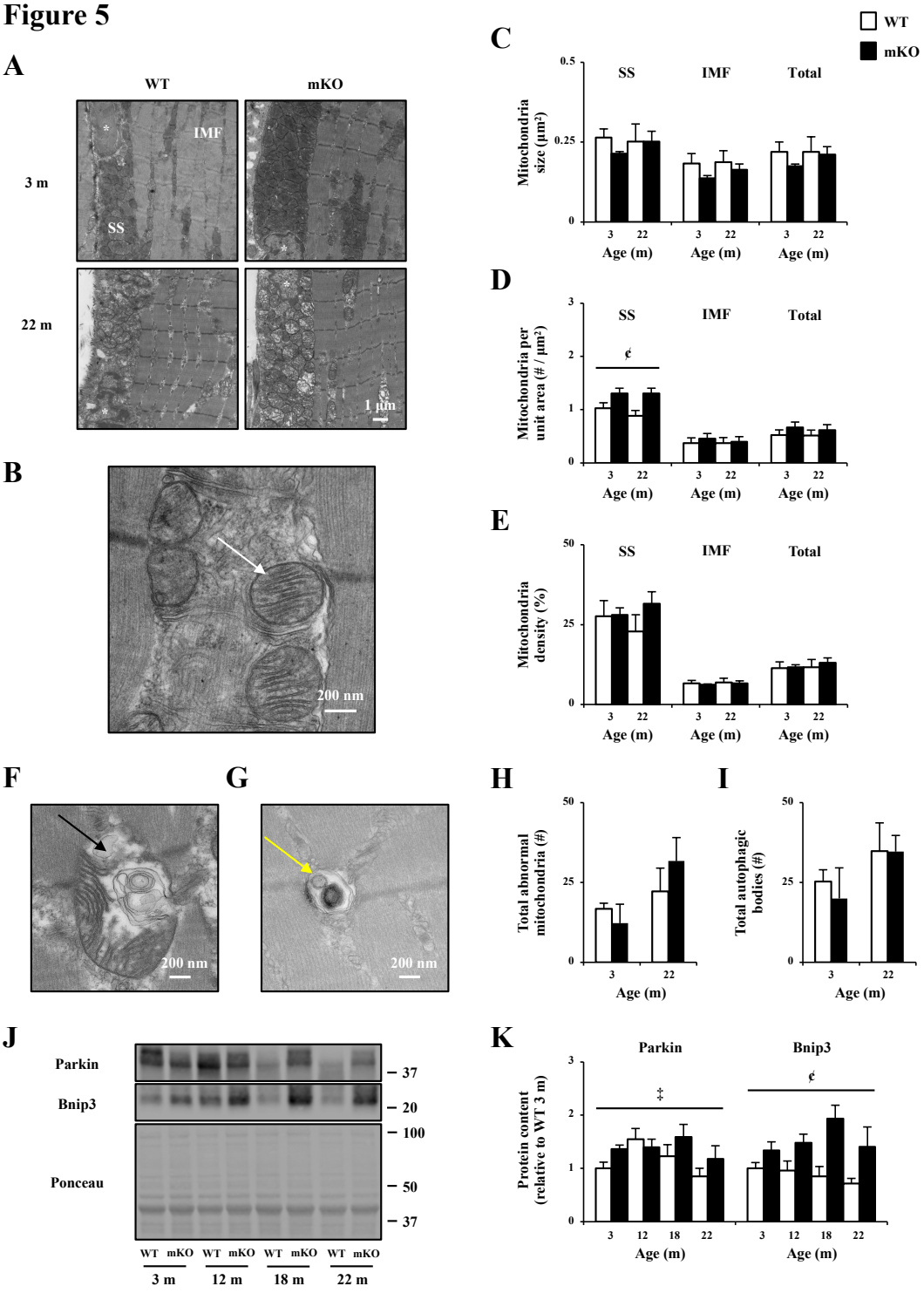
A
WT
mKO
3 m
22 m
IMF
SS
1 µm
B
200 nm
C
WT
mKO
SS
IMF
Total
Mitochondria size (µm²)
Age (m)
D
Mitochondria per unit area (# / µm²)
¢
E
Mitochondria density (%)
F
200 nm
G
200 nm
H
Total abnormal mitochondria (#)
I
Total autophagic bodies (#)
J
Parkin
Bnip3
Ponceau
37
20
100
50
37
WT mKO WT mKO WT mKO WT mKO
3 m
12 m
18 m
22 m
K
Parkin
Bnip3
Protein content (relative to WT 3 m)
‡
¢

Figure 6

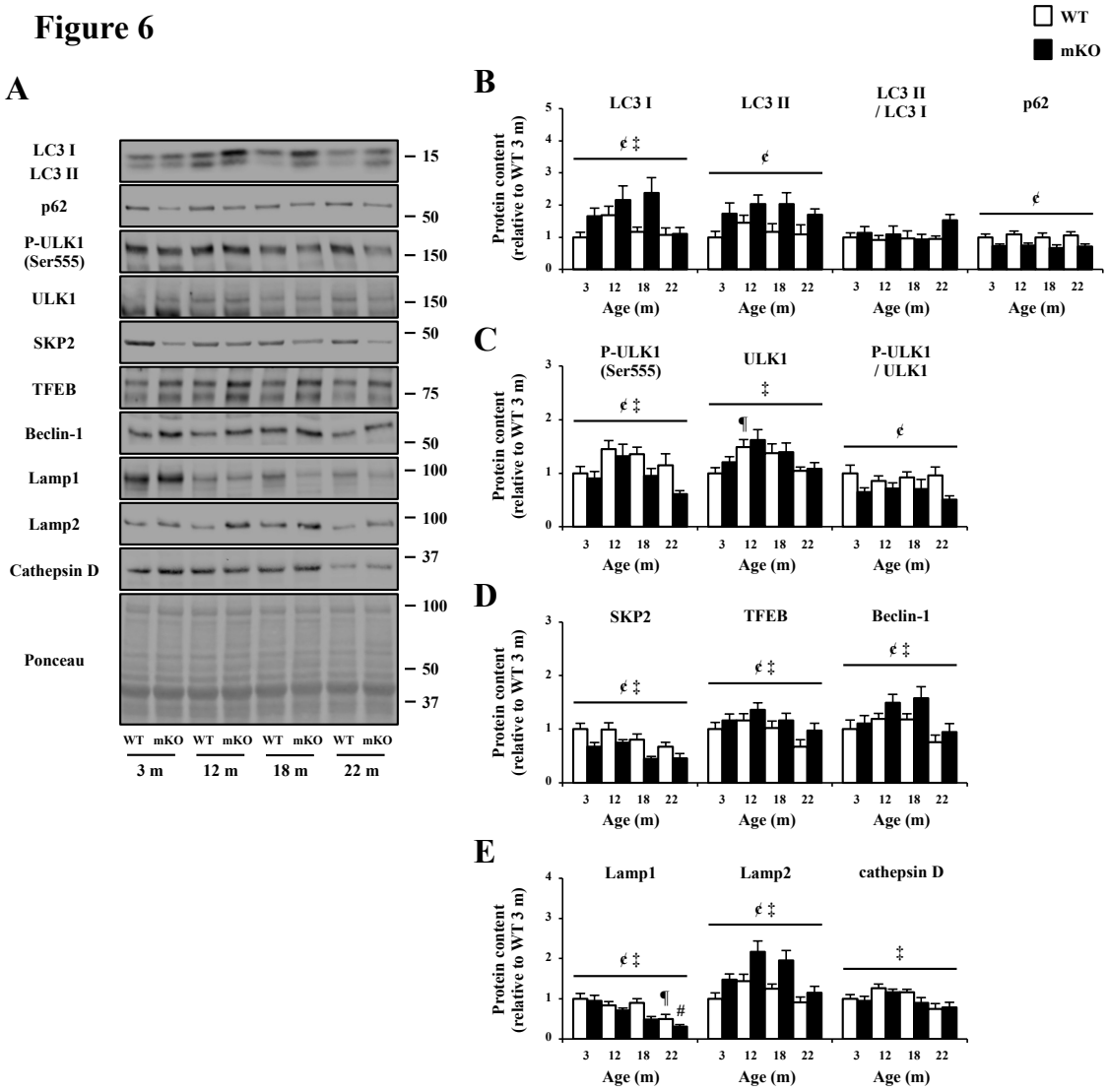
A
LC3 I
LC3 II
p62
P-ULK1 (Ser555)
ULK1
SKP2
TFEB
Beclin-1
Lamp1
Lamp2
Cathepsin D
Ponceau
15
50
150
150
50
75
50
100
100
37
100
50
37
WT mKO WT mKO WT mKO WT mKO
3 m
12 m
18 m
22 m
WT
mKO
B
LC3 I
LC3 II
LC3 II / LC3 I
p62
C
P-ULK1 (Ser555)
ULK1
P-ULK1 / ULK1
D
SKP2
TFEB
Beclin-1
E
Lamp1
Lamp2
cathepsin D
Protein content (relative to WT 3 m)
Age (m)
3 12 18 22

Figure 7

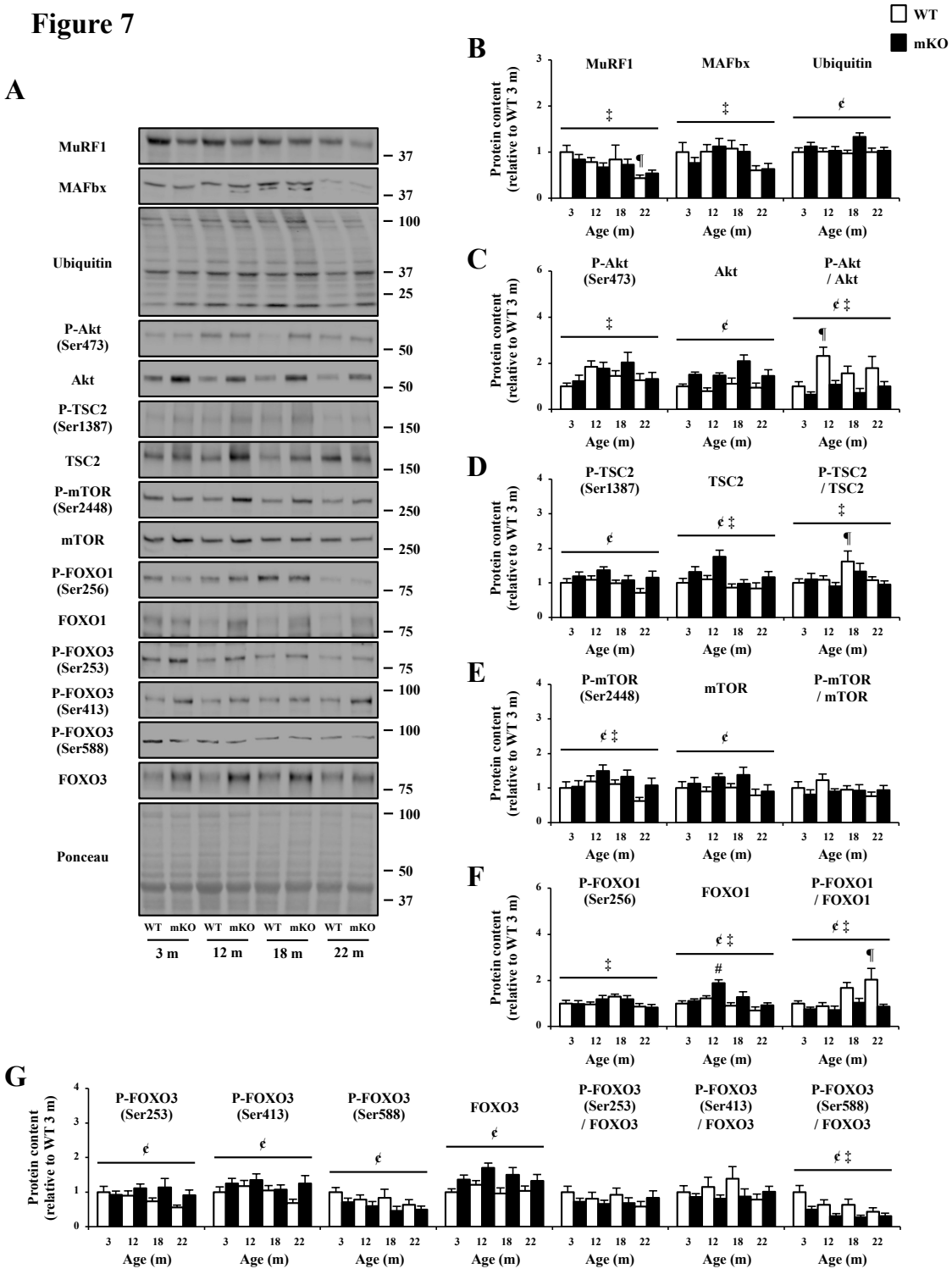
A
MuRF1
MAFbx
Ubiquitin
P-Akt (Ser473)
Akt
P-TSC2 (Ser1387)
TSC2
P-mTOR (Ser2448)
mTOR
P-FOXO1 (Ser256)
FOXO1
P-FOXO3 (Ser253)
P-FOXO3 (Ser413)
P-FOXO3 (Ser588)
FOXO3
Ponceau
37
37
100
37
25
50
50
150
150
250
250
75
75
75
100
100
75
100
50
37
WT mKO WT mKO WT mKO WT mKO
3 m
12 m
18 m
22 m
WT
mKO
B
MuRF1
MAFbx
Ubiquitin
C
P-Akt (Ser473)
Akt
P-Akt / Akt
D
P-TSC2 (Ser1387)
TSC2
P-TSC2 / TSC2
E
P-mTOR (Ser2448)
mTOR
P-mTOR / mTOR
F
P-FOXO1 (Ser256)
FOXO1
P-FOXO1 / FOXO1
G
P-FOXO3 (Ser253)
P-FOXO3 (Ser413)
P-FOXO3 (Ser588)
FOXO3
P-FOXO3 (Ser253) / FOXO3
P-FOXO3 (Ser413) / FOXO3
P-FOXO3 (Ser588) / FOXO3
Protein content (relative to WT 3 m)
Age (m)
3 12 18 22

Chapter 5:

Integrated Discussion

5.1 Introduction

The work outlined in this thesis provides evidence that CARM1 is a critical regulator of skeletal muscle plasticity. We first sought to determine whether CARM1 is required to maintain muscle mass under basal conditions. We demonstrated, for the first time, that CARM1 mKO mice have reduced muscle mass (Chapters 2-4). This finding appeared primarily driven by aberrant autophagic and atrophic processes downstream of the master neuromuscular phenotypic modifier AMPK. Furthermore, we aimed to develop a more comprehensive understanding of CARM1 function during various atrophy-inducing stimuli. We desired to determine whether knocking out CARM1 in skeletal muscle would mitigate the progression of muscle wasting following neurogenic muscle disuse (Chapter 2), prolonged food deprivation (Chapter 3), and the sarcopenia of aging (Chapter 4). This thesis provides evidence that CARM1 mKO attenuates the progression of denervation-induced muscle atrophy (Chapter 2). We also demonstrate that CARM1 mKO mitigates fasting-induced muscle wasting (Chapter 3). However, it remains unclear whether the curtailment in muscle loss was due to a protective effect of CARM1 deletion, or due to mKO muscles already nearing maximal atrophy, or a combination thereof. Unlike neurogenic muscle disuse and food deprivation, CARM1 mKO does not prevent aging-induced muscle wasting. Notably, skeletal muscle-specific deletion of CARM1 exacerbates the sarcopenia of aging (Chapter 4). CARM1 mKO resulted in a shorter lifespan and weakened muscle strength. Taken together, this thesis highlights the importance of CARM1 for the maintenance and plasticity of skeletal muscle.

5.2 Significance of Studies

5.2.1 CARM1 is required to maintain muscle mass under basal conditions.

Prior to Chapter 2 being published, the dearth of in vivo studies investigating PRMTs in muscle (Stouth et al., 2017; vanLieshout and Ljubicic, 2019) limited our understanding of the physiological impact of CARM1. Since CARM1 was identified as a crucial component of autophagy in non-muscle cells (Shin et al., 2016), and autophagy was shown to be necessary for the preservation of muscle mass (Masiero et al., 2009), it was hypothesized that knocking out CARM1 would result in lower muscle mass. In chapters 2, 3, and 4, we provide evidence that supports this hypothesis.

In this thesis (Chapters 2, 3, and 4), we demonstrate muscle-specific differences in the role of CARM1 in the maintenance of skeletal muscle mass. For example, muscle mass of faster, more glycolytic TA, EDL, and GAST was lower in CARM1 mKO versus WT mice, whereas slower, more oxidative SOL was similar between genotypes. EDL CSA was also reduced mKO animals compared to their WT littermates, while no differences were detected in the SOL. These results align with previous work demonstrating that deficiency of PRMT1, a family member of CARM1, causes muscle loss in the TA, EDL, and GAST, but not the SOL (Choi et al., 2019). Interestingly, relative to other muscles, CARM1 is expressed the least in the SOL (Chapter 2). Furthermore, knocking out CARM1 alters the fiber type composition of specific muscles. For instance, myosin heavy chain (MHC) type I was lower and MHC type IIA was greater in mKO versus WT SOL muscle, whereas fiber type composition was similar between genotypes in the EDL (data not shown).

Collectively, these data indicate that CARM1 is required to maintain muscle mass, and that knocking out CARM1 elicits muscle-specific remodeling.

We sought to determine whether other PRMT(s) compensate for the loss of CARM1 in muscle (Chapters 2, 3, and 4). Arginine methylation is a widespread posttranslational modification (Larsen et al., 2016), and muscle-specific deletion of PRMT1 results in greater CARM1 expression (Choi et al., 2019). Although compensatory mechanisms exist between CARM1 and other PRMTs in non-muscle cells (Cheng et al., 2020), PRMT expression and markers of global methyltransferase activity in muscle, for the most part, were unaffected by CARM1 mKO. More work is needed to determine whether CARM1 functions independently or cooperatively with other PRMTs in the maintenance of muscle mass.

We addressed whether CARM1 mKO alters the autophagy-lysosome and ubiquitin-proteasome signaling pathways under basal conditions (Chapters 2, 3, and 4), as these are two major protein degradation pathways that contribute to loss of muscle mass (Sandri, 2013). Since autophagy is a highly dynamic process (Klionsky et al., 2021; Triolo and Hood, 2021), we assessed autophagy flux using colchicine treatment in WT and mKO mice under fed conditions (Chapter 3). We show that LC3-II flux is lower in mKO versus WT muscle, suggesting that CARM1 deletion hinders autophagosome turnover in muscle. Moreover, we detected greater myonuclear TFEB and FOXO3 content in mKO animals compared to their WT littermates during fed settings (Chapter 3). TFEB and FOXO3 are master transcriptional regulators of the autophagy and atrophy programs (Triolo and Hood, 2021). To complement this work, we performed RNA sequencing (RNA-seq) analysis to elucidate global transcriptional changes in mKO versus WT muscle (data not shown). Of

the total 277 downregulated and 206 upregulated differentially expressed genes (DEGs), there were 161 downregulated and 98 upregulated DEGs in mKO mice related to muscle atrophy. Thus, the studies herein strongly suggest that CARM1 mKO alters autophagic and atrophic processes.

It was previously demonstrated that mitochondrial dysfunction contributes to muscle loss (Romanello and Sandri, 2016; Ferri et al., 2020). Here, we show that CARM1 mKO results in greater PGC-1α protein content (Chapters 2, 3, and 4). PGC-1α is a powerful regulator of muscle remodeling, as it is responsible for mitochondrial biogenesis and resistance to muscle atrophy, among others (Ljubicic et al., 2014). We assessed mitochondrial content with transmission electron microscopy (Larsen et al., 2012) and mitochondrial function *in situ* in permeabilized muscle fibers (Kuznetsov et al., 2008). Consistent with elevated PGC-1α protein content, there was a strong trend towards elevated mitochondrial content and function in mKO muscle (Chapters 3 and 4). However, in accordance with reduced autophagic flux, we detected aberrant markers of mitophagy, such as excessive Parkin puncta, in mKO animals compared to their WT littermates (Chapter 3). Given that mitochondrial biogenesis is balanced by organelle turnover via the mitophagy pathway (Hood et al., 2019), and that PGC-1α overexpression serves to protect against mitochondrial dysfunction (Yeo et al., 2019), we speculate that greater PGC-1α protein content in mKO muscle is a compensatory mechanism to offset the accumulation of damaged mitochondria, in an effort, to spare muscle mass. Thus, future studies should examine the impact of CARM1 mKO on mitophagy flux, to develop a more comprehensive understanding of the molecular mechanisms by which CARM1 mKO reduces muscle mass.

Skeletal muscle-specific deletion of CARM1 not only results in reduced muscle mass but also decreased functional capacity. We noted lower muscle strength and balance in mKO versus WT mice (Chapter 4). We also observed NMJ degeneration and inferior *in situ* force assessment in mKO compared to WT animals (data not shown). These results align with previous work demonstrating that autophagy impairment evokes NMJ instability and negatively affects muscle strength (Carnio et al., 2014). Together, these studies demonstrate that in addition to preserving muscle mass, CARM1 is important for supporting muscle function. Overall, CARM1 is a key player in skeletal muscle plasticity (Figure 1).

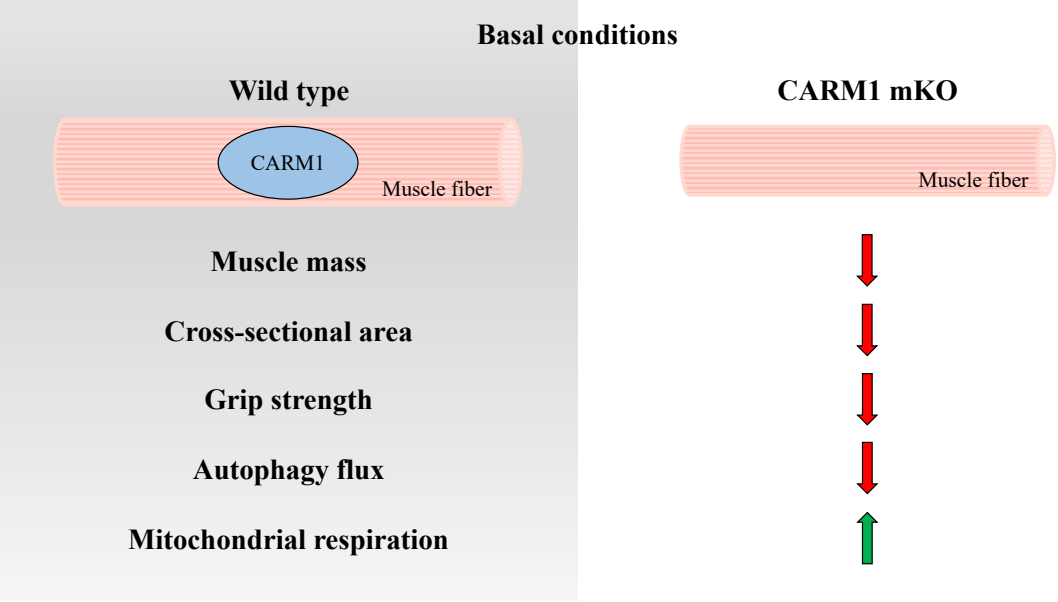

Figure 1. CARM1 mKO evokes skeletal muscle remodeling. CARM1 mKO results in lower muscle mass, cross-sectional area, grip strength, and autophagy flux. Conversely, CARM1 mKO increases mitochondrial respiration in 3-month-old mice.

5.2.2 The role of CARM1 during skeletal muscle atrophy.

Clinical conditions and chronic diseases can elicit loss of muscle mass, which in turn, can lead to muscle weakness and increased risk of mortality (Bodine and Baehr, 2014). For example, limb immobilization, bed rest, mechanical ventilation, spinal cord injury, prolonged fasting, aging, cancer cachexia, and muscular dystrophies result in muscle wasting. Skeletal muscle atrophy is a complex process that involves varying contributions from the autophagy-lysosome and ubiquitin-proteasome signaling pathways (Sandri, 2013). Despite recent advances in the literature, our knowledge of the molecular mechanisms that control muscle loss remains limited.

Previous work has shown that CARM1 expression is elevated following neurogenic muscle disuse (Stouth et al., 2018), and that transient knockdown of CARM1 mitigates the progression of denervation-induced atrophy (Liu et al., 2019). Since CARM1 plays a direct role in the autophagy-lysosome and ubiquitin-proteasome proteolytic systems (Kim et al., 2014; Shin et al., 2016; Yu et al., 2020), we sought to test whether CARM1 mKO would influence muscle loss after neurogenic muscle disuse (Chapter 2), food deprivation (Chapter 3), and the sarcopenia of aging (Chapter 4). In the current thesis, we employed various atrophy-inducing stimuli to gain a more comprehensive understanding of the mechanisms that govern muscle wasting. We demonstrate that CARM1 mKO attenuates the progression of atrophy in response to denervation and fasting (Chapters 2 and 3). However, CARM1 deletion negatively affects muscle function and does not prevent loss of muscle mass with aging (Chapter 4). Altogether, our work suggests that CARM1 mKO differently impacts muscle wasting in response to distinct models of atrophy.

The studies in the current thesis strongly suggest that CARM1 regulates muscle loss by way of AMPK. Earlier work in non-muscle cells reported a link between CARM1 and AMPK in signaling cascades that mediate catabolic processes (Kim et al., 2014; Shin et al., 2016; Yu et al., 2020). Denervation-induced muscle atrophy was also found to be associated with elevated CARM1 expression and AMPK activation (Stouth et al., 2018). Notably, AMPK regulates the autophagy-lysosome and ubiquitin-proteasome signaling pathways during muscle wasting through phosphorylation of its downstream targets (Kjobsted et al., 2018). In the current thesis, we utilized genetic, physiologic, and pharmacologic approaches to demonstrate that CARM1 regulates AMPK and its downstream signaling network in skeletal muscle (Chapter 2). Here, we show that CARM1 mKO curtails AMPK activation following neurogenic muscle disuse (Chapter 2), food deprivation (Chapter 3), and the sarcopenia of aging (Chapter 4). In turn, CARM1 deletion resulted in aberrant autophagic and atrophic signaling, particularly AMPK site-specific activation of ULK1^{Ser555} and FOXO3^{Ser588}. Since AMPK deficiency protects muscle from disuse- and fasting-induced muscle loss (Bujak et al., 2015; Egawa et al., 2015; Guo et al., 2016), through inhibition of autophagy and protein degradation (Triolo and Hood, 2021), it is reasonable to posit that CARM1 mKO affects skeletal muscle atrophy by modulating AMPK activity. Given that autophagy impairment in muscle evokes precocious aging (Carnio et al., 2014), and AMPK depletion accelerates the aging process (Bujak et al., 2015), altered AMPK signaling and dysregulated downstream autophagic processes may represent a mechanism for CARM1 mKO exacerbating the sarcopenia of aging. Thus, CARM1 appears to contribute to muscle wasting by mediating AMPK activity (Figure 2).

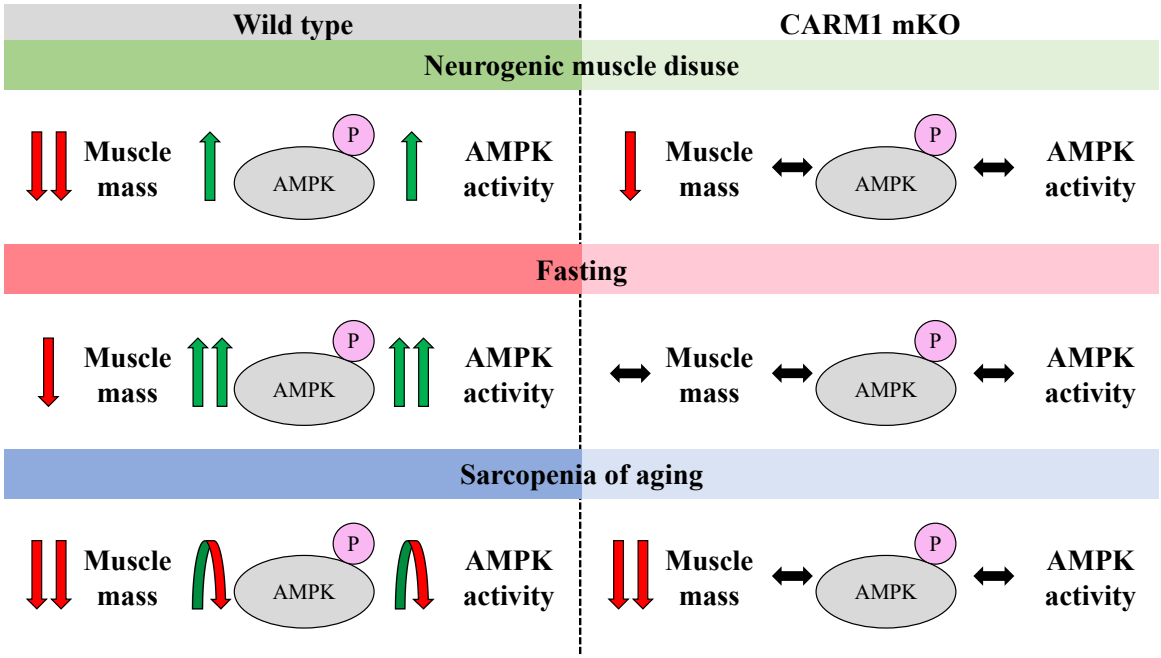

Figure 2. The impact of CARM1 mKO on denervation-, fasting-, and aging-induced skeletal muscle atrophy. Graphical representation of muscle wasting and AMPK activity in wild type (left) and CARM1 mKO (right) mice following neurogenic muscle disuse (green), fasting (red), and the sarcopenia of aging (blue). CARM1 mKO mitigates the progression of denervation- and fasting-induced muscle atrophy. However, CARM1 mKO does not prevent loss of muscle mass with aging. In each model, CARM1 mKO alters the phosphorylation (P) of AMPK^{Thr172} (AMPK activation), as well as autophagic and atrophic processes downstream of AMPK.

There are limited studies that have examined CARM1 biology in response to skeletal muscle atrophy. Consistent with previous studies (Stouth et al., 2018; Liu et al., 2019), we show that denervation elicits greater CARM1 expression and methyltransferase activity (Chapter 2). Here, we assessed asymmetric arginine dimethylation of pan-CARM1 marked substrates (Cheng et al. 2018; Cheng et al., 2020), along with bona fide CARM1

targets BAF155me2a^{Arg1064} and PABP1me2a$^{Arg455/Arg460}$ (Lee and Bedford, 2002; Wang et al., 2016) to evaluate CARM1 activity in muscle. A novel finding of this thesis is that CARM1 methylates AMPK shortly after neurogenic muscle disuse, coincident with increased CARM1-AMPK binding and AMPK activation (Chapter 2). These data further our knowledge of the interplay between CARM1 and AMPK in muscle. Since CARM1 prefers to methylate proline-enriched motifs (Cheng et al. 2018), we speculate that the methyltransferase marks the catalytic AMPK α1 subunit at the Arg538. Future studies should confirm predicted methylation sites of AMPK by CARM1. In Chapters 3 and 4 of the current thesis, we also measured CARM1 expression and methyltransferase activity in muscle during food deprivation (Chapter 3) and the sarcopenia of aging (Chapter 4). It was previously demonstrated that CARM1 levels are elevated in liver tissue with fasting (Shin et al., 2016), whereas CARM1 content in cardiomyocytes remains unchanged with aging (Li et al., 2017). Here, we found that CARM1 expression and methyltransferase activity were largely unaffected by fasting and aging in muscle, except for specific decreases in CARM1 function revealed by lower BAF155me2a^{Arg1064} and PABP1me2a$^{Arg455/Arg460}$ levels (Chapters 3 and 4). These are the first reports of CARM1 biology in skeletal muscle during prolonged food deprivation and the sarcopenia of aging. Evidently, our work indicates that the function of CARM1 on atrophy-induced remodeling depends on the stimuli, as well as the tissue.

There is considerable evidence that the signaling networks controlling muscle wasting are specific for each catabolic condition. Indeed, the autophagy-lysosome and ubiquitin-proteasome signaling pathways variably contribute to the loss of muscle mass in

different models of atrophy (Sandri, 2013). We observed a general upregulation of autophagy-related genes, as well as atrogenes, following denervation and fasting (Chapters 2 and 3), whereas mostly no changes or downregulation was observed with aging (Chapter 4). These results align with previous work demonstrating that FOXO3-dependent transcriptional activity is upregulated during acute atrophies and downregulated during more chronic muscle wasting conditions (Sanchez et al., 2014). The time course of disuse atrophy also bears some consideration, as muscle protein breakdown is adaptively reduced with longer periods of disuse (Atherton et al., 2016). To advance our current understanding of CARM1 function during skeletal muscle atrophy, we sought to compare global transcriptional changes in mKO versus WT mice across different atrophy-inducing stimuli using RNA-seq analysis. Of the total downregulated and upregulated DEGs, there were only 5 commonly downregulated, and 7 commonly upregulated DEGs in mKO muscle with denervation-, fasting-, and aging-induced muscle wasting. Therefore, these results further support the notion that the role of CARM1 during the loss of skeletal muscle mass depends on the model of atrophy (Figure 3).

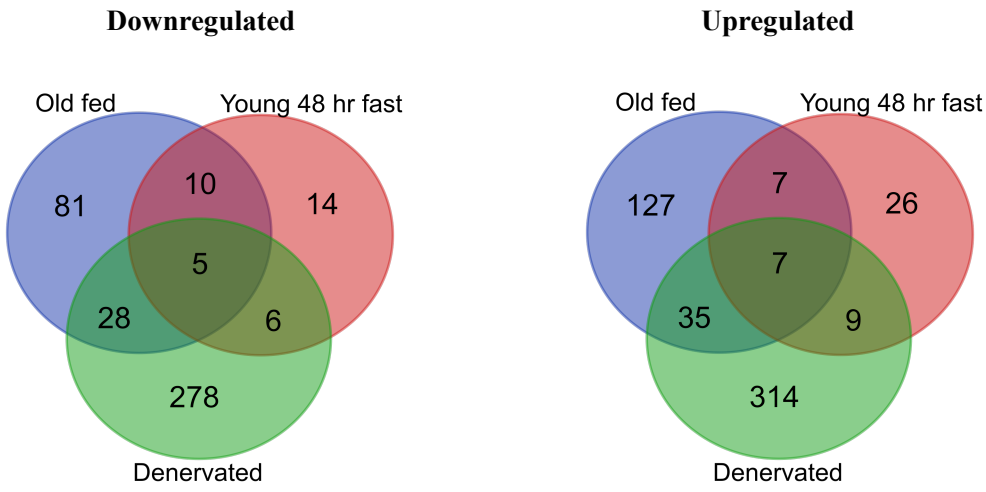

Figure 3. Transcriptional analysis of CARM1 mKO in response to various atrophy-inducing stimuli. Venn diagram representation of the number of significantly down- and upregulated differentially expressed genes (DEGs) based on RNA sequencing (RNA-seq). n = 4. Data represent CARM1 mKO versus wild type muscle after 7 days of neurogenic muscle disuse (green; Denervated), 48 hours of fasting (red; Young 48 hr fast), and 22 months of aging (blue; Old fed).

5.3 Limitations and future directions

We acknowledge several limitations in this thesis. First, we generated and employed CARM1 mKO mice to develop a more comprehensive understanding of CARM1 function in skeletal muscle during various atrophy-inducing stimuli (Chapters 2, 3, and 4). An inducible CARM1 mKO model, for instance, evoked by tamoxifen treatment (McCarthy et al., 2012), would introduce temporal specificity to the deletion of CARM1 in muscle. Pharmacological inhibition of CARM1 activity (Drew et al., 2017; Nakayama et al., 2018; Greenblatt et al., 2018) would also control for any compensatory or confounding adaptations that may have occurred in the animals across a lifetime without the enzyme. Second, only male mice were examined in Chapters 2 and 3, at a certain age, and during fixed periods of neurogenic muscle disuse and food deprivation. It is possible that female mice, or mice of a different age, would have different responses to CARM1 mKO. Utilizing longer durations of denervation and fasting, or different models of disuse atrophy (e.g., immobilization, hind limb suspension, microgravity), would advance our knowledge of CARM1 in diverging signaling networks that govern muscle wasting. Third, data from animal and human studies emphasize both similarities and differences (Atherton et al., 2016). Since the molecular mechanisms that drive muscle atrophy in humans are not

identical to murine muscle, future work is needed to test and extend the current findings in human skeletal muscle. Lastly, we (Chapter 2 and data not shown) and others (Liu et al., 2019) have identified target proteins (e.g., AMPK, TFEB, and FOXO3) that are methylated by CARM1 in muscle. However, further work is needed to confirm the predicted methylation site(s). Other putative CARM1 targets, plus arginine methylome profiling of skeletal muscle during atrophy, also requires further investigation.

The data presented in the current thesis are novel and demonstrate that CARM1 mKO impacts skeletal muscle remodeling in response to neurogenic muscle disuse, food deprivation, and the sarcopenia of aging. Here, we demonstrate that knocking out CARM1 in muscle attenuated the progression of denervation- and fasting-induced muscle atrophy (Chapters 2 and 3). This may have been due to a specific effect of CARM1 deletion, or perhaps mKO muscles already nearing maximal atrophy prior to introducing the stimulus, or a combination thereof. It would be interesting to extend studies from Chapter 2 and 3 with an inducible CARM1 mKO model, or with pharmacological inhibition of CARM1 activity, to determine whether manipulating the expression and/or activity of CARM1 in skeletal muscle offers a viable therapeutic strategy for mitigating disuse muscle wasting.

We provide evidence that CARM1 mKO exacerbates the sarcopenia of aging (Chapter 4). Survival analysis revealed that mKO mice have a significantly shorter lifespan, as well as reduced functional capacity, compared to their WT littermates. We plan to perform pathologic and clinical frailty assessments in the future to complement our current results. Since NMJ dysfunction and elevated levels of fibrosis contribute towards sarcopenia (Tintignac et al., 2015; Mahdy, 2019), and CARM1 mKO affects NMJ

morphology and collagen-specific gene transcription (data not shown), it would be interesting to extend Chapter 4 to investigate whether CARM1 mKO aggravates NMJ morphology and/or causes excessive accumulation of extracellular matrix components, such as collagen, with aging.

The influence of CARM1 mKO, as well as the effects of pharmacological CARM1 inhibition on cancer cachexia-induced muscle wasting is unknown. The involvement of CARM1 in neuromuscular disorders also remains to be fully understood. Since CARM1 mKO does not attenuate muscle loss after 14 days of denervation (data not shown), it stands to reason that CARM1 deletion and/or inhibition protects muscle against acute atrophies instead of chronic muscle wasting conditions. While our data support the notion that CARM1 is a potential therapeutic target for mitigating short-term muscle loss, further elucidation of the molecular mechanisms by which CARM1 influences atrophy is needed.

5.4 Conclusions

In summary, the major findings of this thesis demonstrate that CARM1 is required to maintain muscle mass, and that CARM1 is involved in the molecular mechanisms that regulate denervation-, fasting-, and aging-induced skeletal muscle atrophy. CARM1 mKO mitigated the progression of muscle loss that occurs early after neurogenic muscle disuse and food deprivation. However, CARM1 mKO exacerbated the sarcopenia of aging. Overall, this thesis advances our understanding of the role of CARM1 in governing skeletal muscle plasticity. Further investigation is therefore warranted to determine whether CARM1 is a viable therapeutic target for combating muscle wasting in various conditions.

5.5 References

Bodine, S. C., & Baehr, L. M. (2014). Skeletal muscle atrophy and the E3 ubiquitin ligases MuRF1 and MAFbx/atrogin-1. American journal of physiology. Endocrinology and metabolism, 307(6), E469–E484.

Bujak, A. L., Crane, J. D., Lally, J. S., Ford, R. J., Kang, S. J., Rebalka, I. A., Green, A. E., Kemp, B. E., Hawke, T. J., Schertzer, J. D., & Steinberg, G. R. (2015). AMPK activation of muscle autophagy prevents fasting-induced hypoglycemia and myopathy during aging. Cell metabolism, 21(6), 883–890.

Carnio, S., LoVerso, F., Baraibar, M. A., Longa, E., Khan, M. M., Maffei, M., Reischl, M., Canepari, M., Loefler, S., Kern, H., Blaauw, B., Friguet, B., Bottinelli, R., Rudolf, R., & Sandri, M. (2014). Autophagy impairment in muscle induces neuromuscular junction degeneration and precocious aging. Cell reports, 8(5), 1509–1521.

Cheng, D., Vemulapalli, V., Lu, Y., Shen, J., Aoyagi, S., Fry, C. J., Yang, Y., Foulds, C. E., Stossi, F., Treviño, L. S., Mancini, M. A., O'Malley, B. W., Walker, C. L., Boyer, T. G., & Bedford, M. T. (2018). CARM1 methylates MED12 to regulate its RNA-binding ability. Life science alliance, 1(5), e201800117.

Cheng, D., Gao, G., Di Lorenzo, A., Jayne, S., Hottiger, M. O., Richard, S., & Bedford, M. T. (2020). Genetic evidence for partial redundancy between the arginine methyltransferases CARM1 and PRMT6. The Journal of biological chemistry, 295(50), 17060–17070.

Choi, S., Jeong, H. J., Kim, H., Choi, D., Cho, S. C., Seong, J. K., Koo, S. H., & Kang, J. S. (2019). Skeletal muscle-specific Prmt1 deletion causes muscle atrophy via deregulation of the PRMT6-FOXO3 axis. Autophagy, 15(6), 1069–1081.

Drew, A. E., Moradei, O., Jacques, S. L., Rioux, N., Boriack-Sjodin, A. P., Allain, C., Scott, M. P., Jin, L., Raimondi, A., Handler, J. L., Ott, H. M., Kruger, R. G., McCabe, M. T., Sneeringer, C., Riera, T., Shapiro, G., Waters, N. J., Mitchell, L. H., Duncan, K. W., Moyer, M. P., … Ribich, S. A. (2017). Identification of a CARM1 Inhibitor with Potent In Vitro and In Vivo Activity in Preclinical Models of Multiple Myeloma. Scientific reports, 7(1), 17993.

Egawa, T., Goto, A., Ohno, Y., Yokoyama, S., Ikuta, A., Suzuki, M., Sugiura, T., Ohira, Y., Yoshioka, T., Hayashi, T., & Goto, K. (2015). Involvement of AMPK in regulating slow-twitch muscle atrophy during hindlimb unloading in mice. American journal of physiology. Endocrinology and metabolism, 309(7), E651–E662.

Ferri, E., Marzetti, E., Calvani, R., Picca, A., Cesari, M., & Arosio, B. (2020). Role of Age-Related Mitochondrial Dysfunction in Sarcopenia. International journal of molecular sciences, 21(15), 5236.

Greenblatt, S. M., Man, N., Hamard, P. J., Asai, T., Karl, D., Martinez, C., Bilbao, D., Stathias, V., Jermakowicz, A. M., Duffort, S., Tadi, M., Blumenthal, E., Newman, S., Vu, L., Xu, Y., Liu, F., Schurer, S. C., McCabe, M. T., Kruger, R. G., Xu, M., … Nimer, S. D. (2018). CARM1 Is Essential for Myeloid Leukemogenesis but Dispensable for Normal Hematopoiesis. Cancer cell, 33(6), 1111–1127.e5.

Guo, Y., Meng, J., Tang, Y., Wang, T., Wei, B., Feng, R., Gong, B., Wang, H., Ji, G., & Lu, Z. (2016). AMP-activated kinase α2 deficiency protects mice from denervation-induced skeletal muscle atrophy. Archives of biochemistry and biophysics, 600, 56–60.

Hood, D. A., Memme, J. M., Oliveira, A. N., & Triolo, M. (2019). Maintenance of Skeletal Muscle Mitochondria in Health, Exercise, and Aging. Annual review of physiology, 81, 19–41.

Kim, D., Lim, S., Park, M., Choi, J., Kim, J., Han, H., Yoon, K., Kim, K., Lim, J., & Park, S. (2014). Ubiquitination-dependent CARM1 degradation facilitates Notch1-mediated podocyte apoptosis in diabetic nephropathy. Cellular signalling, 26(9), 1774–1782.

Kjøbsted, R., Hingst, J. R., Fentz, J., Foretz, M., Sanz, M. N., Pehmøller, C., Shum, M., Marette, A., Mounier, R., Treebak, J. T., Wojtaszewski, J., Viollet, B., & Lantier, L. (2018). AMPK in skeletal muscle function and metabolism. FASEB journal: official publication of the Federation of American Societies for Experimental Biology, 32(4), 1741–1777.

Klionsky, D. J., Abdel-Aziz, A. K., Abdelfatah, S., Abdellatif, M., Abdoli, A., Abel, S., Abeliovich, H., Abildgaard, M. H., Abudu, Y. P., Acevedo-Arozena, A., Adamopoulos, I. E., Adeli, K., Adolph, T. E., Adornetto, A., Aflaki, E., Agam, G., Agarwal, A., Aggarwal, B. B., Agnello, M., Agostinis, P., … Tong, C. K. (2021). Guidelines for the use and interpretation of assays for monitoring autophagy (4th edition)1. Autophagy, 17(1), 1–382.

Kuznetsov, A. V., Veksler, V., Gellerich, F. N., Saks, V., Margreiter, R., & Kunz, W. S. (2008). Analysis of mitochondrial function in situ in permeabilized muscle fibers, tissues and cells. Nature protocols, 3(6), 965–976.

Larsen, S., Nielsen, J., Hansen, C. N., Nielsen, L. B., Wibrand, F., Stride, N., Schroder, H. D., Boushel, R., Helge, J. W., Dela, F., & Hey-Mogensen, M. (2012). Biomarkers of mitochondrial content in skeletal muscle of healthy young human subjects. The Journal of physiology, 590(14), 3349–3360. https://doi.org/10.1113/jphysiol.2012.230185

Larsen, S. C., Sylvestersen, K. B., Mund, A., Lyon, D., Mullari, M., Madsen, M. V., Daniel, J. A., Jensen, L. J., & Nielsen, M. L. (2016). Proteome-wide analysis of arginine monomethylation reveals widespread occurrence in human cells. Science signaling, 9(443), rs9.

Lee, J., & Bedford, M. T. (2002). PABP1 identified as an arginine methyltransferase substrate using high-density protein arrays. EMBO reports, 3(3), 268–273.

Li, C., Yu, L., Xue, H., Yang, Z., Yin, Y., Zhang, B., Chen, M., & Ma, H. (2017). Nuclear AMPK regulated CARM1 stabilization impacts autophagy in aged heart. Biochemical and biophysical research communications, 486(2), 398–405.

Liu, Y., Li, J., Shang, Y., Guo, Y., & Li, Z. (2019). CARM1 contributes to skeletal muscle wasting by mediating FoxO3 activity and promoting myofiber autophagy. Experimental cell research, 374(1), 198–209.

Mahdy M. (2019). Skeletal muscle fibrosis: an overview. Cell and tissue research, 375(3), 575–588.

Masiero, E., Agatea, L., Mammucari, C., Blaauw, B., Loro, E., Komatsu, M., Metzger, D., Reggiani, C., Schiaffino, S., & Sandri, M. (2009). Autophagy is required to maintain muscle mass. Cell metabolism, 10(6), 507–515.

McCarthy, J. J., Srikuea, R., Kirby, T. J., Peterson, C. A., & Esser, K. A. (2012). Inducible Cre transgenic mouse strain for skeletal muscle-specific gene targeting. Skeletal muscle, 2(1), 8.

Nakayama, K., Szewczyk, M. M., Dela Sena, C., Wu, H., Dong, A., Zeng, H., Li, F., de Freitas, R. F., Eram, M. S., Schapira, M., Baba, Y., Kunitomo, M., Cary, D. R., Tawada, M., Ohashi, A., Imaeda, Y., Saikatendu, K. S., Grimshaw, C. E., Vedadi, M., Arrowsmith, C. H., … Brown, P. J. (2018). TP-064, a potent and selective small molecule inhibitor of PRMT4 for multiple myeloma. Oncotarget, 9(26), 18480–18493.

Romanello, V., & Sandri, M. (2016). Mitochondrial Quality Control and Muscle Mass Maintenance. Frontiers in physiology, 6, 422.

Sanchez, A. M., Candau, R. B., & Bernardi, H. (2014). FoxO transcription factors: their roles in the maintenance of skeletal muscle homeostasis. Cellular and molecular life sciences: CMLS, 71(9), 1657–1671.

Sandri M. (2013). Protein breakdown in muscle wasting: role of autophagy-lysosome and ubiquitin-proteasome. The international journal of biochemistry & cell biology, 45(10), 2121–2129.

Shin, H. J., Kim, H., Oh, S., Lee, J. G., Kee, M., Ko, H. J., Kweon, M. N., Won, K. J., & Baek, S. H. (2016). AMPK-SKP2-CARM1 signalling cascade in transcriptional regulation of autophagy. Nature, 534(7608), 553–557.

Stouth, D. W., Manta, A., & Ljubicic, V. (2018). Protein arginine methyltransferase expression, localization, and activity during disuse-induced skeletal muscle plasticity. American journal of physiology. Cell physiology, 314(2), C177–C190.

Stouth, D. W., vanLieshout, T. L., Shen, N. Y., & Ljubicic, V. (2017). Regulation of Skeletal Muscle Plasticity by Protein Arginine Methyltransferases and Their Potential Roles in Neuromuscular Disorders. Frontiers in physiology, 8, 870.

Tintignac, L. A., Brenner, H. R., & Rüegg, M. A. (2015). Mechanisms Regulating Neuromuscular Junction Development and Function and Causes of Muscle Wasting. Physiological reviews, 95(3), 809–852.

Triolo, M., & Hood, D. A. (2021). Manifestations of Age on Autophagy, Mitophagy and Lysosomes in Skeletal Muscle. Cells, 10(5), 1054.

vanLieshout, T. L., & Ljubicic, V. (2019). The emergence of protein arginine methyltransferases in skeletal muscle and metabolic disease. American journal of physiology. Endocrinology and metabolism, 317(6), E1070–E1080.

Wang, L., Zhao, Z., Meyer, M. B., Saha, S., Yu, M., Guo, A., Wisinski, K. B., Huang, W., Cai, W., Pike, J. W., Yuan, M., Ahlquist, P., & Xu, W. (2016). CARM1 Methylates Chromatin Remodeling Factor BAF155 to Enhance Tumor Progression and Metastasis. Cancer cell, 30(1), 179–180.

Yeo, D., Kang, C., Gomez-Cabrera, M. C., Vina, J., & Ji, L. L. (2019). Intensified mitophagy in skeletal muscle with aging is downregulated by PGC-1alpha overexpression in vivo. Free radical biology & medicine, 130, 361–368.

Yu, Y. S., Shin, H. R., Kim, D., Baek, S. A., Choi, S. A., Ahn, H., Shamim, A., Kim, J., Kim, I. S., Kim, K. K., Won, K. J., & Baek, S. H. (2020). Pontin arginine methylation by CARM1 is crucial for epigenetic regulation of autophagy. Nature communications, 11(1), 6297.